UNIVERSITY OF NOTTINGHAM

Permanent Deformation in Bituminous Mixtures

by

Shahab Khanzada, B.Sc, MIHT, MIAT

Thesis submitted to the University of Nottingham
for the degree of Doctor of Philosophy

June, 2000

DEPARTMENT OF CIVIL ENGINEERING

To my parents

Acknowledgements

This research project was suggested by Dr Andrew Collop who also acted as my research supervisor. I am greatly indebted to him for his invaluable advice, encouragement and enthusiasm towards this project. I would also like to express my appreciation to him for reviewing my thesis a number of times during the write up notwithstanding his own heavy workload and offering valuable suggestions and comments. I am grateful to Professor S. F. Brown for his valuable suggestions and many long fruitful discussions. I would also like to thank Dr N. H. Thom and Dr G. Airey for extending their help during the course of this project.

I am grateful to Barry Broderick who detected and solved all the electronic problems and provided valuable technical support during the course of this research. I am thankful to the technical staff, especially Gerry Barnes and Garry Hayes for their help throughout these years. I would like to extend my thanks to the unsung heroes in the bitumen laboratory, Ehsan, Shane and Mick for making countless specimens for my experimental work. I would also like to mention all the researchers of the Pavements and Geotechnics Group with whom, I had lots of discussions from which I learnt a great deal. I am thankful to my friend Dr Mohammad Tufail for extending his help and company during my stay at Nottingham. Thanks to all those who have helped me in some way but not mentioned above by name.

This research was funded by the Commonwealth Commission in the United Kingdom, and I am grateful for their generous and continuos support.

I would like to thank my family, in particular my parents, Dr Ronaq Zaman Khanzada and Mrs Khalida Gul, my brother Dr Faisal Khanzada for their constant encouragement.

Finally, a very special person who really made it possible for me, during all these years of hard work is my wife Farah. Her support and understanding are beyond any thanks.

Declaration

The research described in this thesis was conducted at the University of Nottingham, Department of Civil Engineering between October 1996 and September 1999. I declare that the work is my own and has not been submitted for a degree of another university.

Shahab Khanzada
Nottingham
June 2000

Summary

This thesis is concerned with improving current understanding of the permanent deformation behaviour of bituminous mixtures. The approach used has been to investigate the steady-state deformation behaviour of idealised bituminous mixtures and binders and extend this to investigate the steady-state deformation behaviour of more realistic bituminous mixtures. A detailed literature review covering modelling approaches and test methods is given in Chapter 2.

Chapter 3 describes testing carried out in the Dynamic Shear Rheometer (DSR) to determine the dynamic mechanical properties of the binders used in this project. Creep tests have also been performed using the DSR to characterise the steady-state deformation behaviour of the binders over a wide range of stress levels. A simple model has been developed which relates steady-state stress to shear strain rate. It is concluded that the deformation behaviour of the binders is linear at lower stress levels (<100 kPa) and non-linear with a creep exponent of approximately $n = 2.4$ at higher stress levels (>100 kPa).

Chapter 4 describes compressive uniaxial experiments carried out on both idealised (sand asphalts) and realistic mixtures over a wide range of stress levels, strain rates and temperatures. The steady-state deformation behaviour of both the idealised and the realistic mixtures is found to be of the same form as that of the pure bitumen with the aggregate acting to stiffen the mixture.

The deformation behaviour of the idealised and the realistic mixtures is investigated under more complicated stress conditions in Chapter 5, which describes the results from compressive triaxial experiments. It is observed that at a constant stress ratio, the steady-state deformation behaviour of the idealised mixtures and the realistic mixtures has the same form as that of the pure bitumen. The behaviour is found to be dependent on both the mean stress and the deviator stress. The stiffening factor (between the pure bitumen and the mixture) is found to be a function of the volume fraction of the aggregate and the stress ratio (mean stress divided by the deviator

stress). Measurements of radial strain have shown that both the idealised and realistic mixtures are observed to dilate under compressive triaxial stresses.

Chapter 6 contains details of Repeated Load Axial (RLA) testing carried out using the Nottingham Asphalt Tester (NAT) on the idealised and realistic mixtures over a range of temperatures and applied stress levels. It is concluded that this simplified test, that operates at relatively low stress levels, may not be sufficient to fully characterise the permanent deformation behaviour of these types of mixtures, particularly in the non-linear region.

More simulative wheel tracking tests have been performed on the idealised and realistic bituminous mixtures over a range of temperatures and applied stress levels and results are presented in Chapter 7. It is concluded that the rutting process (as measured in the wheel tracking test) for the mixtures tested can be non-linear with respect to the applied load at realistic stress levels. The measured creep exponents from the wheel tracking test for the idealised as well as the realistic mixtures are found to be similar to the non-linear creep exponent measured from compressive uniaxial and triaxial tests on these mixtures.

Chapter 8 describes the development of a model based on the theory of linear viscoelasticity to predict the steady-state rutting rates obtained from the wheel tracking tests on the idealised and realistic mixtures. The method uses non-linear material properties determined from the uniaxial and triaxial testing. A linearised approach is developed to predict the non-linear deformation behaviour of bituminous mixtures. The predicted and the measured rutting rates for both the idealised and realistic mixtures show good agreement over a range of stress levels and temperatures. It is concluded that the model has the ability to predict non-linear deformation behavior of bituminous mixtures.

Summary, conclusions and recommendations for further research are presented in Chapter 9.

Contents

Page

Acknowledgements i
Declaration ii
Summary iii
Contents v
List of Figures x
List of Tables xvi
Nomenclature xvii

1 Introduction 1

1.1 Problem Definition 1
1.2 The Research Project 4
1.3 Figures 6

2 Literature Review 7

2.1 Introduction 7
2.2 Permanent Deformation Criteria 8
2.3 Mechanism of Permanent Deformation in Bituminous Materials 8
2.4 Permanent Deformation Behaviour of Pure Bitumen 11
2.5 Permanent Deformation Behaviour of Idealised Bituminous Mixtures 15
2.6 Permanent Deformation Behaviour of Realistic Mixtures 18
2.6.1 Early rutting models 18
2.6.2 'Layer-strain' based prediction models 19
2.6.3 Viscoelastic based prediction models 24
2.7 Material Testing for Permanent Deformation 28
2.7.1 Uniaxial and Triaxial Creep Tests 29
2.7.2 Uniaxial and Triaxial Repeated Load Tests 30
2.7.3 Simple Shear Tests 32
2.7.4 Tests on Hollow Cylinder Specimens 35
2.7.5 Wheel Tracking Tests 36
2.8 Summary 38
2.9 Research Needs 40
2.10 Figures 42

3 Binder Testing 52

3.1 Introduction 52
3.2 Dynamic Shear Rheometry (DSR) 53
3.2.1 Apparatus 56
3.2.2 Preparation of Apparatus 56
3.2.3 Test Specimen Preparation and Test Procedure 57
3.2.4 Test Conditions 58
3.3 Time-Temperature Superposition Principle 58
3.3.1 Shift Factors 60
3.3.2 Master Curves 63
3.4 SHRP Rutting Parameter 63
3.5 DSR Results 64
3.6 Creep Shear Tests 66
3.6.1 DSR Creep Model 67
3.7 Conclusions 72
3.8 Figures 74

4 Uniaxial Tests on Idealised and Realistic Bituminous Mixtures 86

4.1 Introduction 86
4.2 Idealised Mixtures 87
4.2.1 Specimen Preparation 88
4.2.2 Compaction of Test Specimen 89
4.2.3 Testing Procedure 91
4.3 Experimental Results 92
Idealised Mixtures (Mixture A/D and Mixture A) 92
4.4 Realistic Mixtures 95
4.4.1 Test Specimens 96
4.4.1.1 30/10 Hot Rolled Asphalt (HRA) 96
4.4.1.2 Dense Bitumen Macadam (DBM) 97
4.4.2 Compaction of Test Specimens 97
4.5 Experimental Results 98
30/10 HRA Mixture 98
HRA Mortar 99
10mm DBM Mixture with 50 Pen Binder 99
10mm DBM Mixture with 100 Pen Binder 100
4.6 Discussion 100
4.7 Conclusions 102
4.8 Figures 104

5 Triaxial Tests on Idealised and Realistic Bituminous Mixtures 118

5.1 Introduction 118
5.2 Triaxial Testing 119
5.2.1 Test Equipment 119
5.2.2 Membrane Preparation 120
5.3 Testing Procedure 121
5.4 Experimental Results 123
5.4.1 Idealised Mixtures (mixture A/D and mixture A) 123
5.4.2 Realistic Mixtures (HRA and DBM Mixtures) 126
5.5 Unbound Granular Material Testing 128
5.5.1 Specimen Preparation 128
5.6 Experimental Results 129
5.7 Discussion 130
5.8 Conclusions 132
5.9 Figures 134

6 Repeated Load Axial Tests on Idealised and Realistic Bituminous Mixtures 150

6.1 Introduction 150
6.2 Repeated Load Axial (RLA) Test 151
6.2.1 The Nottingham Asphalt Tester (NAT) 151
6.3 Test Specimens 152
6.3.1 Test Conditions 153
6.4 Results for the Idealised Mixtures 154
6.5 Analysis of Test Results 154
6.6 Results for Realistic Mixtures 157
6.7 Analysis of Test Results 157
6.8 Comparison of $G^*/\sin\delta$ with RLA Test Data 158
6.9 Discussion 159
6.10 Conclusions 161
6.11 Figures 162

7 Wheel Tracking Tests on Idealised and Realistic Bituminous Mixtures 170

7.1 Introduction 170
7.2 Wheel Tracking Test at Nottingham 171
7.3 Equipment Development 171

7.3.1 Image Analysis 172
7.3.2 Mechanical Profilometer 172
7.4 Test Procedure 173
7.4.1 Compaction of Test Specimens 174
7.4.2 Density Measurements 174
7.4.3 Test Conditions 177
7.5 Results for the Idealised Mixtures 177
7.6 Analysis of Results 178
7.7 Results for Realistic Mixtures 180
7.8 Analysis of Test Results 180
7.9 Comparison of Wheel Tracking and RLA Test Data 181
7.10 Comparison of G*/sinδ with Wheel Tracking Test Data 182
7.11 Discussion 182
7.12 Conclusions 184
7.13 Figures 186

8 A Visco-Elastic Model for Rutting in Asphaltic Mixtures 200

8.1 Introduction 200
8.2 Theoretical Rutting Model Formulation 200
8.3 Determination of Asphalt Mixture Extensional Viscosity 203
8.3.1 Viscosity Model from Uniaxial and Triaxial Tests 203
8.3.2 Calculation of Stress Ratio and Von Mises Equivalent Stress in Wheel Tracking Test 205
8.3.3 Predicted Viscosities 207
8.4 Linearisation Approach 207
8.5 Calculation of Rutting Influence Function 209
8.6 Rut Depth Predictions 209
8.6.1 Idealised Mixtures (mixtures A and A/D) 209
8.6.2 Realistic Mixtures (HRA and DBM) 212
8.7 Discussion 213
8.8 Conclusions 214
8.9 Figures 216

9 Summary, Conclusions and Recommendations 226

9.1 Summary 226
9.2 Conclusions 229
9.2.1 Chapter 2: Literature Review 229
9.2.2 Chapter 3: Binder Testing 229
9.2.3 Chapter 4: Uniaxial Tests on Idealised and Realistic Bituminous Mixtures 230
9.2.4 Chapter 5: Triaxial Tests on Idealised and

Realistic Bituminous Mixtures 231
9.2.5 Chapter 6: Repeated Load Axial Tests on Idealised and Realistic Bituminous Mixtures 232
9.2.6 Chapter 7: Wheel Tracking Tests on Idealised and Realistic Bituminous Mixtures 233
9.2.7 Chapter 8: A Visco-Elastic Model for Rutting in Asphaltic Mixtures 234
9.3 Recommendations for Future Work 234
9.3.1 Quasi-static behaviour of modified binders and mixtures 234
9.3.2 Further investigation into the Dilation Gradient 235
9.3.3 Field Verification 235
9.3.4 Finite Element Implementation of Rutting Model 235
9.3.5 Extension to Transient Behaviour 236

References 237

List of Figures

Page

1.1 Typical flexible pavement structure 6
1.2 Structural and Non-Structural rutting 6
2.1 Idealised strain response of a bituminous mixture 42
2.2 Accumulation of permanent strain under repeated loading 42
2.3 Effect of number of passes on transverse surface profiles 43
2.4 A stress/temperature deformation mechanism map for 50 Pen grade of bitumen in tension 43
2.5 Constant strain rate tests of 64% mix at 20°C 44
2.6 Deformation map for mixture with 64% by volume sand and 50 Pen bitumen 44
2.7 Permanent deformation – Time relationship 45
2.8 Inability to model shear displacement adjacent to the wheel path 45
2.9 Comparison of predicted permanent deformation with measured values for Dense Bitumen Macadam (DBM) 46
2.10 Correlation between the predicted and observed rut depth 46
2.11 Maxwell model with Voigt model in series (4-element (Burger's) model) 47
2.12 Ability to model shear displacement adjacent to the wheel path 47
2.13 Comparison between the predicted and measured rut depth in the wheel tracking test 48
2.14 Predicted contribution to deformation from bound layers 48
2.15 Predicted and measured rutting 49
2.16 Conceptual view of the simple shear at constant height test 49
2.17 Conceptual view of the frequency sweep at constant height test 50
2.18 The development of Tertiary flow as a function of repeated shear loading 50
2.19 Section showing hollow cylinder specimen test configuration 51
2.20 Idealised stress conditions in a hollow cylinder test: loading and stresses on wall element 51
3.1 Dynamic Shear Rheometer (DSR) 74
3.2 Principles of operation of torsional-type Dynamic Shear Rheometers 75
3.3 Definitions of moduli obtained from DSR tests 75

3.4 Viscoelastic behaviour of bitumen 76
3.5 Linear viscoelastic response of bitumen 76
3.6 Time-temperature superposition principle 77
3.7 Comparison of Arrhenuis and WLF equation with manually obtained Shift factors for 50 Pen bitumen 77
3.8 Comparison of Arrhenuis and WLF equation with manually obtained Shift factors for 100 Pen bitumen 78
3.9 Phase angle master curve from $|G^*|$ derived shift factors (50 Pen) 78
3.10 Isochronal plot at 0.1 Hz for 50 and 100 Pen grade bitumens 79
3.11 Isochronal plot at 1 Hz for 50 and 100 Pen grade bitumens 79
3.12 Isochronal plot at 10 Hz for 50 and 100 Pen grade bitumens 80
3.13 Isochronal plot of viscosity for 50 Pen grade bitumen 80
3.14 Isochronal plot of viscosity for 100 Pen grade bitumen 81
3.15 Isothermal plots of complex modulus for 50 Pen grade bitumen 81
3.16 Isothermal plots of phase angle for 50 Pen grade bitumen 82
3.17 Complex modulus master curves for 50 and 100 Pen grade bitumens 82
3.18 Phase angle master curves for 50 and 100 Pen grade bitumens 83
3.19 Creep test result for 50 Pen grade bitumen at 20°C 83
3.20 Creep test result for 100 Pen grade bitumen at 20°C 84
3.21 Deformation behaviour of 50 Pen grade bitumen at 20°C 84
3.22 Deformation behaviour of 100 Pen grade bitumen at 20°C 85
3.23 DSR testing geometry 85
4.1 Schematic showing compaction mould and Kango hammer foot 104
4.2 Photograph showing split mould and Kango compactor 104
4.3 Photograph of Mixture A/D specimen with loading arrangement (Size Ø75×150mm) 105
4.4 Constant strain rate test results for mixture A/D at 20°C 106
4.5 Constant strain rate test results for mixture A at 20°C 106
4.6 Constant strain rate test results for mixture A/D at 30°C 107
4.7 Constant strain rate test results for mixture A at 30°C 107
4.8 Creep test result for mixture A/D at 20°C 108
4.9 Creep test result for mixture A at 20°C 108
4.10 Steady-state deformation behaviour of mixture A/D at 20°C and 30°C 109

4.11 Steady-state deformation behaviour of mixture A at 20°C and 30°C 109
4.12 Design grading for 30/10 Hot Rolled Asphalt 110
4.13 Idealised section through a gap graded material 110
4.14 Design grading for 10mm Dense Bitumen Macadam 111
4.15 Idealised section through a continuously graded material 111
4.16 Constant strain rate test results for 30/10 HRA at 20°C 112
4.17 Creep test result for 30/10 HRA at 20°C 112
4.18 Steady-state deformation behaviour of 30/10 HRA at 20°C 113
4.19 Constant strain rate test results for HRA mortar at 20°C 113
4.20 Steady-state deformation behaviour of HRA mortar and mixture at 20°C 114
4.21 Constant strain rate test results for 10mm DBM at 20°C 114
4.22 Creep test result for 10mm DBM at 20°C 115
4.23 Steady-state deformation behaviour of 10mm DBM at 20°C 115
4.24 Constant strain rate test results for 10mm DBM with 100 Pen Bitumen at 20°C 116
4.25 Steady-state deformation behaviour of 10mm DBM with 100 Pen binder at 20°C 116
4.26 Variation of stiffening factor *S* with volume fraction of aggregate 117
5.1 Triaxial Test Equipment (general view) 134
5.2 Schematic diagram of triaxial experimental setup 135
5.3 Photograph of the Triaxial cell 136
5.4 Schematic showing arrangement for radial strain measurement 136
5.5 Schematic of the Triaxial Cell 137
5.6 Specimen fitted with a radial strain transducer 138
5.7 Schematic showing the triaxial co-ordinate system 138
5.8 Triaxial creep test result for mixture A/D at 20°C (stress ratio 0.8) 139
5.9 Steady-state deformation behaviour of mixture A/D at various triaxial stress states at 20°C 139
5.10 Triaxial creep test result for mixture A at 20°C (stress ratio of 0.8) 140
5.11 Steady-state deformation behaviour of mixture A at various triaxial stress states at 20°C 140
5.12 Dependence of the radial strain on the axial strain for a creep test at 20°C (mixture A) 141
5.13 Variation of volumetric strain with distortional strain for triaxial

creep tests on mixture A/D 141
5.14 Variation of volumetric strain with distortional strain for triaxial creep tests on mixture A 142
5.15 Triaxial creep test result for 30/10 HRA at 40°C (stress ratio of 0.6) 142
5.16 Steady-state deformation behaviour of 30/10 HRA mixture at 40°C (stress ratio of 0.6) 143
5.17 Variation of volumetric strain with distortional strain for triaxial creep tests on 30/10 HRA mixture at 40°C (stress ratio of 0.6) 144
5.18 Triaxial creep test result for 10 mm DBM (100 Pen) at 40°C (stress ratio of 0.6) 144
5.19 Steady-state deformation behaviour of 10 mm DBM mixture (100 Pen) at 40°C (stress ratio of 0.6) 145
5.20 Variation of volumetric strain with distortional strain for triaxial creep tests on 10 mm DBM mixture at 40°C (stress ratio of 0.6) 146
5.21 Specimen preparation (unbound granular material) 146
5.22 Creep test result for 10 mm DBM mixture without bitumen at stress ratio of 0.6 147
5.23 Constant strain rate test results for DBM mixture and aggregate 147
5.24 Direct shear box test 148
5.25 Variation of dilation gradient with volume fraction of aggregate 149
6.1 The Nottingham Asphalt Tester (NAT) configured in Repeated Load Axial (RLA) test mode 162
6.2 Repeated load axial tests at 40°C (mixture A/D) 163
6.3 Repeated load axial tests at 30°C (mixture A/D) 163
6.4 Repeated load axial tests at 20°C (mixture A/D) 164
6.5 Repeated load axial tests at 30°C (mixture A) 164
6.6 Repeated load axial tests at 20°C (mixture A) 165
6.7 Steady-state deformation rates for mixture A 165
6.8 Steady-state deformation rates for mixture A/D 166
6.9 Repeated load axial tests at 40°C (30/10 HRA mixture) 166
6.10 Repeated load axial tests at 40°C (10 mm DBM mixture) 167
6.11 Steady-state deformation rates for 30/10 HRA mixture at 40°C 167
6.12 Steady-state deformation rates for 10 mm DBM mixture at 40°C 168
6.13 Comparison of steady-state deformation rate with $G^*/\sin\delta$ 168

6.14 Effect of void content on steady-state deformation rate (mix A & mix A/D) . 169
6.15 Effect of void content on steady-state deformation rate (10 mm DBM & 30/10 HRA) 169
7.1 Schematic of Wheel tracking apparatus at Nottingham 186
7.2 Schematic of image analysis arrangement for capturing rut profile 186
7.3 Comparison of rut profile captured by image analysis and LVDT 187
7.4 Mechanical Profilometer fitted on the slab 187
7.5 Validation of rut profile captured by mechanical profilometer with vernier calliper 188
7.6 Transverse rut profile captured with mechanical profilometer (mixture A/D) 188
7.7 Schematic showing Laboratory Roller Compactor 189
7.8 Position of core samples from mixture A/D 189
7.9 Area ratio for mixture A at 30°C 190
7.10 Area ratio for mixture A/D at 30°C 190
7.11 Area ratio for 30/10 HRA at 45°C 191
7.12 Area ratio for 10 mm DBM at 45°C 191
7.13 Wheel tracking tests at 40°C (Mixture A/D) 192
7.14 Wheel tracking tests at 30°C (Mixture A/D) 192
7.15 Wheel tracking tests at 20°C (Mixture A/D) 193
7.16 Wheel tracking tests at 40°C (Mixture A) 193
7.17 Wheel tracking tests at 30°C (Mixture A) 194
7.18 Wheel tracking tests at 20°C (Mixture A) 194
7.19 Steady-state rutting rates for mixture A 195
7.20 Steady-state rutting rates for mixture A/D 195
7.21 Wheel tracking tests at 45°C (30/10 HRA mixture) 196
7.22 Wheel tracking tests at 45°C (10 mm DBM mixture) 196
7.23 Steady-state rutting rates for 30/10 HRA mixture 197
7.24 Steady-state rutting rates for 10 mm DBM mixture 197
7.25 Comparison of steady-state rutting rates from the Wheel tracking and RLA tests 198
7.26 Comparison of steady-state rutting rate with $G^*/\sin\delta$ (wheel tracking tests) . 198
7.27 Effect of void content on the steady-state rutting rate (mixture A/D) 199
7.28 Effect of void content on the steady-state rutting rate (HRA and DBM

mixture) 199
8.1 Viscosity asymptotes at various stress ratios (mixture A at 20°C) 216
8.2 Contours of Von Mises equivalent stress (values in MPa) 216
8.3 Contours of constant mean stress (values in MPa) 217
8.4 Contours of constant stress ratio 217
8.5 Constant of constant viscosity mixture A at 20°C (values in GPa.s) 218
8.6 Variation of viscosity with depth 'z' and 'x' distance (HRA at 45°C) 218
8.7 Variation of stress ratios with depth 'z' and radial distance 'x' 219
8.8 Transverse rut profile for higher viscosity value
(mixture A at 20°C & 1000 kPa) 219
8.9 Viscosity-depth profiles (mixture A/D at 20°C) 220
8.10 Slab section divided into sub-layers (mixture A/D at 20°C) 221
8.11 Predicted and measured rutting rates for mixture A at 20°C 222
8.12 Predicted and measured rutting rates for mixture A at 30°C 222
8.13 Predicted and measured rutting rates for mixture A at 40°C 223
8.14 Predicted and measured rutting rates for mixture AD at 20°C 223
8.15 Predicted and measured rutting rates for mixture AD at 30°C 224
8.16 Predicted and measured rutting rates for mixture AD at 40°C 224
8.17 Predicted and measured rutting rates for 30/10 HRA at 45°C 225
8.18 Predicted and measured rutting rates for 10mm DBM at 45°C 225

List of Tables

Page

3.1 Shift Factors 62

3.2 DSR Model Parameters 71

4.1 Air Void Content Analysis (mix A and mix A/D) 91

4.2 Air Void Content Analysis (HRA and DBM) 98

5.1 Dilation Gradients for Idealised and Realistic Mixtures 125

6.1 Air Void Content Analysis (RLA test specimens) 153

6.2 Summary of Repeated Load Axial Test Results (Idealised Mixtures) 156

6.3 Summary of Repeated Load Axial Test Results (Realistic Mixtures) 158

6.4 Percentage Variation of Steady-State Rutting Rate Measured from Replicate Repeated Load Axial Tests 160

7.1 Air Void Content Analysis (outside loaded area) 177

7.2 Summary of Wheel Tracking Test Results (Idealised Mixtures) 179

7.3 Summary of Wheel Tracking Test Results (Realistic Mixtures) 181

7.4 Percentage Variation of Steady-State Rutting Rate Measured from Replicate Wheel Tracking Tests 184

8.1 Viscosity Constants for Equations 8.4 & 8.5 205

8.2 Measured and Predicted Steady-State Rutting Rate Data Analysis (Idealised Mixtures) 211

8.3 Measured and Predicted Steady-State Rutting Rate Data Analysis (Realistic Mixtures) 213

Notation

CBR	California Bearing Ratio
DBM	Dense Bitumen Macadam
HRA	Hot Rolled Asphalt
LCPC	Laboratoire Centrale des Ponts et Chaussees
LVDT	Linear Variable Differential Transformer
MCM	Modified Cross Model
NAT	Nottingham Asphalt Tester
PTF	Pavement Test Facility
SHRP	Strategic Highway Research Program
TRL	Transport Research Laboratory
VMA	Voids in Mixed Aggregate (volume of bitumen + volume of air voids)
WLF	Williams-Landel-Ferry

$\dot{\varepsilon}$	Uniaxial strain rate (s^{-1}) (tensile or compressive)
σ	Uniaxial stress (tensile or compressive)
σ_o	Reference stress
$\dot{\varepsilon}_o$	Reference strain rate
τ	Shear stress
τ_d	Average DSR shear stress
$\dot{\gamma}$	Shear strain rate
$\dot{\gamma}_d$	Average DSR shear strain
S	Stiffening factor
η_s	Pre-exponential for viscosity (Pa.s)
T_s	Reference temperature (°C)
R	Universal gas constant (J mol^{-1} K^{-1})
ρ	Density (kg/m^3)
λ_{eq}	Equivalent viscosity (Pa.s)
ν	Poisson's ratio
Σ	Deviator stress
Σ_m	Mean stress
s	Dilation gradient
n_c & n	Creep exponent
σ_e	Bitumen Von Mises equivalent stress
δ_{ij}	Kronecker delta

$$\delta_{ij} = \begin{cases} 0 & if \quad i \neq j \\ 1 & if \quad i = j \end{cases}$$

σ'_{ij} Deviatoric stress tensor

$$\sigma'_{ij} = \sigma_{ij} - \frac{1}{3}\delta_{ij}\sigma_{kk}$$

$$= \begin{bmatrix} \sigma_{11} - \frac{1}{3}(\sigma_{11}+\sigma_{22}+\sigma_{33}) & \sigma_{12} & \sigma_{13} \\ \sigma_{21} & \sigma_{22} - \frac{1}{3}(\sigma_{11}+\sigma_{22}+\sigma_{33}) & \sigma_{23} \\ \sigma_{31} & \sigma_{32} & \sigma_{33} - \frac{1}{3}(\sigma_{11}+\sigma_{22}+\sigma_{33}) \end{bmatrix}$$

$$\sigma_e = \left\{\frac{3}{2}\sigma'_{ij}.\sigma'_{ij}\right\}^{\frac{1}{2}}$$

$$= \left\{\frac{3}{2}\left[(\sigma'_{11})^2 + (\sigma'_{12})^2 + (\sigma'_{13})^2 + (\sigma'_{21})^2 + (\sigma'_{22})^2 + (\sigma'_{23})^2 + (\sigma'_{31})^2 + (\sigma'_{32})^2 + (\sigma'_{33})^2\right]\right\}^{\frac{1}{2}}$$

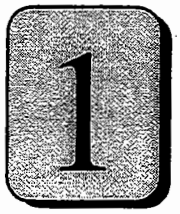

Introduction

1.1 Problem Definition

There are two principal forms of load associated failure in flexible pavements; cracking and rutting. The cracking, or fatigue, phenomenon is due to repeated tensile strains (and stresses) induced in the bituminous material and is traditionally thought to be initiated at the base of the bituminous materials [20], (see Figure 1.1), although recent observations suggest that this can also initiate at the surface, particularly in thick pavements [104]. Further detailed information about the fatigue behaviour of bituminous mixtures can be found in [116, 117] and will not be repeated here as it is outside the bounds of this thesis.

Rutting is the formation of longitudinal depressions (ruts) in the vehicle wheel paths and is of concern for two main reasons. Firstly, rutting interferes with the normal run-off of water from pavements and increases the hazards of wet weather driving. The ruts trap water, which creates a potential for hydro-planing (particularly for light passenger cars). Secondly, safety is a concern if the ruts progress in depth, as this may lead to steering difficulties for vehicles. Both of these can put the safety of road users at risk [129].

Rutting may be caused by permanent deformation in all the layers of the pavement or by permanent deformation in only the bituminous materials. The former mechanism is

usually termed structural rutting and is typically associated with excessive permanent deformation in the subgrade and represents failure of the pavement. The latter is known as non-structural rutting since it is confined to the upper bituminous layers of the pavement. Rutting due to deformations within the bituminous material can generally be distinguished from structural rutting by the cross-section of the rut at the surface, which is characterised by the formation of "shoulders" at the edge of the ruts (see Figure 1.2), due to the lateral flow of the material [66].

In most thick flexible pavements constructed in the UK rutting is associated mainly with permanent deformation in the bituminous layers. The permanent deformation resistance of the granular and unbound layers often does not constitute a major problem. Bituminous materials are used in the majority of road construction and maintenance works in this country, and if permanent deformation is a major problem in these materials so it has a major effect on pavement serviceability and maintenance. Therefore, the bituminous mixtures being strong and durable is not only important to the engineer but also to the road user who must ultimately pay for the construction and maintenance of roads.

The permanent deformation behaviour of bituminous mixtures can be affected by several significant factors such as: type of aggregate, gradation of aggregate, binder type and content, degree of compaction (air void content), method of compaction, temperature and magnitude and frequency of loading. The structural strength of a bituminous mixture relies essentially on two factors; mechanical interlock between aggregate particles, and the mechanical properties of the binding agent (bitumen). A dense aggregate grading with a relatively low voids in mineral aggregate (VMA) is generally equated with good deformation resistance provided that the mixture is not over filled with binder and it is satisfactorily compacted. In mechanical tests, deformation resistance has been shown to increase as binder content decreases, but there is clearly some limit to this. The quantity of binder introduced to the gradation is critical, as too much, or too little will adversely affect the mixture properties, but it must be realised that similar consequences may result from variations in the aggregate grading. The majority of work associated with the design of bituminous mixtures has addressed the problem of identifying an optimum binder content. However, recently

effort has been concentrated on understanding the influence of the mechanical properties of the binder on the mixture.

The properties of bituminous mixtures are dependent upon the properties of the binder. Therefore, it is necessary to understand the mechanical properties of bitumen. The bitumens which are used in highway engineering in the UK are classified by hardness, or penetration grade, which is obtained through an empirical test. All bitumens display thermoplastic properties, which means they become softer when heated and harder when cooled. As permanent deformation is primarily associated with the viscous response of the material, it is at high temperatures combined with long loading times which create ideal conditions for this mode of distress. Concerning mixture design and resistance to permanent deformation, it is necessary to concentrate on the binder performance together with the aggregate gradation. The most comprehensive specification of binder properties is in the Strategic Highway Research Programme (SHRP) Superpave system. One of the major products of the SHRP research was a suite of tests which are used for the classification of binders by their performance characteristics.

Research into the behaviour of bituminous materials in pavements has attracted a great deal of worldwide attention for the past 30 years. A lot of progress has been made during this time in the understanding and mathematical modelling of the permanent deformation behaviour of bituminous mixtures. The prediction of rut depth, however, is complicated especially so when one compares it with the simple task of measuring the rut depth using a straight edge and a steel rule. The problem is not only limited to material characterisation, but also to the accurate assessment of environmental conditions and calculations of the appropriate stress distribution within the pavement structure. Due to increasing traffic (both in terms of volume and axle loads) and associated road maintenance costs, it is increasingly important to have accurate models for predicting the permanent deformation behaviour of these types of materials.

1.2 The Research Project

The work described in this thesis is part of a joint research project undertaken with the University of Cambridge, which started in October 1994. The objectives of the research at Nottingham were to experimentally investigate the permanent deformation behaviour of idealised and realistic bituminous mixtures and develop a simplified approach for rut depth prediction in these materials.

The overall research philosophy has been to start from a fundamental understanding of the deformation mechanisms in pure bitumen and extend this to develop a fundamental understanding of the deformation behaviour of simplified idealised bituminous mixtures and more realistic bituminous mixtures. A large experimental program has been undertaken to characterise the permanent deformation behaviour of the idealised and realistic mixtures at a fundamental level. Results from this programme have been used, together with a simplified modelling procedure, to predict results from laboratory scale rolling wheel tests which simulate real traffic loading conditions.

This thesis is organised into 9 chapters. Chapter 2 reviews the literature concerning the deformation behaviour of bituminous materials and predictive methodologies. It also provides a brief description of the test methods used to characterise the permanent deformation behaviour of the bituminous mixtures. Chapter 3 describes testing carried out in the Dynamic Shear Rheometer (DSR) to determine the dynamic mechanical properties of the binders used in this project. It also contains details of creep tests performed using the DSR to characterise the deformation behaviour of pure bitumen in the linear and non-linear regions. Chapter 4 describes the uniaxial experiments carried out on the idealised and realistic mixtures over a wide range of stress levels, strain rates and temperatures. The deformation behaviour of the idealised and the realistic mixtures is investigated under more complicated stress conditions in Chapter 5, which describes the results from triaxial experiments. Chapter 6 contains details of repeated load axial testing carried out using the Nottingham Asphalt Tester (NAT) on the idealised and realistic mixtures. Rheological measurements using the DSR performed on the bitumen (Chapter 3) and the results, in terms of the Strategic

Highway Research Program (SHRP) rutting parameter ($G^*/\sin\delta$), have been correlated to results from the RLA test. Chapter 7 discusses experimental developments and investigates the relationship between the rutting performance of idealised and realistic mixtures measured using a wheel tracking test. Results from DSR tests on the bitumen in terms of the SHRP rutting parameter ($G^*/\sin\delta$), are compared with results from the wheel tracking test. Chapter 8 describes the development of a model which is developed using the theory of linear viscoelasticity to predict the steady-state rutting rates obtained from the wheel tracking tests on the idealised and realistic mixtures. Conclusions and recommendations for further research are presented in Chapter 9.

1.3 Figures

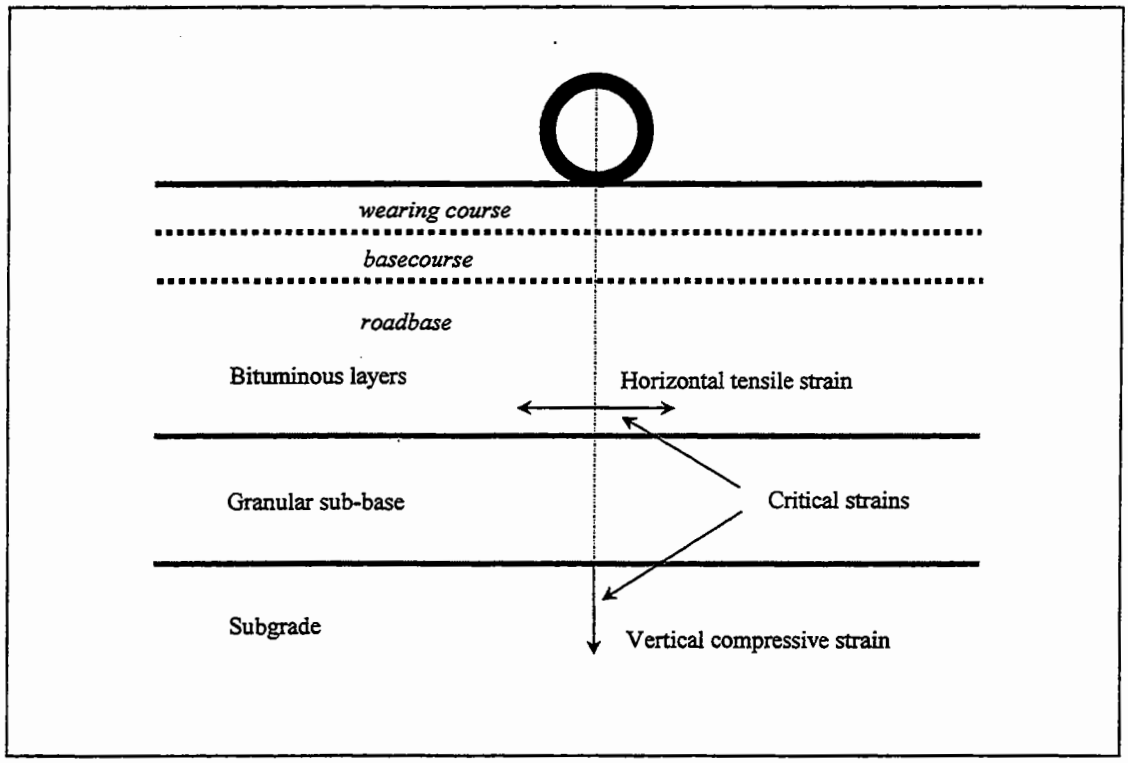

Figure 1.1 Typical flexible pavement structure.

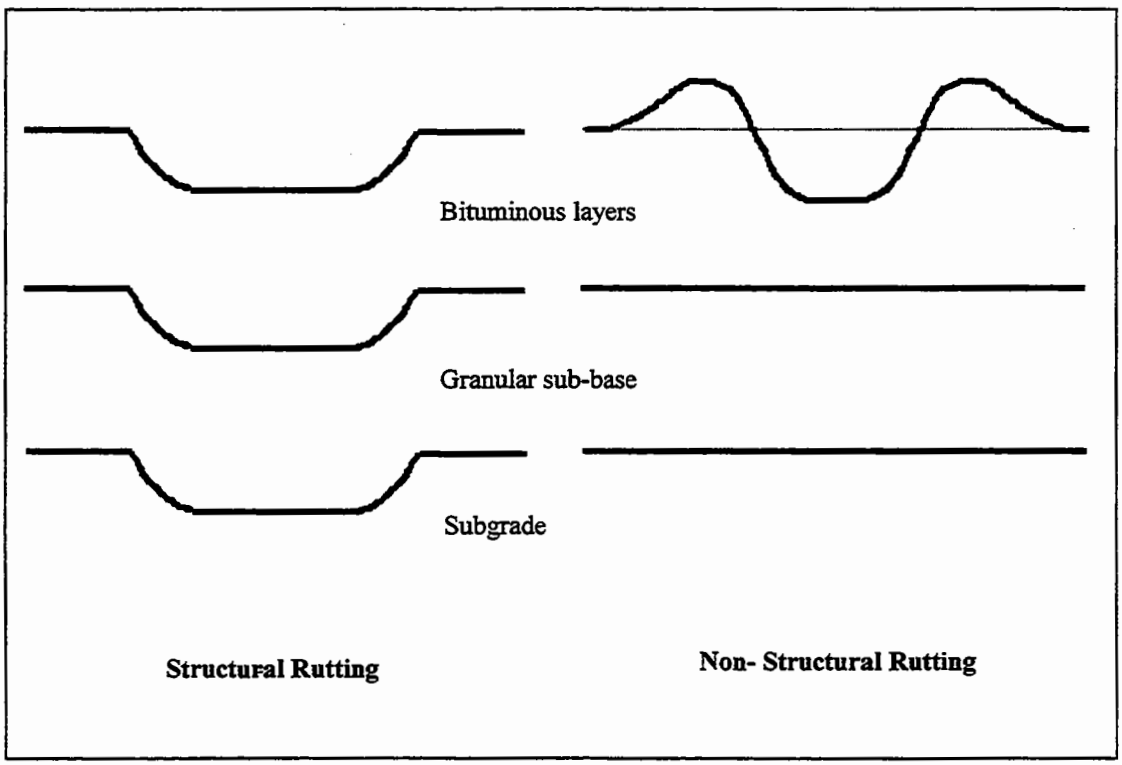

Figure 1.2 Structural and non-structural rutting.

Literature Review

2.1 Introduction

Rutting in asphalt pavements is a major mode of distress in many parts of the world. Although rutting is well recognized, the methodologies for its prediction and elimination are far from perfect and substantial research has been directed towards modelling the phenomenon of rutting. This chapter begins by reviewing literature relating to the mechanism of permanent deformation in bituminous mixtures. The permanent deformation behaviour of pure bitumen and idealised bituminous mixtures is also briefly reviewed. Major research efforts directed towards predictive methodologies for rutting in realistic mixtures have also been reviewed with an emphasis on techniques for prediction of permanent deformation (rutting) in the upper bitumen bound layers of pavement structures. Finally, laboratory test methods associated with the predictive methodologies which include 1) uniaxial and triaxial creep tests (confined or unconfined); 2) uniaxial and triaxial repeated load tests (confined or unconfined); 3) simple shear tests; 4) Hollow cylinder testing, and 5) wheel tracking tests have been highlighted. An evaluation of these test methodologies, either existing or new, that have the potential to characterise the propensity of rutting in bituminous mixtures has also been presented.

2.2 Permanent Deformation Criteria

Pavements do not fail suddenly but gradually deteriorate in serviceability to a terminal level which may be defined as failure. In the U.K., failure is taken to be a 20 mm rut in the nearside wheel track or extensive cracking. The point at which deterioration starts to accelerate rapidly is known as the "Critical Life" of the pavement. This is defined in the U.K as a 10 mm rut [20] or the onset of wheelpath cracking. Maintenance is recommended at (or before) the Critical Life of the pavement, so that structural integrity is largely retained.

Rutting causes ponding of water, which is an obvious hazard causing automobiles travelling at high speeds to hydroplane. In the United States the Federal Administration has classified rut depth into four levels of severity: 1) hydroplaning (0.2 to 0.25 in); 2) low (0.25 to 0.5 in); 3) medium (0.5 to 1 in); 4) high (1 in) [129].

2.3 Mechanism of Permanent Deformation in Bituminous Materials

Pure Bitumen has been shown to exhibit very complex stress-strain behaviour [40, 41, 42, 43]. It behaves as an elastic solid at low temperatures and high frequencies of loading, and as a viscous fluid at high temperatures and low loading frequencies. In the intermediate range, it exhibits visco-elastic behaviour. As the response of the bituminous mixture is also in part viscous under the application of the load, this element of the total strain is irrecoverable and with the repeated load application accumulates, leading to the formation of surface ruts. Figures 2.1 and 2.2 show an idealised strain response to an applied stress pulse and the accumulation of permanent strain under repeated loading [66]. Recently the research has also been focused on the constitutive models that reflect the complex non-linear behaviour of bituminous materials (see for example [124, 130, 131, 140]).

There are two main mechanisms responsible for permanent deformation in bituminous materials:

1. Densification or compaction (decrease in volume, hence increase in density), and

2. Shear displacement (lateral movement of the material at a constant volume).

Densification is where the aggregate skeleton becomes more closely packed and can be a problem in pavements which are poorly compacted during construction. Densification tends to occur relatively early in the life of a pavement. Shear displacements tend to be associated with a flow of material in a constant volume process and occur throughout the life of the pavement. Properties associated with mixture volumetrics like the percentage voids in mineral aggregate (VMA) have also been shown to influence the performance of the mixture. An increased binder content affects the mixture's ability to resist permanent deformation. Mixtures with high binder contents have lower air voids when compacted which indicate that the void space is becoming filled with the bitumen. As a result the binder film between the aggregate particles becomes thicker due to increase in binder content otherwise separated by a very tight network of air voids. This phenomenon causes mixtures with high binder content to be more susceptible to permanent deformation. To reduce a mixture's susceptibility to permanent deformation a minimum of 3% air voids is recommended. Cooper et al [52] found that good resistance to permanent deformation requires a low percentage of voids in the mineral aggregate (VMA). However, they cautioned that the lowest theoretical VMA could be undesirable as it may not allow sufficient voids in the aggregate for enough binder to ensure satisfactory compaction without the mixture becoming overfilled.

Hofstra and Klomp [77] indicated that shear displacement was the primary factor responsible for rutting. They emphasized that material should be well compacted to higher densities in order to minimize shear deformation. A range of temperatures from 20-60°C were investigated, during which the asphalt *stiffness*[1] decreased by a factor of approximately 60 and the permanent deformation increased by a factor between 250 and 300. A series of tests was carried out to investigate the effect of different mixture variables, namely binder type, binder content and aggregate type on permanent deformation. It was found that mixtures containing higher stiffness binders were less susceptible to permanent deformation than mixtures containing lower

[1] The stiffness of a viscoelastic material is analogous to Young's modulus for a linear elastic material. It is defined as the ratio between the stress and the strain which in case of a viscoelastic material, depends on the loading time and the temperature.

stiffness binders. The same effect was found for mixtures with low binder contents and/or high coarse aggregate contents. Hofstra and Klomp [77] found that the rut depth per wheel pass decreased with an increasing number of wheel passes, as the mixture builds up a resistance to flow due to the binder being expelled from between the aggregate particles producing greater aggregate interlock. They also observed that the permanent deformation through the asphaltic layers was greatest near to the surface and gradually decreased with depth due to decreasing stresses.

Trenching studies performed after the AASHO Road Test [72], further indicated that the surface rut depth reached a limiting value for asphalt layer thicknesses of approximately 10 in (25cm) and it was concluded that thicker layers were less susceptible to additional rutting. Uge and Van de Loo [139] also reported that under the action of a moving load (pneumatic tires), permanent deformation no longer increased with increasing layer thickness beyond a certain threshold which was found to be 13cm (in their case).

Eisenmann and Hilmer [59] confirmed that, if the pavement is well compacted during construction, permanent deformation is due mainly to shear flow. Wheel tracking tests were conducted on a pavement section which consisted of a 50 mm wearing course and a 180mm base course supported on a rubber foundation of a specified stiffness. They found that, in the initial stage of trafficking, the increase in irreversible deformation below the tyres was distinctly greater than the increase in the upheaval zones at the tyre edges. Therefore, in the initial phase, post compaction due to traffic has an important influence on rutting. After the initial stage, the volume decrement beneath the tyres was found to be approximately equal to the volume increment in the adjacent upheaval zones as shown in Figure 2.3. This is an indication that further rutting is caused essentially by shear flow of the material at a constant volume. They suggested that rutting could be controlled in two ways:

1. optimizing mixture composition, and
2. optimizing the design of heavy-duty trucks.

Their investigations also revealed that an increase in wheel load at a constant inflation pressure mainly causes an increase of deformation in the lower regions of the asphalt pavement, whereas a change of inflation pressure has a particular influence on the

deformation in the upper regions of the asphalt layers near to the pavement surface. In order to quantify the influence of wheel load and tyre inflation pressure a regression analysis was conducted using results from laboratory tests resulting in the following equation:

$$y = a + b(N)^{0.5} \tag{2.1}$$

where y = rut depth
N = number of load repetitions, and
a & b = laboratory determined parameters

Because of the substantial evidence that operating tyre pressures of heavy trucks have been increasing, higher tyre pressures have been perceived as contributing to pavement rutting and cracking [62, 83, 87, 122, 125]. This perception has focused considerable research on various aspects of operating tyre pressures which include, influence of tyre type on pressures, relationship between tyre inflation pressures, tyre-pavement contact pressures, and distribution of contact pressures within the contact area. More recent research on pavement response to dynamic tyre forces can be found in [45, 67]. Because pavement rutting can be controlled both by reducing tyre-pavement contact pressures and by increasing resistance to the contact pressures through improved mixture design, research and other developments have occurred in the mixture design area to limit rutting in the asphaltic layers [61, 127].

2.4 Permanent Deformation Behaviour of Pure Bitumen

There has been considerable progress in the understanding of the mechanical behaviour of pure bitumen in recent years and a wide range of new tools and modelling techniques have become available. During the 1960's, Van der Poel [142] succeeded in correlating the stiffness of the bitumen with two empirical parameters, namely the *penetration*[2] at 25°C and the *ring & ball softening point*[3] as determined by

[2] The penetration is the distance travelled into a bitumen sample by a standard needle under a standard load (100g) for a period of time (5sec) measured in decimeters [34].
[3] The ring & ball softening point in the British Standard method is the temperature at which the bitumen sample is contained in a brass ring under the loading of a steel ball will touch a base plate 25mm below the ring when the bath temperature is raised below at 5°C per minute [33].

routine tests. It should be noted that the Van der Poel's ring & ball softening point was based on American Society of Testing Materials (ASTM) method[4]. Van der Poel summarized the mechanical behaviour of the bitumen as a function of temperature and loading time in the well known Van der Poel Nomograph [142].

In the later years, Volume Dilatometry, Differential Thermal Analysis (DTA) and subsequently Differential Scanning Calorimetry (DSC) were employed, to characterise the thermal behaviour of bitumen subject to a controlled heating or cooling programme [40]. More comprehensive reviews regarding the structure of bitumen can be found in [147].

Cheung [40] developed mathematical models for the mechanical behaviour of a 50 Pen grade of bitumen with a softening point of 53.5°C (BS method) over a wide range of stress conditions, strain-rates, temperatures and pressures. Various physical models were proposed using the results of uniaxial tension and compression tests, shear tests and published data from the literature. The mechanical behavior was illustrated in the form of a deformation mechanism map (see Figure 2.4). Six regimes were identified, all of which were described by physical models, based on the best understanding of the molecular structure of pure bitumens. It was hypothesised that the behaviour of many varieties of bitumens encountered in practice would exhibit the same deformation mechanisms but at different temperatures, stresses and strain rates.

Based on his experimental results, Cheung [40] found that, at temperatures above the *glass transition*[5], the deformation behaviour of the 50 pen grade of bitumen tested was linear viscous at low stress levels and power law creep at high stress levels with a creep exponent of approximately 2.3. The transition stress at which there was a change from linear to power law behaviour was found to be a measure of the failure strength of the structural linkages in a bitumen, beyond which extensive pseudoplastic flow would be observed. The value of this transition stress determined the extent with which the viscosity decreased as a function of strain-rate. The value for the transition stress was found to be approximately 115kPa.

---

[4] The American Society for Testing Materials (ASTM) also specifies a similar softening point test to British Standard method but with the use of stirrer in the liquid bath. Consequently, the ASTM test gives values for softening point about 1.5°C higher than the British Standard method.

[5] The glass transition temperature, T_g, is defined as the temperature range at which bitumens change from a glassy to a fluid condition. The usual range of T_g for bitumens is between –40°C and 0°C [40].

The steady-state uniaxial behaviour of the bitumen was described by the Modified Cross Model (MCM) [40]:

$$\frac{\sigma}{\sigma_o} = \frac{\dot{\varepsilon}}{\dot{\varepsilon}_o}\left(\frac{1}{1+\left(\frac{\dot{\varepsilon}}{\dot{\varepsilon}_o}\right)^{n_c}}\right) \tag{2.2}$$

where σ & $\dot{\varepsilon}$ = uniaxial stress and strain rate respectively

σ_o & $\dot{\varepsilon}_o$ = material constant for 50 pen grade bitumen

n_c = creep exponent (material constant)

Cheung [40] also found that the temperature dependence of bitumen was activation energy controlled (Arrhenius equation) at low temperatures (T ≤ 20°C for his bitumen) and is given by:

$$\eta_{oT} = \frac{\sigma_o}{\dot{\varepsilon}_o} = \eta_{oc}^{\left(\frac{Q_c}{RT}\right)} \tag{2.3}$$

where η_{oc} = pre-exponential for viscosity with value 5.66×10^{-34} Pa.s

Q_c = thermal activation energy with value 2.28×10^{3} J mol^{-1}, and

R = Universal gas constant with value 8.314 J mol^{-1} K^{-1}

At higher temperatures (T ≥ 20°C) Cheung [40] found that the temperature dependence was free volume controlled (WLF equation) which is given by:

$$\eta_{oT} = \eta_s \exp\left(-\frac{2.303c_1^s(T-T_s)}{c_2^s+(T-T_s)}\right) \tag{2.4}$$

where η_{oT} = limiting viscosity when $\dot{\varepsilon} \to 0$,

η_s = pre-exponential for viscosity with the value 214×10^3 Pa.s

c_1^s & c_2^s = universal constants with the values 8.86 & 101.6

T_s = reference temperature with the value 35.2°C

The reference temperature of 35.2°C was chosen because Cheung [40] noted that for his bitumen it fitted the data more accurately than any other value of reference temperature. From an extensive set of tensile, shear and compression tests, Cheung [40] showed that the 3-Dimensional steady-state constitutive behaviour of bitumen was given by:

$$\frac{\dot{\varepsilon}_{ij}}{\dot{\varepsilon}_o} = \frac{3}{2}\left(\frac{\sigma_e}{\sigma_o}\right)^n \frac{\sigma'_{ij}}{\sigma_o} \tag{2.5}$$

where $\dot{\varepsilon}_{ij}$ = strain rate tensor

$\dot{\varepsilon}_o$ = reference strain rate

σ_o = reference stress

σ_e = Von Mises equivalent stress

σ'_{ij} = deviator stress tensor

n = creep exponent (n=1 for low stress levels and n=2.3 for high stress levels)

It was concluded that, for modelling purposes, the multi-axial behaviour of bitumens at temperatures above the glass transition could be deduced from the tensile behavior in terms of a Von Mises effective stress and strain-rate [40].

The concept of zero shear viscosity of the binder for assessing the potential of bituminous mixtures to permanent deformation has been recently introduced [112]. The zero shear viscosity is the viscosity that would be obtained from a dynamic test at a frequency of zero. The dependence of viscosity on shear rate and stress arises when flow generates a significant deviation of molecular colloidal system from equilibrium 'no-flow' condition (see [112]). The relevance of this for rutting emerges from the observation that pavement loading is generally considered to take place in the linear

region in most of the pavement design methods. This is good reason for considering the zero shear viscosity as an appropriate viscosity for correlating with rutting. However, the research described herein gives an insight into the viscous behaviour which covers both the linear and the non-linear regions of material behaviour. One of the important consequences of using the current approach is that the binder contribution to rutting from purely viscous process, and the corresponding particle contribution (which in turn increases the viscosity of the mixture) is also accounted for in the linear and non-linear regimes of the mixture behaviour (see section 2.5).

2.5 Permanent Deformation Behaviour of Idealised Bituminous Mixtures

Using a similar approach, Deshpande [53, 54] investigated the mechanisms controlling the deformation of idealised bituminous mixtures operating under different states of stress, strain-rate and temperature. The same grade of bitumen tested by Cheung [40] was used in the idealised mixtures and uniaxial and triaxial compression tests were performed.

Various types of idealised mixtures, with different volume fraction of rigid inclusions in the range of 40% to 85% were tested:

1. Glass spheres 1.7mm diameter, 4% volume air voids.
2. Glass spheres 1.7mm diameter, 20% volume air voids.
3. Sand particles between 300μm and 600μm, 4% volume air voids.
4. Sand particles between 1.18mm and 2.36mm, 150μm and 300μm, and rounded stones, 4% volume air voids.

The specimens were manufactured in cylindrical moulds and were compacted in three layers using a single plunger compression method under a static compressive stress of 10 MPa. Studies in which the structure of the aggregate has been examined in detail have shown that the orientation of aggregate particles can vary with the method of compaction. The aggregate structure has a strong influence on resistance to permanent deformation and it has been found that the use of different laboratory compaction techniques has produced differences in the results [66]. Various compaction methods

were tried which included compression methods along with the kneading compaction[6]. However the techniques were only limited to static compression methods for most of the idealised specimens. These compaction techniques gave a uniform density profile along the height of the specimen. Consequently, no other method such as vibratory hammer or a gyratory compactor was used. Also static compaction is likely to be unimportant for idealised mixtures because of the more uniform nature of the particles. Two types of uniaxial tests were conducted on these idealised mixtures. In the constant strain-rate tests, a constant velocity was applied to the specimen, whereas in the constant stress creep tests, a constant force was applied to the specimen. Constant strain-rate tests were performed at 20°C and 40°C and the resulting nominal stress was plotted against the nominal strain (Figure 2.5). It was observed that, at a particular strain-rate, the stress increased until the strain reached approximately 4%, beyond which the stress started to decrease (see Figure 2.5). Creep tests were also performed at 20°C and 40°C.

This maximum observed stress corresponding to a particular combination of strain-rate and temperature was defined as the steady-state creep stress [40]. At a constant temperature, the value of the steady-state creep stress was found to increase with increasing applied strain-rate. The steady-state behaviour was obtained from two sets of tests on 64% mixture (Sand particles between 300μm and 600μm) and was plotted against steady-state stress for temperatures ranging from 0°C to 40°C. The curve obtained by Cheung [40] for pure bitumen at 20°C was also reproduced. Interestingly, in his investigations, Deshpande found that the idealised mixture curve exhibited the same behaviour as the pure bitumen curve at the same temperature, over five decades of strain-rate and three decades of stress levels. The main difference that he observed between the curves was a decrease in the steady-state strain-rate in the mixture compared to pure bitumen at the same stress, *i.e.* the mixture was stiffer than the pure bitumen, see Figure 2.6.

Consequently, the model proposed by Cheung [40] (Equation 2.2), was modified by replacing $\dot{\varepsilon}/\dot{\varepsilon}_0$ with $S\dot{\varepsilon}/\dot{\varepsilon}_0$ to describe the creep behavior of the idealised mixtures over the temperature and stress ranges tested, resulting in:

[6] This process involves mechanical compaction that imparts a kneading action to the mixture by a series of individual impressions made with a ram.

$$\frac{\sigma}{\sigma_o} = \frac{S\dot{\varepsilon}}{\dot{\varepsilon}_o}\left(\frac{1}{1+\left(\frac{S\dot{\varepsilon}}{\dot{\varepsilon}_o}\right)^{n_c}}\right) \tag{2.6}$$

where $n_c, \sigma_o, \dot{\varepsilon}_o$ = material constants for the 50 pen grade of bitumen

S = the stiffening factor due to the presence of aggregates

The value of S was found to be 1000 for the 64% mixture (*i.e.* for the same stress level the 64% mixture has steady-state strain about 1000 times lower than pure bitumen, see Figure 2.6). The constants n_c and σ_o determine the form of Equation 2.6, whilst $\dot{\varepsilon}_o$ is the reference strain-rate. Deshpande found that all the idealised mixtures tested followed a similar behaviour with only difference being in the stiffening factor.

The following conclusions can be drawn from Cheung [40] and Deshpande's [53] work on uniaxial and triaxial compression tests of idealised mixtures:

1. The steady-state behaviour of idealised bituminous mixtures follows a similar pattern to the steady-state behaviour of pure bitumen. The form of the constitutive law governing the mixture and its temperature dependence are the same as that for the pure bitumen.

2. The stiffening effect is approximately the same in the linear and non-linear regimes of mixture behaviour.

3. The steady-state behaviour of the mixtures is a function of the mean stress and the deviator stress. The stiffening factor is a function of the volume fraction of aggregate and the stress ratio.

4. The steady-state behaviour of the idealised mixtures is independent of the size of the inclusions up to 2 mm.

5. The behaviour of the idealised mixtures is not strongly dependent on the shape of the particles. However, this conclusion may not be extendible to inclusions with high angularity and a wider distribution of particle sizes, where frictional effects in the form of interlocking of the particles may become dominant.

6. The steady-state deformation behaviour of the mixture is affected by the volume fractions of voids. Though the form of the behaviour remains unchanged the stiffness of a mixture with a large volume fraction of voids is less than that of more dense mixtures.

2.6 Permanent Deformation Behaviour of Realistic Mixtures

2.6.1 Early rutting models

Early approaches to limiting rutting in flexible pavement structures were based around limiting the vertical compressive elastic strain in the subgrade. Dormon and Metcalf [57, 58] developed rut limiting criteria in the form of relationships between the vertical compressive strain at the top of subgrade and the number of load repetitions. The method gained popularity amongst researchers as an alternative to purely empirical design methods. The use of this parameter as a criterion in thickness design serves principally to guard against structural rutting, although rutting in the bituminous material is implicitly included. Analytical methods for the design of flexible pavements, such as the Nottingham method [20] are based upon predicting failure through fatigue cracking or rutting by limiting the magnitudes of critical strains at the bottom of the asphalt layer and on the top of the subgrade. Other analytical methods based upon the critical strains at the bottom of the bound layer are:

- The Shell Pavement Design Manual [6],
- NAASRA Pavement Design [7],
- AASHTO Guide for Design of Pavement Structures [8],
- MS-1 – Thickness Design [9],
- Road Note 29 [55] and
- Road Note 31 [138].

The subgrade strain criterion, used by many researchers can be viewed in the literature (see for example [21, 119]). Some researchers modelled the criterion as a function of the number of load repetitions, whilst others included subgrade properties such as the CBR or stiffness or road class as independent variables [65, 90]. During recent years, the focus has been to develop subgrade strain models with an additional element to explicitly predict permanent deformation in the asphaltic layers (see, for example [92, 113, 141]). Claessen at al [44] proposed an improvement to the Shell method which included an additional analysis to estimate the amount of rutting occurring in the bound asphalt layers of the pavement. The method suggested that the final design thickness satisfying the subgrade strain criterion should be checked for permanent deformation in the bituminous layers.

2.6.2 'Layer-strain' based prediction models

Most of the rutting models developed in the 1970's were based on the "layer-strain" approach. Barksdale [14] and Romain [120] first proposed the general principle of this method. To predict the amount of permanent deformation that would occur after a given number of wheel load applications, the pavement layers are divided into sub-layers, and the elastic stress state is calculated at the centre of each sub-layer directly beneath the wheel load. A linear or non-linear relationship between the elastic stress field and permanent deformation in each layer is then assumed to calculate permanent deformation. The permanent deformation characteristics of the various pavement materials as a function of stress state, number of load repetitions, temperature, density, etc. are determined usually through triaxial testing. The total rut depth for a given number of load repetitions is obtained by summing up the average plastic strains occurring at the centre of each sub-layer combined with the corresponding sub-layer thickness.

$$\Delta p = \sum_{i=1}^{n} \left[(\varepsilon_i^p)(\Delta z_i) \right] \tag{2.7}$$

where Δp = total rut depth

ε_i^p = average plastic strain in the i'th layer

Δz_i = thickness of the i'th sublayer

n = total number of sublayers

The layer-strain approach is a flexible method for the prediction of rut depth and permits the use of either linear or non-linear elastic properties. The layer strain approach assumes that permanent deformation is only dependent on the elastic stresses in the pavement and independent of the material viscosity. One of the disadvantages of the models based on the layer strain methodology is that they cannot account for the characteristic ridge formed adjacent to the wheel path. Haas and Papagiannakis [69] also reported that the stress state induced by the triaxial tests under which the plastic material properties are usually determined is not representative of the stress conditions in real pavements, and the effects of moving traffic can only be taken into account indirectly by adjusting the rate of loading of the test.

Morris et al [101] proposed a rutting model for the asphaltic layers where the permanent deformation characteristics were determined from triaxial tests as a function of stress state i.e. vertical and horizontal stress, temperature and number of load repetitions. The bituminous material was tested in two stress modes, compression and tension to simulate the behaviour of the bituminous layer. The predicted rut depth values were compared with the measured values from the Brampton Test Road in Canada by plotting total yearly permanent deformation against a period of 7 years (permanent deformation-time relationship) (see Figure 2.7). The model predicted that the permanent deformation had occurred in the tension zone due to lateral distortion of the material, which was in agreement with observations from the test section. Based on their findings they concluded that if moderate tensile stresses exist in the field the mechanism of rutting is entirely due to the lateral distortion in the tension zone, where the resistance to stresses and strains is provided by the binder alone [101].

Meyer and Haas [94] proposed a rutting model based on the Morris et al approach. For the model to be more realistic the unbound granular materials were also included in the model. To simulate field conditions, dynamic triaxial tests were carried out for characterising the permanent deformation characteristics of both the asphalt and

granular base materials, under a variety of loading rates, temperatures, and densities. To verify the model with field results, the materials used were similar to those used in the construction of Brampton Test Road in Canada. Rut depths were calculated in a number of typical pavements based on stresses determined using Finite Element methods and verified using measured rut depths from test roads, particularly the Brampton Test Road. From these results, the primary factors affecting rutting were found to be the thickness and stiffness of the bituminous layers, the stiffness of the subgrade material, and the number of wheel load repetitions. Meyer and Haas concluded that there was an optimum bituminous layer thickness to produce a minimum depth of rutting. In order to apply the prediction model, various tests were carried out and the variables resulting in minor stress changes were eliminated.

Brown and Bell [27] noted that Barksdale and Romain [14, 120] related permanent strain to vertical and horizontal stresses. They proposed the use of stress invariants as the most appropriate method of representing the stress state for material characterization. Following this approach, the stress conditions at any point can be characterized by the mean normal stress, p, and the octahedral shear stress, τ_{oct}, where:

$$p = 1/3*[\sigma_1+\sigma_2+\sigma_3] \tag{2.8}$$

$$\tau_{oct} = 1/3*[(\sigma_1-\sigma_2)^2 + (\sigma_2-\sigma_3)^2 + (\sigma_3-\sigma_1)^2]^{1/2} \tag{2.9}$$

Where σ_1, σ_2, and σ_3 are the principal stresses. For simplicity the shear stress term, q can be defined as:

$$q = \left(3/\sqrt{2}\right)*\left(\tau_{oct}\right) \tag{2.10}$$

In the triaxial compression test situation, the shear stress, q, can be written as:

$$q = \sigma_1 - \sigma_3 \tag{2.11}$$

This is known as the deviator stress. The mean normal stress p represents the volumetric stress whereas q represents the shear stress. The corresponding strain invariants are the volumetric strain (v) and shear strain (e), can be defined as:

$$v = \varepsilon_1 + \varepsilon_2 + \varepsilon_3 \tag{2.12}$$

$$e = (2/3)*[(\varepsilon_1-\varepsilon_2)^2 + (\varepsilon_2-\varepsilon_3)^2 + (\varepsilon_3-\varepsilon_1)^2]^{1/2} \tag{2.13}$$

Where ε_1, ε_2, and ε_3 are the principal strains. Brown and Bell, obtained a relationship for the plastic behaviour of the material by inducing p-q stress conditions in the triaxial test. The off-axis loading conditions (stress not directly under the load) were considered in the compression and tension zone of the asphalt layer. It was found that in the tension zone of the asphalt layer, where the principal stresses cannot be reproduced in the triaxial test, the corresponding values of the stress invariants generally can be reproduced, and p and q in the pavement structure can be calculated using elastic layered theory or finite element programs. They also found that substantial errors in both p and q develop if the shear stresses are ignored in the determination of stress state, and underestimation of plastic strain by as much as 40% may be expected.

The predicted rut depths, calculated using the layer strain approach, were compared to those measured in the Nottingham Pavement Test Facility (PTF). The agreement was found to be reasonably good, but again, the model could not account for the shoulder, or ridge, formed due to the shear displacement of the material, which accounted for the inability of the layer strain approach (see Figure 2.8).

Monismith et al [98] proposed a model to predict the rut depth in flexible pavements occurring under repeated traffic loading also using a constitutive relationship derived from triaxial compressive testing on paving materials. They found that the time of loading in the triaxial testing was a very significant factor in the rut prediction of asphalt. The contributions to permanent deformation from all pavement layers and subgrade were taken into consideration. Their method used ELSYM[7], for the

[7] A computer program which calculates stresses, strains and displacements in an elastic multi-layer system.

computation of stresses and strains [1], and the total rut depth was calculated by summing up the contributions from each layer. The vertical plastic strain in the asphalt layer was calculated using the equation:

$$\varepsilon_p = R\,[\sigma_z - 1/2*(\sigma_x + \sigma_y)] \qquad (2.14)$$

where $\sigma_x, \sigma_y, \sigma_z$ = normal stress components

R = ratio of total effective strain $[2/3*(\varepsilon_1 - \varepsilon_3)]$, to the equivalent stress $(\sigma_1 - \sigma_2)$.

Poisson's ratio was assumed to be 0.5 for the asphalt layer. The calculations from the model for rut prediction were verified by studying pavement sections in San Francisco. The difference in the predicted and measured rut depth was found to be approximately 0.25 cm (2.5 mm).

Kirwan et al [88] proposed a relationship between static and dynamic loading required to give the same rate of deformation. The rut prediction model was based on a non-linear elastic Finite Element model used for the stress computations. The permanent deformation characteristics of the asphaltic materials were obtained from triaxial tests. The results of these tests were compared to results from static creep tests. It was found that the equivalent static creep test loading is 61% of the peak to peak value of a sinusoidal dynamic load. To test this proposition, a series of tests were carried out at the University of Nottingham on cylindrical specimens of Dense Bitumen Macadam (DBM). A number of specimens were subjected to dynamic vertical stress pulses of sinusoidal pattern and constant vertical stress. Kirwan et al [88] concluded that, except at low stress levels, good agreement was obtained between predicted and measured values (see Figure 2.9).

Verstraeten et al [146] proposed a simplified rut prediction model based on a permanent deformation law for each layer in the pavement structure. The model expressed the permanent strain as a function of elastic strain and number of load repetitions. Theoretical results were found to be in excellent agreement with field observation in Belgium (see Figure 2.10).

2.6.3 Viscoelastic based prediction models

Viscoelastic based rutting models directly incorporate the time-dependent response of bituminous materials to define the states of stress and strain at particular points in the pavement structure. This type of model assumes that ruts form primarily by shear flow of the pavement materials. Permanent deformation is assumed to be dependent on the viscous properties of the pavement materials and is assumed to be independent of the elastic properties. Unlike the "layer strain" approach the viscoelastic approach can account for the characteristic ridge formed adjacent to the wheel path. The viscoelastic properties of the asphalt are typically determined from confined or unconfined creep testing. Over the years researchers at Shell and other parts of the world have found a good correlation between rutting and confined or unconfined creep tests (see section 2.7.1). Bitumen is a viscoelastic material which is stress, strain rate and temperature dependent. As the permanent deformation is primarily associated with the viscous response of the binder, consequently, in the creep test longer loading times are involved which when combined with high temperatures create ideal conditions for viscous behaviour to dominate.

Representative models generally use a combination of springs and dashpots in various arrangements to represent time-dependent behaviour. A typical example of a viscoelastic model is a 4-element Burger's model (a Maxwell model with a Voigt model in series) shown in Figure 2.11. An important advantage of this approach is that the moving wheel loads can be considered directly, which results in the correct rate of loading to be applied to each material element. This permits estimates to be made of the lateral viscous flow of material from beneath the moving wheel, resulting in the formation of a shoulder adjacent to the wheel path.

One of the limitations of the viscoelastic theory based prediction models is that pavement behaviour is, in general, non-linear and the materials cannot be characterized adequately by a linear viscosity. A non-linear viscoelastic model is more prohibitive, both in terms of computational effort and the scale of laboratory work necessary to establish appropriate non-linear, time–dependent constitutive equations. Thus, linear viscoelastic models are the only types that can be readily implemented for modelling the accumulation of permanent deformation both in terms

of laboratory and computational work involved [69, 129]. Recently, due to the increased availability of fast computer systems and software many developments have been made in modelling the non-linear constitutive properties of bituminous mixtures (see for example [124, 130, 131, 140]). However, the scale of laboratory work which involves manual determination of non-linear constitutive material properties from test measurements is still a tedious, time consuming process.

Battiato et al [16] proposed a two-layer viscoelastic model for the prediction of permanent deformation in asphalt pavements. The subgrade was assumed to be elastic and the asphalt layer was idealised using a Maxwell model (spring and dashpot in series). The material properties were evaluated using unconfined creep tests. This model accounts for the ridge formed adjacent to the wheel path (see Figure 2.12). Their results also showed that if the subgrade was assumed to be elastic in behaviour, the permanent deformation due to the passage of a single wheel is independent of the subgrade stiffness.

Huschek [81] proposed a linear viscoelastic theory for calculating the permanent deformation in a layered pavement system. To model material behaviour the non-bituminous materials were considered to be elastic, only the bituminous layers were considered to have time-dependent material properties. A Maxwell model was again used to represent the response of asphaltic material. The material was characterized using both conventional and cyclic unconfined compression creep tests. Using the computer program BISAR[8], the stress and strain distributions in a pavement under the influence of a standard wheel load (contact stress: 600kN/m^2) were calculated. Huschek suggested that the specimen should be confined to better include the influence of the internal friction of the aggregate. The temperature distribution in the pavement, transverse distribution of traffic and vehicle speed were also taken into account. The total rut depth was obtained by summing the permanent deformation values in the various viscoelastic layers. The calculated results were verified by comparing with the actual measurements of rutting on a test road in Switzerland. Good agreement was found between the measured and calculated rut depths. The test

[8] BISAR (Bitumen Stress Analysis in Roads): A computer program developed by Shell which calculates stresses, strains and displacements in an elastic muti-layer system.

road had five sections and it was found that most of the rutting in all these sections was due to viscous flow and rutting due to compaction was almost negligible.

Kenis [85] summarized the analytical methods and procedures which formed the basis of US Federal Highway Administration's VESYS-II model for the prediction of rut depth. The permanent deformation characteristics of the pavement materials were determined by triaxial testing using a haversine load pulse. A probabilistic viscoelastic model was used to compute stress and strain in the pavement structure. The model represents the pavement as a three layered, semi-infinite continuum, with the upper two layers having a finite thickness and the bottom having infinite depth. The permanent deformation behaviour of the asphalt was expressed as a function of plastic strain versus number of load repetitions. The model was verified by comparing predicted rut depths with the measured values from the Pennsylvania State University test facility.

Thrower [135] analyzed the permanent deformation of an idealised pavement structure composed of viscoelastic materials, subjected to a pulsed load. He suggested that separative methods, based on deriving the permanent deformation from experimentally determined material deformation properties, in association with a stress distribution determined separately not considering the permanent deformation, may lead to serious distortions in assessing the role of the various layers in contributing to permanent deformation. He proposed a linear viscoelastic model for rutting where a multilayer elastic program is supplied with equivalent viscous parameters instead of elastic constants[9]. He concluded that, in a viscoelastic system, the permanent deformation is independent of the elastic properties and depends only on the viscous properties of the pavement materials. The results compare well with Battiato's findings [16], suggesting that the model can successfully describe the ridge formed adjacent to the wheel path under a moving load.

Based on Thrower's findings, Nunn [105] developed a method of predicting the deformation in the bituminous layers of the pavement using linear viscoelastic theory. He conducted uniaxial creep tests to determine the viscous properties of the bituminous materials. As stated by Thrower the resulting permanent deformation is

[9] Elastic-Viscoelastic Correspondence Principle.

dependent on the viscous properties rather then the elastic properties and the rate of development of permanent deformation is related to viscous parameters in precisely the same way that the resilient response is related to elastic modulus in a multi-layered structure. Using this concept, Nunn used a multilayer elastic computer program by supplying it with viscous parameters (axial viscosity and deformational Poisson's ratio), analogous to elastic Young's modulus and Poisson's ratio respectively. Comparisons between predicted and actual measured rut depth were made. The tests were carried out in different regimes of loading, ranging from simple laboratory wheel tracking test (see Figure 2.13) to more complex conditions encountered on actual roads (see Figure 2.14). It was found that viscous analysis predicted the permanent deformation better than the methods based on the elastic analysis.

Hopman et al [78] modelled the rutting and fatigue behavior of asphalt pavements using the viscoelastic approach. The pavement structure was characterized as a visoelastic half space loaded by a moving point force. A 4-element (Burger's) model was adopted to model instantaneous elasticity, delayed elasticity and permanent deformation. In the case of permanent deformation, the viscous properties from the Burger's model were determined by a repeated unconfined uniaxial creep test, at 40°C using the Nottingham Asphalt Tester (NAT). They concluded that the viscosity in the Voigt model and the elastic elements were relatively constant, whereas, the viscosity in the series dashpot increased with an increasing number of load repetitions. The permanent deformation occuring in the repeated creep test was attributed to the series dashpot in the Burger's model. It was also found that the elements of the Burger's model were dependant on the mode of loading i.e. tensile versus compressive.

Collop et al [46] also suggested a viscoelastic approach based on Thrower's analysis to predict rutting in flexible pavements. Their method used the VESYS computer program reported by Kenis [85], in which the pavement is modelled as a semi-infinite linear elastic layered structure supported on an elastic half space. The influence function for rate of permanent deformation was calculated by supplying VESYS with viscous rather than elastic material properties. Temperature effects were taken into account by using temperature sensitive viscosities. After an initial compaction phase, the model predicts that permanent deformation per wheel pass is proportional to the

static axle load and inversely proportional to the vehicle speed. They proposed a theoretical method for determining the viscosities of asphalt mixtures operating under a wide range of environmental conditions from routine test data based on one parameter q, that needed to be fitted to experimental data. For the mixtures tested by Hills et al [73] in a wheel tracking test, a value of q =0.47 was found to fit the measured deformation data. To obtain a reasonable estimate of asphalt mixture viscosity, longer loading times and lower effective stiffness of the asphalt mixture were taken into account for sufficient strain contributions from viscous deformation. Subsequently, a new equation was developed enabling the viscosity of the asphalt mixture to be estimated from the viscosity of bituminous binder and the mixture composition (VMA). The rutting model (with q = 0.47) was successfully validated using the results of a full wheel tracking test in France [109] (see Figure 2.15).

2.7 Materials Testing for Permanent Deformation

The development of predictive methods requires suitable techniques not only for calculating the response of the pavement but also for realistically characterising the material. Laboratory tests are typically performed to determine the representative parameters for modelling permanent deformation behaviour in asphalt mixtures. Generally, from an analysis of these models of permanent deformation, the primary factors that affect rutting are found to be temperature, number of load applications or time of loading, mixture properties, and the state of stress.

The overall objective of materials testing should be to reproduce, as closely as is practical, in-situ pavement conditions, including the general stress state, temperature and general condition of the material. Types of tests presently used to characterise the permanent deformation response of pavement material include the following:

- Uniaxial and Triaxial creep tests
- Uniaxial and Triaxial repeated load tests
- Simple shear tests
- Hollow Cylinder Testing

- Wheel tracking tests

These tests are typically used to evaluate the elastic, viscoelastic, plastic and shear strength parameters of asphaltic mixtures.

2.7.1 Uniaxial and Triaxial Creep Tests

The creep test (confined or unconfined) has been used to measure mixture characteristics for a variety of predictive methods. This test gained wide acceptance, principally due to ease of specimen preparation, the simplicity of test procedure and the low cost of test equipment. It was developed in the 1970's by the Shell organisation in Amsterdam for testing bituminous mixtures [74]. A detailed description of the compressive creep test for bituminous mixtures can be found in [143]. Typically, a bituminous specimen with flat and parallel ends is placed between two hardened steel platens, one of which is fixed and the other movable. A constant load is applied to the movable platen, and the compressive deformation of the specimen is measured as a function of time. Early versions of the equipment generally used a dead weight to apply the load via a mechanical lever arm [75]. Lubrication is necessary to prevent the load platens from laterally constraining the specimen, resulting in a non-uniform stress distribution. Deformation (strain), measured as a function of the loading time at a constant temperature, is the usual test output.

Researchers at Shell conducted extensive studies using results from the unconfined creep test as a basis for predicting rutting in bituminous materials [73, 143, 144, 145]. They found that the method under-predicted rut depths measured in the trial pavements [73]. This was attributed to the effects of repeated loading producing higher deformations in the wheel tracking tests [145]. Eventually, an experimentally derived correction factor that varied according to the mixture type was introduced into the creep analysis to account for these effects.

To obtain good comparisons between rut depths observed in a test track and those calculated using creep test data Van de Loo [145] recommended that the creep test should be performed at relatively low stress levels within the linear range of the materials. He later concluded [144], that tests performed at 103.4 kPa (15 psi) gave

acceptable results. The need to use a stress level within the linear range has been attributed to the fact that the loading time in situ is small compared to the loading time in the creep test and the permanent deformation per wheel pass remains in the linear range of stiffness.

In the United Kingdom, unconfined creep tests have been typically carried out at 100 kPa axial stress and at a test temperature of 30°C [121] and at 40°C [29, 66]. In the Netherlands, the unconfined creep test has been carried out at 100 kPa at 40°C [79]. In the United States, unconfined creep testing is normally conducted within the stress levels of 100-200 kPa, at temperature of 40°C [70], and the confined creep test has been conducted at 200-350 kPa with confining pressures of 34.5-138 kPa [99].

Recently, Brown and Foo [32], measured the unconfined and confined creep of a dense graded laboratory mixture under conditions at which rutting is most likely to occur in Hot Mix Asphalt (HMA) pavements. The relationship between sample air voids and the unconfined, as well as the confined creep test were evaluated in the laboratory and compared to the relationship between in-situ air voids and rutting under traffic. In addition, the effects of mixture preparation and specimen height were also evaluated. They concluded that the confined creep test represents more realistically in-situ performance.

2.7.2 Uniaxial and Triaxial Repeated Load Tests

A variety of loading systems have been used to measure mixture response due to repeated loading. These range from relatively simple mechanical or pneumatic systems to more complex servo-controlled electric-hydraulic systems [128]. Amongst these, pneumatic systems are considered to be more suitable for routine testing. More sophisticated systems generally include a testing chamber that permits careful control of temperature as well as the application of a cyclic confining pressure co-ordinated with the vertical repeated load. Such equipment is capable of applying repeated axial stress (either tension or compression) and lateral stress pulses of any desired shape, with pulses ranging from 0.01 to 1 second, incorporating rest periods between stress pulses ranging from zero to several seconds.

Whichever system is used, it is necessary to apply an axial load that varies with time in a manner representative of the pavement situation. Various pulse shapes, for example sinusoidal, square, triangular, and trapezoidal have been used for this purpose [22, 23]. A further consideration concerning repeated load application is whether to cycle continuously or incorporate some rest periods between pulses.

Furthermore, the influence of pulse shape and duration on the permanent deformation measurements has brought great concerns among the researchers in duplicating conditions existing in the actual pavement. In the early 70's Barksdale [15], presented data with which to determine the length of the pulse that corresponds to various vehicle speeds and depths in the pavement.

Later investigations at the University of Nottingham [26] confirmed that rest periods are not significant for permanent deformation tests on asphaltic materials and cohesive soils. For resilient measurements, however, a short interval between pulses was recommended to allow for the delayed elastic recovery in asphaltic materials [22]. For granular materials, where the shear resistance depends mainly on interparticle friction, the number of load cycles is more significant than the pulse time.

Permanent vertical and horizontal strains are most easily measured using Linear Variable Differential Transformers (LVDT's) located on the axial loading ram and the lateral strain gauges glued to the specimen. Resilient modulus, permanent strain and Poisson's ratio as a function of the number of load repetitions, can be obtained from these measurements [82].

More recent use of triaxial tests on bituminous mixtures was reported by Brown and Cooper [24, 25]. They conducted triaxial quasi-static creep tests as well as triaxial repeated load tests on a wide variety of paving mixtures. It was established that the volumetric strain rates depend on hydrostatic stress only, whilst deviator strain rates depend on both the hydrostatic stress and the deviator stress. Moreover, it was found that repeated load tests using a square wave form generally caused higher permanent strains than creep tests in compression at corresponding stress levels. Tests in tension and compression with the same deviator stress produced similar strains under repeated

loading but different responses under creep loading. They also found that the deformation resistance was greater for continuously graded mixtures than for gap graded mixtures. The deformation resistance of continuously graded dense bitumen macadam was found not to be influenced strongly by the grade of the binder. This indicates that the effect of aggregate interlock is more important than the viscous properties of the bitumen. Based on extensive testing, Barksdale [14] concluded that repeated load triaxial tests appear to better characterise rutting compared to results from the creep test. Similar conclusions were drawn by Monismith and Tayebali [99], and more recently by Molenaar [95].

2.7.3 Simple Shear Tests

Simple shear tests have been widely used in the measurement of soil deformation properties [18, 19, 149]. The simple shear test can approximate field conditions that are characterised by a pure shear stress state and consequently is a suitable tool for investigating the rutting propensity of bituminous materials.

The Superpave Simple Shear Tester (SST) [86], developed by Strategic Highway Research Program (SHRP) to perform shear tests on bituminous mixtures consists of a closed loop, servo-hydraulic loading system with two perpendicular load actuators and an environmental chamber. The shear table holds the specimen and can be actuated to impart shear loads. LVDT's are fixed to specimens and measure the response of specimens to applied testing loads. The LVDT's make it possible for the system to control the applied testing loads. For example, the compressive (axial) load can be continually controlled by feedback from the shear deformation. The environmental control unit controls the temperature and air pressure inside the testing chamber at a constant level. The unit is capable of providing temperatures within a wide range from 1°C to 80°C. Air pressure is normally applied at a rate of 70 kPa per second up to a maximum value of 840 kPa.

The test specimen is 150 mm in diameter and is trimmed to a thickness of 50 to 65 mm. For the tests that require no confining pressures, the specimen is glued between two platens. An epoxy-type gluing device is used to squeeze the specimen between the platens while the glue cures. The gluing device rigidly holds the platens and

specimen to ensure that the platens are parallel. A different specimen configuration is used for confined tests. Test specimens are still placed between platens, however, no glue is used. A rubber membrane surrounds the specimen. A radial LVDT is fixed by a collar that surrounds the perimeter of the specimen. Axial LVDT's are fixed to the platens.

Tests Conducted with the SST

The following tests are performed using the SST (detailed procedures can be found in [71], and will not be repeated here):

- Simple shear test at constant height
- Frequency sweep test at constant height
- Repeated shear test at constant stress ratio / constant height

Simple Shear Test at Constant Height

In this test a shear stress is applied whilst maintaining the specimen at constant height and the corresponding shear strain is measured. Figure 2.16 shows the application of stresses during the test. A controlled shearing stress is applied at a constant strain-rate to a test specimen. As the specimen is sheared, it dilates, which increases its height. A variable axial stress is applied continually to keep the specimen height constant as the specimen is horizontally displaced or deformed. During the test, axial and shear loads and deformations are measured and recorded. The following response variables are measured:

σ_{11} = variable axial stress applied to maintain a constant height, kPa.

σ_{12} = shear stress applied, kPa.

δ_H = horizontal displacement, mm.

h = height of the specimen, mm.

$\varepsilon_o = \delta_H/2h$

Frequency Sweep at Constant Height

For this test the load is applied at a series of frequencies and different temperatures. No confining pressures are applied. The shear stress is adjusted to provide a small shear strain and an axial stress is applied to maintain constant height. Figure 2.17 presents the key parameters of this test in schematic form. The frequency sweep data is used to determine the linear visco-elastic properties (i.e., complex modulus and phase angle). The following variables are measured:

σ_{11} = variable axial stress applied to maintain a constant height, kPa.

σ_{12} = shear stress applied, kPa.

ϕ = phase angle, degrees.

G^* = Complex shear modulus, kPa.

Repeated Shear Test at Constant Stress ratio / Constant Height

Repeated shear tests at constant height and constant stress ratio provide a tool for mixture evaluation and analysis, as a guard against catastrophic mixture failures. The repeated shear test at constant height was developed through the SHRP asphalt research program, but is not a part of the Superpave 2 system. It can be used for quick estimation of rut depth. The repeated shear test at a constant stress ratio provides information related to tertiary creep (failure) of the bituminous mixtures and is regarded as a screening test to identify mixtures that exhibit tertiary plastic flow leading to instability and premature rutting. Test conditions must be specific to the location in the pavement structure, the temperature of the environment, and the amount of the traffic to be carried.

A plot of the log of plastic strain versus the log of number of repetitions is made as shown in Figure 2.18. If the mixture remains in steady-state secondary creep the mixture passes. When the mixture passes the screening requirements, the mixture is subjected to the series of tests for the characterisation of permanent deformation, fatigue cracking and low temperature cracking. If the plastic strain enters the tertiary creep phase, the mixture fails the screening test. When the mixture fails the screening

test, it will be necessary either to make adjustments to the mixture proportioning or to redesign the mixture completely.

2.7.4 Tests on Hollow Cylindrical Specimens

Controlled changes in the magnitude and direction of the principal stresses on a material element are extremely difficult to reproduce in the laboratory. In triaxial testing, the principal stresses are fixed in one direction, and only an interchange of principal stress direction can take place. Rotation of the principal stress axes can only be accomplished in equipment such as the hollow cylinder apparatus in which shear stresses can also be applied to the specimen. A laboratory simulation of principal stress rotation involves subjecting hollow cylindrical specimens to axial load and torque about a central axis, and to internal and external radial pressures respectively. Due to the symmetry of the hollow cylinder specimen, the normal and shear stresses are uniformly applied. Testing of specimens of a hollow cylindrical shape has been performed for many years on solids such as metals and concrete and also on soils and granular material [76].

The Hollow Cylinder Apparatus developed at Nottingham was designed by O'Reilly [108] and modified by Thom [136], Chan [39] and Richardson [118]. It is a device which not only allows repeated loading but also permits the direction of the principal stresses to be rotated, or stated another way, for shear stresses to be applied to the specimen. A schematic diagram of the specimen in testing configuration is shown in Figure 2.19. A cylindrical specimen of 280 mm outside diameter, height 500 mm and wall thickness 28 mm is used in the test. Two actuators are used to apply axial loads and torques. Figure 2.20 shows the stress conditions on an element in the wall of the cylinder. When the specimen is only subjected to static axial and radial compression (from the cell pressure), it is similar to a pavement element at rest. When cyclic torque is directly applied, rotation of principal stress is induced. A maximum confining pressure of 500 kPa can be applied by compressed air both outside and inside the cylinder. Since the two pressures can be controlled separately, it is possible to vary the radial stresses, as well as the circumferential stresses, on the specimen. The limitation of the Hollow Cylinder Apparatus is that only small or scaled-down aggregates can be tested due to the thin wall (28 mm) of the cylinder. It is thus used

primarily as a research tool in which to investigate the effects of repeated stress rotation so that this effect can be properly allowed for in design procedures which are based on more simple tests. Furthermore, the equipment is quite sophisticated with much more complex testing procedures it is not suitable for routine application.

Recently Alavi [3, 4], investigated the permanent deformation characteristics of asphalt concrete mixtures subjected to axial and shear dynamic loading in a hollow cylinder test configuration. The hollow cylinder specimens used were 200 mm (8 in) in height, with 90 mm (3.5 in) inner and 115 mm (4.5 in) outer radii. The effects of combined axial and shear dynamic loading on the accumulation of permanent axial and shear strains were studied. The importance of shear dilatancy effect on permanent strain magnitudes was also investigated. The shear stress was shown to have a dilatancy effect on the permanent axial strain magnitudes. Consequently, Alavi [3, 4] concluded that for the combined mode of loading, the magnitude of permanent axial strain can be affected by shear dilation and this phenomenon should be taken into consideration in any permanent deformation investigation of asphalt concrete mixtures. During the preliminary stages of his investigations he also observed that, for a given mixture, application of excessive stress might affect the proper ranking of permanent deformation parameters. It was therefore recommended that stress magnitudes be selected such that the specimens would at least undergo a sufficient number of load applications before failure. However, these findings did not account for the effects of confining pressure i.e. the effects of the three dimensional stress states on the viscoelastic and permanent deformation characteristics of asphalt concrete mixtures.

2.7.5 Wheel Tracking Tests

Bonnot [17] reported that for design applications, laboratory simulation of rutting should duplicate stress conditions in actual pavements. Wheel tracking tests have been in use for many years for the assessment of resistance to permanent deformation since they are simple in principle and simulative in nature. The test is widely used throughout Europe [49, 103] and the USA [132] as a main tool for the validation of proposed methods for estimating rutting. It is a device that generates ruts due to the repeated passage of a wheel over a prismatic asphalt specimen. The specimen can be

obtained from an actual pavement but is more generally made and compacted in the laboratory.

In the Laboratoire Centrale des Ponts et Chaussees (LCPC) procedure, each specimen is a slab measuring 500 by 150 mm and is 100 mm thick [17]. The slab specimen is tracked by a pneumatic tyred wheel with an inflation pressure of 600 kPa (6 bar) and an applied load of 5 kN. Rutting is measured by the relative reduction in the thickness of asphaltic mixture in the wheel path. The test is terminated after 10^5 cycles, unless the rut depth exceeds 15 percent of the specimen thickness (15mm) prior to this time. Tests are conducted over the temperature range of 50°C to 60°C to reproduce the most extreme conditions expected in-situ. The tyre passes over the centre of the specimen twice per second, and the loading time at the centre of the slab is approximately 0.1 second.

The Nottingham Pavement Test Facility (PTF) [31] allows instrumented pavement sections, 16 ft. long and 8 ft. wide, to be constructed in a 5 ft. deep test pit. The PTF is a half scale testing facility in which trial pavements can be constructed and subjected to simulated vehicle loading under controlled conditions. The loading system is a linear tracking, servo-controlled, hydraulic apparatus and was designed to be capable of applying a load of up to 10 kN through a driven wheel at a speed of up to 14 km/hr. Either unidirectional or bi-directional tracking can be employed and the tracking frame has also a traversing facility to simulate lateral wander. The loading wheel is fitted with a pneumatic tyre that can be inflated to give a maximum contact pressure of around 650 kPa. Pavement temperature can be maintained constant anywhere within the range of 15°C to 30°C.

Full scale accelerated pavement test facilities (APT) have also been developed in France [13, 49], Germany [38], Australia [84], Netherlands [68], and South Africa [80]. A comprehensive report on Accelerated Pavement Testing (APT) has been written by Metcalf [93] and the proceedings of the international conference on APT, held recently in Reno Nevada [115], gives up-to-date information from United States and around the world. However, there is some concern about their efficiency (in terms of time required for a test) to study the development of permanent deformation under

repeated trafficking. Recently, it was reported that circular test tracks may be useful for studying fatigue characteristics of bituminous mixtures [89].

2.8 Summary

The loads applied by traffic on pavement structures are repeated in nature. As traffic moves along the pavement, a large number of stress pulses are applied rapidly to each element of material below and at some lateral distance from the wheel path. A wheel load moving along a surface in the direction of an element of material introduces axial, radial, and shear stresses on that element. Recent investigations have shown that densification in the early stages of a pavement's life, and shear deformation in the later stages are the primary mechanisms of rutting.

None of the traditional methods to model the permanent deformation behaviour of bituminous mixtures are capable of predicting all the observed phenomena in a consistent manner. A number of empirical models approximating the behaviour are available. Most of the models have been reasonably successful in ranking the mixtures based on their performance. However, their quantitative application to modelling permanent deformation always requires the addition of calibration factors. The important deformation properties of pure bitumens and idealised bituminous mixtures as noted by Cheung [40] and Deshpande [53] were highlighted in sections 2.4 and 2.5. Based on their extensive review of composite theories they concluded that, for modelling the deformation behaviour of bituminous mixtures where no definite micro-structure can easily be defined due to the high volume fraction of particulates, no existing models are applicable. Although bituminous mixtures are usually assumed to be linear viscoelastic materials, they are generally non-linear in their response to applied load. The suitability of any approach for modelling the deformation behaviour of bituminous mixtures needs to include these observations.

Two basic methodologies used to predict rutting have been reviewed. The layer-strain approach assumes that rutting is dependent on the elastic material properties whereas the viscoelastic approach assumes that rutting is dependent on the viscous material properties.

The layer-strain method is considered to be an attractive engineering theory for calculating rut depth which allows use of either linear or non-linear elastic theory together with the permanent deformation characteristics of asphalt mixtures. The method, however, has certain limitations. Firstly, testing the plastic behaviour of the materials is usually performed by triaxial testing which is a stress state substantially different than the conditions of plastic deformation in the field. Secondly, the disadvantage of the layer-strain approach is that it does not consider the interaction of shear deformation between the adjacent columns, required for the formation of the characteristic ridge adjacent to the wheel path. However, it should be noted that the shear deformation of the material within a given column is properly taken into account by the testing procedure. This is a limitation in situations where modelling of the transverse rut profile is attempted by dividing the pavement structure in column elements transverse to the direction of vehicle travel. Thirdly, the effect of the moving traffic can be taken into account indirectly. The effect of traffic speed is simulated by the rate of loading in the repeated dynamic tests. In order to capture the effects of widely varying traffic speeds with the complexity of these tests, it is impossible to conduct them at a variety of load frequencies.

The viscoelastic theory based rutting models are theoretically more appealing and provide a direct means for calculating the effects of moving loads on pavement permanent deformation. In addition, they can effectively model the shear deformation that results in the formation of a ridge adjacent to the wheel path. It appears that the simple uniaxial creep test (unconfined and confined) provides a reliable and convenient method of characterising the properties of bound materials for models using the viscoelastic approach. One of the limitations of the viscoelastic approach is that pavement behaviour is non-linear and cannot be adequately captured by the viscoelastic models. Because of the mathematical complexities and difficulty in defining an appropriate material model with non-linear viscoelastic analysis, the linear model is most frequently used and can be realistically implemented. However, if permanent deformation laws are developed based on the tests that apply states of stress comparable to those encountered in pavements near the tyre edges and if viscoelastic models are developed that can incorporate these laws, more accurate predictions can be expected.

From the information summarised in section 2.7, the primary difficulty in laboratory testing of bituminous mixtures is the replication of in-situ stress conditions. Standard test procedures are very limited in the range of stress states that can be applied to bituminous specimens. For rut prediction, characterisation of the pavement material requires a level of sophistication beyond both simple mixture design, where the aim is to optimise and compare the performance of candidate mixtures, and also beyond performance specification where the aim is to make quantitative assessment of mixture behaviour. Consequently, tests to be used in a predictive methodology will, therefore, generally be more rigorous.

For prediction methodology, firstly, a test should have the capacity to simulate field conditions, which includes a state of stress representative of the shear stresses causing permanent deformation, repeated or dynamic loading representative of traffic loading and in general other environmental conditions which directly or indirectly affect the performance of the material. Secondly, the test should be simple and require minimum cost for new equipment or supplemental devices. The specimens should be easy to fabricate and require minimum quantities of fabricating material in the laboratory and the equipment should be able to test cores obtained from the existing pavements.

2.9 Research Needs

An important reason for the limited progress in the detailed understanding of deformation behaviour of bituminous mixtures is the lack of theoretical framework to describe the mechanical behaviour of bituminous mixtures. This is partly because of the complexity of the problem and partly because, in the past, understanding of the behaviour of bituminous materials has been derived through empirical means. These empirical approaches have only shown limited success in modelling the failure mechanisms in bituminous mixtures. Significant new developments are required before sufficiently reliable test procedures, analytical models and design systems are available. They will provide the basis for development of a theoretically sound analysis procedure and related test methodology which will permit more reliable mixture designs and more appropriate modelling of the real conditions under which rutting occurs.

To predict rutting in asphalt pavements suitable techniques need to be developed not only for calculating the response of the pavement to traffic loading but also for realistically characterising material properties. One of the urgent research needs is that the materials should be tested to reproduce as closely as possible in-situ pavement conditions including the general stress state, moisture, temperature and general conditions of the material. Shear deformation is the main mechanism causing rutting, but suitable laboratory test methods and theoretical models are not yet available for properly treating shear induced permanent deformation. In fact, creep testing of bituminous mixtures in compression either uniaxially or triaxially, remains the main source of material characterisation regarding the long term permanent deformation behaviour of pavements.

The research described in this thesis provides further insights into the physical mechanisms of deformation of bituminous mixtures. It investigates the mechanism of rutting in bituminous mixtures and development of a simplified approach to predict rutting in asphalt pavements. Two particular types of bitumen commonly employed for pavement construction in the UK are investigated and are used as binders in mixtures. As a first step towards understanding the deformation behaviour of bituminous mixtures, uniaxial and triaxial compression tests have been performed on idealised mixtures.

Research is further extended to realistic mixtures which include Hot Rolled Asphalt and Dense Bitumen Macadam. The mechanisms controlling the deformation behaviour of these mixtures are evaluated and brought to light in the subsequent chapters. More routinely used performance related tests, such as the repeated load axial test and a more simulative wheel tracking test, are used to compare the performance of the idealised and realistic mixtures under a wide range of stress levels and temperatures. Experimentation is developed for testing the material in wheel tracking equipment under wide ranges of temperature and stresses. Dynamic mechanical analysis of the binder has been performed in Dynamic Shear Rheometer and rutting is characterised using the SHRP rutting parameter $G^*/\sin\delta$. An attempt has been made to model the steady-state rutting rates from the wheel tracking test using the results from uniaxial and triaxial tests in a viscoelastic model.

2.10 Figures

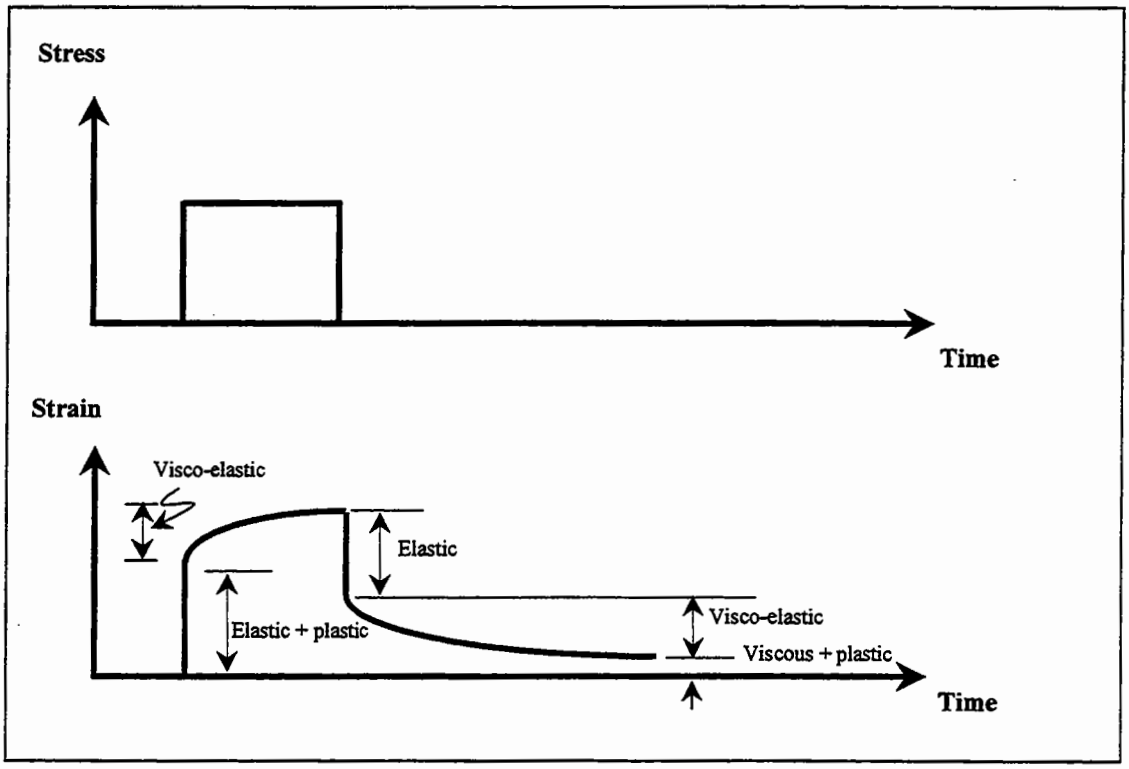

Figure 2.1 Idealised strain response of a Bituminous mixture.

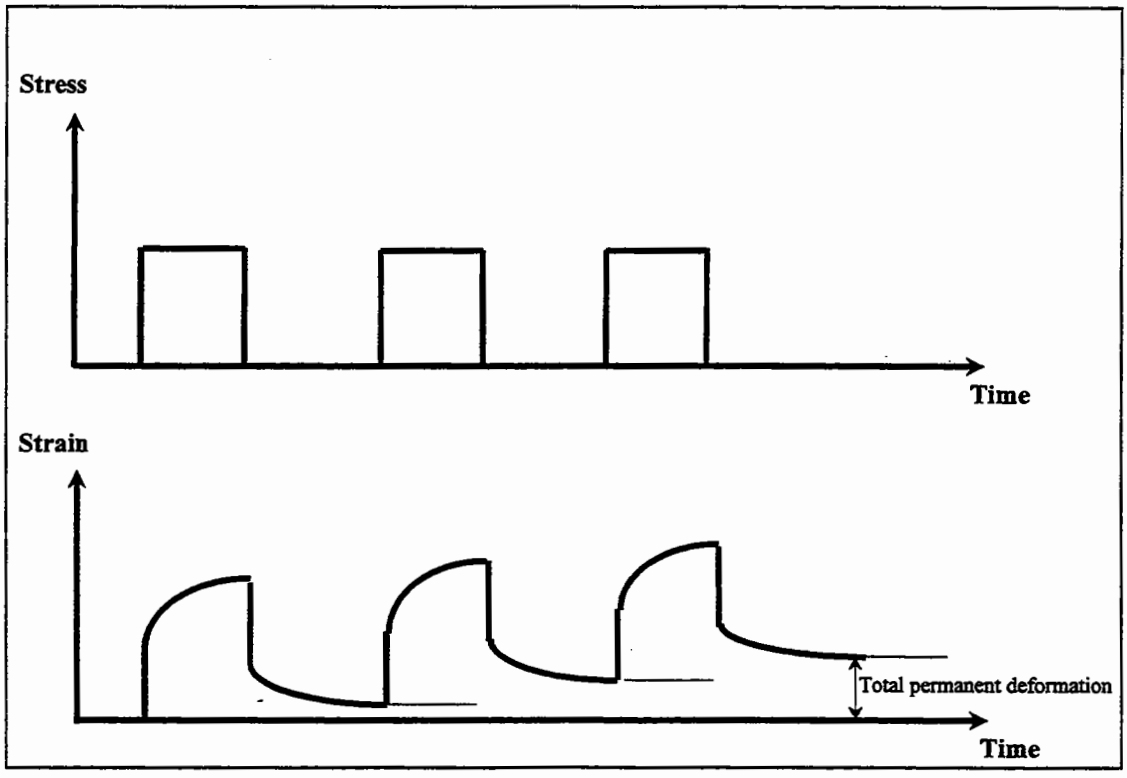

Figure 2.2 Accumulation of Permanent strain under repeated loading.

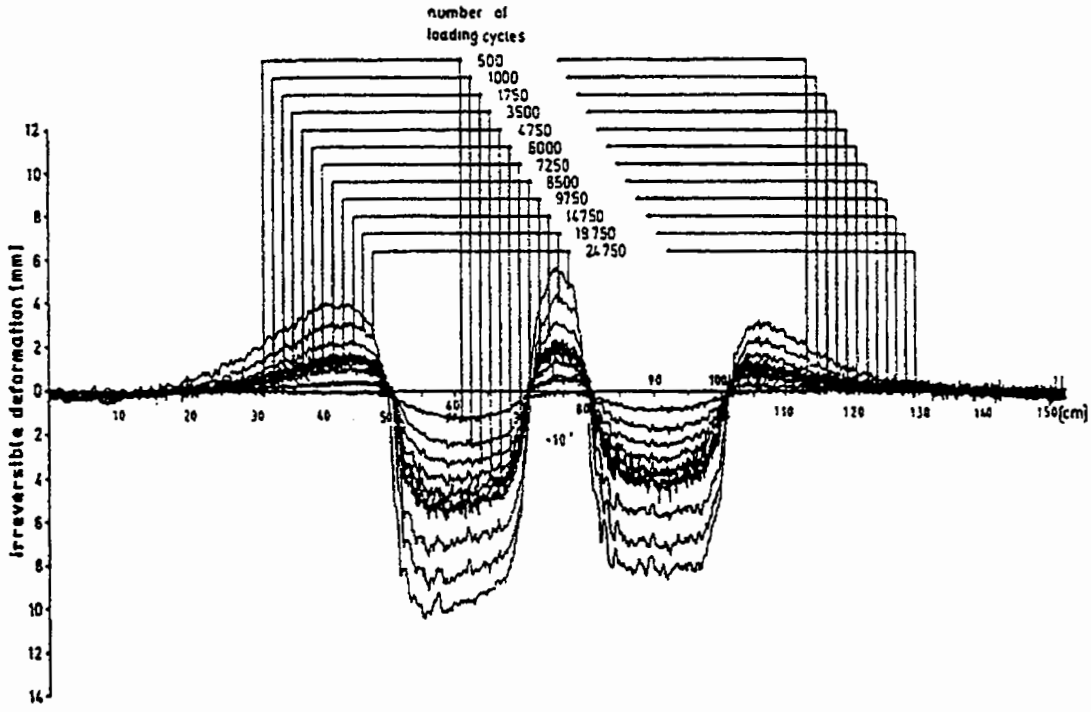

Figure 2.3 Effect of number of passes on transverse surface profiles. (reproduced from [59]).

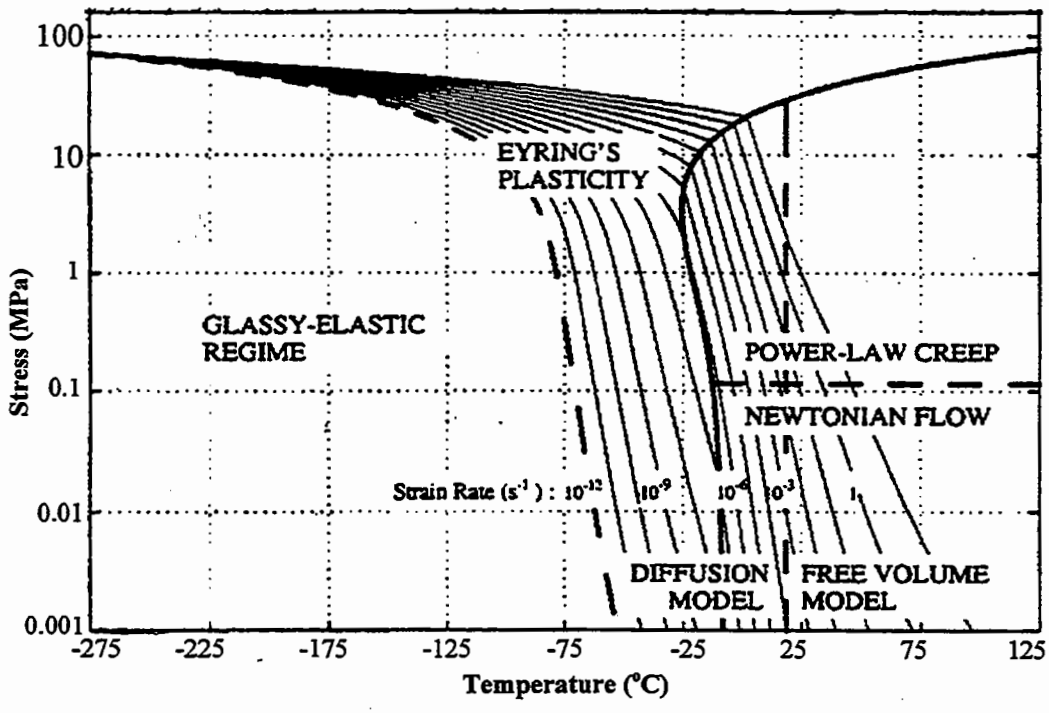

Figure 2.4 A stress/temperature deformation-mechanism map for 50 pen grade of bitumen in tension (reproduced from [40]).

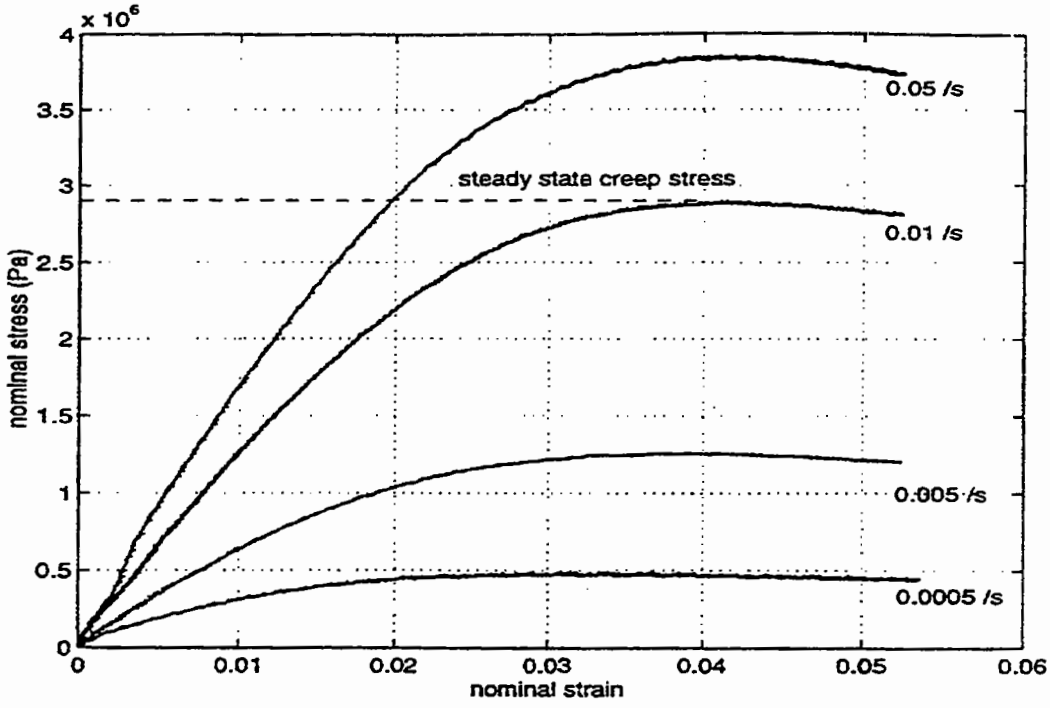

Figure 2.5 Constant strain rate tests of 64% mix at 20°C (reproduced from [53]).

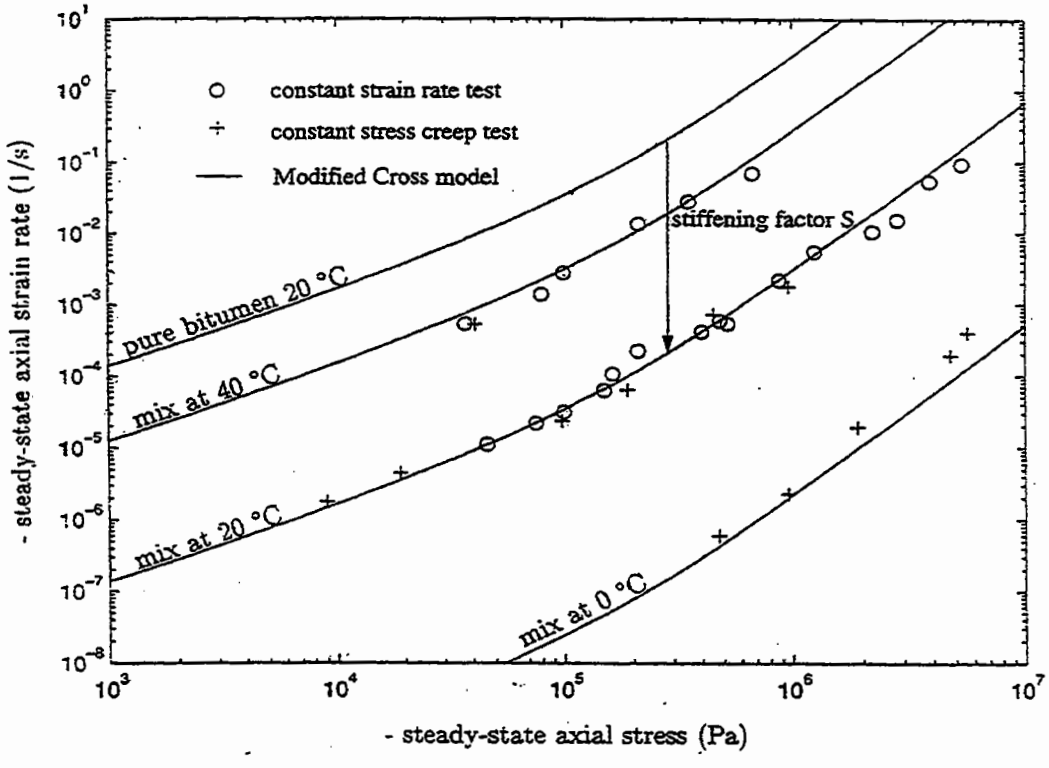

Figure 2.6 Deformation map for mixture with 64% by volume sand and pure 50 Pen bitumen (reproduced from [53]).

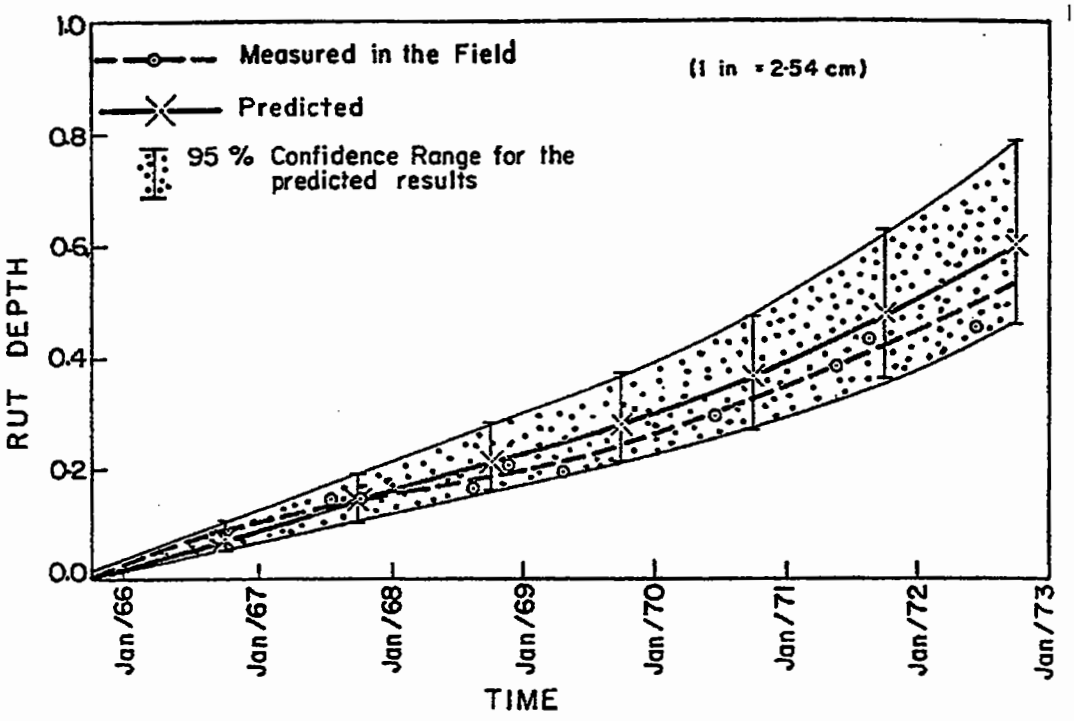

Figure 2.7 Permanent deformation – Time relationship (reproduced from [101]).

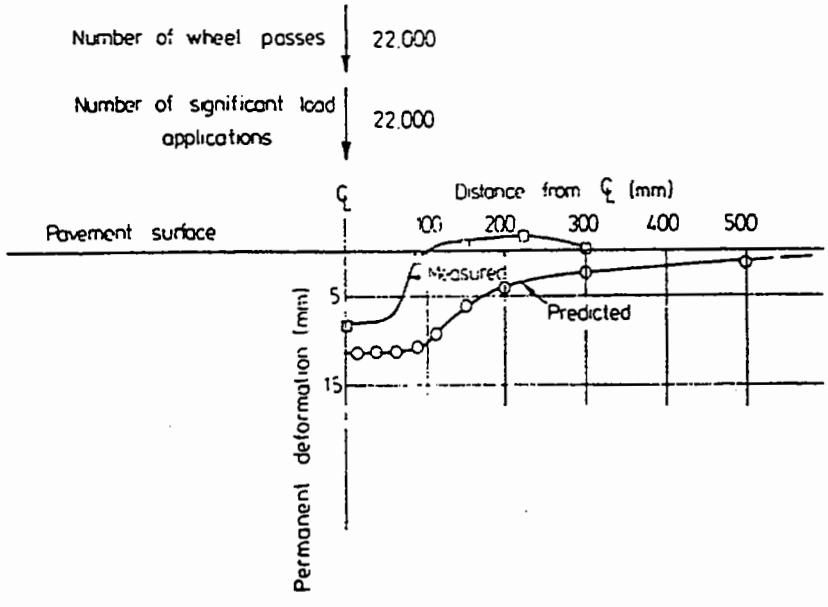

Figure 2.8 Inability to model shear displacement adjacent to the wheel path (reproduced from [27]).

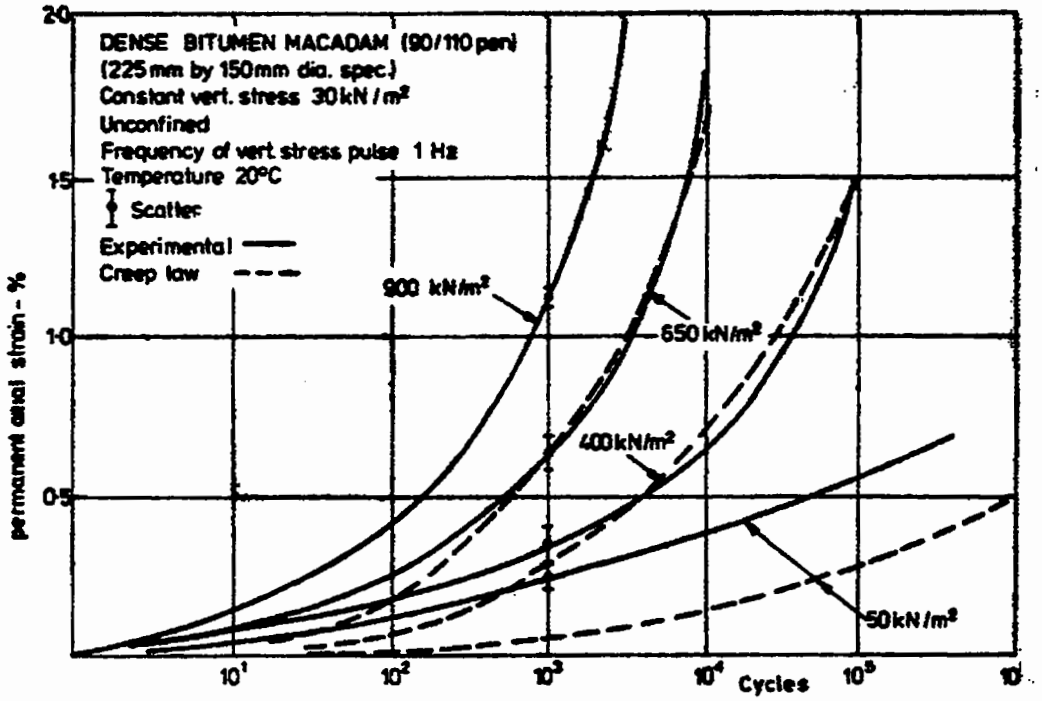

Figure 2.9 Comparison of predicted permanent deformation with measured values for a Dense Bitumen Macadam (DBM) (reproduced from [88]).

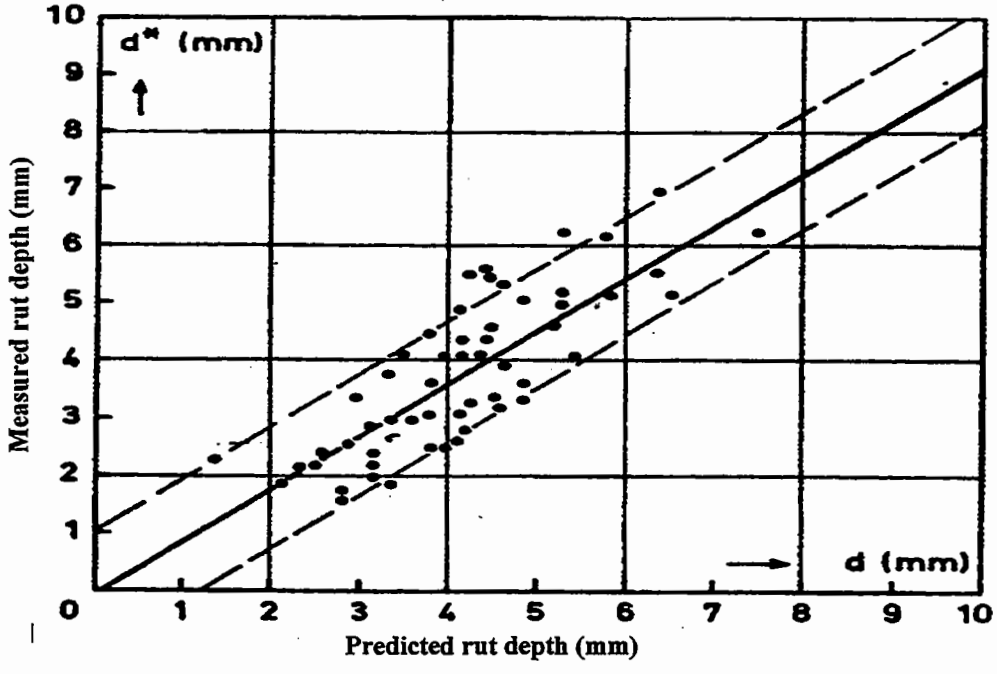

Figure 2.10 Correlation between the predicted and observed rut depth (reproduced from [146]).

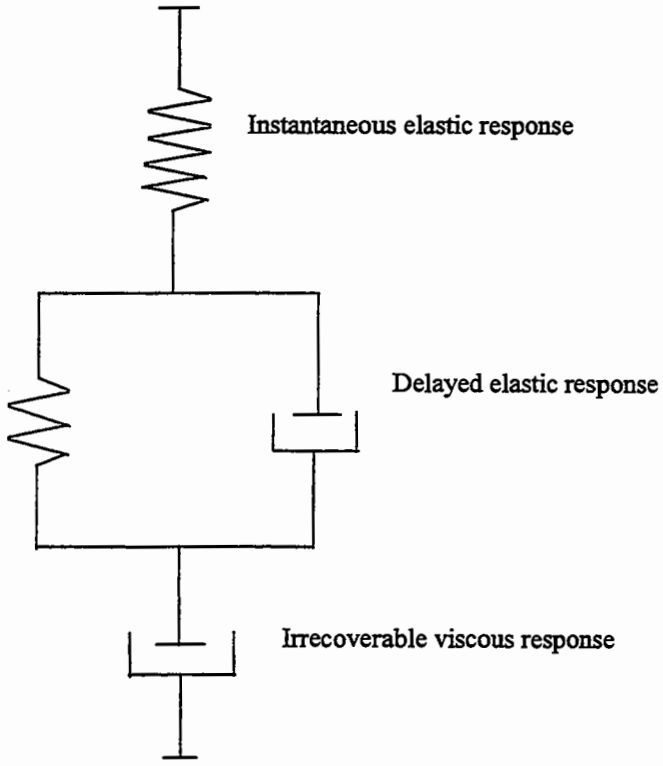

Figure 2.11 Maxwell model with Voigt model in series (4 - element (Burger's) model).

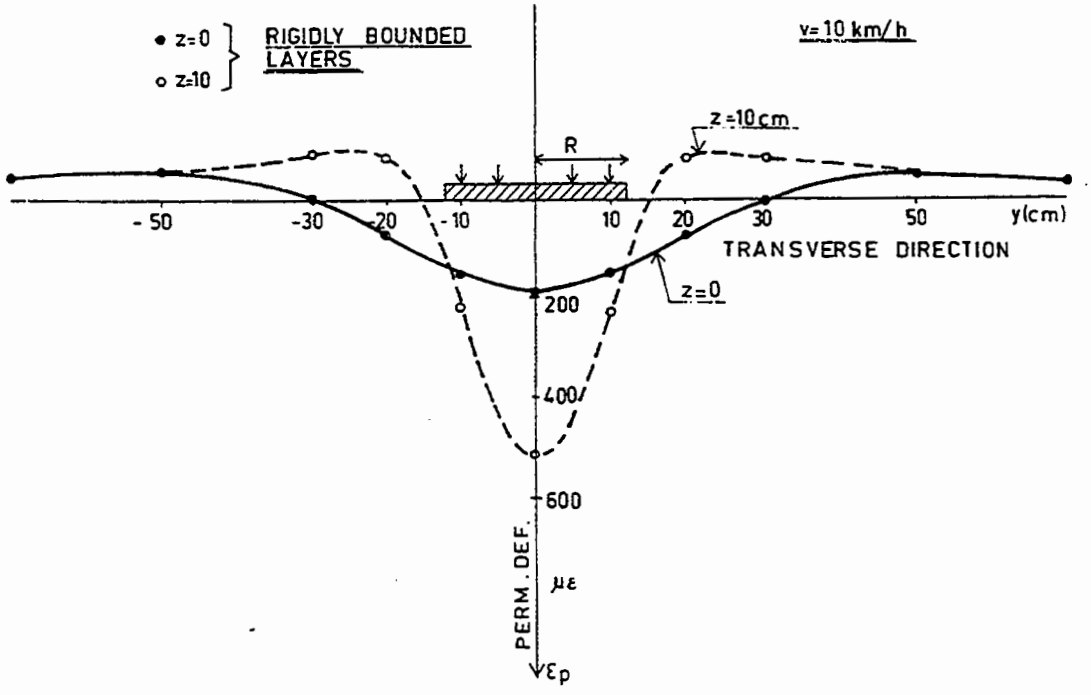

Figure 2.12 Ability to model shear displacement adjacent to the wheel path (reproduced from [16]).

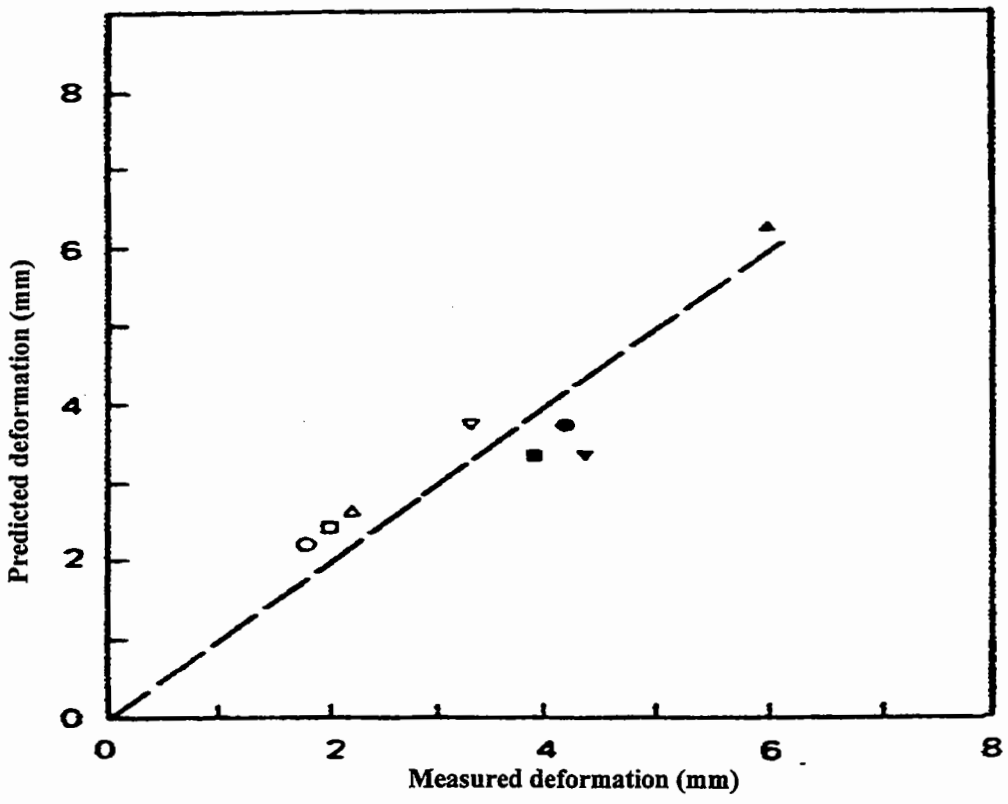

Figure 2.13 Comparison between predicted and measured rut depth in the wheel tracking test (reproduced from [105]).

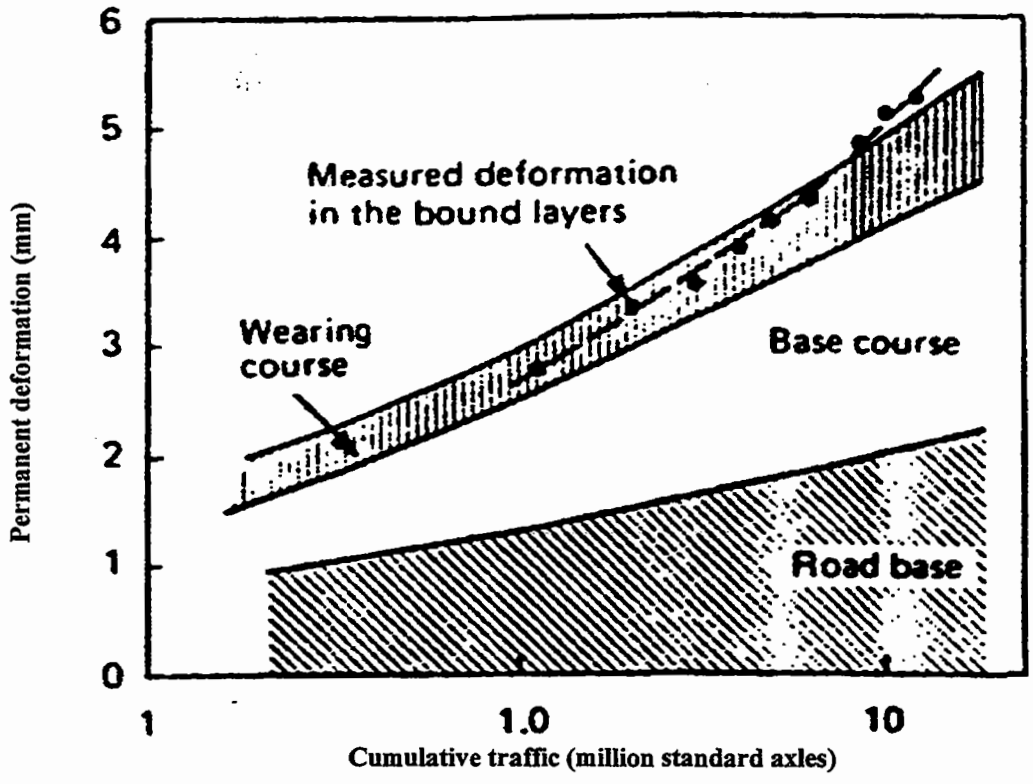

Figure 2.14 Predicted contribution to deformation from bound layers [105].

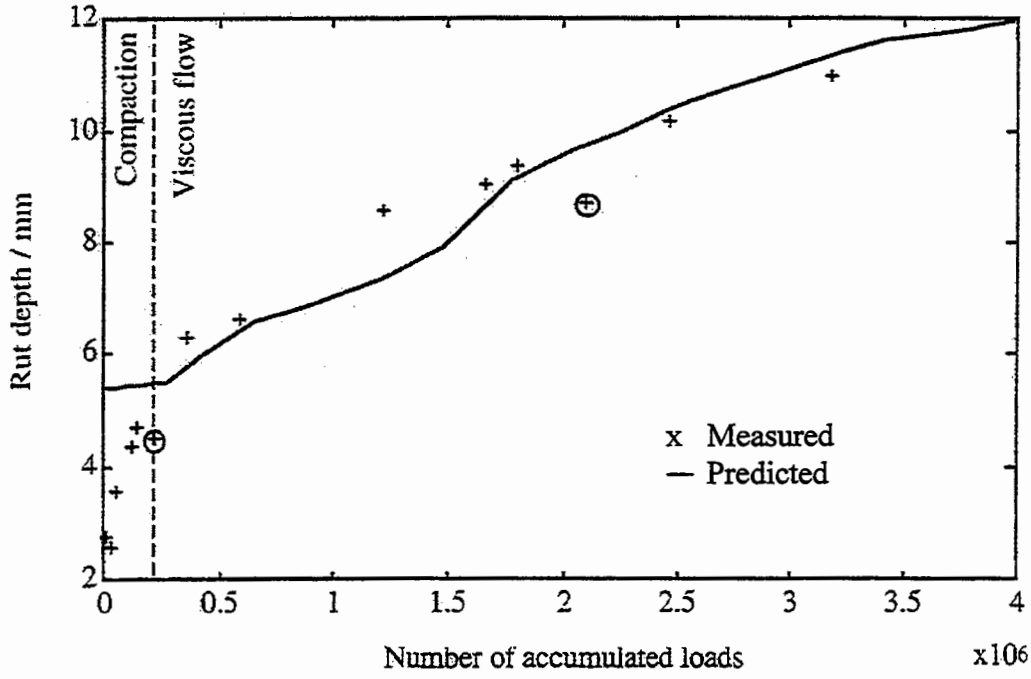

Figure 2.15 Predicted and measured rutting (reproduced from [46]).

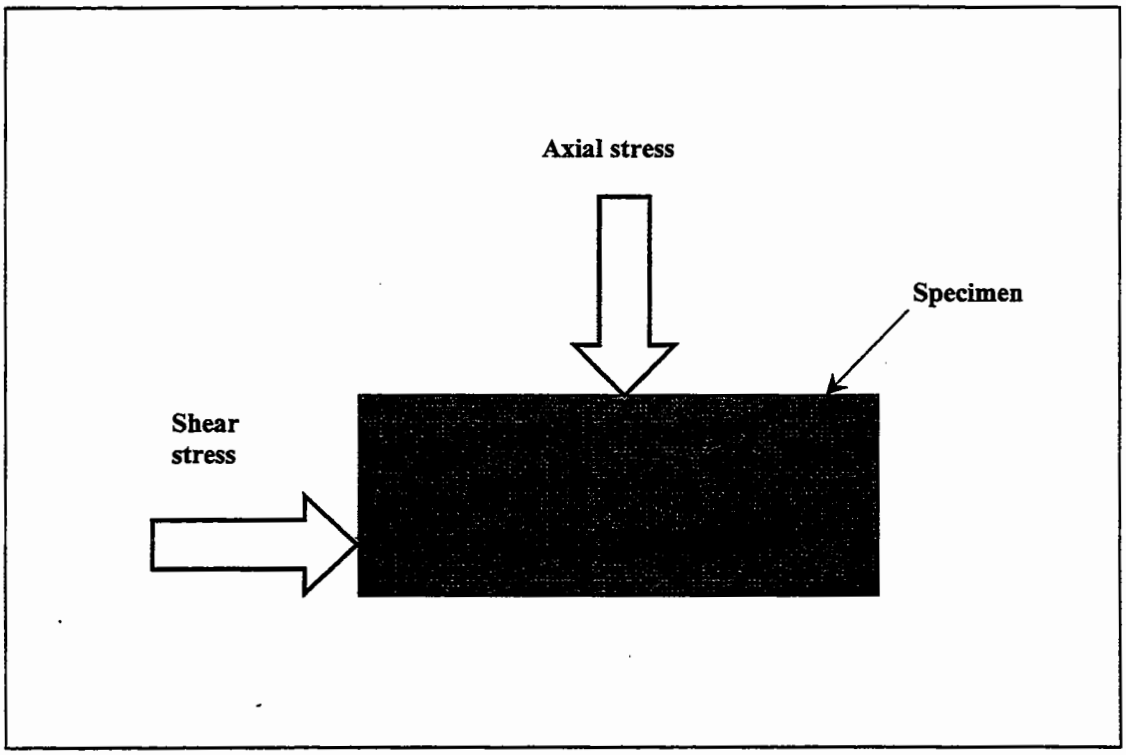

Figure 2.16 Conceptual view of the simple shear at constant height test.

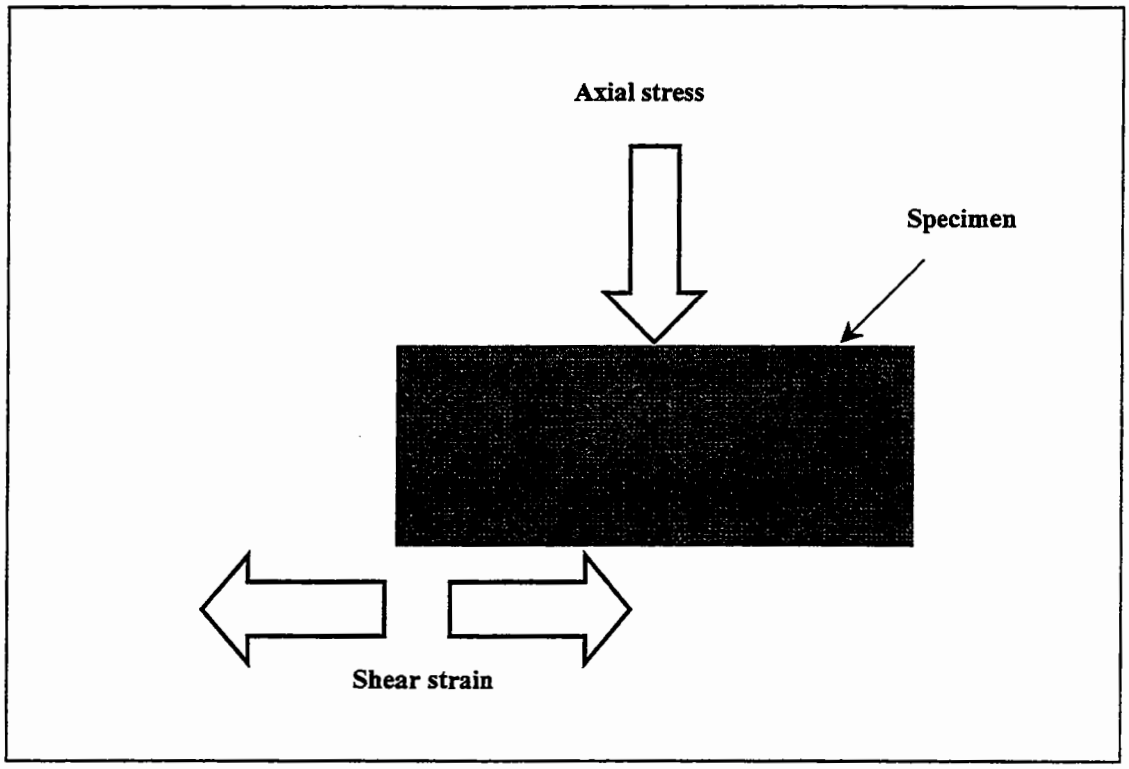

Figure 2.17 Conceptual view of the frequency sweep at constant height test.

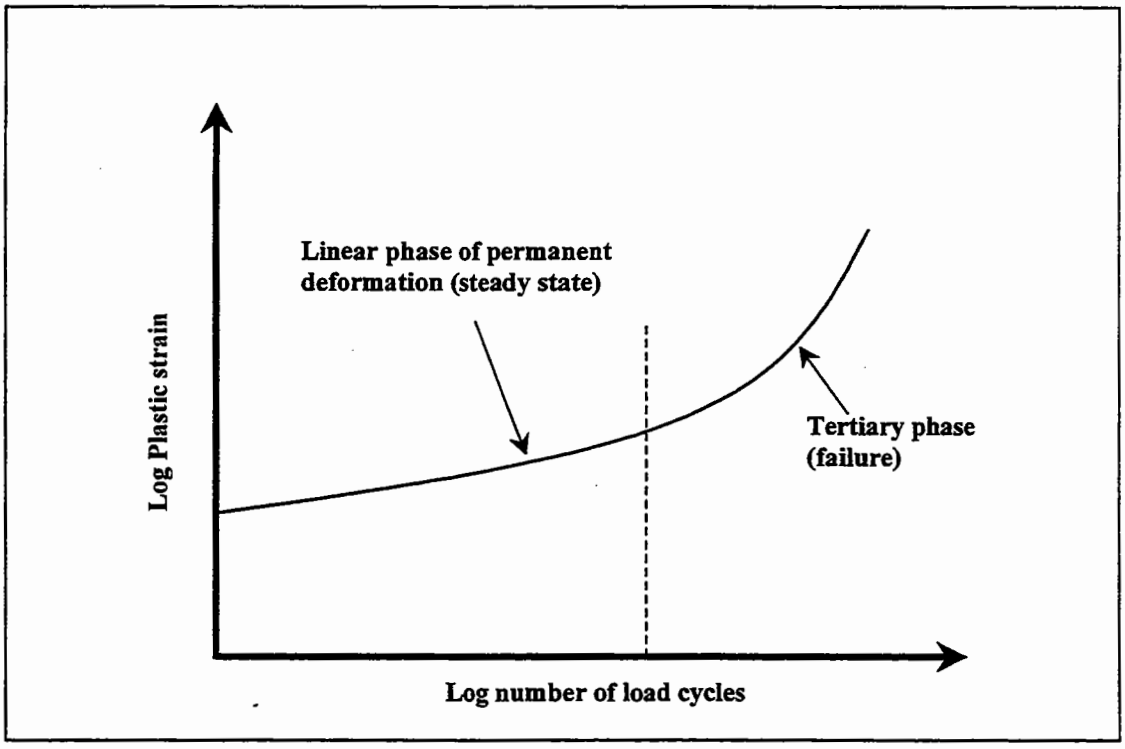

Figure 2.18 The development of tertiary flow as a function of repeated shear loading.

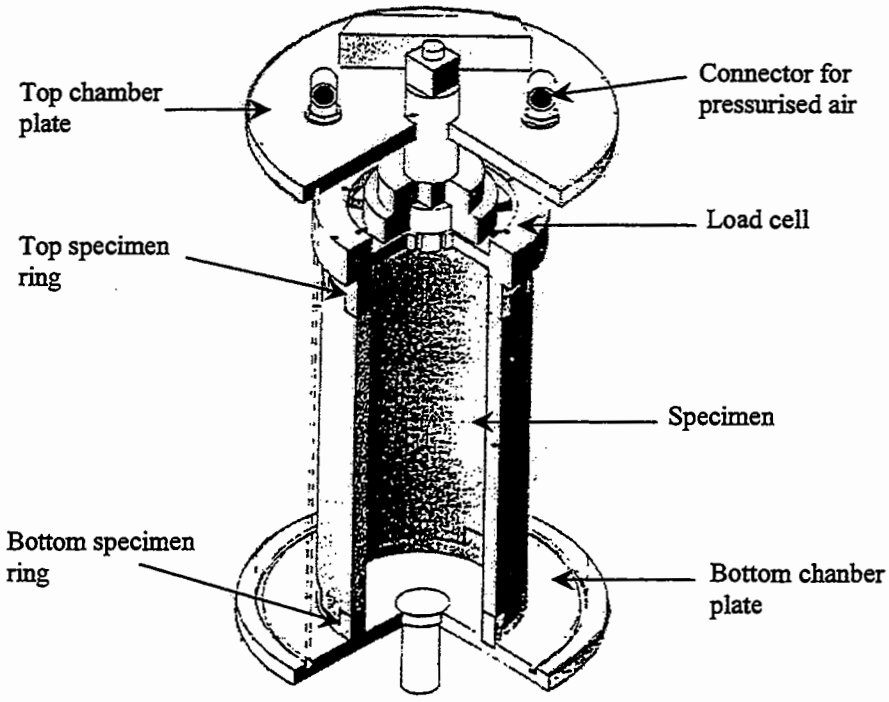

Figure 2.19 Section showing hollow cylinder specimen test configuration.

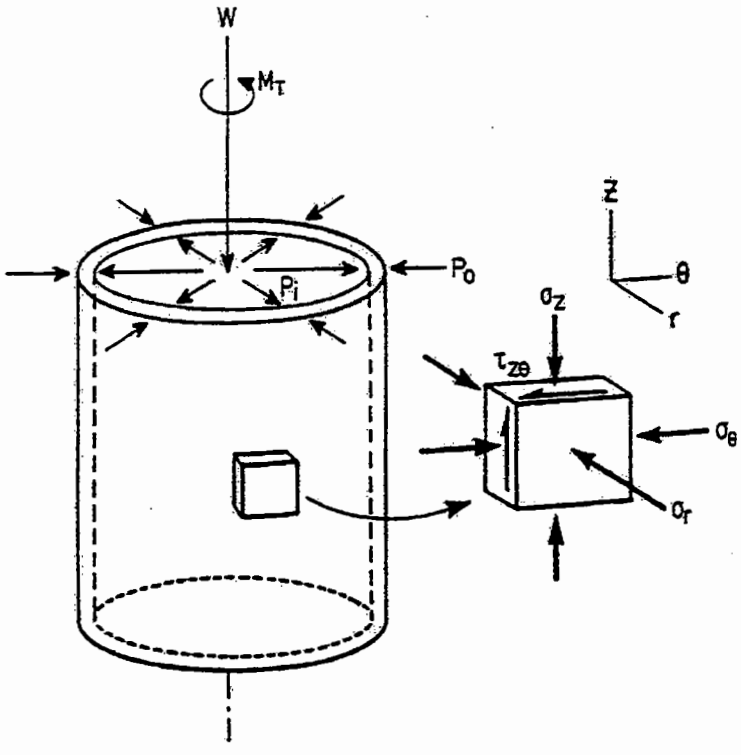

Figure 2.20 Idealised stress conditions in a hollow cylinder test: loading and stresses on wall element.

Binder Testing

3.1 Introduction

The viscoelastic characteristics of bitumens directly and significantly influence the performance of mixtures that use the bitumens as a binder. Knowledge of these characteristics is therefore very important to ensure good long-term performance when designing asphalt mixtures. Dynamic Shear Rheometers (DSR's) are used to measure the rheological characteristics, such as complex modulus and phase angle, of bitumen from which elastic and viscous properties can be defined [2, 123]. The DSR has become accepted as a test method for determining the properties of binder in the linear region [5, 10].

This chapter describes tests performed using the Bohlin DSR50 Dynamic Shear Rheometer on 50 Pen and 100 Pen grade bitumens over a range of frequencies, stress levels and temperatures. The bitumens selected for the rheological investigation were the binders used in the idealised and realistic mixtures in this research project. The test methodology used with the Bohlin DSR50 Dynamic Shear Rheometer is described, and the dynamic shear behaviour of the bitumens is described in terms of rheological master curves that show the variation in viscous and elastic components with loading frequency and temperature. Finally, the results from creep shear tests performed on these two types of bitumens are presented and the results are compared to previous results from uniaxial creep testing. A model is developed which describes the deformation behaviour of the bitumen subjected to shear loading in the DSR.

3.2 Dynamic Shear Rheometry (DSR)

A photograph of the Bohlin Dynamic Shear Rheometer is shown in Figure 3.1. The principles involved in the DSR test are illustrated schematically in Figure 3.2. The bitumen is sandwiched between a spindle and a base plate. The spindle, which can be either disc-shaped or conical, is allowed to rotate while the base plate remains fixed during testing. The test is performed by oscillating the spindle about its own axis such that a radial line through Point A moves to Point B, then reverses direction and moves past Point A to Point C, followed by a further reversal and movement back to Point A. This oscillation which is smooth and continuous as illustrated in Figure 3.2, comprises one cycle which can be continuously repeated during the test. Normally DSR tests are carried out over a range of frequencies and temperatures.

DSR tests can be carried out in controlled stress or controlled strain mode. In the controlled stress mode, a specified magnitude of shear stress at half the radius of the disc (R/2) is applied to the bitumen by application of a torque to the spindle. The resultant spindle rotation is measured, from which the magnitude of the shear strain is calculated at the edge of the disc (R). In the controlled strain mode, the magnitude of spindle rotation (i.e., magnitude of shear strain at the edge of the disc) is specified and the required torque needed to achieve this is measured. In a DSR test, assuming a sinusoidal shear stress of the form:

$$\tau = \tau_o e^{i\omega t} \tag{3.1}$$

where τ = shear stress

τ_o = shear stress amplitude

i = $\sqrt{-1}$

ω = angular frequency, rad/sec

the resulting shear strain, for a linear material, will be of the form:

$$\gamma = \gamma_o e^{i(\omega t - \delta)} \tag{3.2}$$

where γ = shear strain

γ_o = shear strain amplitude

δ = phase angle, degrees

Consequently, a complex shear modulus can be defined as:

$$G^* = \frac{\tau}{\gamma} = \frac{\tau_o}{\gamma_o} e^{i\delta} = \frac{\tau_o}{\gamma_o} (\cos\delta + i\sin\delta) \tag{3.3}$$

It can be seen that Equation 3.3 comprises real and imaginary parts that relate to the elastic (storage modulus) and viscous (loss modulus) responses respectively and are given by:

$$G' = \frac{\tau_o}{\gamma_o} \cos\delta = |G^*| \cos\delta \tag{3.4}$$

$$G'' = \frac{\tau_o}{\gamma_o} \sin\delta = |G^*| \sin\delta \tag{3.5}$$

where G' = storage modulus, Pa

G'' = loss modulus, Pa

The magnitude of the complex shear modulus is given by:

$$|G^*| = \sqrt{G'^2 + G''^2} = \frac{\tau_o}{\gamma_o} \tag{3.6}$$

In either mode of testing, the complex shear modulus, G^*, is calculated as the ratio of shear stress or shear strain as shown in Figure 3.3.

The relationship between the moduli obtained from a DSR test can be represented graphically on a plane Cartesian coordinate system such as that shown in Figure 3.4. The axes of the graph represents the extremes of the bitumen behaviour. This means

that the vertical axis represents completely viscous or fluid-like behaviour, whereas, the horizontal axis represents completely elastic or glass-like behaviour. At moderate to low temperatures, viscous behaviour can be achieved through long-term or very slow shear loading and at moderate to high temperatures, elastic behaviour can be realised through very rapid shear loading. In the vast majority of circumstances to which bituminous mixtures are subjected, the temperature and loading conditions are such that the behaviour of the bitumen lies somewhere between the two axes, which is represented by a vector with magnitude $|G^*|$ and direction δ degrees anti-clockwise from the horizontal axis. The phase angle indicates how much of the total complex modulus, G^*, is attributable to viscous behaviour and how much is attributable to elastic behaviour.

A viscosity value for the bitumen can also be obtained from the dynamic oscillatory test. This viscosity is known as the complex viscosity and is defined as the ratio of the complex modulus and the angular frequency:

$$\eta^* = \frac{G^*}{\omega} \tag{3.7}$$

where η^* = complex viscosity, (Pa.s)

The complex viscosity can also be termed the complex dynamic shear viscosity. Since the complex viscosity is a function of a complex number pair, a real part and an imaginary part of the complex viscosity can also be defined. The real part of the complex viscosity is termed the dynamic viscosity and defined as:

$$\eta' = \frac{G''}{\omega} \tag{3.8}$$

where η' = dynamic viscosity, (Pa.s)

the imaginary part of the complex viscosity is called the out of phase component of η^* and defined as:

$$\eta'' = \frac{G'}{\omega} \tag{3.9}$$

where η'' = out of phase component of η^* (Pa.s)

3.2.1 Apparatus

The DSR test system consists of parallel metal plates, an environmental chamber, a loading device and a control and data acquisition system. The metal plates are 8 mm or 25 mm in diameter with smooth polished surfaces and the base plate consists of a flat 2 mm raised plate with a 25 mm diameter. An environmental water chamber controls the temperature of the test specimen. Water is pumped through the test chamber by a separate circulating bath temperature control unit. The environmental water chamber and the temperature control unit can control the temperature of the specimen to an accuracy of ± 0.1°C [2].

The chamber completely encloses the top and bottom plates to minimise thermal gradients. The loading device applies a sinusoidal oscillatory torque to the specimen at various frequencies. When the load is strain controlled, the loading device applies a cyclic torque sufficient to cause an angular rotational strain accurate within 100 μrad of the specified strain. If the load is stress controlled, the loading device applies a cyclic torque accurate to within 10 mN.m of the specified torque. The control and data acquisition system provide a record of the test temperature, frequency, angular rotation and torque. In addition, the system calculates and records the shear stress, shear strain, complex modulus, $|G^*|$, and phase angle, δ.

3.2.2 Preparation of Apparatus

A 25 mm diameter spindle was firmly mounted on the upper test plate of the DSR. A zero gap between the upper and lower test plates was established, by manually spinning the moveable top plate. While the plate was spinning, the gap was closed until the movable plate touched the bottom fixed plate. The zero gap was reached when the plate stopped spinning completely. Finally, a gap setting of 1 mm plus 0.05 mm (for the 25 mm diameter test specimen) was established by moving the plates

apart. The same procedure was followed for the creep shear testing (see later) but with a 8 mm spindle and a gap setting of 2 mm. For the both 25 mm and 8 mm spindles, the gap settings of 1 mm and 2 mm respectively were taken from the Superpave binder testing specification manual [134].

3.2.3 Test Specimen Preparation and Test Procedure

The rheological properties of the 50 and 100 Penetration grade of binder used in the idealised and realistic bituminous mixtures (supplied by Shell Bitumen) were investigated. The bitumen was heated, stirring occasionally (to ensure homogeneity and to remove air bubbles) during the heating process until it was sufficiently fluid to pour. The plates in the environmental water chamber were heated to a temperature of approximately 65°C. The cover of the environmental water chamber was removed and the loading mechanism was raised along with upper plate to provide enough room to pour the bitumen specimen. The surfaces of both the plates were dried to ensure that the bitumen specimen adhered to both the plates uniformly.

A sufficient amount of bitumen was poured onto the centre of the bottom fixed plate to ensure that the bitumen was uniformly squeezed out between the plates for trimming. The loading mechanism and the upper plate were lowered to the required gap width plus 0.05 mm, squeezing out the excess bitumen from between the two plates. By moving a heated trimming tool around the upper and lower plate perimeters, the excess bitumen was trimmed from the specimen. When the trimming was completed, the gap was decreased by 0.05 mm to the desired testing gap. Finally, the cover of the environmental water chamber was replaced, ensuring that both the upper and lower plates and the bitumen specimen were immersed in water. The test was started after the temperature had remained at the desired temperature ± 0.1°C for at least 10 minutes (see [2, 10, 11] for further details).

3.2.4 Test Conditions

The combination of frequencies and temperatures used were:

- 7 frequencies (0.1, 0.2, 0.5, 1, 2, 5 and 10 Hz),
- 3 temperatures (20, 30 and 40°C).

These test conditions chosen relate to a range (low to high) of frequencies and temperatures. The main purpose for testing the binder in these conditions was to compare the SHRP rutting parameter with the repeated load axial test and the wheel tracking test results conducted at range of stress levels and corresponding temperatures (see Chapters 6 and 7).

3.3 Time-Temperature Superposition Principle

One of the primary analytical techniques used in analysing dynamic mechanical data involves the construction of master curves for thermorheologically simple materials. Research by various researchers has found that there is an interrelationship between temperature and frequency (or temperature and loading time) which, through the use of shift factors, can bring measurements performed at different temperatures to fit one overall continuous curve expressed as a function of reduced frequency or time scale. This continuous curve represents the binder behaviour at a given temperature for a large range of frequencies. The principle that is used to relate the equivalency between time and temperature and thereby produce the master curve is known as the time-temperature superposition principle or the method of reduced variables [2, 10].

Complex modulus curves at low temperatures and high frequencies tend to group together tending to a horizontal asymptote. This limiting elastic behaviour is found to be approximately independent of temperature [2]. This asymptote is called the glassy modulus, G_g. However, under viscous conditions, there is no convergence to a single viscous asymptote as viscosity strongly depends on temperature and therefore each temperature gives rise to a separate viscous flow asymptote (see Figure 3.5).

Because the limiting viscous behaviour is strongly temperature dependent and the elastic behaviour is not, it is possible to separate the influence of frequency and temperature. The concept of frequency-temperature superposition and time-temperature superposition is shown in Figure 3.6 which shows an asymptote pair for an arbitrary reference temperature T_r. If the temperature is increased from T_r to T there is a corresponding decrease in viscosity and hence $|G^*|$ by a factor a(T). However, the elastic asymptote shows negligible change during this temperature rise. The result is that the asymptote pair appears to be shifted a distance log a(T) along the log *f* axis, because the viscous asymptote has a unit slope.

The general viscoelastic response of a bitumen is represented by the transition region between the viscous asymptotic and elastic response and is represented by the curve for T_r. If a change in temperature causes the complex modulus curves to shift together over the same distance log a(T), the material is called "thermorheologically simple". A reference temperature can be chosen and the next higher modulus curve shifted to coincide with the reference temperature curve to obtain a value for the horizontal shift factor log a(T) and a more extended modulus curve. This procedure is repeated for all the other curves in succession to obtain the continuous modulus curve called a master curve. The effect of temperature on complex modulus is, therefore, to shift the curve of log $|G^*|$ versus log *f* along the log *f* axis without changing its shape.

The extended time or frequency scale used in a master curve is referred to as the reduced time or frequency scale, where reduced frequency scale is defined as:

$$\log f_r = \log f + \log a(T) \tag{3.10}$$

where f_r = reduced frequency, Hz
f = frequency, Hz
$a(T)$ = shift factor

The time-temperature superposition principle can be expressed mathematically as:

$$G^*(\omega, T) = G^*(\omega a(T), T_r) \tag{3.11}$$

where G^* = modulus and may be G′, G″, or $|G^*|$

$a(T)$ = shift factor

ω = loading frequency

T = temperature

T_r = reference temperature

The time-temperature superposition principle can be used to determine master curves and shift factors using the following procedure [2]:

- Dynamic data are first collected over a range of temperatures and frequencies,
- A standard reference temperature is then selected (typically 25°C or 0°C),
- The data at all other temperatures are then shifted with respect to time until the curves merge into a single smooth function.

The shifting may be done based on any of the viscoelastic functions, such as $|G^*|$, and if the time-temperature superposition principle is valid the other viscoelastic functions should all form continuous functions after shifting.

3.3.1 Shift Factors

The temperature dependence of the viscoelastic behaviour of bitumen is indicated by means of shift factors and expressed as:

$$a_T = a_T(T, T_{ref}) \tag{3.12}$$

and therefore depends, for a given system, only on the temperature.

Viscosity-temperature equations are used to characterise the temperature dependence of bitumens and therefore determine the shift factors needed for the time-temperature superposition principle. The Williams Landel and Ferry (WLF) equation [148] has been widely used to describe the relationship between the shift factors and temperature and thereby determine the shift factors for bitumens. The equation is

based on the free volume theory [40] and makes use of temperature differences which makes it suitable for practical applications. The WLF equation is given by:

$$\log a(T) = \log \frac{\eta_o(T)}{\eta_o(T_r)} = -\frac{c_1(T - T_r)}{c_2 + (T - T_r)} \tag{3.13}$$

where $a(T)$ = shift factor at temperature T

$\eta_o(T)$ = Newtonian viscosity at temperature T

$\eta_o(T_r)$ = Newtonian viscosity at the reference temperature T_r

c_1, c_2 = empirically determined coefficients

The WLF equation requires three constants to be determined, namely c_1, c_2 and T_r. The constants c_1 and c_2 can be calculated with respect to the reference temperature, T_r, from the slope and intercept of rearranged form of the WLF equation:

$$-\frac{T - T_r}{\log a(T)} = \frac{c_2}{c_1} + \frac{1}{c_1}(T - T_r) \tag{3.14}$$

The temperature dependency of bitumens can be described by one parameter T_r if universal constants are used for c_1 and c_2 in the WLF equation. Williams et al [148] proposed that if T_r is suitably chosen for each material then c_1 and c_2 could be allotted universal values of 8.86 and 101.6 respectively. For the T_r value they proposed that it was related to the glass transition temperature T_g by the relationship:

$$T_r - T_g = 50°C \tag{3.15}$$

An alternative equation that can be used to describe the relationship between the shift factors and temperature is the Arrhenius equation, which depends on the activation energy controlled and is given by:

$$\log a(T) = \frac{\Delta H_a}{2.303R}\left(\frac{1}{T} - \frac{1}{T_r}\right) \tag{3.16}$$

where $a(T)$ = horizontal shift factor

ΔH_a = activation energy, (160 - 260 kJ/mol)

R = universal gas constant (8.314 J/° K-mol)

T = temperature, °C

T_r = reference temperature, °C

The Arrhenius equation requires only one constant to be determined, which is the activation energy ΔH_a (for 50 and 100 Pen it was taken as 190kJ/mol). The reference temperature, T_r, can be arbitrarily chosen. Recently, Cheung [40] found that, at temperatures above the glass transition, the WLF equation is capable of describing the temperature dependence of the pure bitumen whereas, at temperatures lower than the glass transition, the Arrhenius equation is applicable. More comprehensive reviews about the shift factors can be found in [2, 40] and will not be repeated here.

The shift factors for both the 50 Pen and 100 Pen bitumens are given in Table 3.1. They were obtained by manually shifting the data to produce smooth $|G^*|$ master curves (see sub-section 3.3.2). In order to quantify the $|G^*|$ shift factors for both the 50 and 100 Pen bitumens they were compared with WLF and Arrhenius (Equations 3.14 & 3.16) determined shift factors (see Figures 3.7 & 3.8). Since DSR tests on the two bitumens were carried out at an intermediate range of temperatures (20°C, 30°C and 40°C), it can be seen from these figures that both the equations compare well with the manually obtained shift factors. The reference temperature was taken as 30°C.

Table 3.1 Shift Factors

Bitumen	Test Temp (°C) (T)	Temp. Difference ($T-T_r$)	Shift Factor Modulus $\|G^*\|$, Log a(T)	Shift Factor Phase angle δ, Log a(T)
50 Pen	20	-10	1.02	1.08
	30 (T_r)	0	0	0
	40	+10	-0.96	-1.11
100 Pen	20	-10	1.03	1.23
	30 (T_r)	0	0	0
	40	+10	-1.01	-1.30

It can be seen from Table 3.1 that, in addition to the complex modulus shift factors, the shift factors for phase angle master curves are also given. It can also be seen that for both bitumens the shift factors are slightly different for $|G^*|$ and δ. Differences in the shift factors for construction of the master curves for $|G^*|$ and δ for the same bitumen have been noted by many researchers (for example [2, 64]). It was found that using the shift factors derived from the complex modulus master curves did not produce smooth master curves for the phase angle [2, 64] (see for example Figure 3.9). Consequently, for $|G^*|$ and δ different shift factors were derived for a construction of smooth master curves for both 50 and 100 Pen bitumens.

3.3.2 Master Curves

In their simplest form, master curves are produced by manually shifting the modulus or phase angle verses frequency plots (isotherms) at different temperatures along the logarithmic frequency axis. Breaks in the smoothness of the master curve can indicate the presence of structural changes with temperature within the bitumen, as would be found for waxy bitumens, highly structured 'GEL' type bitumens and polymer modified bitumens [2].

3.4 SHRP Rutting Parameter

The Strategic Highway Research Program (SHRP) have developed a number of rheological tests to measure fundamental binder mechanical properties which have been used to develop performance related specifications [2]. A measurement of non-recoverable deformation of bitumen at high temperatures was established as a suitable rutting parameter for bitumen. A loading time of 0.1 seconds was chosen to represent the loading time within the pavement, which can be attributed to a truck tyre travelling at 80 km/h [111]. For dynamic mechanical analysis using the DSR, a sinusoidal loading frequency of 10 rad/s (1.59Hz) was recommended by SHRP [2].

For permanent deformation the specification was taken as the inverse of the loss compliance (1/J") which can be shown to be equivalent to the magnitude of the complex shear modulus divided by the phase angle ($G^*/\sin\delta$) from the DSR [2].

3.5 DSR Results

Isochronal[1] plots of complex modulus $|G^*|$ and phase angle δ, at frequencies of 0.1Hz, 1Hz and 10Hz for 50 Pen and 100 Pen grade bitumens are shown in Figures 3.10, 3.11 and 3.12. It can be seen from these figures that, as expected, with an increase in temperature there is a decrease in complex modulus and an increase in the phase angle indicating more viscous behaviour.

At low temperatures $|G^*|$ values are higher and the phase angle values tend to be lower. It can also be seen from these figures that, at a particular temperature, as the frequency tends towards a higher value there is a subsequent increase in the $|G^*|$ values. For example, at 20°C for both 50 and 100 Pen bitumens there was an increase in $|G^*|$ by approximately one order of magnitude when the loading frequency was increased from 0.1 Hz to 10 Hz (see Figures 3.10 and 3.12). Similar behaviour can be seen at 30°C and 40°C. As it can be seen from these figures, $|G^*|$ values for 50 Pen grade bitumen are higher than the 100 Pen bitumen.

The effect of loading frequency on the phase angle for both the bitumens is clearly illustrated in Figures 3.10, 3.11 and 3.12. It can be seen from these figures that the phase angle decreases with an increase in the loading frequency. The isochronal plot for the phase angle in Figure 3.10 shows that the 50 Pen bitumen is slightly more viscous then the 100 Pen bitumen at low loading frequencies. At a loading frequency of 10Hz (Figure 3.12), it can be seen that 50 Pen bitumen demonstrates more elastic behaviour compared to 100 Pen bitumen.

The isochronal plots of viscosity[2] against temperature for the 50 Pen bitumen at seven frequencies (0.1-10Hz) are shown in Figure 3.13. It can be seen from this figure that, as expected, the viscosity decreases with an increase in temperature. It can also be seen that, at a particular temperature, the viscosity decreases as the loading frequency is increased. Similar findings were observed for 100 Pen bitumen (see Figure 3.14).

[1] In a dynamic test such as DSR test, an isochronal plot or isochrone is an equation or a curve on a graph, representing the behaviour of a system at a constant frequency or loading time.
[2] Dynamic shear viscosity calculated from Equation 3.8.

A typical logarithmic isothermal[3] plot for the 50 Pen bitumen is shown in Figure 3.15, where the magnitude of the complex modulus is plotted against frequency. As expected, there is an increase in $|G^*|$ values at higher frequencies and lower temperatures and a decrease in $|G^*|$ at higher temperatures and lower frequencies.

Figure 3.16 shows a typical isothermal plot of phase angle against log of frequency for the 50 Pen bitumen. Again, it can be seen from this figure that the behaviour of the bitumen changes from viscous to more elastic behaviour at higher loading frequencies.

The complex modulus and phase angle master curves for the 50 and 100 Pen bitumens are shown in Figures 3.17 and 3.18. It can be seen from Figures 3.15 and 3.16, that the curves for 50 Pen bitumen in Figures 3.17 and 3.18 were shifted horizontally with respect to one reference temperature to form a one continuous curve over a reduced time scale. The shift factors for both the bitumens are given in Table 3.1. It can be seen from Figure 3.17, that at low temperatures or short loading times, the values of $|G^*|$ for both the bitumens change only slightly with frequency, which is typical for viscoelastic materials in the glassy region. At intermediate frequencies, the modulus decreases with decreasing frequency at an increasing rate, denoting more viscous behaviour at long loading times or high temperatures.

The phase angle master curves for 50 and 100 Pen bitumens are shown in Figure 3.18. They are produced using the shift factors given in Table 3.1. However, unlike the complex modulus master curves, the phase angle master curves differ in appearance. It can be seen from this figure that at high temperatures or low loading frequencies the phase angle is around 80° for both the bitumens, which indicates highly viscous behaviour. As the frequency increases there is a transition from viscous behaviour to elastic behaviour. Between phase angles of 50°-70°, the bitumen exhibits both viscous and elastic properties. It can also be seen from the figure that, as the loading frequency increases or the temperature decreases, the phase angle reduces further indicating more elastic behaviour.

[3] In a dynamic test, an isothermal plot or isotherm is an equation or a curve on a graph, representing the behaviour of a system at a constant temperature.

3.6 Creep Shear Tests

In order to investigate the steady-state deformation properties of the binders, constant stress creep tests were performed on 50 and 100 Pen bitumens using the DSR. An 8-mm spindle with a gap setting of 2 mm was used for this testing programme. Tests were conducted at 20°C over a range of stress levels that were expected to cover both linear and non-linear behaviour [40].

Typical test results from creep tests on the 50 and 100 Pen binders are shown in Figures 3.19 and 3.20 respectively, where the creep shear strain at the outside of the disc is plotted as a function of time elapsed after the application of the stress. It can be seen from these figures that the creep curve can be divided into three regions: a primary region where the strain rate decreases, a secondary creep region where the strain rate is approximately constant and a tertiary creep region where the strain increases. The secondary creep region is used to define the steady-state shear strain rate (see Figure 3.19).

Steady-state creep behaviour observed for the 50 and 100 Pen bitumens is presented in Figures 3.21 and 3.22, where the steady-state shear strain rate (calculated at the outside of the disc) is plotted against the steady-state creep stress (calculated at half the disc radius). The figures illustrate that the steady-state deformation behaviour of both the 50 Pen and 100 Pen grades of bitumens is similar in shape. However, the 100 Pen grade of bitumen was found to have higher strain rates at a particular applied stress level compared to the 50 Pen grade of bitumen (i.e. 100 Pen bitumen is softer than 50 Pen bitumen). To account for variability associated with sample preparation, various creep test repeats were conducted at particular stress levels. These are also shown in these figures. It can be seen from Figure 3.21 and 3.22 that at low stress levels (<70kPa) the experimental points tend to lie on a straight line with a slope of 1. This indicates that the deformation behaviour in this region is linear viscous flow. However, above 70 kPa the points tend to lie again on a straight line but with a slope of approximately 2.4, indicating a non-linear (power law) creep behaviour.

However, interpretation of DSR results is complicated because the shear strain rate varies from zero at the centre of the bitumen disc to maximum value at the outer edge. Consequently a simple model was developed to aid interpretation of these results.

3.6.1 DSR Model

Consider a bitumen ring of thickness 'δr', a distance 'r' from the centre of the disk (see Figure 3.23). If the shear stress acting on the ring is τ_r, the torque (δT) required to generate this shear stress is given by:

$$\delta T = \tau_r 2\pi r^2 \delta r \tag{3.17}$$

Consequently, the total torque for a disc of radius 'R' is given by:

$$T = 2\pi \int_0^R \tau_r r^2 dr \tag{3.18}$$

Assuming that below a certain radius, R_1, the quasi-static stress-strain rate behaviour of the bitumen is linear, and is given by:

$$\tau = \eta \dot{\gamma} \tag{3.19}$$

where τ = shear stress

$\dot{\gamma}$ = shear strain-rate

η = shear viscosity (linear region where $n_c = 1$)

Above this radius, R_1, it will be assumed that the quasi-static stress-strain rate behaviour of the bitumen is non-linear and is given by:

$$\tau = \eta_1 \dot{\gamma}^m \tag{3.20}$$

where η_1 = shear viscosity (non-linear region)

m = inverse of the creep exponent ($m = 1/n_c$ where $n_c = 2.4$)

Equation 3.19 and 3.20 can now be substituted into Equation 3.18 to give:

$$T = 2\pi\left[\eta\int_0^{R_1}\dot{\gamma}\,r^2\,dr + \eta_1\int_{R_1}^{R}\dot{\gamma}^m r^2\,dr\right] \tag{3.21}$$

In a DSR test, the stress and strain rate parameters calculated are:

$$\tau_d = \frac{2T}{\pi R^3} \tag{3.22}$$

$$\dot{\gamma}_d = \frac{\dot{\theta}R}{h} \tag{3.23}$$

where τ_d and $\dot{\gamma}_d$ = DSR shear stress and strain respectively

T = torque

R = radius of parallel disk

$\dot{\theta}$ = angular velocity

h = gap between parallel disk

Substituting Equation 3.22 and 3.23 into Equation 3.21 and integrating gives:

$$\tau_d = 4\left[\frac{\eta\dot{\gamma}_d}{4}\left(\frac{R_1}{R}\right)^4 + \frac{\eta_1\dot{\gamma}_d{}^m}{(m+3)}\left(1-\left(\frac{R_1}{R}\right)^{m+3}\right)\right] \tag{3.24}$$

Assuming that the uniaxial transition between linear and non-linear behaviour happens at a uniaxial stress denoted by σ_T, it can be shown that this corresponds to a shear stress of [40]:

$$\tau_T = \frac{\sigma_T}{3} \tag{3.25}$$

where τ_T = transition shear stress

σ_T = transition normal stress

Substituting Equation 3.19, Equation 3.25 gives:

$$\frac{\sigma_T}{3} = \eta\dot{\gamma} = \frac{\eta R_1 \dot{\theta}}{h} \tag{3.26}$$

Substituting Equation 3.23 into Equation 3.26 gives:

$$\frac{R_1}{R} = \frac{\sigma_T}{3\eta\dot{\gamma}_d} \qquad \left(\frac{R_1}{R} \leq 1\right) \tag{3.27}$$

It can now be seen that Equation 3.27 can be used to determine the extent of the linear and non-linear regions within the disc of material. It can be seen from Equation 3.27 that at low strain rates R_1/R tends to 1 (i.e. the whole disc is operating within the linear region) whereas at high strain rates R_1/R tends to 0 (i.e. the whole disc is operating within the non-linear region).

It can be seen from Equation 3.24 that the DSR shear strain rate ($\dot{\gamma}_d$) can be plotted against the DSR shear stress (τ_d) provided the following parameters are known: σ_T, η, η_1 and m. However, since σ_T defines the transition point between linear and non-linear behaviour there is a unique relationship between η and η_1 given by:

$$\eta_1 = 3^{m-1}\eta^m {\sigma_T}^{1-m} \tag{3.28}$$

Figures 3.21 and 3.22 also show Equation 3.24 (solid line). The parameters σ_T, η, and m were chosen to best fit the experimental data and are given in Table 3.2. It can be seen from these figures that the model fits the data well in both the linear and non-

linear regions. In a DSR testing geometry the strain rate varies from the centre to the outer perimeter of the disc, thus it was considered important to investigate whether DSR could be used to characterise the permanent deformation behaviour of the pure bitumen. Recently Cheung [40] modelled the uniaxial tensile behaviour of the pure 50 pen bitumen (see Chapter 2). Consequently, to compare the results with Cheung [40] it is necessary to adjust the shear stress-strain rate data shown in Figure 3.21 and 3.22.

At temperatures above the glass transition, the steady-state deformation behaviour of pure bitumen in uniaxial loading has been described by the following power law equation (see Cheung [40]):

$$\left(\frac{\dot{\varepsilon}}{\dot{\varepsilon}_0}\right)=\left(\frac{\sigma}{\sigma_0}\right)^n \tag{3.29}$$

whilst under pure shear, the behaviour is given by [40]:

$$\left(\frac{\dot{\gamma}}{\dot{\varepsilon}_0}\right)=\sqrt{3}^{n+1}\left(\frac{\tau}{\sigma_0}\right)^n \tag{3.30}$$

where σ and $\dot{\varepsilon}$ = uniaxial stress and strain rate respectively

σ_o and $\dot{\varepsilon}_o$ = material constants for bitumen

τ and $\dot{\gamma}$ = shear stress and strain rate respectively

n = creep exponent (material constant)

It can be seen from Equations 3.29 and 3.30 that bitumen behaviour in tension and in shear is related by the factor $\sqrt{3}^{n+1}$. At low stress levels/strain rates where the bitumen is linearly viscous (n = 1), this factor equals 3, whereas at higher strain rates/stress levels where the bitumen has a power law creep exponent of n = 2.4, this factor equals 6.47.

The uniaxial model developed by Cheung [40] to describe the behaviour of a 50 Pen grade of bitumen is also shown in the Figure 3.21 (dashed line). For comparison the model fitted to the DSR results, adjusted by multiplying the strain rate by 1/3, is also shown (solid line). It can be seen that these two curves agree reasonably well bearing this in mind that the two bitumens tested were from different batches although they were of the same nominal grade (50 Pen). It can also be seen from this figure that the factor of 3 between the shear results and tensile results seems to fit the data both in the linear and non-linear regions. The factor of 6.47 was found not to fit the data very well. Consequently, to better match the tensile results a correction factor of 3 was used. This factor of 3 also agrees with previous results obtained by Cheung [40] for his range of shear tests conducted on the same grade of bitumen and according to him, in the non-linear region, reflects the collapse behaviour of the elastic asphaltene network prior to the steady-state creep behaviour where the expected correlation factor should be $\sqrt{3}^{n+1} \cong 6$ (see Cheung [40] for further details). However, interpretation of shear tests results is more complicated and the reasons are not fully understood. In the non-linear region the strain rates are predominantly high and there may be damage accumulating in the specimen. This requires further investigation.

Table 3.2 DSR Model Parameters

Model Parameters	Bitumen (Penetration grade)	
	50	100
η (Pa.s)	2E+6	6E+5
σ_T (Pa)	225E+3	
m	0.42	

3.7 Conclusions

The following conclusions can be drawn from this chapter:

- DSR testing has been used to understand the rheological behaviour of the 50 Pen and 100 Pen grades of bitumen over a range of frequencies (0.1Hz-10Hz) and 3 temperatures (20°C, 30°C and 40°C).

- Rheological data obtained has been presented in the form of isochronal plots, isothermal plots and master curves.

- The isochronal plots of $|G^*|$ versus temperature show that there is a decrease in complex modulus with an increase in temperature. At a particular temperature $|G^*|$ was found to increase with an increase in loading frequency.

- The phase angle isochronal plots show that there is a reduction in phase angle with the decrease in temperature. At a particular temperature there was found to be a reduction in phase angle as the frequency increased.

- The isochronal plots of viscosity against temperature show that the viscosity decreases with an increase in temperature. It was also found that at a particular temperature, the viscosity decreases as the loading frequency increases.

- The viscoelastic nature of the bitumen was presented in the form of complex modulus and phase angle master curves. It was found that at low temperatures or lower loading times the value of $|G^*|$ increases only slightly with increasing frequency. At intermediate frequencies, the $|G^*|$ decreases with decreasing frequency at an increasing rate, denoting more viscous behaviour at long loading times or high temperatures.

- At high temperatures or low loading frequencies the phase angle value was found to be higher, which indicates highly or a dominant viscous behaviour. As the frequency increases to a higher value there is a transition from a viscous behaviour to elastic behaviour, called the viscoelastic region, where the bitumen exhibits both viscous and elastic properties. As the loading frequency increases or

the temperature decreases, the phase angle reduces further and tends towards more elastic properties until it reaches its limiting phase angle value.

- Creep tests performed on the 50 Pen and 100 Pen bitumens indicate that at low stress levels (≤ 70kPa) the deformation behaviour of the pure bitumen is linear $n = 1$. At higher stress levels the deformation behaviour is non-linear and can be characterised by an effective creep exponent of $n = 2.4$.

- A simple model has been developed which describes the deformation behaviour of the bitumen subjected to shear loading in the DSR. The model relates steady-state shear stress to steady-state shear strain rate and agrees well with experimental results.

- The correction factor of 3 was found to give good results when the DSR model was corrected for uniaxial tensile conditions and compared to data obtained by another researcher.

- Over the regimes tested, the DSR was found to be a convenient test tool in assessing the deformation behaviour of pure bitumen.

3.8 Figures

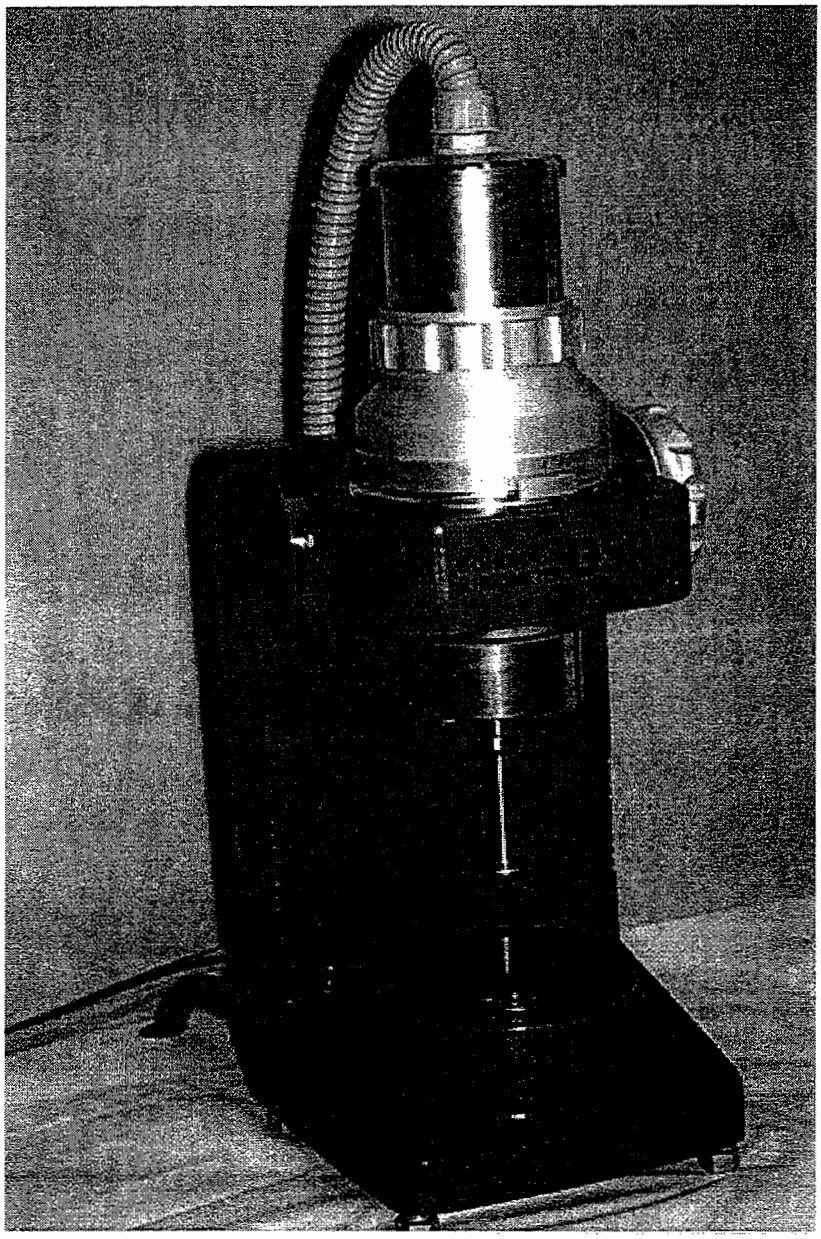

Figure 3.1 Dynamic Shear Rheometer (DSR).

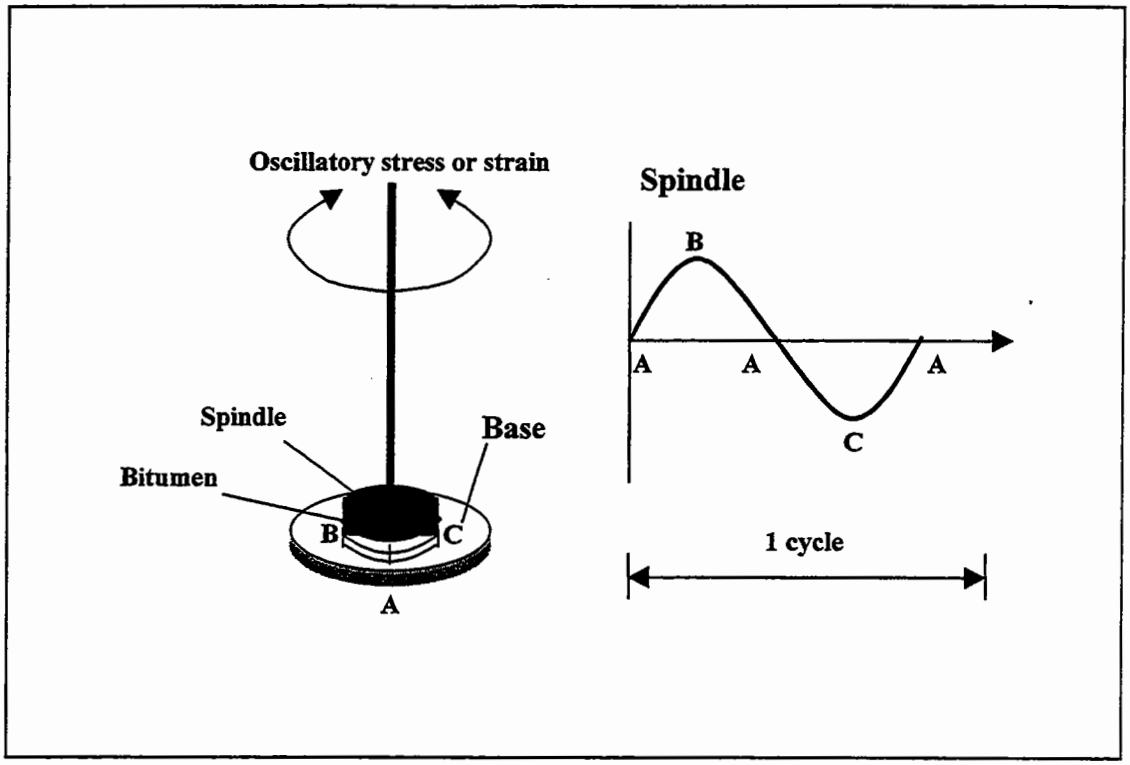

Figure 3.2 Principles of operation of torsional-type Dynamic Shear Rheometers (DSR's).

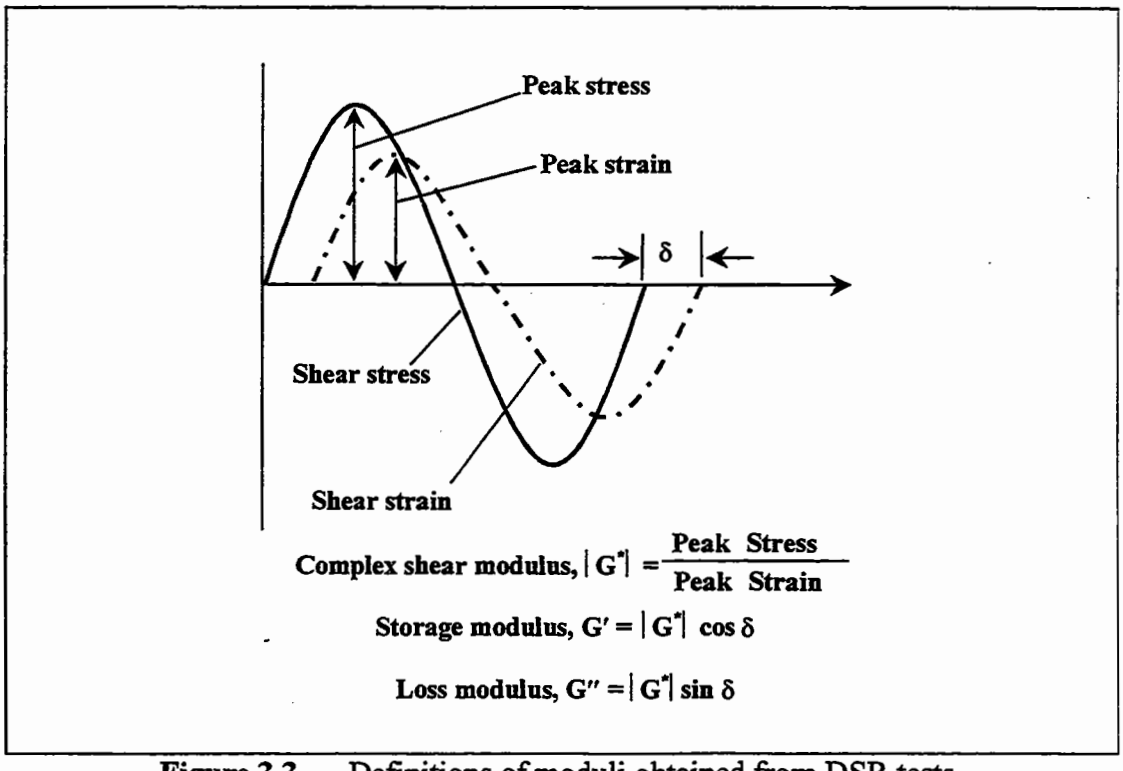

Figure 3.3 Definitions of moduli obtained from DSR tests.

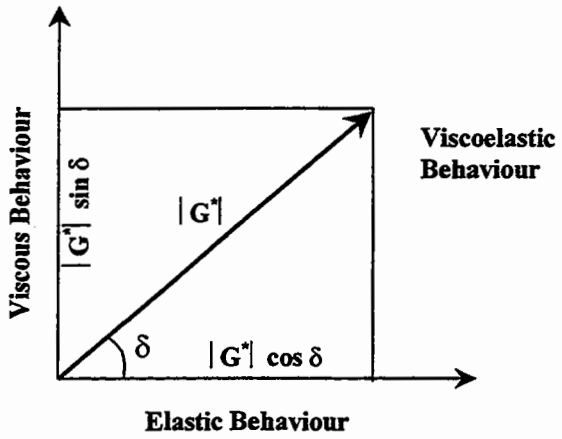

Figure 3.4 Viscoelastic behaviour of bitumen.

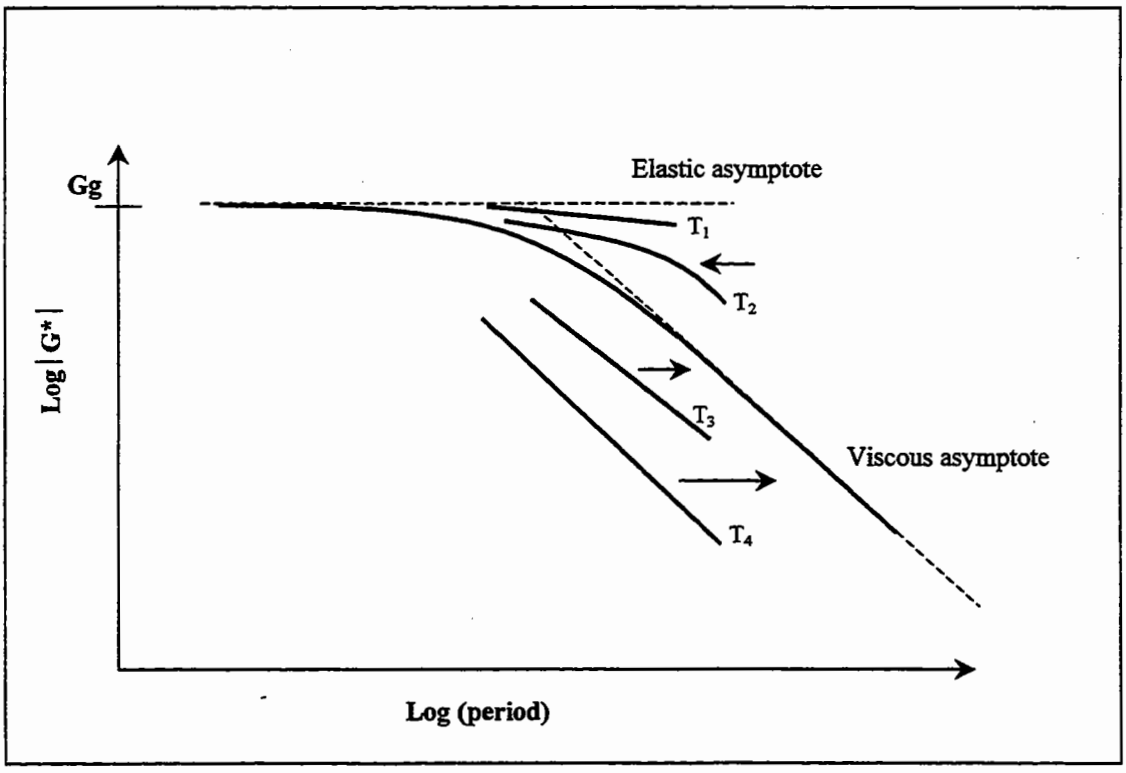

Figure 3.5 Linear viscoelastic response of bitumen.

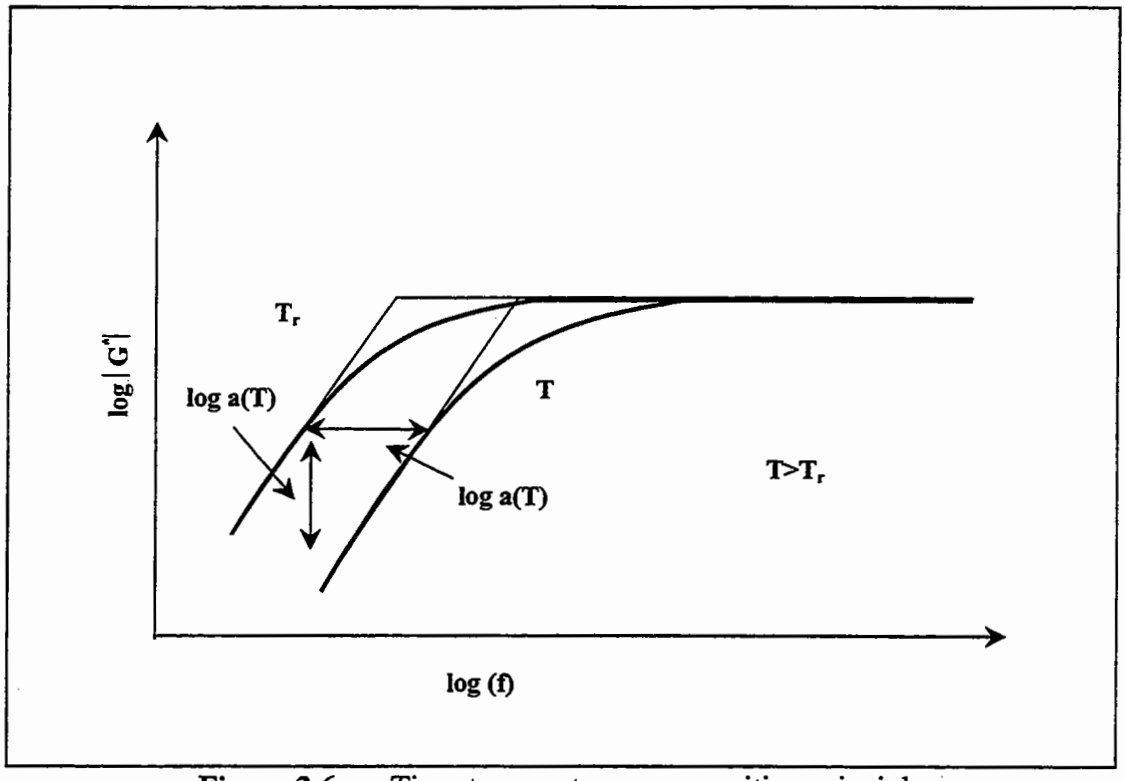

Figure 3.6 Time-temperature superposition principle.

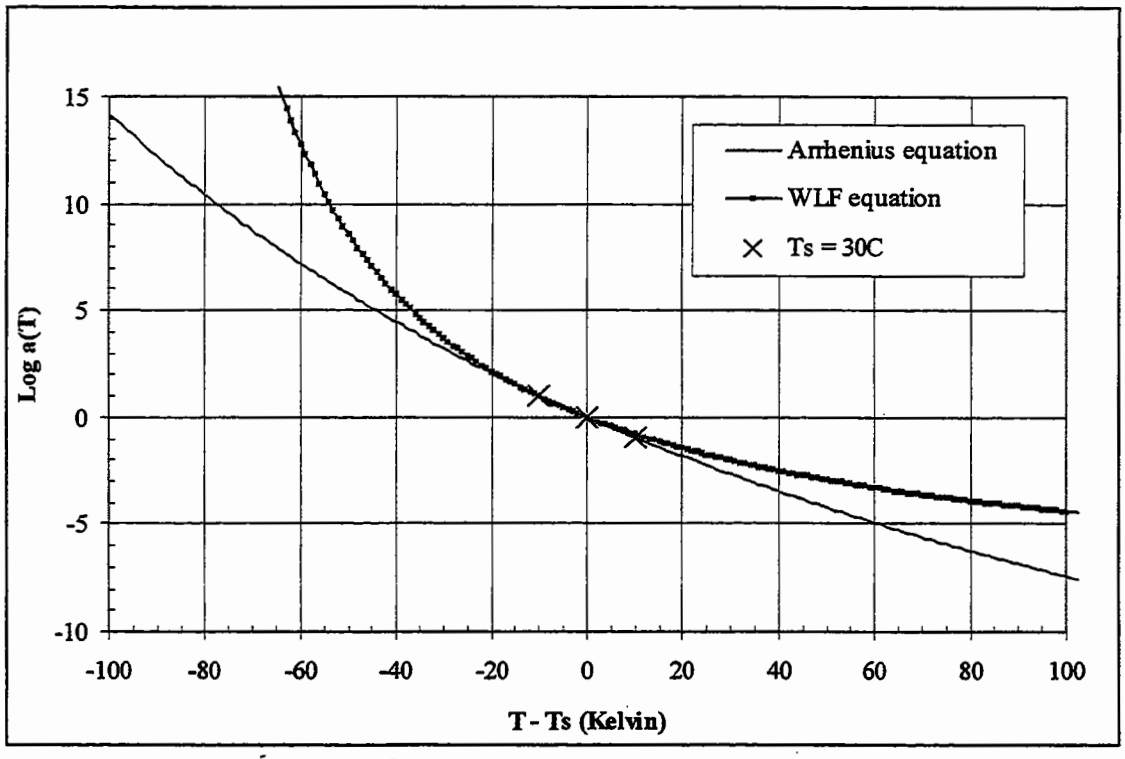

Figure 3.7 Comparison of Arrhenius and WLF equation with manually obtained shift factors for 50 Pen bitumen.

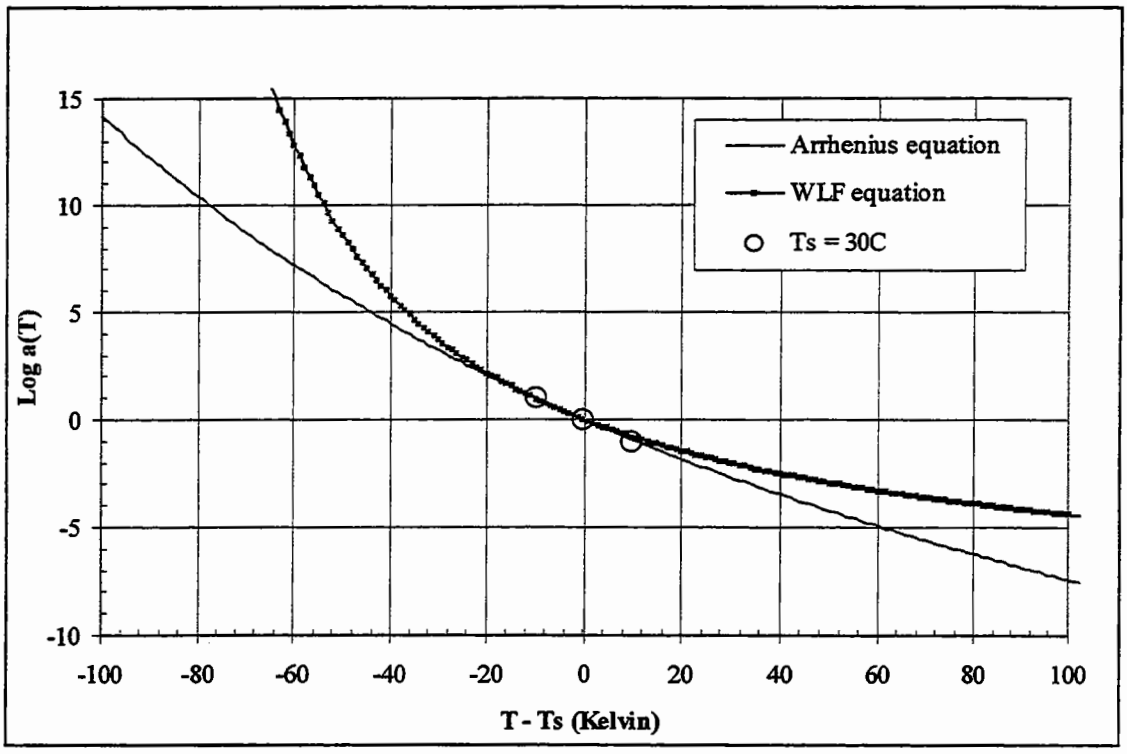

Figure 3.8 Comparison of Arrhenius and WLF equation with manually obtained shift factors for 100 Pen bitumen.

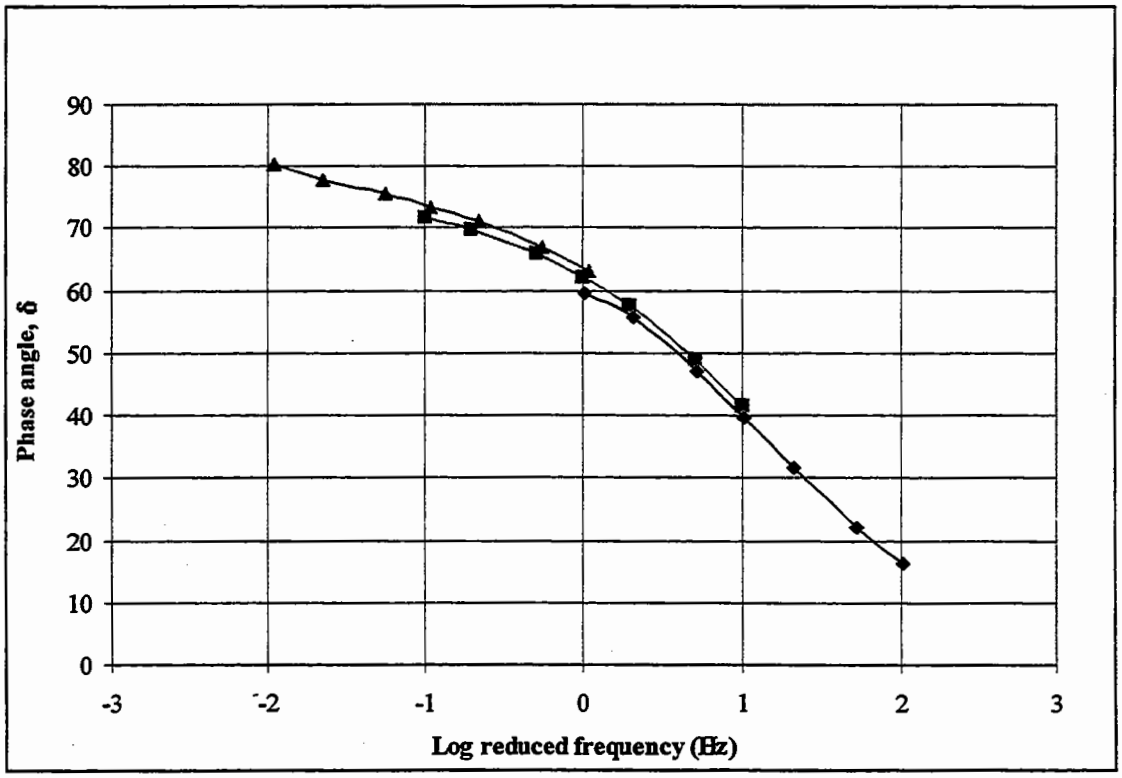

Figure 3.9 Phase angle master curve from $|G^*|$ derived shift factors (50 Pen).

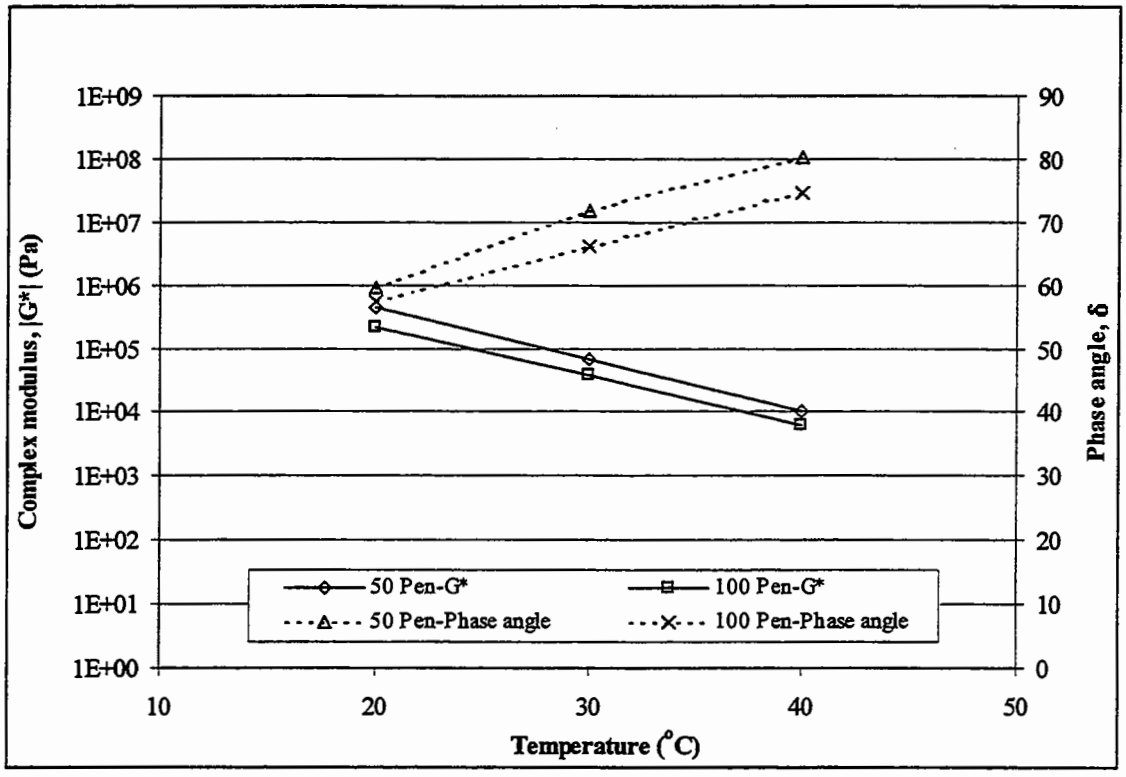

Figure 3.10 Isochronal plot at 0.1 Hz for 50 and 100 Pen grade bitumens.

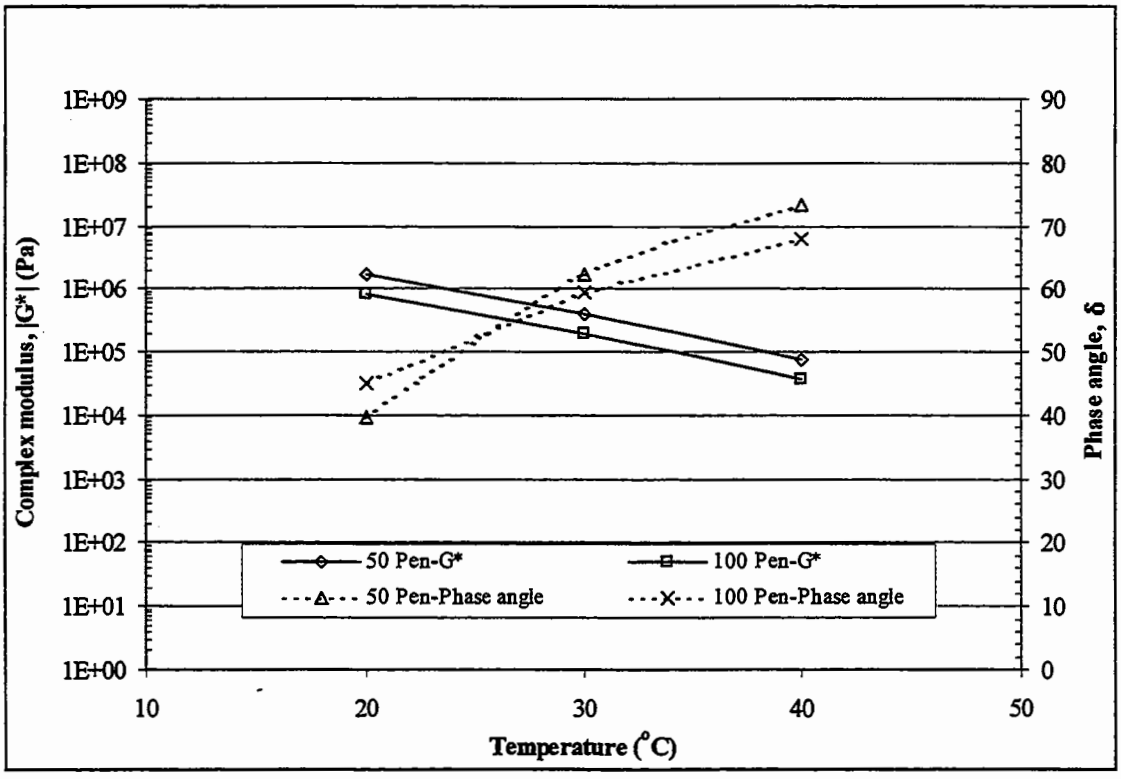

Figure 3.11 Isochronal plot at 1 Hz for 50 and 100 Pen grade bitumens.

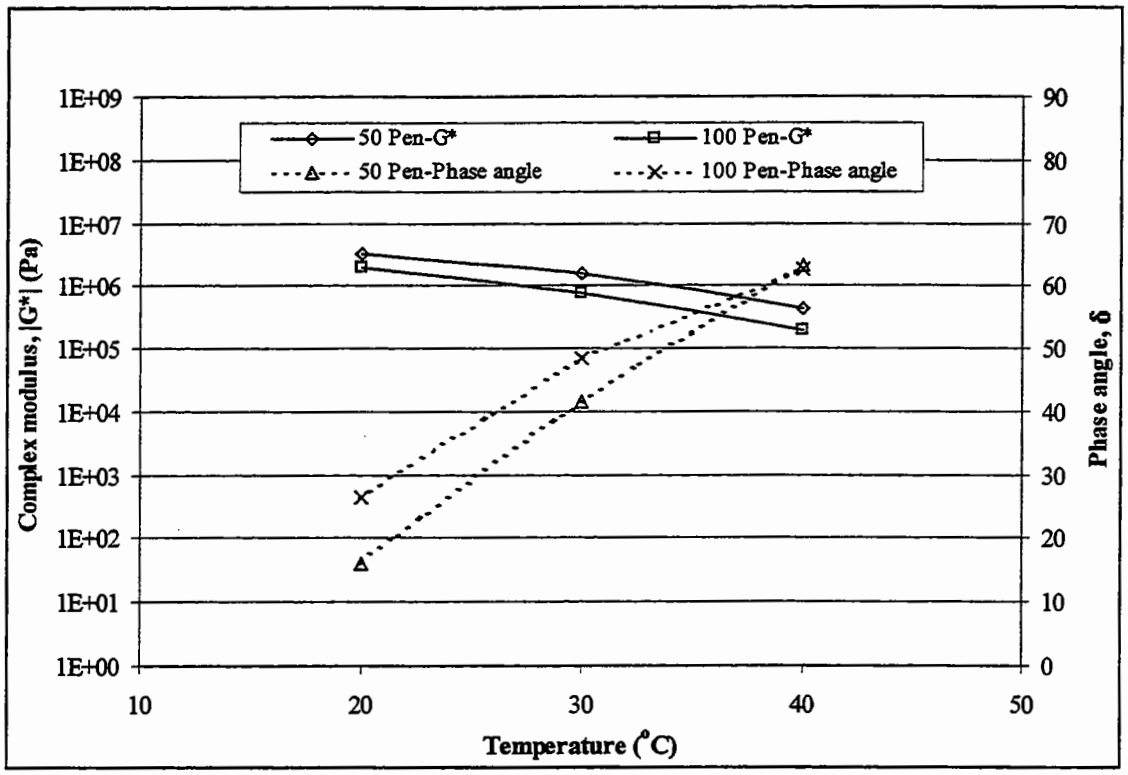

Figure 3.12 Isochronal plot at 10 Hz for 50 and 100 Pen grade bitumens.

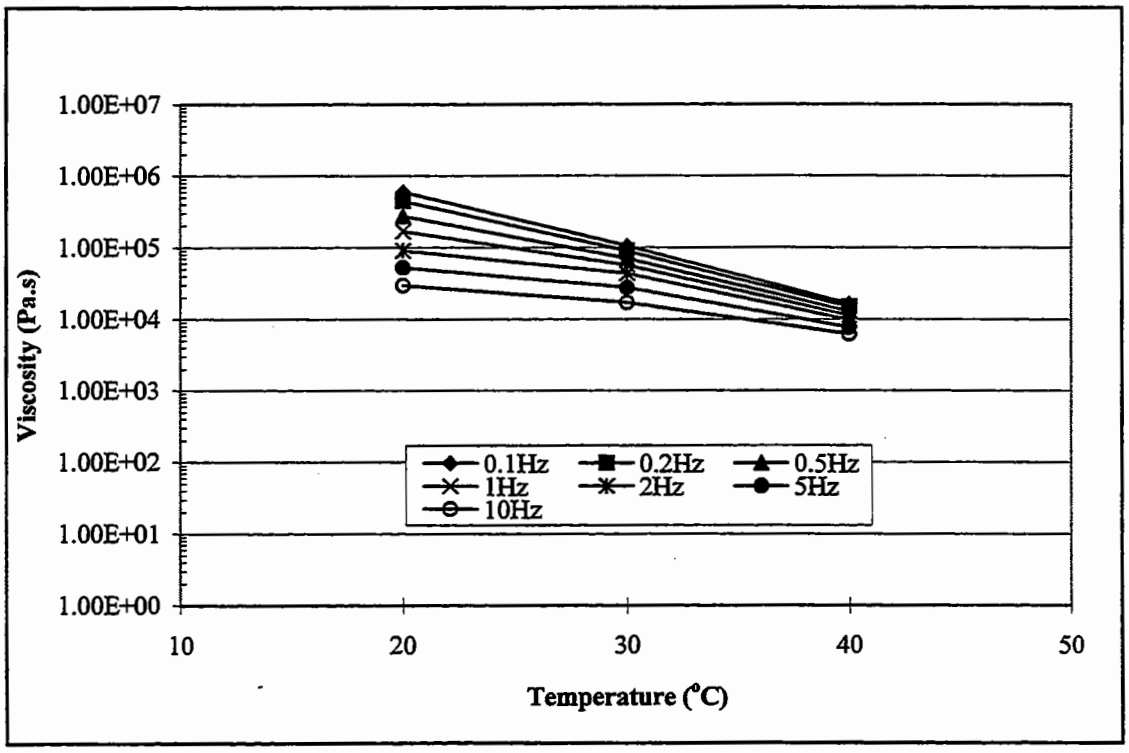

Figure 3.13 Isochronal plot of viscosity for 50 Pen grade bitumen.

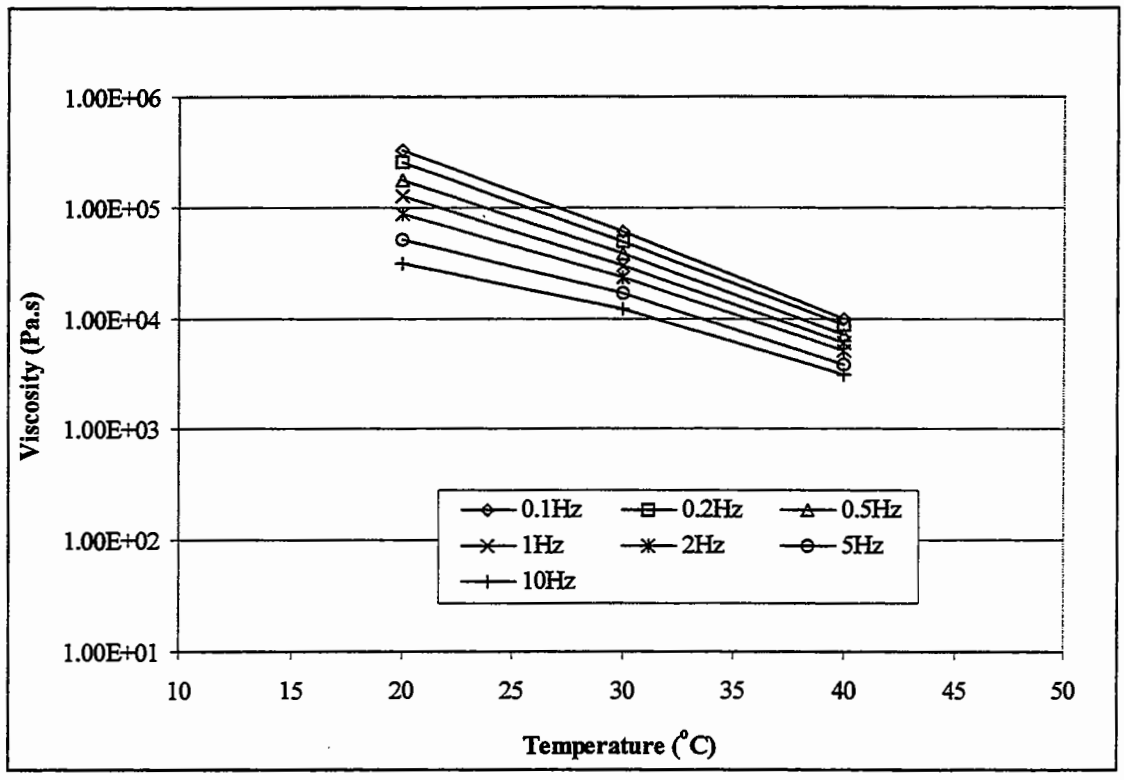

Figure 3.14 Isochronal plot of viscosity for 100 Pen grade bitumen.

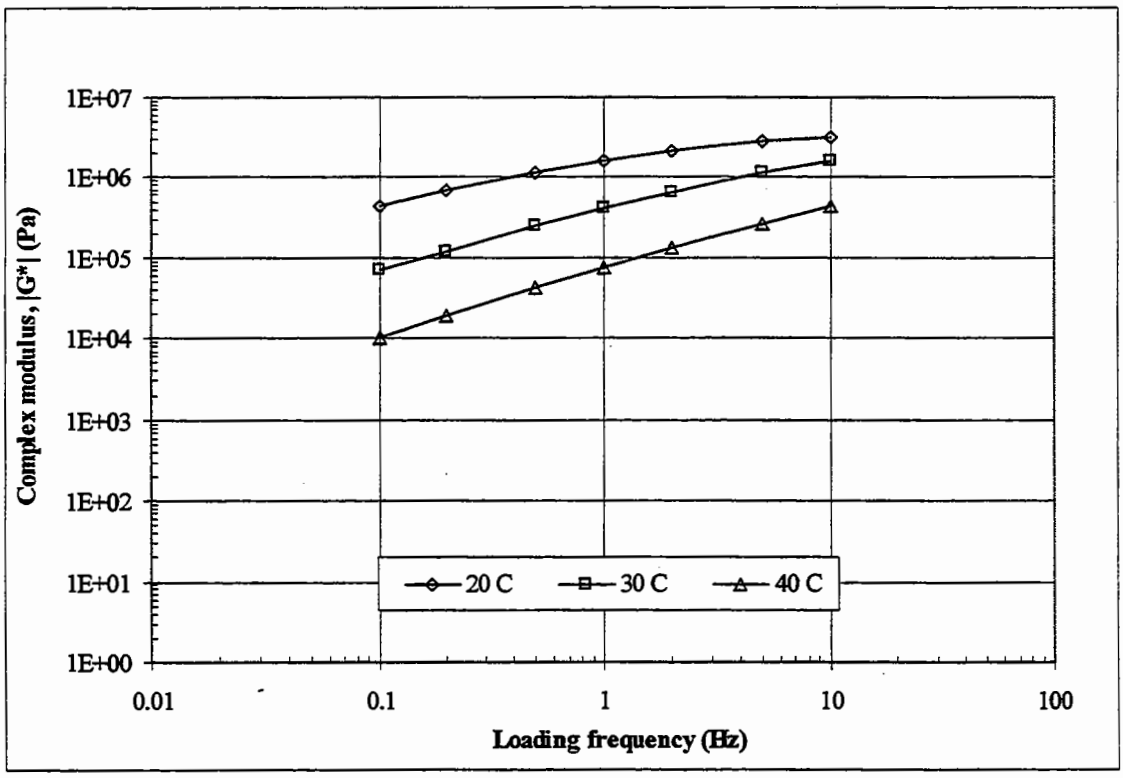

Figure 3.15 Isothermal plot of complex modulus for 50 Pen grade bitumen.

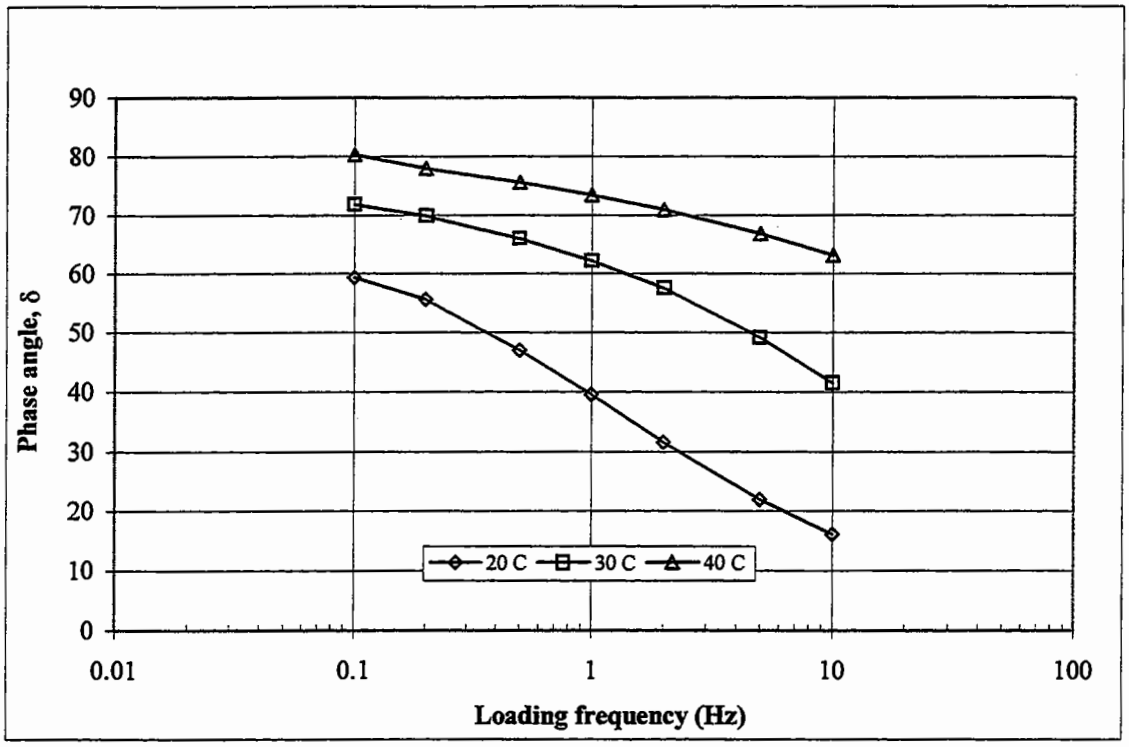

Figure 3.16 Isothermal plot of phase angle for 50 Pen grade bitumen.

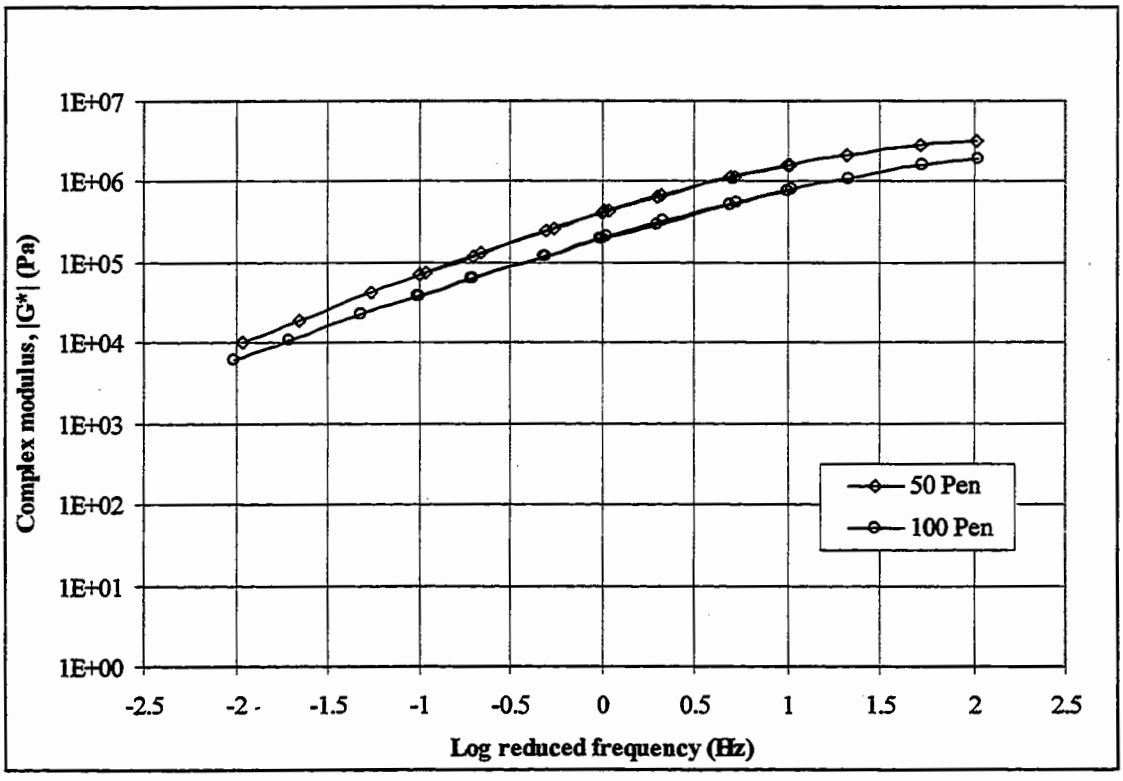

Figure 3.17 Complex modulus master curves for 50 and 100 Pen grade bitumens.

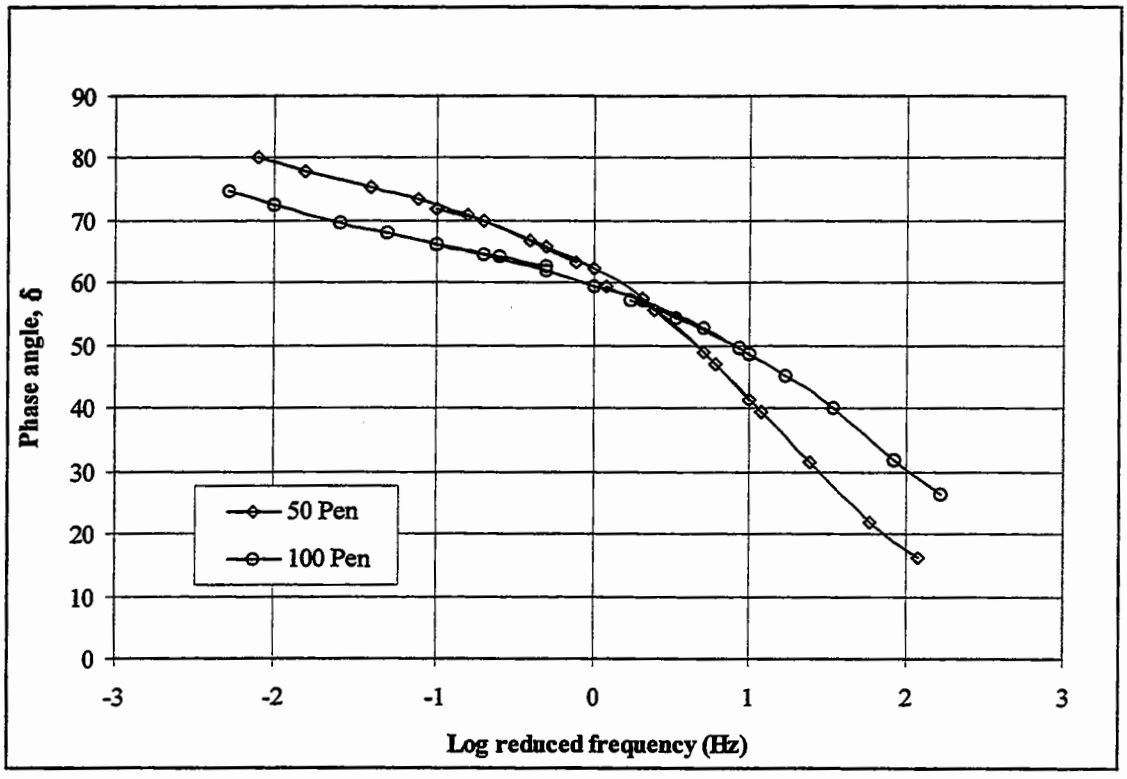

Figure 3.18 Phase angle master curves for 50 and 100 Pen grade bitumens.

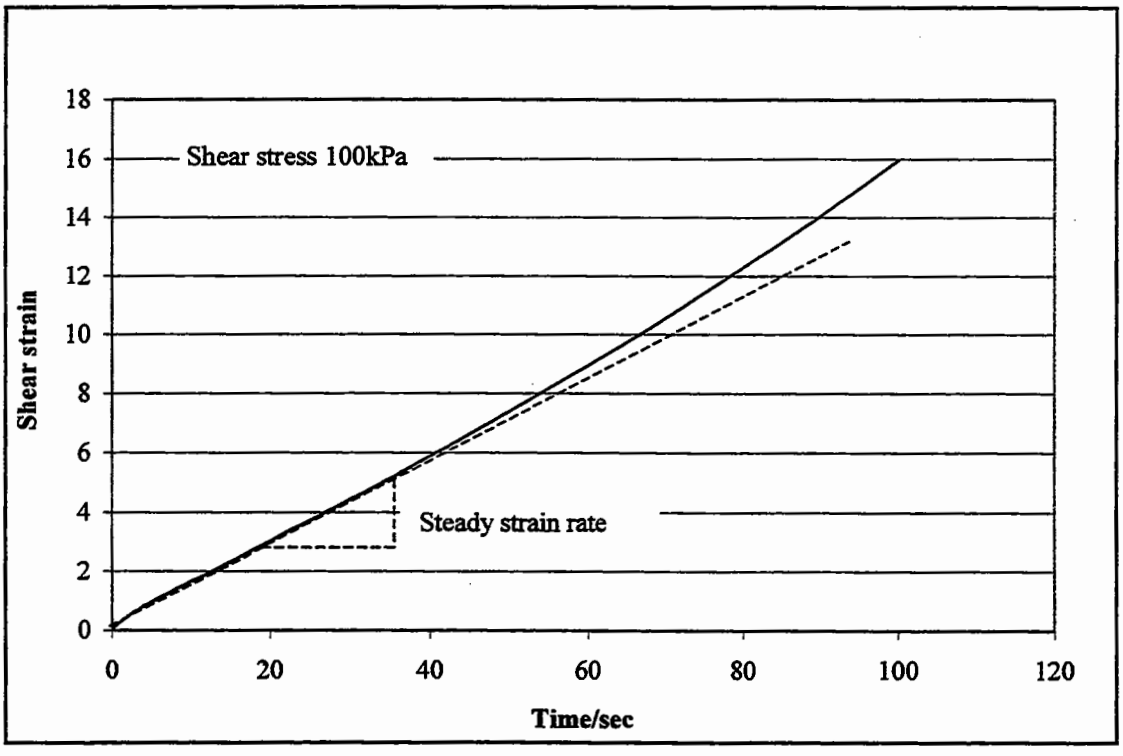

Figure 3.19 Creep test result for 50 Pen grade bitumen at 20°C.

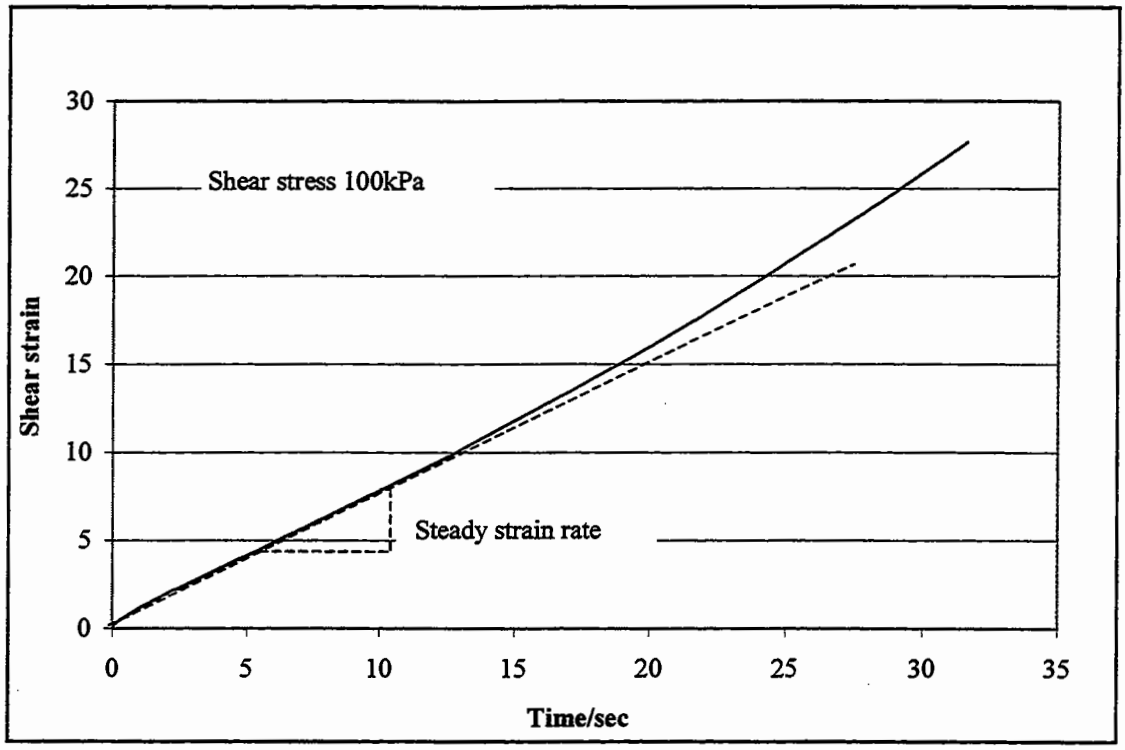

Figure 3.20 Creep test result for 100 Pen grade bitumen at 20°C.

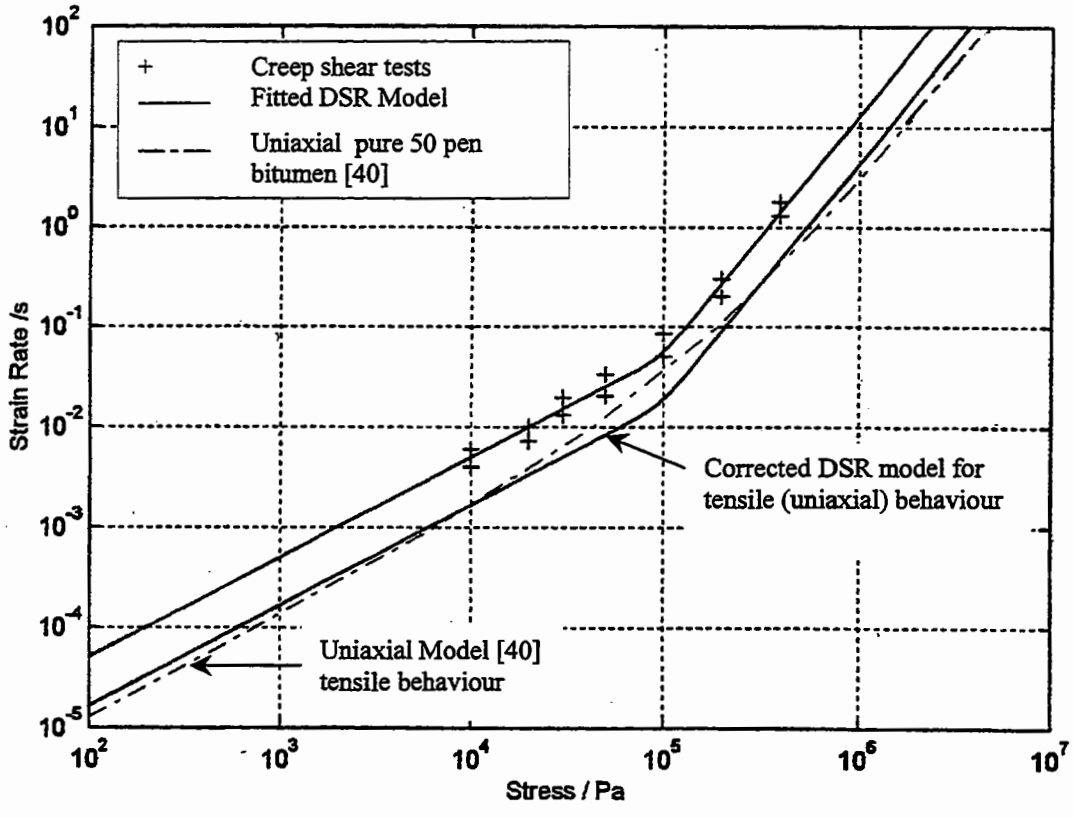

Figure 3.21 Deformation behaviour of 50 Pen grade bitumen at 20°C.

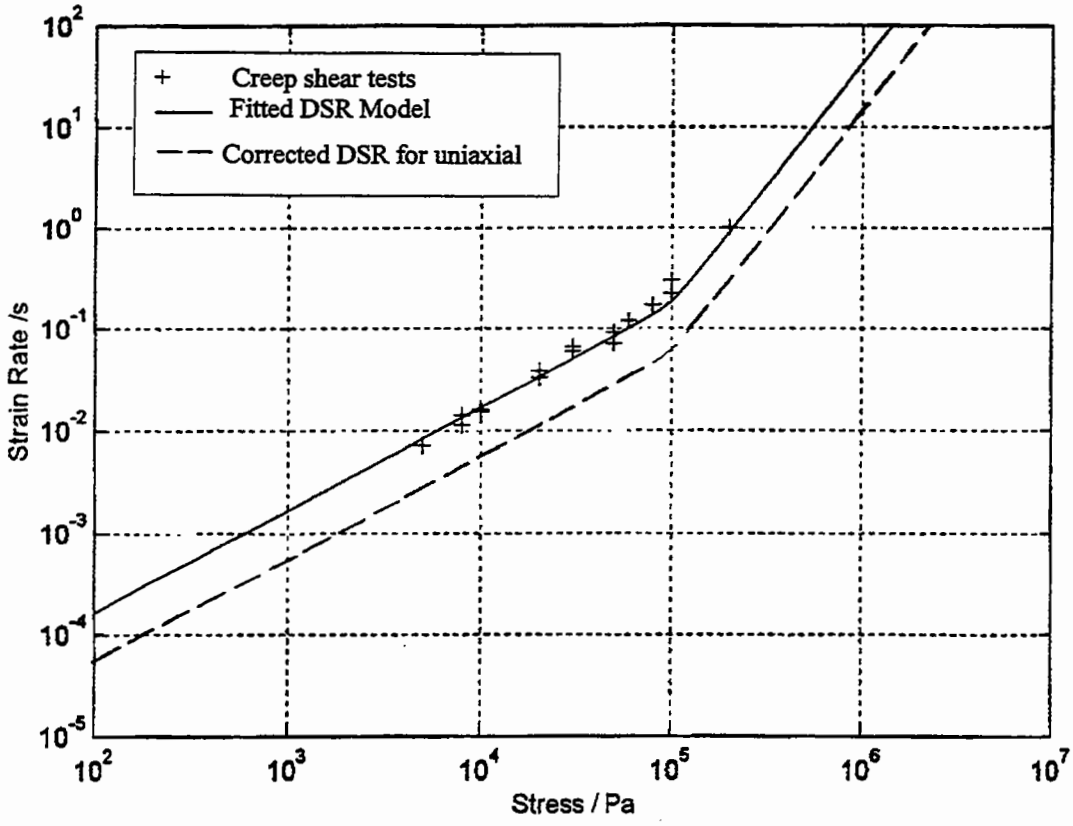

Figure 3.22 Deformation behaviour of 100 Pen grade bitumen at 20°C.

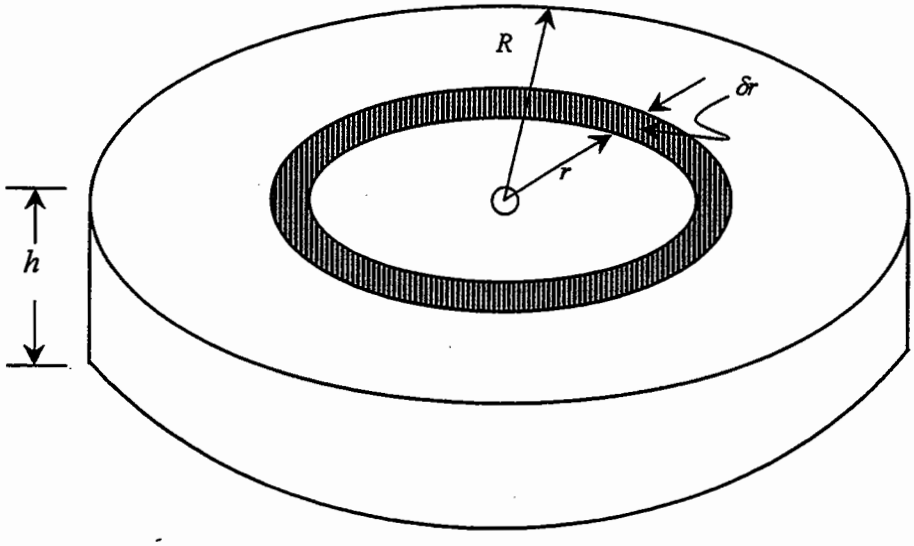

Figure 3.23 DSR testing geometry.

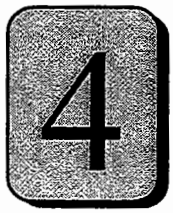

Uniaxial Tests on Idealised and Realistic Bituminous Mixtures

4.1 Introduction

In general, bituminous mixtures can be considered to be three phase composites comprising bitumen, graded aggregate and air voids. The mechanism of permanent deformation in a bituminous mixture is a complicated process and depends on the physical properties and proportions of these three phases. The microstructure of a bituminous mixture depends on the manufacturing process (particularly compaction) [63] and can be idealised as rigid particles embedded in a matrix of voided bitumen. The two main load carrying mechanisms are through aggregate contact, which depends on inter-particle friction and particle interlocking, and through the "stiffness" of the bitumen matrix. Consequently, the mechanical properties of the bitumen can significantly influence the permanent deformation resistance of a bituminous mixture.

The mechanical properties of bitumen have been widely investigated and comprehensive reviews can be found in [40, 53]. Recently, Cheung [40] tested a standard 50 Pen grade of bitumen over a wide range of operating conditions (temperature, stress and strain rate) in uniaxial tension/compression and shear. He found that the bitumen displayed a wide range of steady-state properties. At temperatures above the glass transition, the deformation behaviour was found to be linear viscous at low stress levels and power law creep at higher stress levels with a creep exponent of between 2 and 2.5 [40]. The transition stress was found to be in the

range of 100 kPa to 500 kPa. It should be noted that in Chapter 3 the transition stress was found to be approximately 70 kPa. However, this is a shear stress that equates to a normal stress of approximately 210 kPa which falls in the range (100 kPa to 500 kPa) measured by Cheung and Deshpande [40, 53]. The asymptotic transition stress was found to be 100kPa. This work was extended by Deshpande [53] who examined the steady-state properties of a number of idealised mixtures comprising one (or two) grades of sand and the same 50 Pen grade of bitumen. He found that the behaviour of the idealised mixtures mirrored the behaviour of the binder in terms of the transition from linear to power law behaviour (see [53] for further details).

This chapter contains details of uniaxial compression experiments performed on idealised and realistic bituminous mixtures over a range of stresses, strain-rates and temperatures. As a first step towards understanding the deformation behaviour of realistic mixtures, the behaviour of two idealised mixtures A and A/D are investigated. The research is further extended to investigate the deformation behaviour of realistic mixtures with more complex micro-structures. Hot Rolled Asphalt (HRA) and Dense Bitumen Macadam (DBM), two types of bituminous mixtures commonly used in the UK paving industry, were selected for the experimental investigation. Finally, conclusions regarding the possible mechanisms controlling the deformation behaviour of these mixtures are presented.

4.2 Idealised Mixtures

The idealised mixtures reported herein are denoted mixture A/D and mixture A. Mixture A/D comprised two size sand fractions and was designed to have the following proportions (by mass); 44.9% of each size of sand and 10.2% binder. Mixture A comprised a single size sand fraction and was designed to have the following proportions (by mass); 87.4% sand and 12.6% binder. The same 50 Pen grade of bitumen with a softening point of 53.5°C was used as the binder for these idealised mixtures.

The nominal volumetric properties of the two mixtures are defined below:

1. Mixture A/D (Double size sand mixture)

Size of Sand A	= Sand particles between 1.18mm and 2.36mm,
Size of Sand D	= Sand particles between 150μm and 300μm
% volume sand A	= 37.5
% volume sand D	= 37.5
% volume bitumen	= 22
% volume air voids	= 3

2. Mixture A (Single size sand mixture)

Size of Sand A	= Sand particles between 1.18mm and 2.36mm,
% volume sand A	= 70
% volume bitumen	= 26
% volume air voids	= 4

The volumetrics for these idealised mixtures were chosen to be similar to Deshpande's [53] idealised mixtures, which were prepared to give maximum packing densities and also to promote the viscous response of the binder. For a regular packing of single sized aggregates (for example mixture A), the hexagonal close packed arrangement gives the maximum volume fraction in the range of 70-75% [53].

4.2.1 Specimen Preparation

To simulate realistic compaction conditions, it was intended to core the test specimens from 150 mm thick slabs compacted using a laboratory roller compactor. However, it was observed that coring the samples from mixtures that are rich in bitumen (such as the idealised mixtures being tested) was a difficult and time consuming procedure. Moreover, the cores obtained showed significant surface damage and were not suitable for testing.

A cylindrical split mould was manufactured and used to cast the specimens (see Figures 4.1 and 4.2). The ratio of the height to the diameter of the specimens was chosen to be approximately two. The specimens were 150 mm in height with a diameter of 75 mm. A non-evaporating, heat resistant grease was used to lubricate the inner surface of the mould to prevent sticking of the bituminous mixture during compaction.

4.2.2 Compaction of the Test Specimen

Consequently, a Kango Hammer vibratory compactor was used for specimen compaction. A photograph of the split mould and Kango compactor is shown in Figure 4.2. In order to keep the height of the specimen constant at 150 mm, compaction was stopped when the top of the specimen reached the level indicated on the inside of the mould. A wooden platen was placed on top of the mixture during the compaction process, to avoid bitumen sticking to the hammer foot. The specimen was compacted from both sides and care was taken to ensure the bottom and top surfaces of the specimens were flat and parallel. After compaction the mixture was allowed to cool to room temperature for at least 12 hours. Finally, the mould was opened slowly to avoid any surface damage to the specimen and the specimens were stored at 5°C.

In order to obtain the most homogenous specimens, two compaction techniques were used to compact these samples with the Kango vibratory hammer. Firstly, the specimen was compacted in 3 layers and secondly, in a single layer. After cooling, the cylindrical specimens were removed from the mould and cut into three sections. The density of each section was measured. It was found that the variation in density in the specimens compacted by these two methods was less than 1% for both types of mixtures. Consequently, it was decided to make cylindrical specimens compacted in a single layer.

The theoretical maximum density (ρ_{max}) of the mixture was estimated using was estimated according to BS 598 [37] procedures using:

$$\rho_{max} = \frac{M_A + M_B}{M_B/\gamma_b + M_A/\gamma_a} \times \rho_w \tag{4.1}$$

where M_A = aggregate content percent by mass of total mixture
M_B = binder content percent by mass of total mixture
$M_A + M_B = 100\%$
γ_a = specific gravity of aggregate
γ_b = specific gravity of bitumen
ρ_w = density of water (1000 kg/m^3)

A theoretical maximum density calculation was used rather than a measured maximum density (Rice Density) because the primary concern was the variation in air voids along the specimen and the repeatability of specimens rather than the absolute air void content. The specific gravities for the coarse/fine aggregates and bitumen were supplied by the Bardon Hill aggregate quarry and Shell bitumen UK respectively. The bulk density (ρ) of the specimens was measured by weighing in air and weighing in water after sealing with self adhesive aluminium foil. The specific gravity of the foil (1.650) was accounted for using the following equation:

$$\rho = \frac{M_{au} \times \rho_w}{M_{ac} - M_{wc} - \left(\frac{M_{ac} - M_{au}}{S_{gf}} \right)} \tag{4.2}$$

where ρ = Bulk density of the specimen,

M_{au} = Mass of the specimen in air uncoated (kg),

M_{ac} = Mass of the specimen in air coated with aluminium foil (kg),

M_{wc} = Mass of the specimen in water coated in aluminium foil (kg) and

S_{gf} = Specific gravity of the aluminium foil

ρ_w = Density of water (1000 kg/m^3).

During the density testing the temperature of the water varied between 21°C and 27°C. This variation in temperature was not included in the density of the water (required by Equation 4.2) because a previous study had shown that corrections due to thermal effects in this temperature range were negligible [56]. The percentage volume of voids V_v was calculated using:

$$V_v = \left(1 - \frac{\rho}{\rho_{max}} \right) \times 100 \tag{4.3}$$

The variability in air void content, characterised by a mean value, minimum, maximum and Coefficient of Variation (COV), for mixture A and mixture A/D are given in Table 4.1.

Table 4.1 Air Void Content Analysis (Mix A and Mix A/D)

Mix	No. of Samples	Air Void Content (%)			
		Mean	Minimum	Maximum	COV (%)
A	30	9.7	8.2	10.6	8.5
A/D	30	7.5	6.5	8.6	7.8

It can be seen from table 4.1 that the average void contents for both the mixtures A and A/D are higher than the target void contents. This is because a different method of compaction was used compared to Deshpande's [53] specimens from which target figures were taken.

4.2.3 Testing Procedure

Uniaxial compression testing of idealised mixtures was performed using a hydraulic testing machine located inside a temperature controlled room. Testing was undertaken at temperatures of 20°C and 30°C.

A specimen was placed on the steel platen, the top surface of which was loaded by a moving piston through a circular araldite platen of 80 mm diameter. A photograph of loading arrangement is shown in Figure 4.3. The force applied was measured by a load cell located at the lower end of the ram. A lubricant was applied to the top and bottom surfaces of the platens to minimise friction and thus prevent bulging of the specimen. The lubricating agent was prepared by dissolving natural soap in glycerine which was noted to be effective since the top and bottom platens were not observed to stick to the specimen after the test had been completed.

For each test, the temperature inside the testing room was brought to the desired value and maintained for at least 12 hours before the commencement of the test. The specimen to be tested was kept inside the temperature controlled room for approximately two hours before the test to ensure that it was at a uniform temperature. The conditioning time of 2 hours was found to be sufficient by measuring the

temperature within a dummy core specimen. Moreover, it was also noticed that leaving the specimens for more than 2 hours at high temperatures resulted in distortion of the samples by creep induced due by the self-weight of the specimen.

Two types of tests were conducted. In a constant strain rate test, a constant axial displacement rate (velocity) was applied to the specimen. In a constant stress creep test, a constant force was applied instantaneously to the specimen and maintained until the end of the test. It should be noted that the nominal stress has been calculated rather than the true stress which takes into account the change in cross sectional area of the specimen during the test. The effect of this can be assessed by assuming that the permanent deformation takes place at constant volume and the deformation is uniform. Under these conditions at a strain level of 2% the true stress will be approximately 2% less than the nominal stress which is considered small enough not to include in the analysis. Consequently, nominal value of stress has been used throughout this thesis.

For both types of test (creep and constant strain rate) the axial strain and applied load were measured. The axial strain was measured by a load line displacement LVDT (i.e. no on-sample instrumentation was used). Data were recorded simultaneously by the data logging equipment which were then transferred to a computer for further analysis.

4.3 Experimental Results

Idealised Mixtures (Mixture A/D and Mixture A)

Constant strain rate tests were performed on mixture A/D and mixture A at 20°C and 30°C. Typical results in terms of axial strain plotted against the axial stress for different applied strain rates, at 20°C and 30°C for mixture A/D and mixture A are shown in Figures 4.4 to 4.7. It can be seen from these figures, that for each applied strain rate, the stress increases with the strain up to a point, beyond which it starts to decrease. As proposed by Cheung [40] and Deshpande [53], the maximum stress observed from this type of stress strain curve is defined as a steady-state creep stress (see Figure 4.4), corresponding to a particular combination of strain rate and

temperature. It can also be seen from Figures 4.4 to 4.7 that at a particular strain rate and temperature mixture A/D is stiffer than mixture A i.e. higher axial stress for same strain. This is because mixture A/D has a higher percentage of aggregate with two different aggregate sizes resulting in better interlocking of the aggregate particles and a larger stiffening effect.

Constant creep tests were also performed on mixture A/D and mixture A specimens at 20°C and 30°C. Typical results are shown in Figure 4.8 and 4.9 respectively, in which the axial creep strain is plotted as a function of time elapsed after the application of load. It can be seen from these figures that the creep curve can be divided into three regions: primary creep where the strain rate decreases, secondary creep where the strain rate is approximately constant and tertiary creep where the strain rate increases. The secondary creep region is used to define a steady-state creep strain rate (gradient), corresponding to a particular combination of applied stress and temperature.

The constant strain rate test and the constant stress creep test have previously been found to be complementary experimental tools for investigating the steady-state deformation behaviour of bitumen and bituminous mixtures [40, 53]. At higher temperatures where a low applied stress results in high strain rate, it is more convenient to perform a constant strain rate test where the strain rates can be more easily prescribed and controlled. Conversely, at lower temperatures where the resulting strain rate is much lower, it becomes necessary to perform a constant stress creep test so that the testing machine provides a constant force rather than a low velocity which is difficult to accurately control. Results from the two types of test, in terms of steady-state strain rate and steady-state stress, have been found to agree at intermediate levels of temperatures and strain rates [40, 53].

Steady-state deformation behaviour observed from the two types of tests for mixtures A/D and A at 20°C and 30°C are presented in Figures 4.10 and 4.11, where the steady-state strain rate is plotted against the steady-state creep stress. The complementary nature of the constant strain-rate tests and the creep tests can be clearly seen from these figures. It can also be seen from these figures that the deformation behaviour of mixtures A/D and A follow a similar pattern. At higher stress levels (>500 kPa) the experimental points tend to lie on a straight line (on

double logarithmic scales) with a slope of approximately 2.4. This indicates that the deformation behaviour in this region is non-linear power law creep. At lower stress levels (<70 kPa) the experimental points also tend to lie on a straight line (on double logarithmic scales) but with an approximate slope of 1. This indicates that the deformation behaviour in this region is linear viscous flow. Between 70 kPa and 500 kPa there is a transition region from power law behaviour to linear viscous behaviour [48].

Also shown in Figures 4.10 and 4.11 are results from a model developed by Cheung [40] (Equation 2.2) for the same grade of bitumen tested at 20°C. It can be seen from these results that the curve has a similar shape to the curves for the mixtures indicating that the response of these idealised mixtures is being dominated by the response of the binder [48]. It can also be seen from these figures, that the effect of the aggregate is to decrease the strain rate resulting from a particular value of stress (i.e. stiffening effect). It can be seen from Figures 4.10 and 4.11 that this stiffening factor is approximately 15,000 for mixture A/D and 2,500 for mixture A respectively.

As noted above the solid lines in Figures 4.10 and 4.11 are predictions from a model for this behaviour proposed by Cheung [40] and Deshpande [53]. The model relates steady-state stress to steady-state strain rate using the following equation:

$$\frac{\sigma}{\sigma_o} = \frac{S\dot{\varepsilon}}{\dot{\varepsilon}_o}\left(\frac{1}{1+\left(\frac{S\dot{\varepsilon}}{\dot{\varepsilon}_o}\right)^{n_c}}\right) \tag{4.4}$$

where σ = uniaxial stress

$\dot{\varepsilon}$ = uniaxial strain-rate

$n_c, \sigma_o, \dot{\varepsilon}_o$ = material constants for the bitumen (see Cheung [40]), and

S = stiffening factor due to the aggregate.

It can be seen that if the strain rate $\dot{\varepsilon}$ is large compared to the reference strain rate $\dot{\varepsilon}_o$, Equation 4.1 reduces to a power law creep relationship where $\dot{\varepsilon} \propto \sigma^{1/1-n_c}$ whereas if

the strain rate $\dot{\varepsilon}$ is small compared to the reference strain rate $\dot{\varepsilon}_o$ Equation 4.1 reduces to a linear viscous flow law where $\dot{\varepsilon} \propto \sigma$. It can be seen from Figures 4.10 and 4.11 that there is good agreement between the experimental results and the model predictions for both mixtures over a relatively wide range of stresses and strain rates.

The temperature dependence of the mixture was found to be governed by the bitumen. For the two temperatures investigated herein, the temperature dependence of mixture A and mixture A/D was found to follow the free volume model (WLF equation) (see Figures 4.10 and 4.11) which was be incorporated into Equation 4.4 for temperatures $\geq 20°C$ (see Cheung [40] for further details):

$$\frac{\sigma_o}{\dot{\varepsilon}_o} = \eta_s \exp\left(-\frac{2.303 c_1^s (T - T_s)}{c_2^s + (T - T_s)}\right) \tag{4.5}$$

where $\frac{\sigma_o}{\dot{\varepsilon}_o}$ = limiting viscosity when $\dot{\varepsilon} \to 0$,

η_s = pre-exponential for viscosity with the value 214×10^3 Pa.s

c_1^s & c_2^s = universal constants with the values 8.86 & 101.6

T_s = reference temperature with the value 35.2°C

4.4 Realistic Mixtures

The basic idea of the research was to study the deformation behaviour of idealised mixtures where the behaviour is likely to be governed by the deformation behaviour of the binder. However, to extend the research to investigate the deformation behaviour of more realistic bituminous mixtures it was decided to use mixtures closer to realistic mixtures. Constant strain-rate tests and constant stress creep tests were also conducted on two generic types of bituminous mixtures commonly used in the UK: Hot Rolled Asphalt (HRA) and Dense Bitumen Macadam (DBM). The binder used was the same 50 penetration grade bitumen. Some limited tests were also conducted on the DBM mixture made using 100 penetration grade of bitumen as a binder.

4.4.1 Test Specimens

Test specimens were manufactured according to the aggregate grading specified in BS 4987 [35] and BS 594 [36] for DBM and HRA respectively. The design grading was taken as approximately the midpoint of the limits set out for HRA and DBM mixtures, see Figures 4.12 and 4.14. Both the mixtures were designed to a binder content of 7% by mass. It should be noted that the binder content for the HRA and the DBM would typically be around 7.8% and 5.1% respectively. However it was intended to make these specimens closer to the idealised mixtures as mentioned earlier. The specimens were compacted to achieve 7% air voids. The volumetrics for both the mixtures are given in the following sections.

4.4.1.1 30/10 Hot Rolled Asphalt (HRA)

Hot Rolled Asphalts (HRA's) consist of a sand/filler/bitumen matrix with varying quantities of coarse aggregate generally 'floating' in the matrix, and are known as gap graded mixtures. The term gap graded refers to the omission of a size, or range of sizes, in the aggregate particle distribution, which appears as a 'gap' in the aggregate grading curve. This is illustrated in Figure 4.12, which shows a grading for a typical hot rolled asphalt wearing coarse. A schematic representation of a gap graded mixture is given in Figure 4.13, which shows the coarse aggregate particles distributed in a mortar composed of bitumen, fine aggregate and filler. As there is little or no contact between coarse aggregate particles the mixture resists permanent deformation and transmits load primarily through the mortar, which relies heavily on the properties of the bitumen.

The designation for HRA is in the form of two numbers for example HRA 30/10. The first number (30 in this case) refers to the nominal percentage of coarse aggregate in the mixture and the second number (10 in this case) refers to the maximum nominal aggregate size in millimeters. The specification for these materials is given in B.S. 594 [36]. The volumetric properties for the 30/10 HRA mixture tested is defined below:

% volume coarse aggregate (10mm & 6mm limestone) = 26.5

% volume fine aggregate (hint sand)	= 41
% volume dust/filler	= 12.50
% volume bitumen	= 16
% volume air voids designed to	= 4

4.4.1.2 10 mm Dense Bitumen Macadam (DBM)

These are continuously graded mixtures, so called because the distribution of aggregate particle sizes in the mixture is continuous. DBM's gain their properties by the use of high quality stone, forming a good interlocking aggregate skeleton. Figure 4.14 shows the aggregate grading curve for a typical DBM and Figure 4.15 shows an idealised section through a material of this type. It can be seen from Figure 4.15, that there is stone to stone contact between the coarse aggregate particles, forming a continuous framework through the mixture. The specification of these materials is given in B.S. 4987 [35]. The volumetric properties for the 10mm DBM mixture tested is defined below:

% volume coarse aggregate (10mm & 6mm)	= 50
% volume dust/filler	= 31
% volume bitumen	= 15
% volume air voids designed to	= 4

4.4.2 Compaction of Test Specimens

It was originally intended to compact all the specimen in a similar manner to reduce the variability in the test results due to different compaction techniques. Consequently, the same procedure was adopted for mixing and compaction of test specimens as outlined in section 4.2 for the idealised mixture specimens. Moreover, the compaction method was considered appropriate as the vibratory action of the Kango hammer broadly simulates on-site compaction where the particles are allowed to re-orient themselves and form close contacts. Before testing density measurements were taken again using the same method as detailed for the idealised mixtures. The variability in air void content, characterised by a mean value, minimum, maximum and the Coefficient of Variation, for HRA and DBM, is given in Table 4.2. It can be

seen by comparing Table 4.2 with Table 4.1 that there is higher variability in air void content for the realistic mixtures.

Table 4.2 Air Void Content Analysis (HRA and DBM)

Mix	No. of Samples	Air Void Content (%)			
		Mean	Minimum	Maximum	COV (%)
HRA	15	7.8	6.5	9.8	12.1
DBM	11	8.4	6.4	10.4	15.9

4.5 Experimental Results

30/10 HRA Mixture

Constant strain rate tests and constant stress creep tests were performed on the HRA mixture at 20°C. Figure 4.16 shows typical results from constant strain rate tests. It can be seen from Figure 4.16 that the axial stress increases with the axial strain until it reaches a maximum value, which, as before, is defined as the steady-state stress. It can also be seen from this figure that at particular strain rates this steady-state stress is reached at around 2.5% axial strain.

Constant stress creep tests were also performed on HRA mixtures at 20°C. Figure 4.17 shows a typical creep curve for the HRA mixture. It can be seen from this figure, that similar to the strain rate tests the steady-state strain rate is reached at around 2.5%.

Steady-state deformation behaviour observed from the two types of tests at 20°C for the HRA mixture is presented in Figure 4.18, where the steady-state strain rate is plotted against the steady-state creep stress. It can be seen from this figure that the steady-state deformation behaviour of the HRA mixture can also be described by Equation 4.4 with stiffening factor of approximately 450,000 (this is also shown in Figure 4.18 by the solid line). It can be seen from this figure that HRA mixture follows the same deformation behaviour as observed for the idealised mixtures and

the bitumen and, at higher stress levels (>700kPa), the HRA deforms in a non-linear way with an effective creep exponent of 2.4.

HRA Mortar

Constant strain rate tests were also performed on the HRA mortar since the performance of this type of mixture relies largely on the performance of the mortar. Batch masses were calculated without the inclusion of large size aggregates (10mm and 6mm) to give the following approximate volumetric proportions:

% volume fine aggregate (hint sand)	= 56
% volume dust/filler	= 18
% volume bitumen	= 22
% volume air voids	= 4

Figure 4.19 shows typical data from constant strain rate tests. It can be seen from this figure that the steady-state stress is reached at an axial strain level of approximately 3%. Steady-state deformation behaviour observed from constant strain rate tests for HRA mortar at 20°C is presented in Figure 4.20, where the steady-state strain rate is plotted against the steady-state creep stress. Also plotted in this figure is the steady-state deformation behaviour of HRA mixture. It can be seen from this figure that, as expected, the behaviour of mortar is similar to the behaviour of the mixture and, at stress levels greater then 700 kPa can be characterised with an effective creep exponent of 2.4. The only difference is in the stiffening effect i.e. the mortar is less stiff than the HRA mixture by a factor of approximately 2.25.

10mm DBM Mixture with 50 Pen Binder

Constant strain rate tests and constant stress creep tests were also performed on the 10mm DBM mixture (with the 50 Pen grade of binder) at 20°C. Typical results are shown in Figures 4.21 and 4.22. It can be seen in Figure 4.21 that the steady-state stress was reached at an axial strain of approximately 2.5%. Again the steady-state stress was found to increase with applied strain-rate. It can be seen from Figure 4.22 that steady-state strain rate in the creep tests also occurred around 2.5%.

Figure 4.23 shows the steady-state deformation behaviour of 10mm DBM mixture at 20°C, where the steady-state strain rate is plotted against the steady-state creep stress. As shown in this figure, the steady-state deformation behaviour of the DBM can also be described by Equation 4.4 with a stiffening factor of approximately 500,000. It can be seen from this figure that, although there is some scatter in the results in the power law region (>700kPa), the mixture behaviour can reasonably be characterised with an effective creep exponent of 2.4.

10mm DBM Mixture with 100 Pen Binder

To investigate the effect of the binder on the steady-state deformation behaviour of this type of continuously graded mixture constant strain rate tests were also conducted on a 10mm DBM made using a 100 penetration grade of bitumen. Figure 4.24 shows data from constant strain rate tests. It can be seen that, as before, the steady-state stress occurs at an axial strain of approximately 2.5%. Again the steady-state stress was found to increase with increasing strain rates.

Figure 4.25 shows the steady-state deformation behaviour of DBM with 100 penetration grade bitumen at 20°C, where the steady-state strain rate is plotted against the steady-state creep stress. It can be seen from this figure that the mixture again follows the same deformation behaviour as described by Equation 4.4 with a stiffening factor of approximately 80,000. It can be seen that using softer bitumen (100 Pen) only decreases the stiffening effect. The mixture was found to be approximately 6 times less stiff than DBM mixture with 50 Pen bitumen. As shown in Figure 4.25, the deformation behaviour of the mixture in the power law region can be characterised with an effective creep exponent of 2.4.

4.6 Discussion

From the test results presented in this chapter, it is evident that the steady-state uniaxial deformation behaviour of the idealised and realistic mixtures is of the same form as that of the pure bitumen used as the binder. Tests on the idealised mixtures (mixture A/D and mixture A) suggest that the effect of adding sand aggregate to the

bitumen is to stiffen the mixture without changing the form of the uniaxial steady-state stress-strain rate relationship or the temperature dependence.

The two main mechanisms with which bituminous mixtures resist permanent deformation are interparticle friction due to interlocking and the resistance of the binder to shear deformation. It should be noted that the contribution of coarse aggregate as indicated from the stiffening effect observed from the HRA mortar and mixture is no doubt significant (by a factor of 2). Although there is no aggregate to aggregate contact the coarse aggregate seems to increase the viscosity of the mixture resulting in a stiffer mixture. However, the form of deformation behaviour seems to be dominated by the binder (for this particular HRA). It should be noted that this stiffening effect may be due to the overall increase in the volume fraction of aggregate for the HRA mixture. This requires further investigation. Consequently, it may be expected that the deformation in an HRA type of mixture is a binder dominated process. This is observed from the experimental results.

In continuous graded mixtures like a DBM, aggregate to aggregate contact which initiates friction and interlocking would be expected to overcome binder dominated deformation behaviour. In the manufacturing process of bituminous mixtures graded aggregate is blended, heated and dried before being coated by bitumen in the desired proportions. During laying of the road, the mixture is compacted to reduce air voids. Because of the high volume fraction of aggregate (typically from 70% to 90%), the mixture can be idealised as thin films of bitumen separating the rigid particles. Consequently, the results indicate that the thin films of bitumen separating the aggregate particles govern the uniaxial deformation behaviour of the DBM mixture used in this study. As expected, there was a significant decrease in the stiffening effect of the DBM mixture due to the change of the binder type from harder (50 Pen) to softer grade (100 Pen). However, there was no change in the characteristic slope of 2.4. All these facts suggest that deformation in bituminous mixtures in a uniaxial state of stress is largely governed by the properties of bitumen over the regimes tested.

The stiffening factor was found to be dependent on the volume fraction of rigid inclusions. Similar behaviour was observed from tests on the more realistic HRA and DBM mixtures. The increase in the stiffening factor S with the volume fractions of

aggregate at a temperature of 20°C is shown in Figure 4.26 for all the mixtures that contained the 50 Pen grade of bitumen. Also shown in this figure are the stiffening factors measured by Deshpande [53] for his range of idealised mixtures with different volume fraction of aggregates that contained 50 Pen binder. It can be seen from this figure that increasing the aggregate volume in the mixture (idealised and realistic) results in stiffening of the mixture. It can also be seen from Figure 4.26 that at a volume fraction of 0.75 the stiffening factors are separated by up to 100 times. The dilation gradient '*s*' which is a measure of interlocking of the aggregate is further investigated in Chapter 5. It has been previously found that increasing the dilation gradient *s* results in a higher stiffening factor for mixture with the same volume fraction of aggregate subjected to the same stress ratio (see Chapter 5). Consequently, it is assumed that the stiffening factor for a mixture is dependent on the dilation gradient for that particular mixture which in turn is dictated by the volume fraction of aggregate.

4.7 Conclusions

The following conclusions can be drawn from this chapter:

- The uniaxial steady-state deformation behaviour of mixture A/D and mixture A (idealised mixtures) have the same form as the steady-state deformation behaviour of the bitumen, with the aggregate acting to stiffen the mixture.

- In mixture A/D and mixture A, steady-state conditions were observed at a strain level of approximately 3%.

- The uniaxial steady-state deformation behaviour of HRA mortar and 30/10 HRA mixture was found to have the same form as that of bitumen and idealised mixtures. The aggregates were only found to stiffen the mortar without changing the form of deformation behaviour.

- In HRA mixture and HRA mortar, steady-state conditions were observed at a strain level of approximately 3%.

- The uniaxial steady-state deformation behaviour of the 10mm DBM mixture was also found to be similar to that of pure bitumen and idealised mixtures.

- In the DBM mixture, steady-state conditions were observed at a strain level of approximately 2.5%.

- A reduction in the stiffening effect was observed when 100 Pen grade bitumen was used as the binder in the DBM mixture, without changing the slope of the characteristic curve, which is 2.4 in the power law region.

- The DBM mixture was found to be stiffer than the HRA mixture.

- The uniaxial deformation behaviour of idealised mixtures, HRA and DBM mixtures is dominated by the binder properties over the regimes tested.

- The experimental results indicate that the uniaxial behaviour of the bituminous mixtures tested is not strongly dependent on the shape or angularity of the aggregate particles for the range of mixtures tested.

4.8 Figures

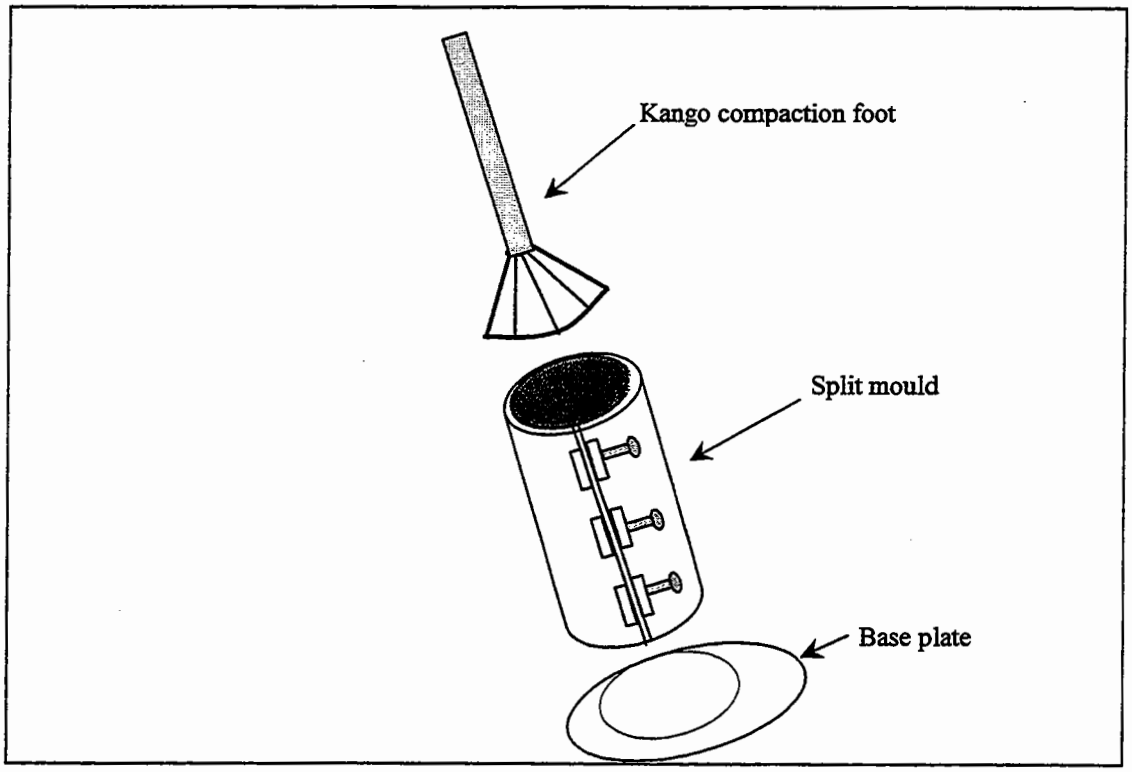

Figure 4.1 Schematic showing compaction mould and Kango Hammer Foot.

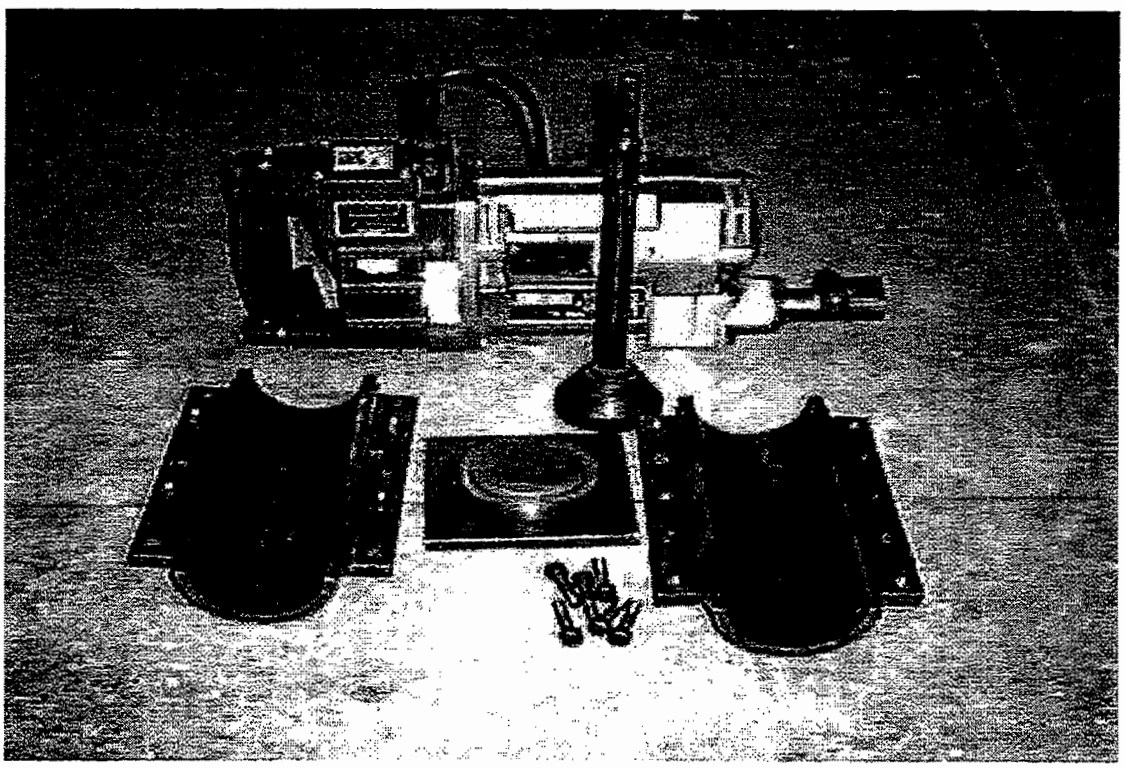

Figure 4.2 Photograph showing split mould and Kango compactor.

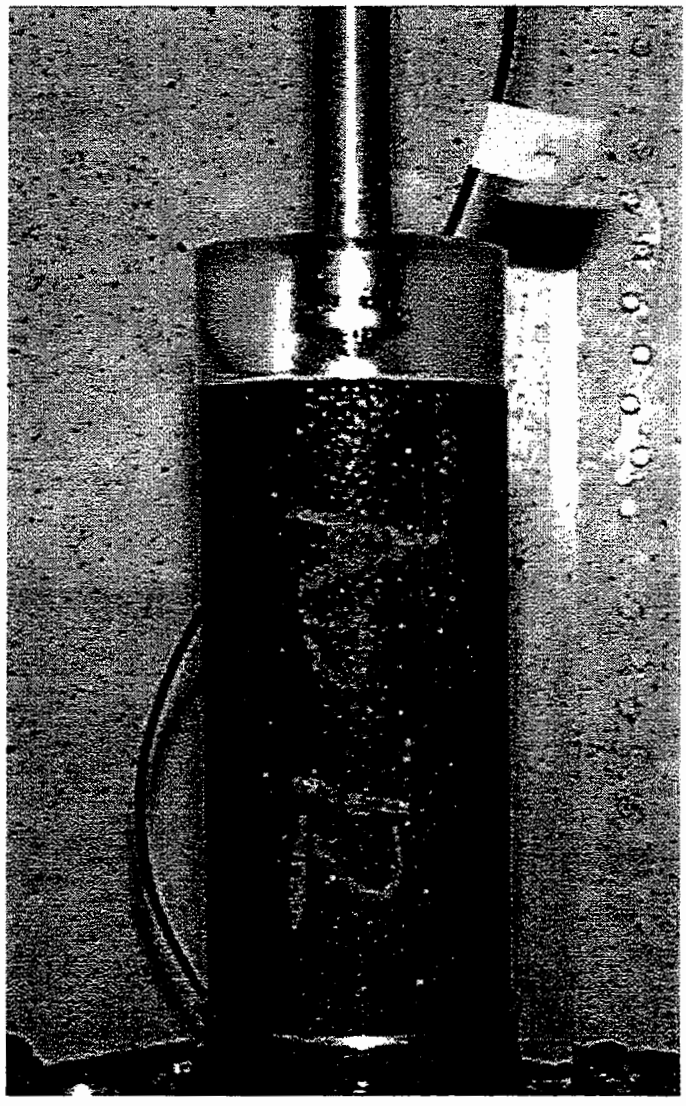

Figure 4.3 Photograph of Mixture A/D specimen with loading arrangement. Sample size Ø75 × 150mm.

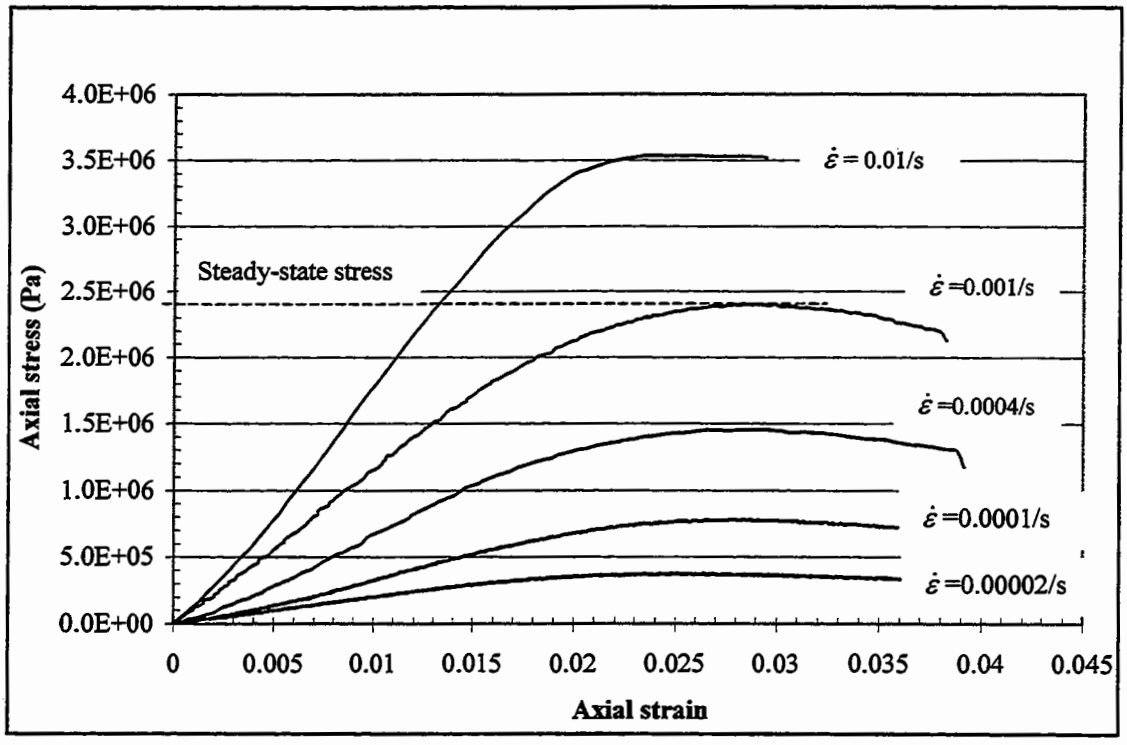

Figure 4.4 Constant strain rate test results for mixture A/D at 20°C.

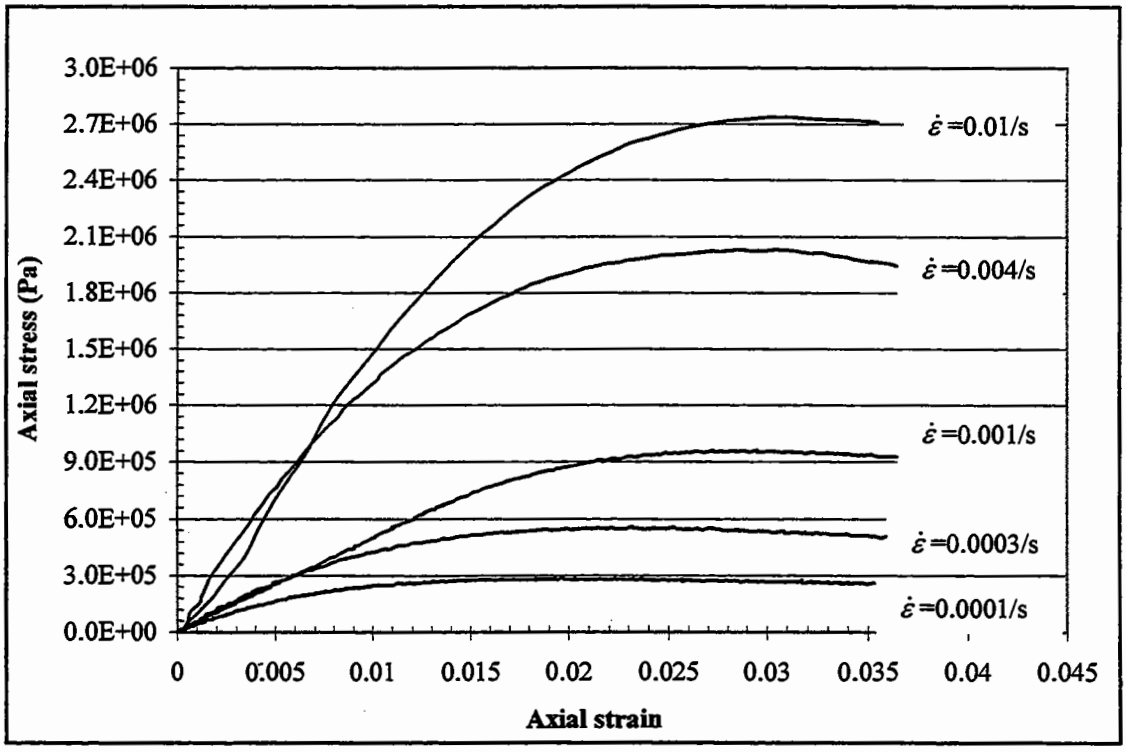

Figure 4.5 Constant strain rate test results for mixture A at 20°C.

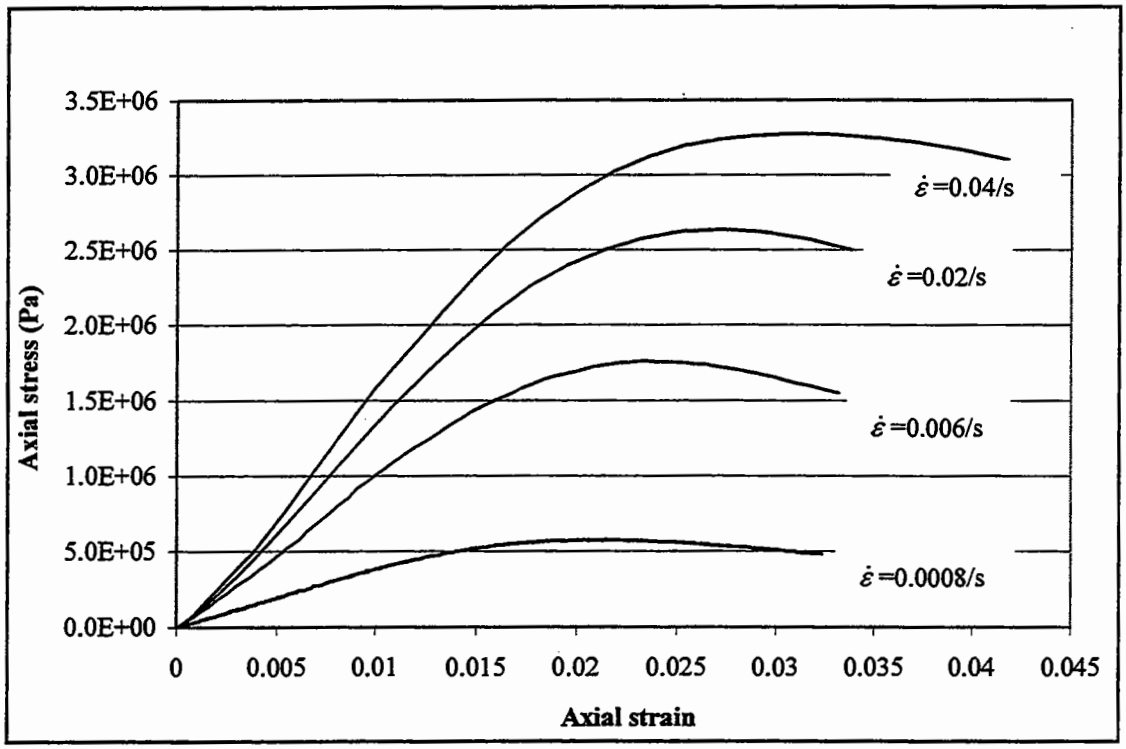

Figure 4.6 Constant strain rate test results for mixture A/D at 30°C.

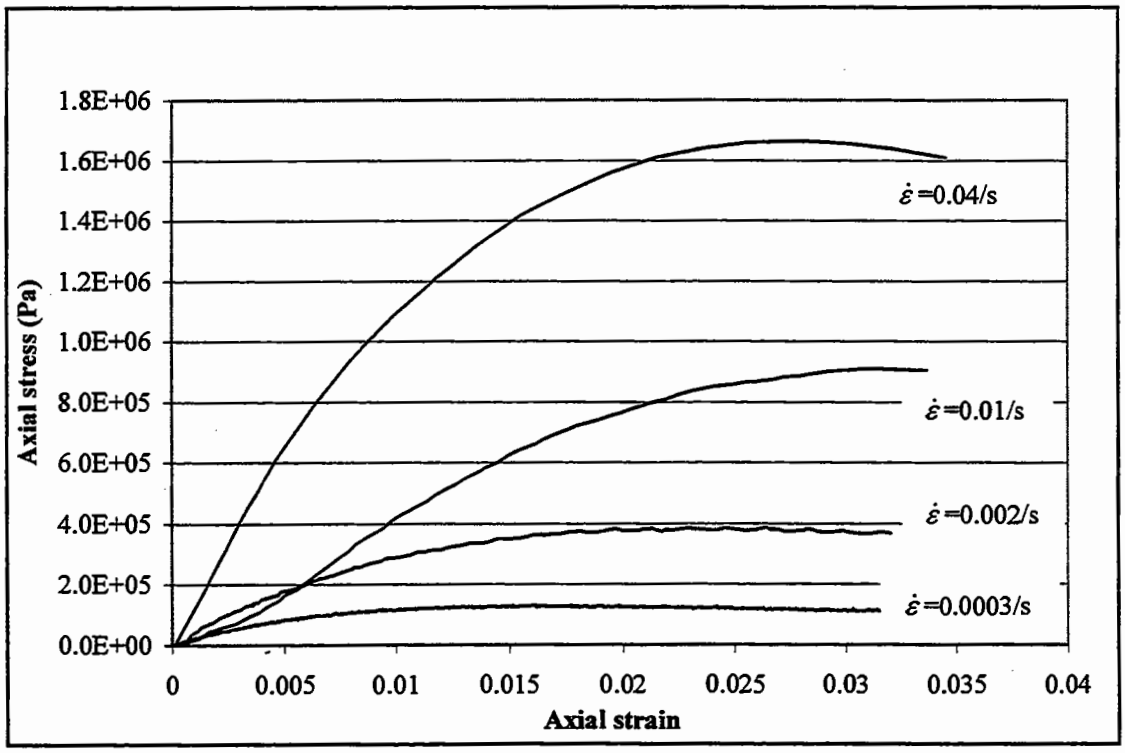

Figure 4.7 Constant strain rate test results for mixture A at 30°C.

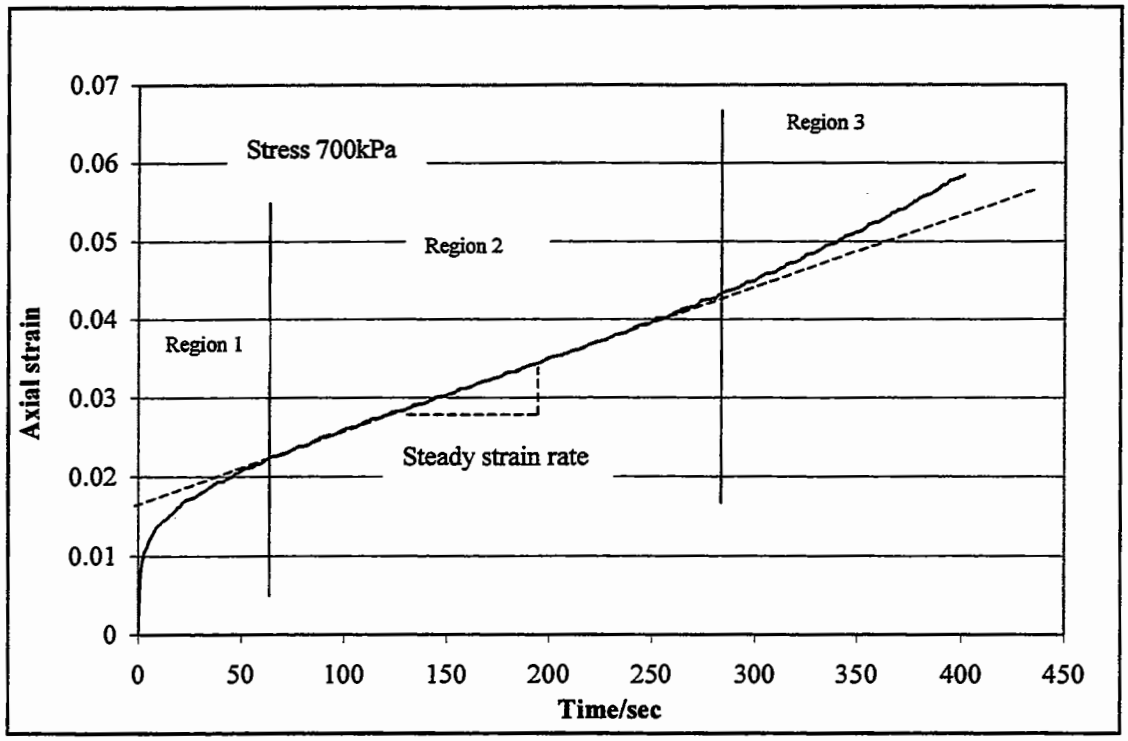

Figure 4.8 Creep test result for mixture A/D at 20°C.

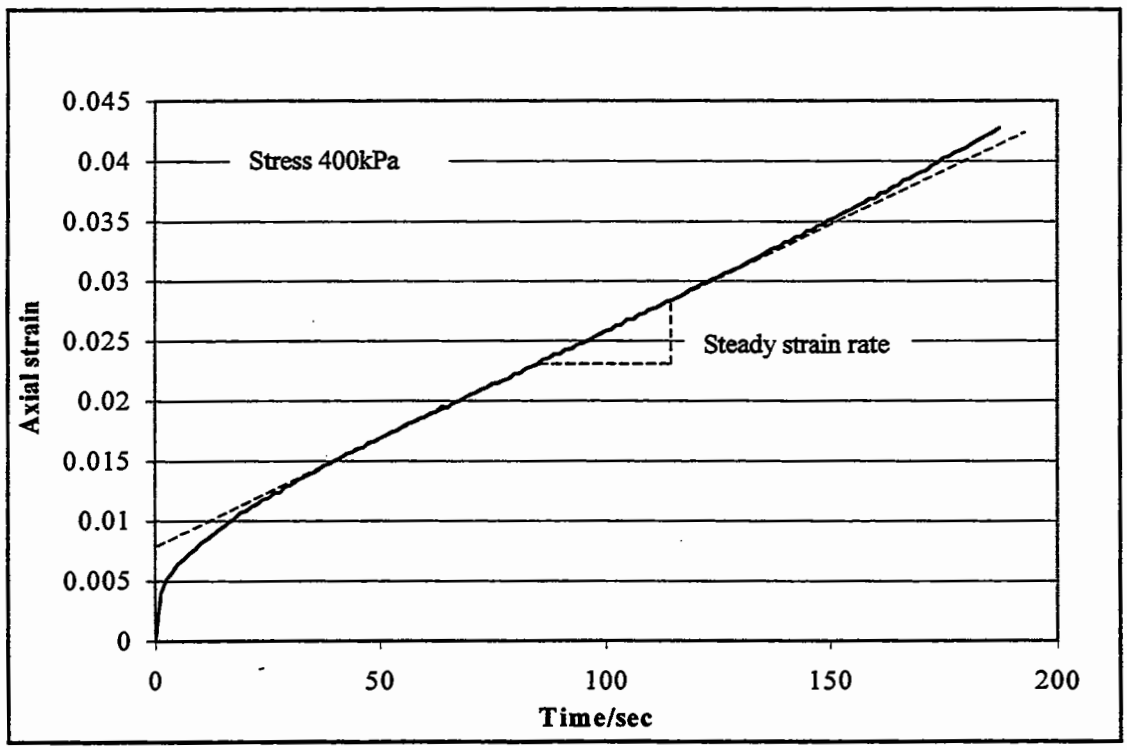

Figure 4.9 Creep test result for mixture A at 20°C.

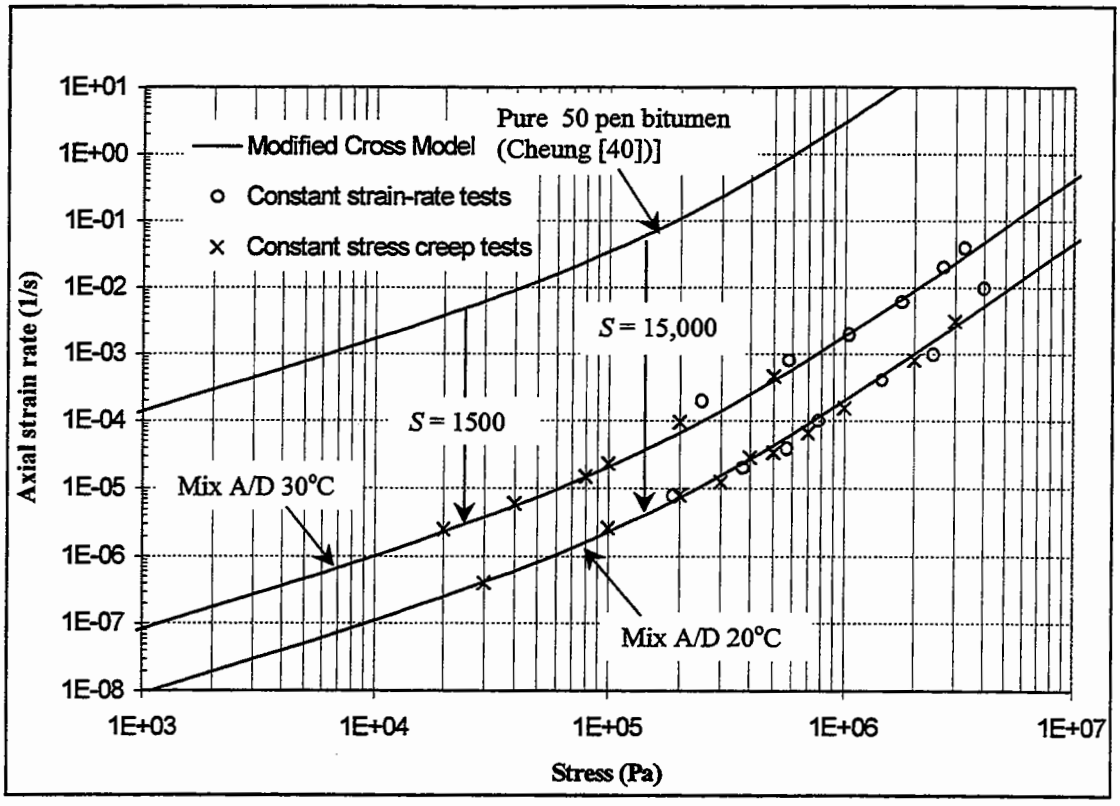

Figure 4.10 Steady-state deformation behaviour of mixture A/D at 20°C and 30°C.

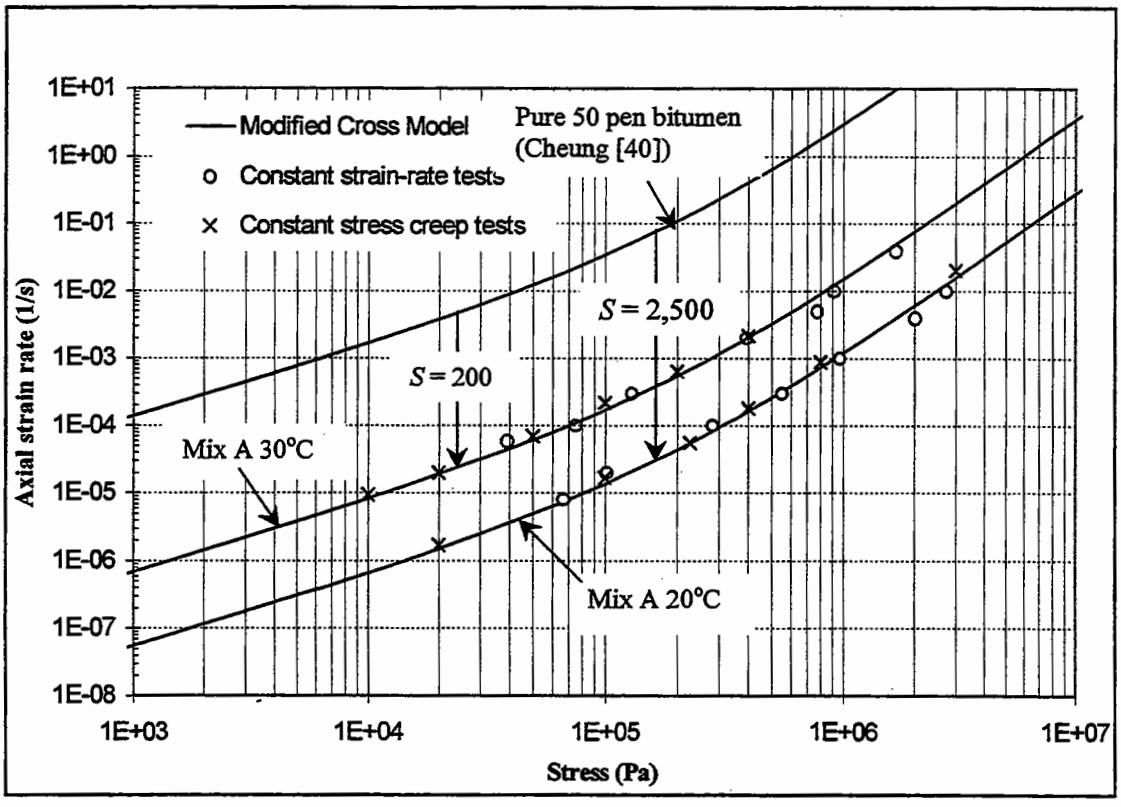

Figure 4.11 Steady-state deformation behaviour of mixture A at 20°C and 30°C.

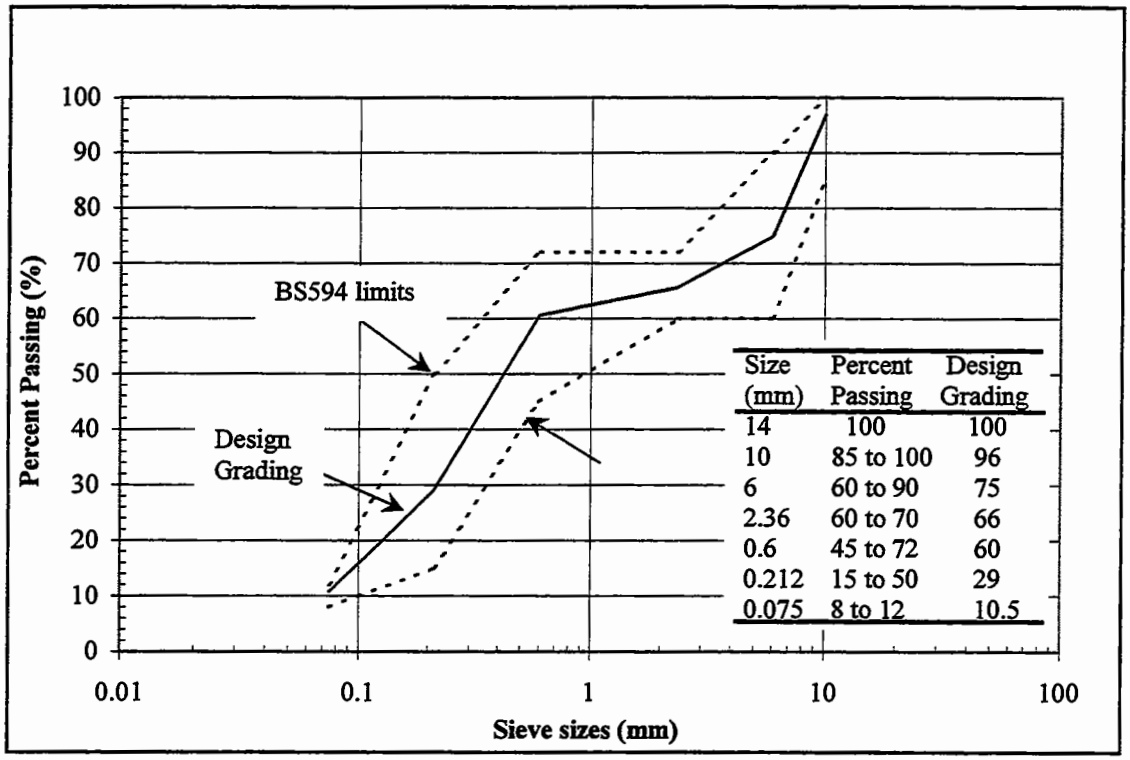

Size (mm)	Percent Passing	Design Grading
14	100	100
10	85 to 100	96
6	60 to 90	75
2.36	60 to 70	66
0.6	45 to 72	60
0.212	15 to 50	29
0.075	8 to 12	10.5

Figure 4.12 Design grading for 30/10 Hot Rolled Asphalt.

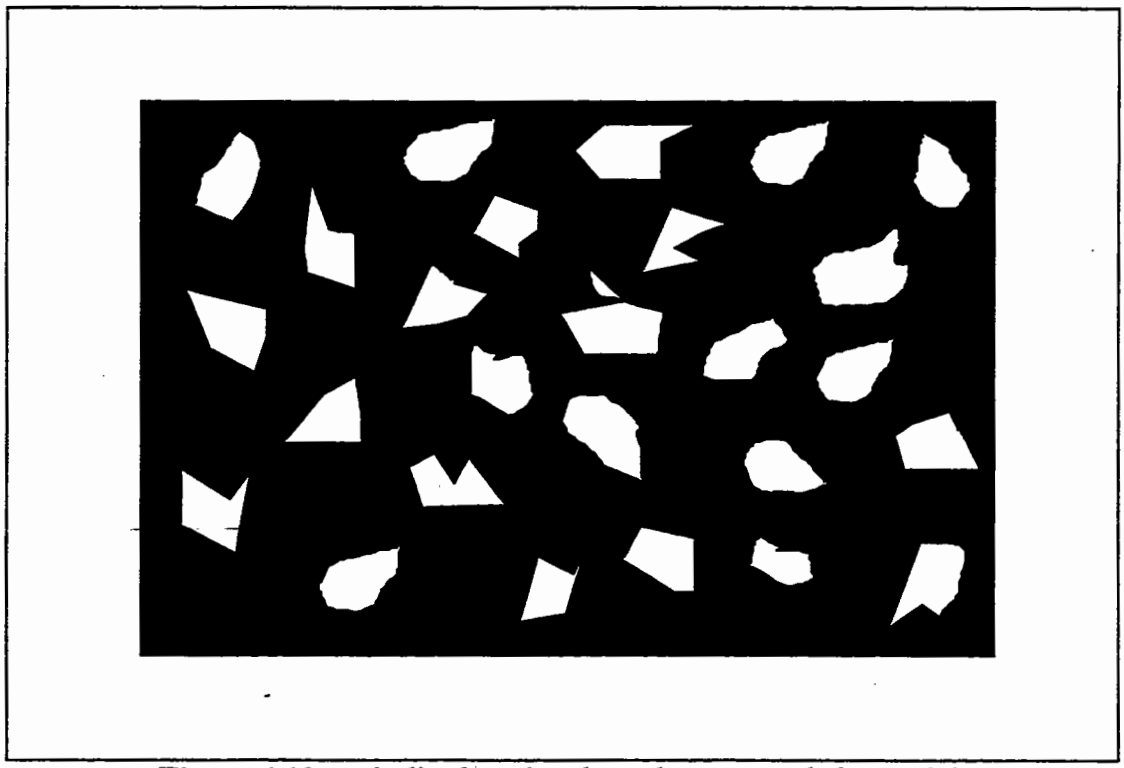

Figure 4.13 Idealised section through a gap graded material.

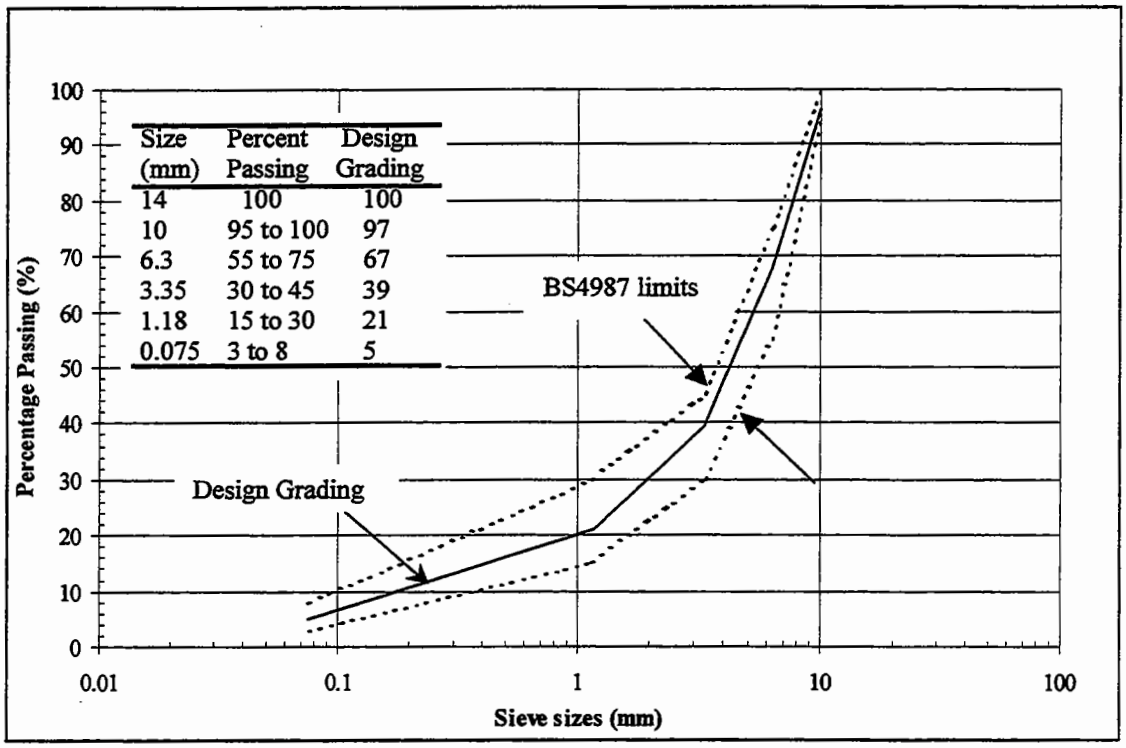

Figure 4.14 Design grading for 10mm Dense Bitumen Macadam.

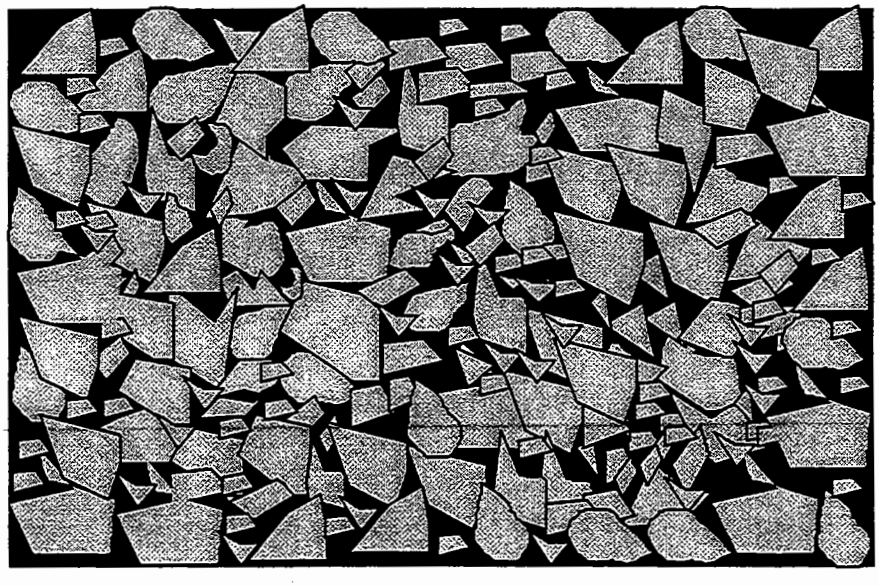

Figure 4.15 Idealised section through a continuously graded material.

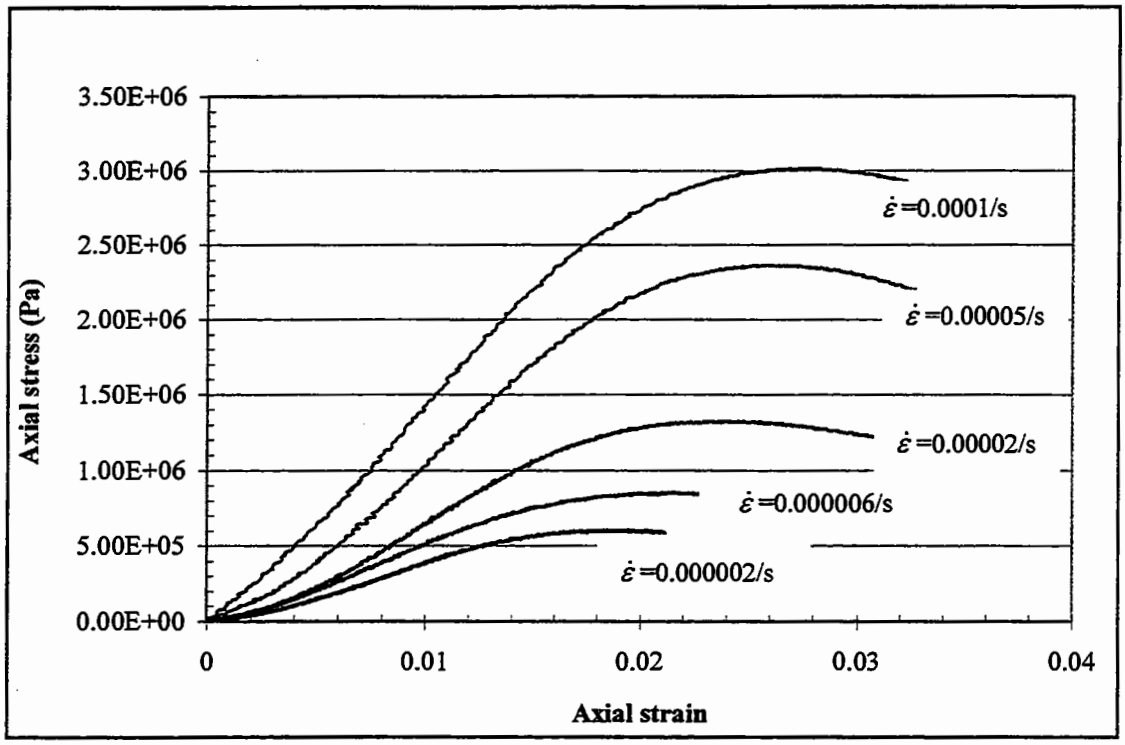

Figure 4.16 Constant strain rate test results for 30/10 Hot Rolled Asphalt at 20°C.

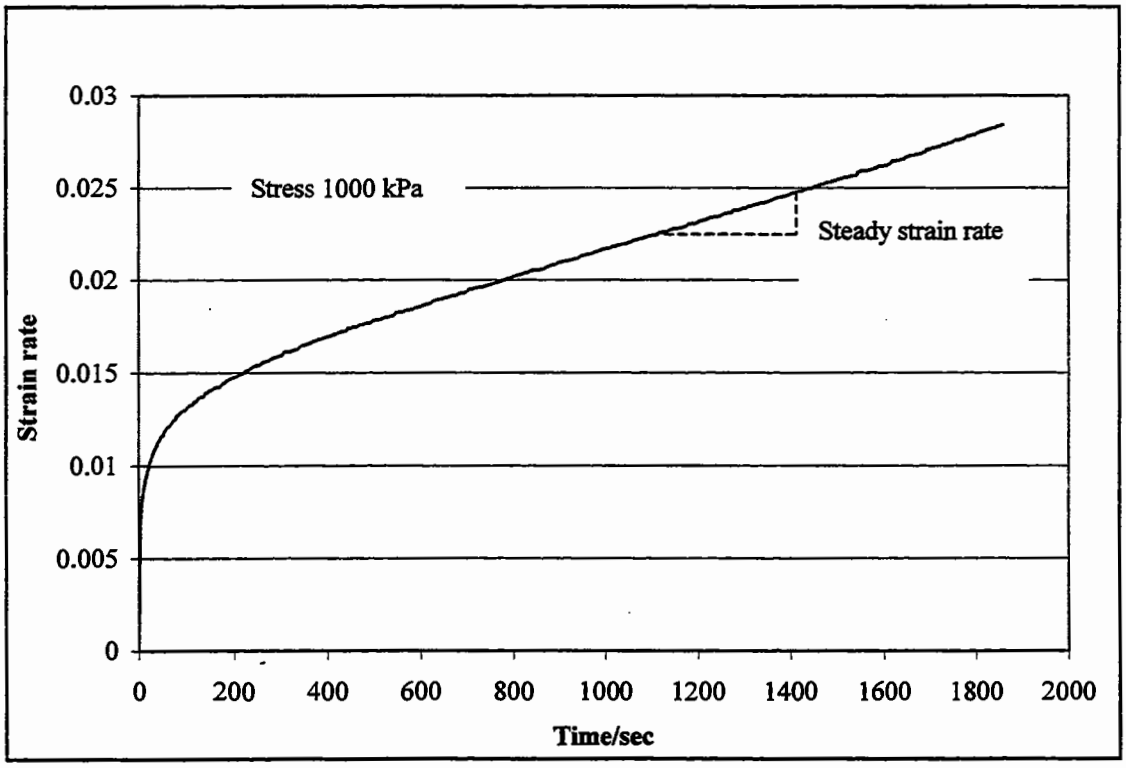

Figure 4.17 Creep test result for 30/10 Hot Rolled Asphalt at 20°C.

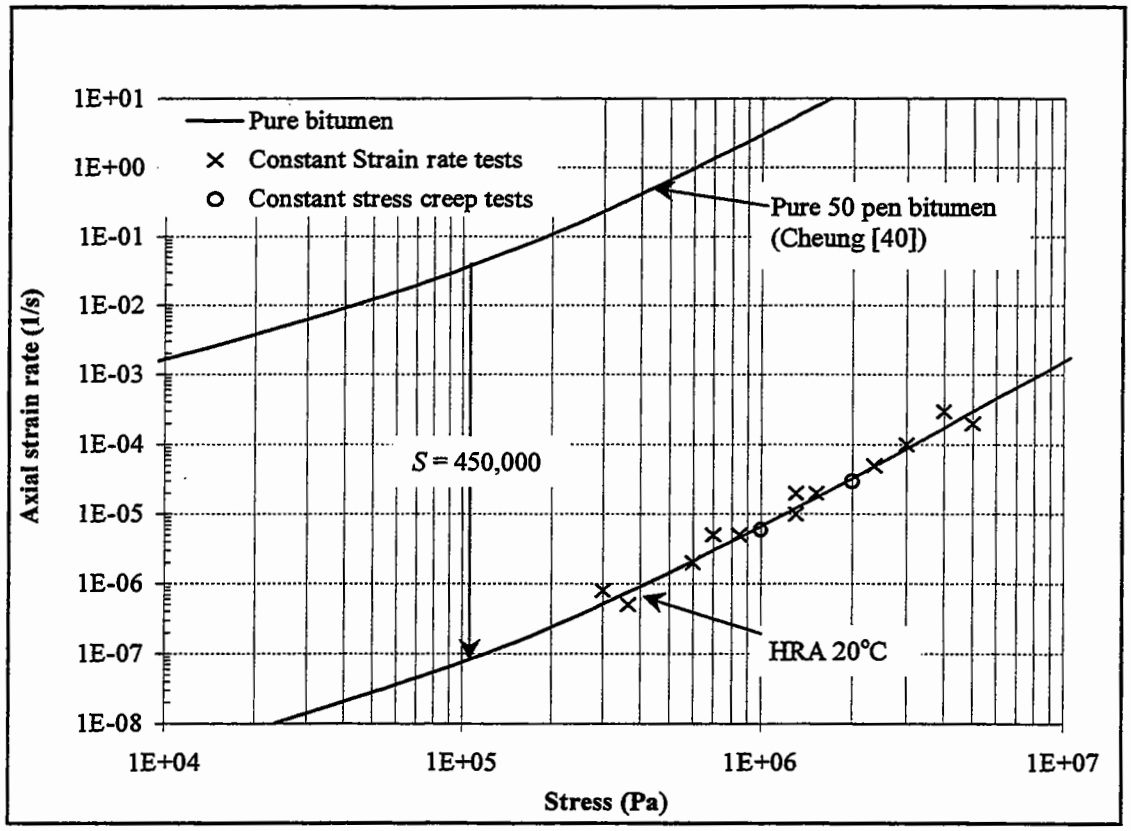

Figure 4.18 Steady-state deformation behaviour of 30/10 Hot Rolled Asphalt at 20°C.

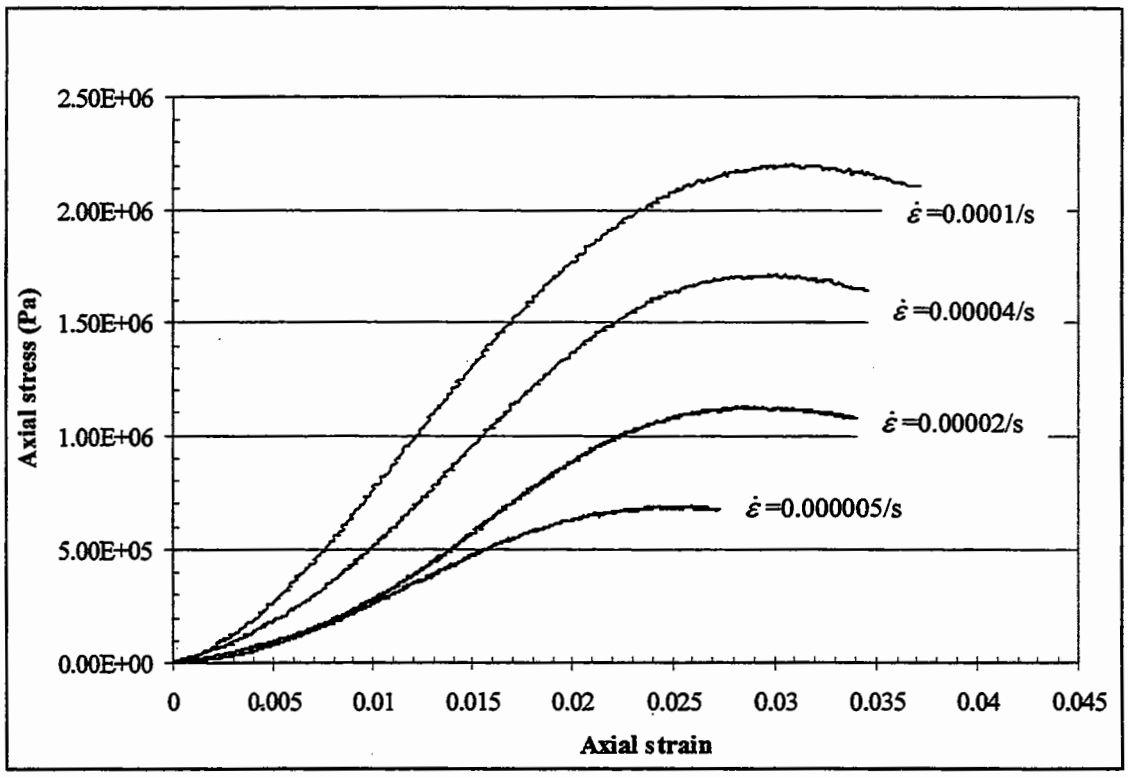

Figure 4.19 Constant strain rate test results for HRA Mortar at 20°C.

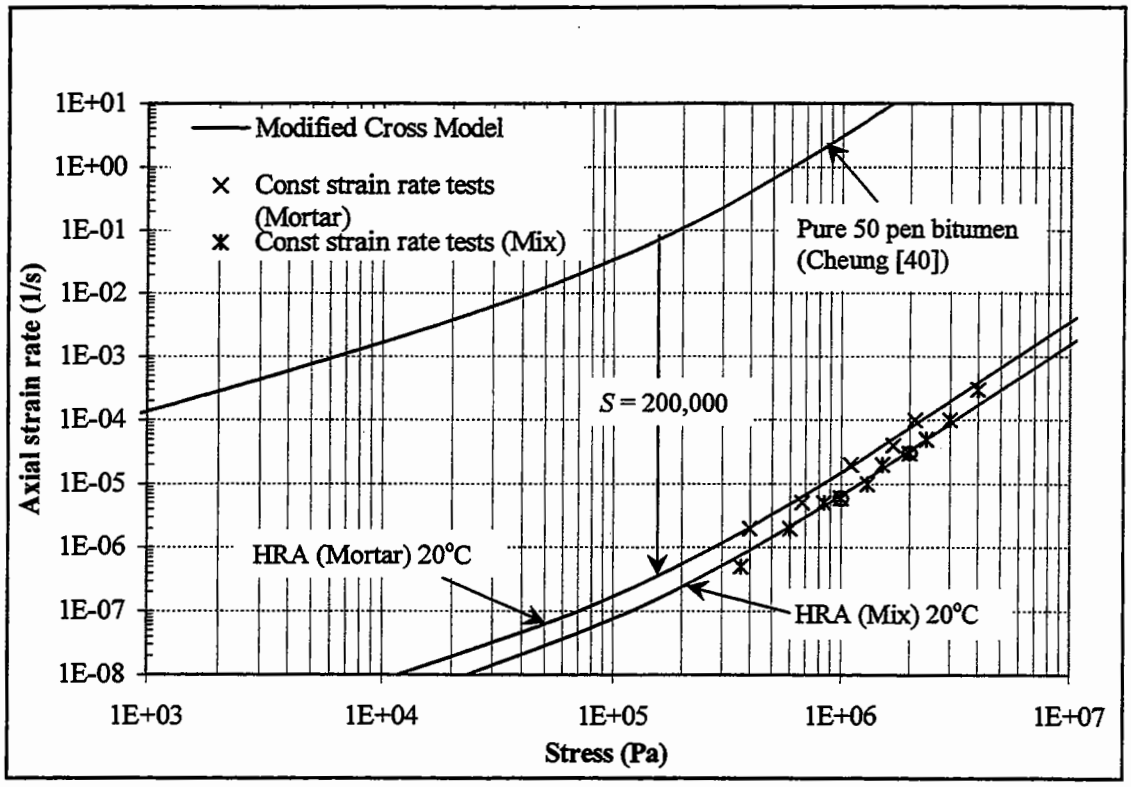

Figure 4.20 Steady-state deformation behaviour of HRA mortar and mixture at 20°C.

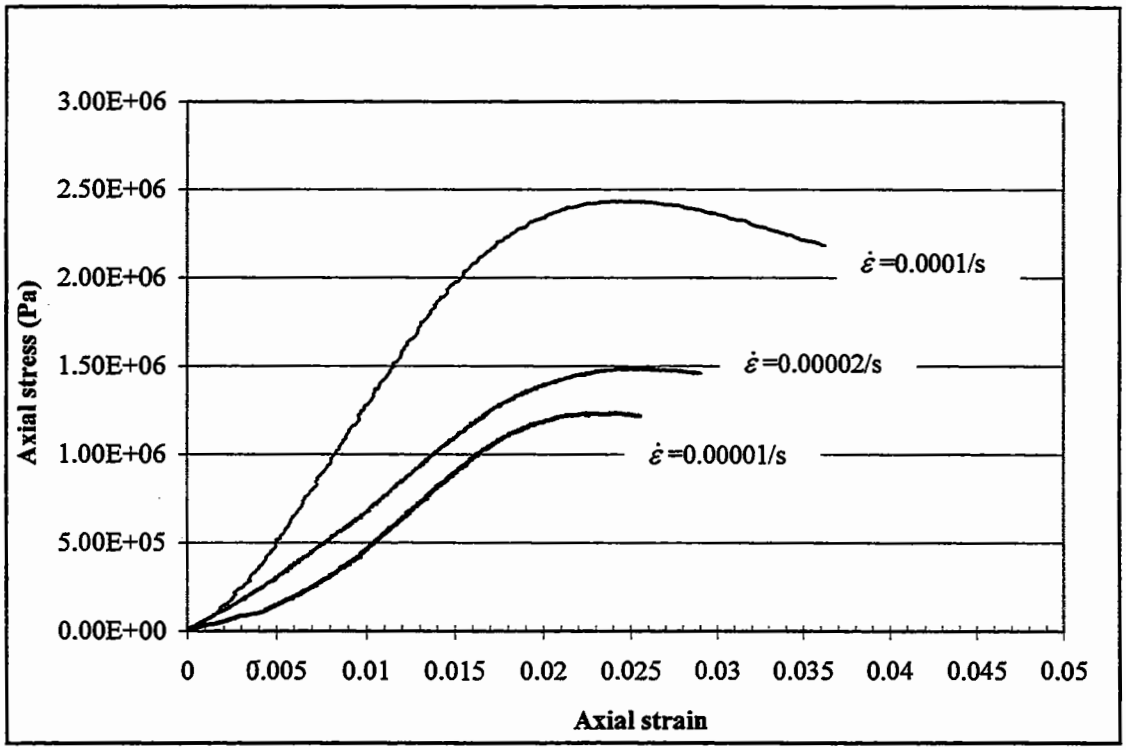

Figure 4.21 Constant strain rate test results for 10mm DBM at 20°C.

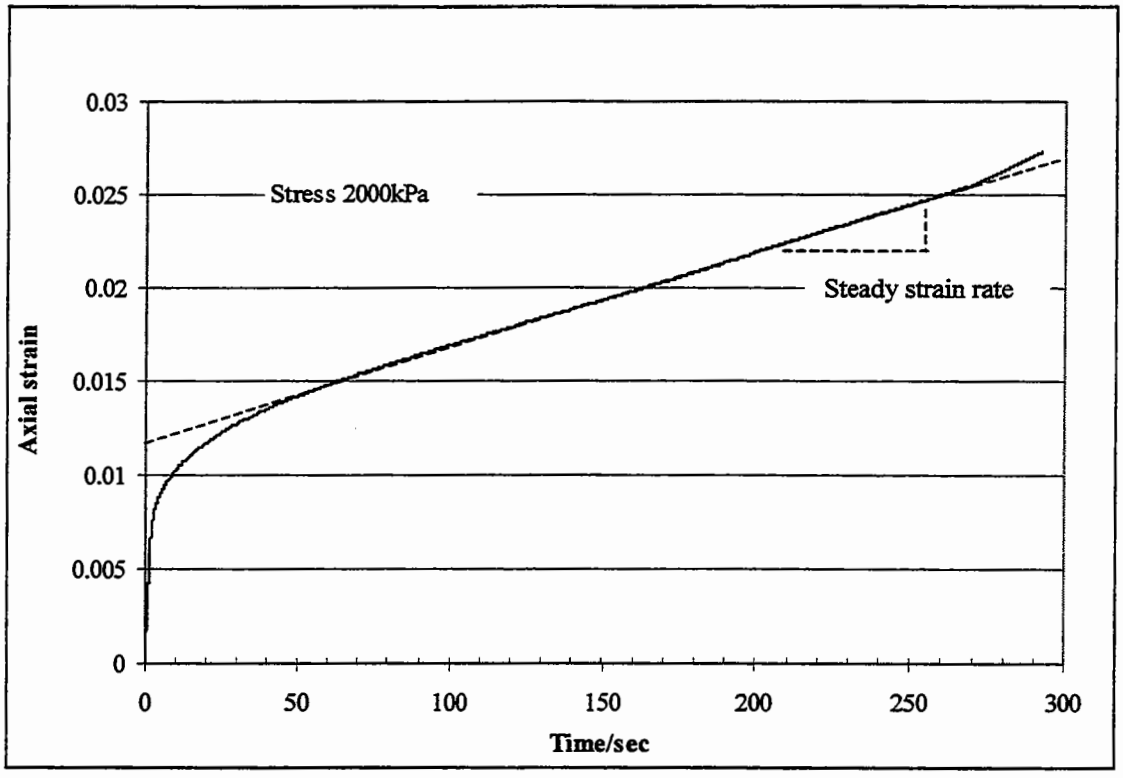

Figure 4.22 Creep test result for 10mm DBM at 20°C.

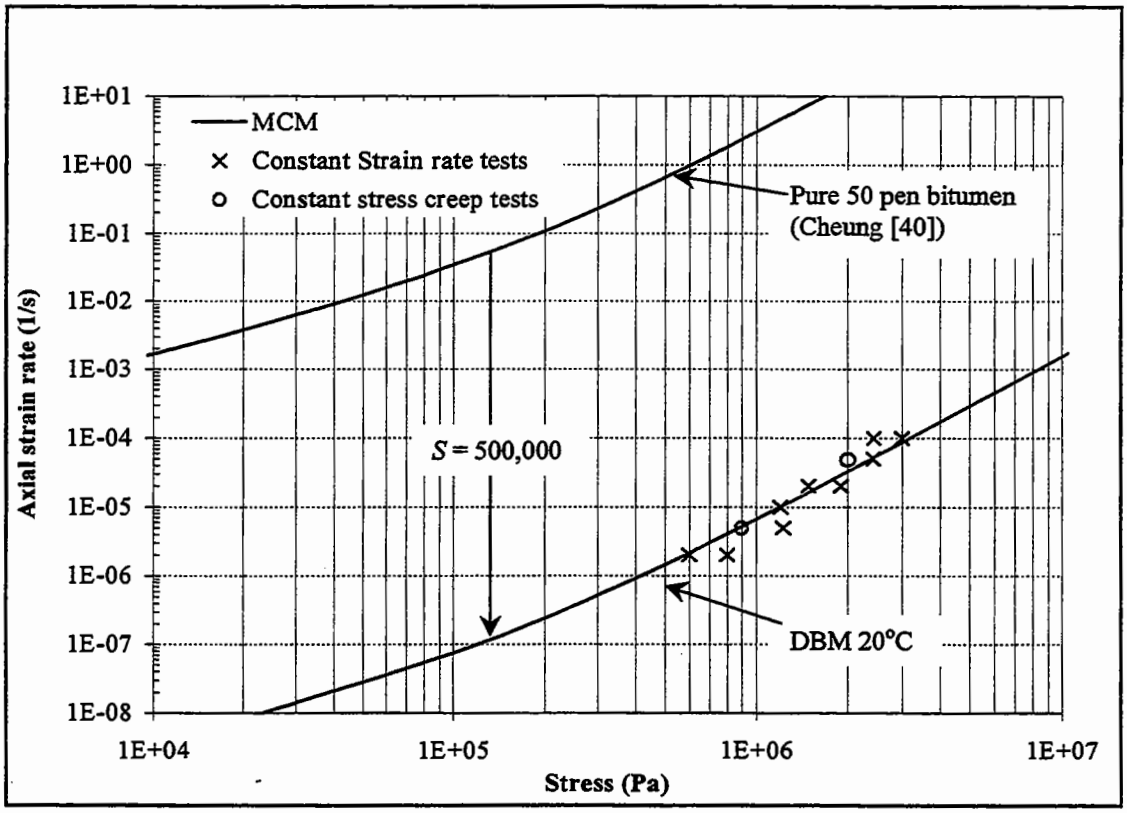

Figure 4.23 Steady-state deformation behaviour of 10 mm DBM at 20°C.

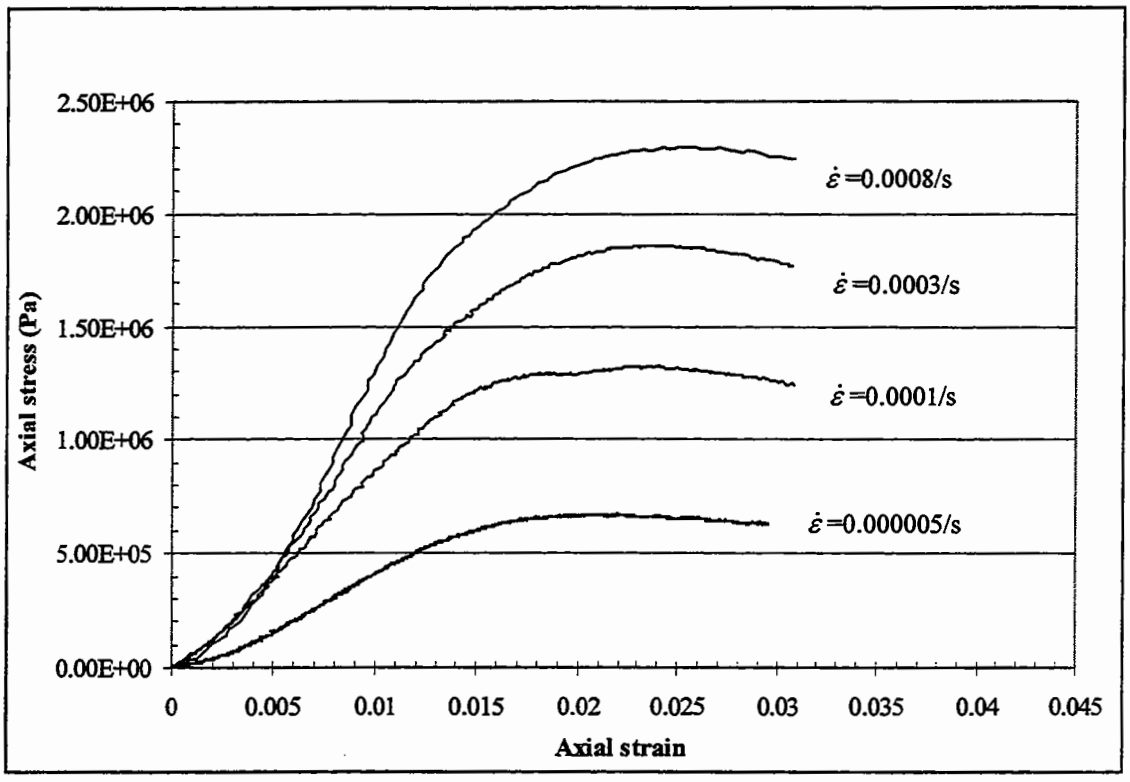

Figure 4.24 Constant strain rate test results for 10mm DBM with 100 Pen Bitumen at 20°C.

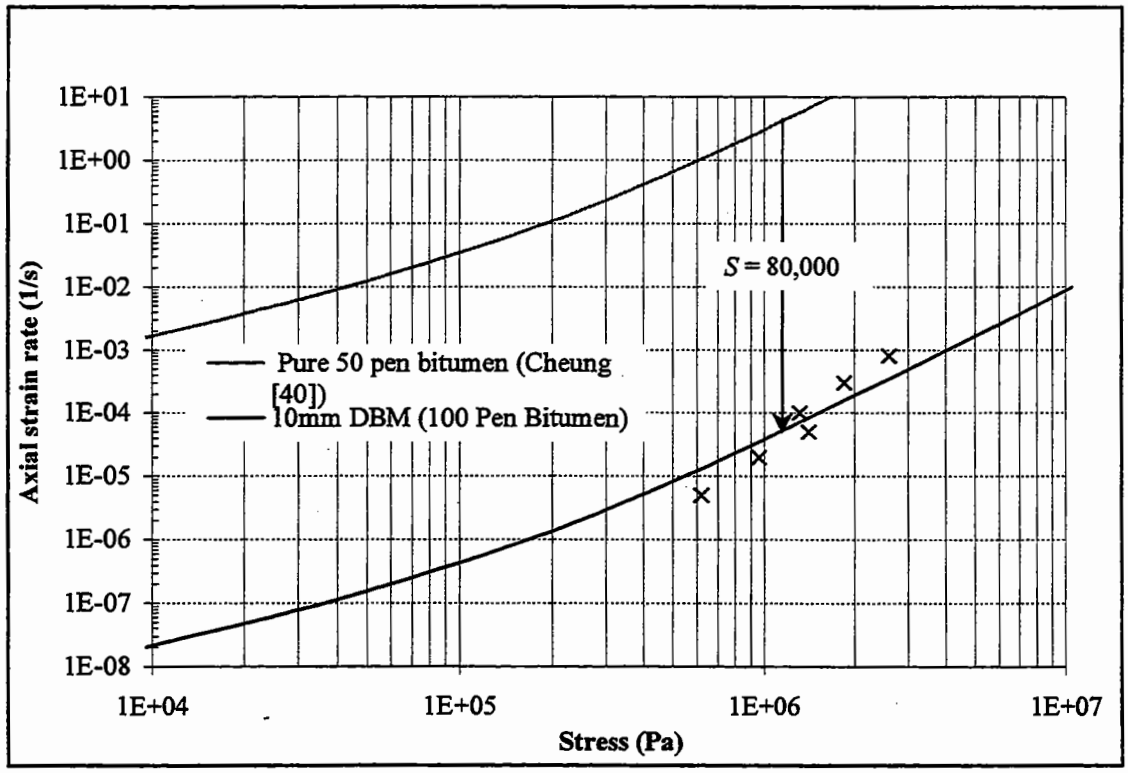

Figure 4.25 Steady-state deformation behaviour of 10mm DBM with 100 Pen Binder at 20°C.

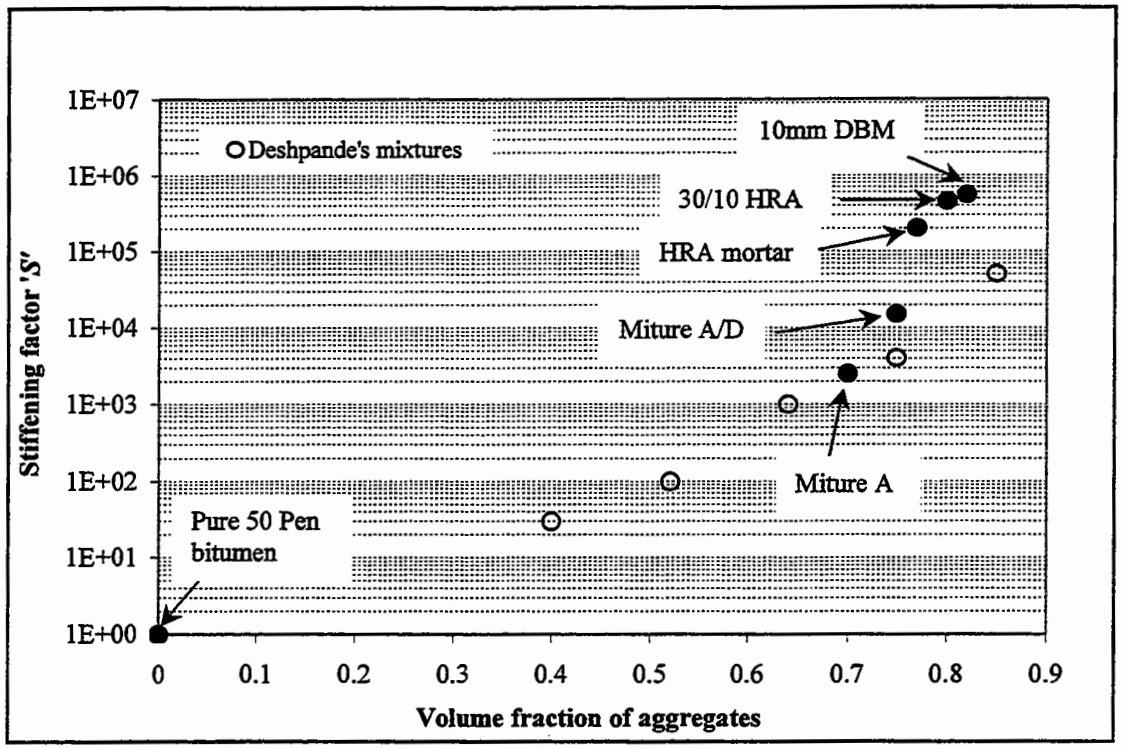

Figure 4.26 Variation of stiffening factor S with volume fraction of aggregates.

Triaxial Tests on Idealised and Realistic Bituminous Mixtures

5.1 Introduction

In soil mechanics the triaxial test has long been recognised as a useful experimental tool for evaluating the shearing resistance, stress-strain characteristics, and strength properties of soils under various stress states. Bituminous mixtures, which are composed of aggregates, bitumen and air voids are to some extent analogous to soils which are composed of soil solids, water and air. Thus it is logical to apply triaxial testing methods developed in soil mechanics to bituminous mixtures. Moreover, to study the response of bituminous mixtures under a wheel load, an understanding of more complicated stress-strain rate relationships is needed (not just uniaxial). For example, Brown and Cooper [24, 25] reported that the deformation behaviour of bituminous mixtures depend on both the hydrostatic (mean) stress and the deviator stress. More recent applications using results from triaxial tests for modelling of experimental studies of bituminous mixtures were reported by Brown and Foo [32] and Low et al [91].

In this chapter triaxial creep tests performed on the idealised mixtures (mixture A/D and mixture A) and the realistic mixtures (30/10 HRA and 10 mm DBM) under various compressive stress states are described. Finally, conclusions regarding the possible mechanism controlling the deformation behaviour of these mixtures in the triaxial state are drawn from the experimental observations.

5.2 Triaxial Testing

5.2.1 Test Equipment

The triaxial testing equipment was located inside a temperature controlled room and consisted of a loading frame, an axially mounted hydraulic actuator, a triaxial cell and instrumentation (including feedback). Figure 5.1 shows a photograph of the test equipment. A controller with data acquisition operated the equipment from outside the temperature controlled room. Hydraulic power was supplied by a pump at a normal operating pressure of 14 MPa. Figure 5.2 shows a schematic layout of the load and control systems. The control system compared the output of the relevant feedback transducer with the input command signal, and the difference was amplified and fed to the servo-valve which adjusted the oil flow to the actuator to reduce the difference between the input and output signals (error signal), so that the actuator responded precisely to the command signal.

The axial load was applied to the sample through a submersible piston, connecting the triaxial cell directly to the hydraulic actuator by sliding smoothly through the end plate of the triaxial cell whilst still providing a fluid tight seal. The load cell was located on the piston above the triaxial cell. The load cell provided the feedback signal required for the control system. There was an option for position control which used a long range LVDT, connected to the load ram to provide the feedback signal.

To ensure that the piston moved freely inside the triaxial cell, a sinusoidal displacement was applied to the piston which was free to move in the triaxial cell without any specimen. The load cell recorded zero load which confirmed that there was minimal friction between the cell and the piston.

The confining fluid used in the triaxial cell was silicone oil. Silicone oil was chosen as the confining fluid due to its low viscosity, excellent electrical insulation properties and the fact that it has no detrimental effect on the membrane, strain gauges or transducers. Air, at the required cell pressure, was directed into the top of the reservoir containing the oil, displacing enough oil to fill the triaxial cell. The air supply was passed through a carbonated filter to avoid any dust or moisture penetrating into the oil. The supply air pressure was monitored by a Bourdon pressure

gauge. A strain gauged diaphragm pressure transducer located in the cell top was used to keep a constant check on the target pressure. If required, the pressure was manually adjusted.

Axial and radial deformations were measured using the in-line displacement transducer fitted to the submersible piston above the triaxial cell, and a radial transducer which was spring loaded through a sealed hole in the membrane at the centre height of the specimen (Figure 5.4). The cable from the radial transducer passed through the bottom of the triaxial cell which was fitted with a microplug and socket. From these deformation measurements, axial and radial strains were calculated.

The triaxial cell was of the standard type commonly used in soil mechanics, modified by Austin [12]. It incorporated an epoxy resin base, perspex side walls and an aluminium cell top. The base was made of resin to eliminate any bi-metallic corrosion caused by different metals on contact with water (the original cell fluid). The cell was designed to test specimens of 150 mm height and 75 mm diameter. It was fitted with castors, to eliminate the need to carry the triaxial cell and limit sample disturbance. A photograph of the triaxial cell is shown in Figure 5.3 (a schematic diagram is shown in Figure 5.5). Analogue outputs from the axial and radial transducers, and the load cell were fed into a personal computer through an analogue to digital converter.

5.2.2 Membrane Preparation

An impervious latex membrane 78 mm in diameter and 267 mm in length was used to seal the specimens from the silicone oil. Measurements were marked on the membrane without stretching it to locate its centre. A soldering iron with a fine tip was then used to puncture the membrane in order to make holes for the studs. These holes were made, such that they were diametrically opposite each other and near the specimen mid-height.

Two curved brass mounting pieces, each with a base width of 20 mm were used to ensure proper seating without imparting any load to the specimen. A piece of sand paper was glued to the bottom of each mounting piece to prevent them sliding during

the test. Small brass threaded studs of diameter 5 mm were screwed into each of the mounting pieces so that they protruded from the membrane. Both the membrane and the mounting piece faces were cleaned with a solvent, and a small amount of adhesive was applied to the membrane, before the studs could be fitted into the holes of the membrane. Each mounting piece was then pressed to the membrane and a nut and washer were screwed over the brass stud such that the membrane was sandwiched between the washer and the mounting piece (see Figure 5.4). Finally a sealing agent was evenly applied to ensure a waterproof seal. The membrane was left overnight to allow the bond to cure.

5.3 Testing Procedure

The experimental setup and the loading arrangement are shown in Figures 5.1 and 5.5. The specimen was placed between the two platens whose surfaces had been lubricated with a mixture of natural soap and glycerine to reduce friction (and thus minimise barelling of the specimen). The latex membrane that surrounded the specimen was fastened to the top and bottom platens by rubber o-rings and aligned so that the studs attached to the membrane made contact with the specimen at the height marked. The radial strain transducer was fitted to the specimen, with a spring holding it in position against the studs so that it was firmly located on the specimen (see Figure 5.6). The spring stiffness was checked to ensure that it imparted enough stress to the mounting pieces to hold them into position without constraining the specimen and causing depressions at point of contact. A visual inspection of the specimens indicated no barelling therefore the radial strain measurements were taken only at mid height of the specimen.

The triaxial cell was filled with silicone oil by pressurising the reservoir with compressed air. Pressure was applied slowly to the cell, and care was taken not leave any air pockets in the cell by bleeding the triaxial cell using the bleed valve on top of the cell, shown in Figure 5.5. The target pressure once achieved, was maintained manually by adjusting the regulator if necessary.

The axial load was applied as quickly as possible and was maintained at that constant value. The axial load, axial displacement, and the radial strain were logged by the computer for the duration of the test.

The principal stresses acting on a cylindrical sample are equal to the pressure (the confining stress), and an additional axial stress (the deviator stress) (see Figure 5.7). As shown in the Figure 5.7, two of these Σ_{22} and Σ_{11} are equal, because of the axial symmetry of the arrangement. The principal stresses are given by:

$$\begin{aligned} \Sigma_{33} &= Q/A + P \\ \Sigma_{22} &= P \\ \Sigma_{11} &= P \end{aligned} \tag{5.1}$$

where Q = applied load
A = nominal cross-sectional area of the specimen
P = confining pressure

Thus the mean stress (Σ_m), and the deviator stress (Σ) acting on the specimen are:

$$\Sigma_m = \frac{\Sigma_{11} + \Sigma_{22} + \Sigma_{33}}{3} = P + Q/3A \tag{5.2}$$

$$\Sigma = \Sigma_{33} - \Sigma_{11} = Q/A \tag{5.3}$$

The triaxial tests were performed over a range of confining and deviator stress states. The stress conditions were characterised by a stress ratio η, defined by Deshpande [53] as:

$$\eta = \Sigma_m/\Sigma \tag{5.4}$$

where η = stress ratio
Σ_m = mean stress

Σ = deviator stress

The stress ratio was varied between 0.6 and 0.8 (it should be noted that a uniaxial test results in a stress ratio of 0.33).

5.4 Experimental Results

5.4.1 Idealised Mixtures (Mixture A/D and Mixture A)

Constant stress creep tests were performed on mixture A/D and mixture A at 20°C. Typical data for triaxial creep tests on mixture A/D are shown in Figure 5.8, where the axial creep strain is plotted as a function of time elapsed from the application of the axial load. It can be seen from this figure that the creep curve has a similar form to results from the uniaxial creep tests described in Chapter 4. Again the creep curve can be divided into three regions: primary creep, secondary creep and tertiary creep where the failure occurs. As before, the secondary creep strain rate has been chosen to represent the deformation behaviour of the mixtures. Tests were performed over a range of confining and deviator stresses. The confining stress ranged from 25 to 500 kPa, whilst the deviator stress ranged from 100 to 1000 kPa.

Figure 5.9 shows the steady-state deformation behaviour of mixture A/D where the axial steady-state axial strain rate is plotted against the deviator stress. Also shown in the figure is the curve representing the uniaxial steady-state deformation behaviour of bitumen at 20°C obtained by Cheung [40]. The dotted line in the figure represents the uniaxial creep behaviour for mixture A/D at the same temperature (see Chapter 4). It can be seen from this figure that, as with the uniaxial behaviour, the steady-state triaxial behaviour can be represented by:

$$\frac{\Sigma}{\sigma_o} = \frac{S\dot{\varepsilon}}{\dot{\varepsilon}_o}\left(\frac{1}{1+\left(\frac{S\dot{\varepsilon}}{\dot{\varepsilon}_o}\right)^{n_c}}\right) \tag{5.5}$$

Equation 5.5 is shown by the solid lines in Figure 5.9. It can be seen from Figure 5.9 that, as the stress ratio increases, the mixture becomes stiffer. For example, S increases from approximately 15,000 for a stress ratio of 1/3 (uniaxial) to 220,000 for a stress ratio of 0.8 indicating that the mixture is becoming harder to deform.

A typical creep curve from a triaxial creep test on the mixture A is shown in Figure 5.10. It can be seen from the figure that this creep curve is similar to the creep curve obtained for mixture A/D. The steady-state deformation behaviour of mixture A under various stress states is shown in Figure 5.11 where the steady-state axial strain rate is plotted against deviator stress. It can be seen that, similar to mixture A/D, the deformation behaviour of mixture A can also be represented by Equation 5.5 where the stiffening factor S is a function of the stress ratio. The uniaxial steady-state deformation behaviour of the bitumen obtained by Cheung [40] is also shown in Figure 5.11. The dotted line represents the uniaxial behaviour of mixture A. As can be seen from this figure, the stiffening factor S increases from approximately 2,500 for stress ratio of 1/3 (uniaxial) to a factor of 20,000 for a stress ratio of 0.8.

Analysis of the radial strains showed that the idealised mixtures were found to dilate under triaxial compressive loading. A plot of radial strain versus the axial strain is shown in Figure 5.12 for mixture A. For both mixtures A and A/D the slope of the dilation curve was found to be approximately 1 in the region where steady-state conditions are achieved. This linear dependence of radial strain on axial strain was found to be independent of the applied stress. Similar results were obtained by Deshpande [53].

For the cylindrical specimens the volumetric strain H is given by:

$$H = 2E_{11} + E_{33} \tag{5.6}$$

E_{11} and E_{33} are the radial and axial strains respectively. The distortional strain E is given by:

$$E = E_{33} - H/3 = 2/3\ (E_{33} - E_{11}) \tag{5.7}$$

Figures 5.13 and 5.14 show the relationship between the distortional strain and the volumetric strain for mixture A/D and mixture A respectively. It can be seen from these figures that this relationship is also linear and can be expressed as:

$$H = s\,|E| \tag{5.8}$$

where s is the dilation gradient or the slope of the line in the figures. For mixtures A and A/D the measured values of s at steady-state conditions are given in Table 5.1. Since the sign convention for dilation is positive the absolute values of the distortional strain are taken in Equation 5.8. It should be noted that, as all the tests were conducted in compression, the sign convention for the axial strain values was taken to be negative in Equations 5.6 and 5.7. The effect of dilation gradient s on the deformation behaviour of bituminous mixtures is discussed later in this chapter (see discussion).

For the idealised mixtures, triaxial testing was only performed at a temperature of 20°C. It was assumed that the temperature dependence of the mixtures under triaxial stress conditions would be the same as that of the idealised mixtures under uniaxial conditions (see Chapter 4).

Table 5.1 Dilation Gradients for Idealised and Realistic Mixtures

Mixture	Mean	Dilation Gradient (range)
A	0.95	0.8 – 1.1
A/D	1.2	1.14 – 1.27
30/10 HRA	1.33	1.29 – 1.37
10 mm DBM	1.38	1.30 – 1.45

5.4.2 Realistic Mixtures (HRA and DBM Mixtures)

30/10 HRA Mixture

Constant stress creep tests were also performed on a 30/10 HRA mixture at 40°C. The binder used in the mixture was a 50 Pen grade bitumen. Typical data from a triaxial creep test on an HRA mixture is shown in Figure 5.15, where the axial strain is plotted as a function of time elapsed since the application of the load. It can be seen from this figure that the curve is similar to the creep curve for the idealised mixtures (mixture A/D and mixture A). The secondary creep region can clearly be identified which, as before, is characterised as the steady-state deformation behaviour of the HRA. It can also be seen from Figure 5.15 that the steady-state strain rate occurs at an axial strain of approximately 2.5 to 3%, which is similar to the behaviour observed under uniaxial conditions for HRA mixtures.

The steady-state deformation behaviour of the HRA mixture under various stress states is shown in Figure 5.16, where the steady-state axial strain rate is plotted against deviator stress. It can be seen that, as with the idealised mixtures, the deformation behaviour of the HRA mixture can again be represented by Equation 5.5 with the stiffening factor S being a function of stress ratio. The deformation behaviour of the HRA mixture in the power law region was characterised by an effective creep exponent of 2.4, indicating binder dominated behaviour under triaxial conditions. The uniaxial steady-state deformation behaviour of the 50 Pen grade of bitumen is shown in the Figure 5.16, while the dotted line represents the uniaxial behaviour of HRA mixture at 20°C. For comparison, the uniaxial deformation behaviour of the HRA mixture at 40°C is also shown in the figure (dashed line). It has been produced assuming the temperature dependence of the HRA mixture is same as that of the pure bitumen (the same 50 Pen grade of bitumen was used). It can be seen from this figure that at the same test temperature (40°C) the stiffening factor S increases from approximately 4,000 for stress ratio of 1/3 (uniaxial) to a factor of 3E+07 for a stress ratio of 0.6.

For the HRA mixture the radial strain was also found to vary linearly with the axial strain. This is shown in Figure 5.17, in terms of volumetric and distortional strain. The

observed ranges for the values of s for the HRA mixtures are given in Table 5.1. It can be seen from this table that the values of s for HRA mixture are higher then the values for idealised mixtures (mixture A and A/D). The implications of this are discussed later in this chapter (see discussion).

10 mm DBM Mixture

Constant stress creep tests were also conducted on the 10 mm DBM mixture at 40°C. The binder used was a 100 Pen grade of bitumen. Figure 5.18 shows data from constant stress creep tests on the 10 mm DBM mixture. It can be seen from this figure that the primary and secondary creep regions can clearly be identified. However, after the secondary region the slope of the curve tends to decrease rather than increase as with the other mixtures. This indicates that the rate of deformation is decreasing and the material is tending to 'lockup'. This is likely to be due to the continuously graded aggregate skeleton and is investigated further in section 5.5.

It can also be seen from Figure 5.18 that the steady-state strain rate occurs at an axial strain of approximately 2.5 to 3%. Data from all the creep tests conducted on the DBM mixture demonstrated a similar trend in which there was a binder dominated linear viscous region occurring at an axial strain of approximately 3% (this linear region was taken as steady-state deformation behaviour) after which the strain rates decreased gradually representing aggregate dominated behaviour.

The steady-state deformation behaviour of the DBM mixture at 40°C and at a stress ratio of 0.6 is shown in Figure 5.19, where the steady-state axial strain rate is plotted against the deviator stress. It can be seen that the data from all the tests can again be characterised with an effective creep exponent of 2.4 in the non-linear region. It can be seen that this binder dominated steady-state deformation behaviour is similar to that observed from the uniaxial tests conducted on the DBM mixture except for the increase in the stiffening factor. The uniaxial steady-state deformation behaviour of the 100 Pen bitumen is also shown in the figure, whilst the dotted line represents the uniaxial behaviour of 10 mm DBM mixture at 20°C. For comparison, the uniaxial deformation behaviour of the DBM mixture at 40°C is also shown in Figure 5.19 (dashed line). As before, it has been produced assuming the temperature dependence

of the DBM mixture to be the same as that of pure bitumen. It can be seen from this figure that at the same test temperature (40°C) the stiffening factor S increases from approximately 12,500 for a stress ratio of 1/3 (uniaxial) to a factor of 6.3E+06 for a stress ratio of 0.6.

The variation of volumetric strain with distortional strain for the DBM mixture is shown in Figure 5.20. The observed ranges for the values of s for the DBM mixtures are given in Table 5.1. It can be seen from this table that the values of s for the HRA and DBM mixtures are higher then the values for idealised mixtures (mixture A and A/D) (see discussion). It can also be seen from this table that the values of s are higher for the DBM as compared to the HRA due to the differences in aggregate grading.

5.5 Unbound Granular Material Testing

Results from triaxial testing on the DBM material indicate that the aggregate skeleton plays an important role in the deformation behaviour during the latter stages of the triaxial creep test. In an attempt to isolate the effects of the aggregate, a dry aggregate mixture of the 10 mm DBM grading was tested, such that the batch proportions for each aggregate size were the same as for the mixture with the bitumen (same aggregate packing density). Triaxial creep and constant strain rate tests were performed on the unbound specimens. The following sections describe the technique used for sample preparation and the results from the testing.

5.5.1 Specimen Preparation

Specimen manufacture was achieved by compacting the aggregate into a cylindrical mould 150 mm in height and 75 mm in diameter. A latex rubber membrane was attached by an 'O' ring to the bottom platen, and stretched up the side of the mould. A vacuum was applied through the wall of the mould which ensured that the membrane lay flat against it (see Figure 5.21). Once the mould was set up the material was placed in five layers each compacted by hand tamping. The top platen was attached, again using an 'O' ring to secure the membrane. The specimen was then placed in the triaxial apparatus, a vacuum was applied internally to the specimen through the

bottom platen to keep the specimen intact and the mould was then carefully removed. During the initial trial tests, it was found that the process of compaction punctured the membrane, therefore another membrane was added at this stage to ensure no leakage. Finally, the triaxial cell was attached to the cell base and the specimen was ready to be tested.

5.6 Experimental Results

Constant stress creep tests and constant strain rate tests were conducted on the dry DBM mixture. The data obtained from the constant stress creep tests are presented in Figure 5.22, where the creep strain is plotted as a function of time elapsed after the application of the load. Tests were carried out at a constant stress ratio of 0.6 which was kept at a constant level by manually adjusting the air pressure valve. Since the deformation behaviour of the unbound aggregate is stress dependent, to accelerate the deformation process the initial applied load was increased during the test from 800 kPa to 1000 kPa and it can be seen from the Figure 5.22 that there is a corresponding increase in the axial strain. It can be seen from Figure 5.22 that there is an initial strain in the material of about 6.5% and after that a gradual increase in strain can be observed. At 1000 seconds when the load was increased, there was again an instantaneous increase in strain to about 8%, after which there was some further increase in the strain until the end of the test. Similar results were obtained from two replicate tests. Consequently, on the basis of this creep test result, it would be logical to assume that the aggregate seems to have a limiting strain value that depends on the magnitude of the applied deviator stress and the stress ratio.

Results from the constant strain rate tests on the dry DBM mixture are shown in Figure 5.23 together with results from the normal DBM mixture (with the bitumen). In this test, a constant confining pressure of 213 kPa was applied to the specimen (it should be noted that in this type of test the stress ratio was not maintained at a constant level). It can be seen from the figure that steady-state stress for the dry mixture occurs at an axial strain of approximately 14%. Also shown in the figure are test results from the DBM mixture (with bitumen) at various strain rates and the same constant confining pressure (213 kPa). For the DBM mixture the steady-state stress as observed from uniaxial tests reaches its limiting value of 1.5 MPa at an axial strain of

approximately 6%. It can be seen from this figure that the dry mixture tested at the same strain rate tends towards a similar value of stress but at a much larger value of strain (>18%). Consequently, on the basis of these limited tests it can be assumed that the mixture has a certain limiting value of stress at which it fails, the form of which is determined by the aggregate grading.

5.7 Discussion

The two mechanisms with which bituminous materials resist permanent deformation are (i) frictional resistance between the particles as they slip during shear distortion and (ii) interlocking of the aggregates. As an example consider the direct shear box test [18] schematically shown in Figure 5.24, with bitumen filling the gaps between the rigid particles. As the relative displacement between the two halves of the shear box is increased by dx, there is an increase in the separation between the two halves of the box by an amount dy. From Figure 5.24 it can be seen that for a displacement in the x direction to occur the aggregates need to 'ride up' over each other, which in turn results in a displacement in the y direction. The quantity dy/dx indicates the rate of dilation of the rigid particles in the shear zone and is a measure of interlocking. If the normal stress σ is increased whilst keeping the shear stress τ constant, a point will be reached when no further deformation is possible implying that beyond a certain critical stress ratio σ/τ no further deformation will take place. Thus, as the stress ratio increases the deformation rate decreases or the stiffening factor increases (see for example Figures 5.9 and 5.11). Since the normal stress is compressive, 'lockup' occurs due to the interlocking of the aggregates. This lockup of the mixtures has been previously found to be controlled by the dilation gradient 's' of the aggregate [53]. Deshpande [53] found that for his idealised mixtures with 64% and 75% volume aggregate fraction lockup occurred at stress ratios of 1.28 and 1.67 respectively. It was also found that increasing the dilation gradient s results in a higher stiffening factor for a mixture with the same volume fraction of aggregates subjected to the same stress ratio (for further details see [53]).

Consequently, high values of dilation gradient not only result in earlier lockup of the mixtures but also an increase in the stiffening of the bituminous mixtures. For mixtures like the DBM with more complex aggregate structure it may be assumed

that, as the load is applied, the bitumen is squeezed out from between the aggregate particles resulting in point to point contact throughout the aggregate skeleton. Once this is achieved, the strain rates are expected to depend to some extent on the geometry and complexity of the aggregate structure. Consequently 'lockup' occurs in the DBM mixture which is also reflected by a higher mean value of the dilation gradient s = 1.38. Figure 5.25 shows the dilation gradients measured for various mixtures plotted as a function of volume fraction of aggregates in the mixture. Also shown in Figure 5.25, is the mean value of dilation gradient measured by Deshpande [53] for his range of idealised mixtures with 64% volume of aggregate. It can be seen from this figure that there is a trend of increasing dilation gradients with increasing volume fraction of aggregate. Based on these results it may be assumed that the dilation gradient increases with the aggregate proportions in the mixture. In other words, as a result of the aggregate, interlocking increases and consequently s increases. This relationship of s to the aggregate properties (e.g. particle shape, size gradation and volume fraction) is not fully understood and requires further research. However, as the dilation gradient s has such a dominant effect on the deformation properties of the mixture, further work into understanding the factors affecting s needs to be undertaken to improve mixture design. It should be noted that the previous research [53] modelled the stiffening effect for various idealised mixtures and used the dilation gradient s as an input to the viscous model. Since the stiffening of the mixture is largely dependent on the values of s as explained earlier, consequently, this parameter which depends on the geometry of the aggregate in a mixture should be taken into account in modelling the permanent deformation behaviour of bituminous mixtures.

While the idealised mixtures (mixture A and A/D) were tested to a maximum stress ratio of 0.8, the realistic mixtures (HRA and DBM) could only be tested to a maximum stress ratio of 0.6. It was found that, on increasing the stress ratio further for these types of mixtures, no significant creep could be induced by the applied load to the test specimen even at a temperature of 40°C. In other words, there was an increase in the stiffening effect and hence decrease in the deformation rate. Consequently, tests on realistic mixtures at high stress ratio (i.e. 0.8) were not feasible. An example of the stress ratio distributions in a wheel tracking slab under a loaded wheel are shown in Figure 8.4 (Chapter 8). A comparison between Figures 8.2

and 8.4 shows that the region of maximum deformation corresponds to a stress ratios in the range of 0.3 to 0.65 (see Chapter 8), hence testing the idealised and the realistic mixtures over stress ratios in the range 0.33 to 0.8 was considered to be sufficient.

5.8 Conclusions

The following conclusions can be drawn from this chapter:

- At a constant stress ratio the triaxial steady-state deformation behaviour of the idealised mixtures (mixture A and A/D) and the realistic mixtures (HRA and DBM) has the same form as that of the pure bitumen.

- The steady-state deformation behaviour of the idealised and the realistic mixtures was found to be dependent on the mean stress and the deviator stress.

- The stiffening factor S was found to be a function of the volume fraction of the aggregate and the stress ratio ($\eta = \Sigma_m/\Sigma$).

- In the later stages of the creep test, the deformation behaviour of the DBM mixture was found to be dependent on the aggregate skeleton.

- Both the idealised and realistic mixtures were observed to dilate under compressive triaxial stresses.

- For the idealised and realistic mixtures the volumetric strain was found to vary linearly with the distortional strain and was independent of the stress ratio and deviator stress.

- The value of the dilation gradient s was observed to be dependent on the volume fraction of aggregates. The mean value of s for mixture A was found to increase from 0.95 to 1.2 for mixture A/D.

- For HRA and DBM mixtures the mean values of dilation gradient s were observed to be higher than for the idealised mixtures at corresponding stress ratios.

- The dilation gradient s was found to have a significant effect on the deformation behaviour of the mixtures. The results indicate that above a critical stress ratio (see discussion) mixtures with high value of s are expected to lockup (i.e. no deformation is possible).

5.9 Figures

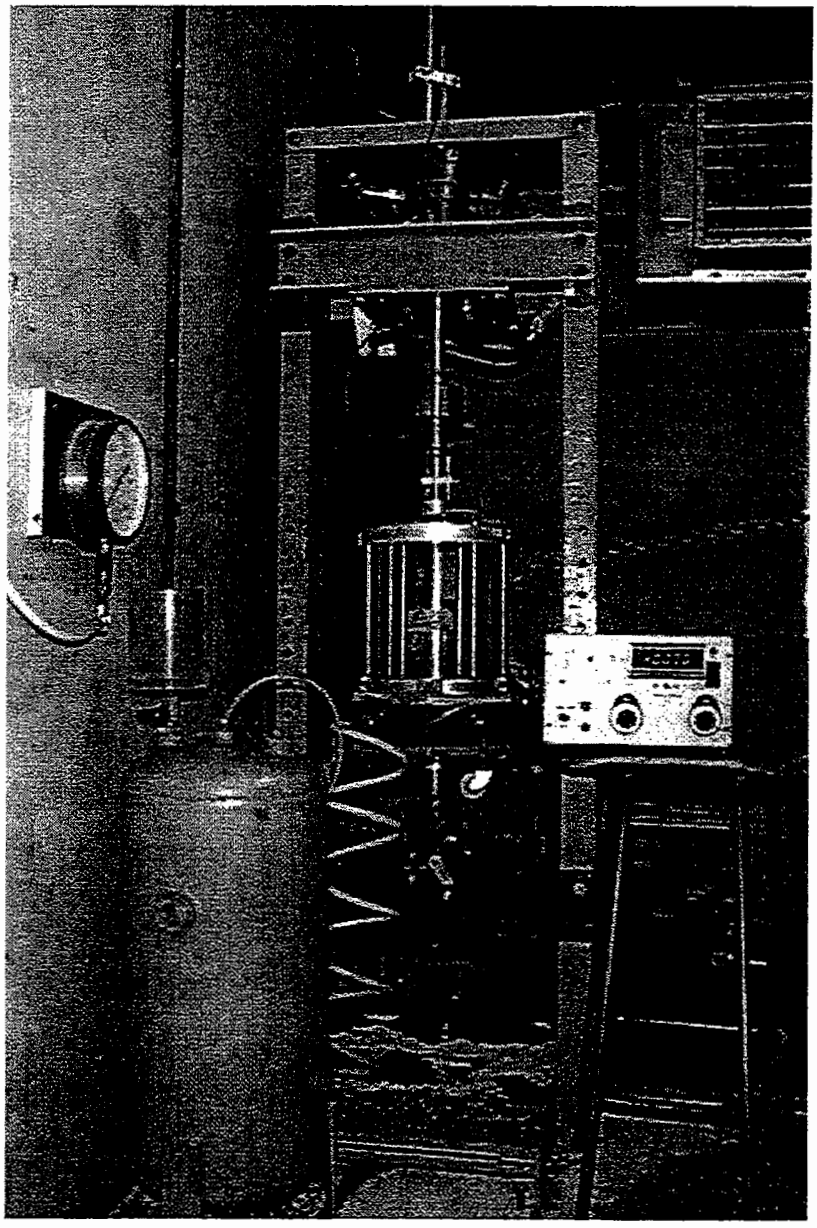

Figure 5.1 Triaxial Testing Equipment (general view).

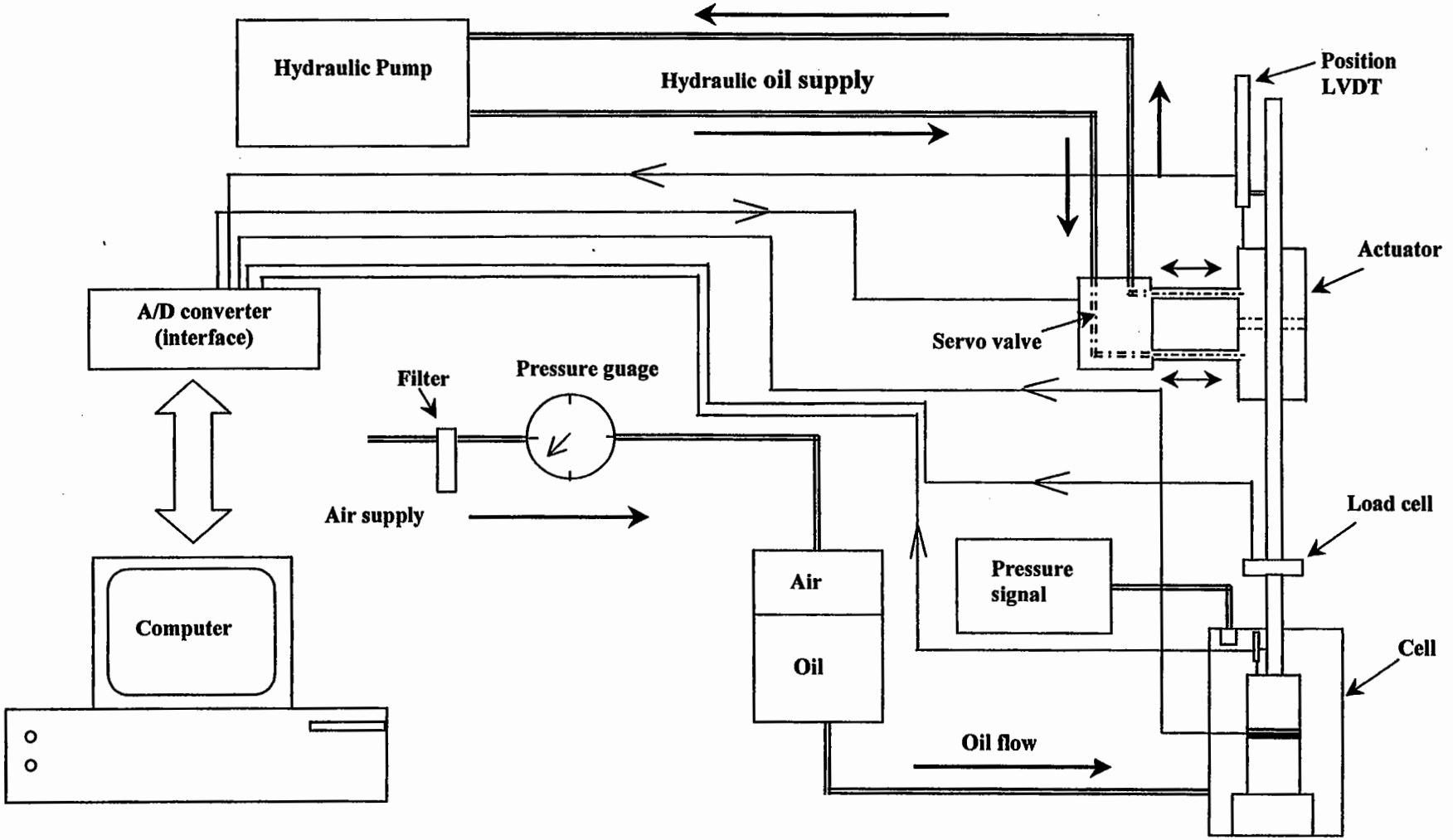

Figure 5.2 Schematic of triaxial experimental setup.

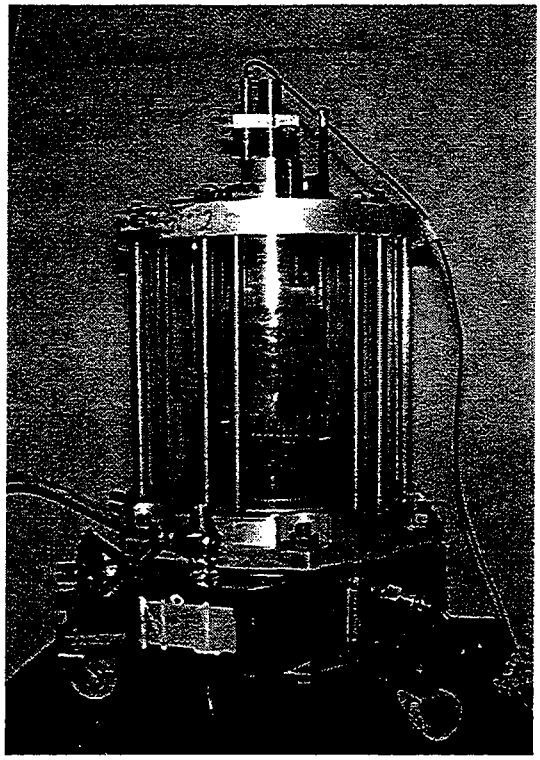

Figure 5.3 Photograph of the Triaxial Cell.

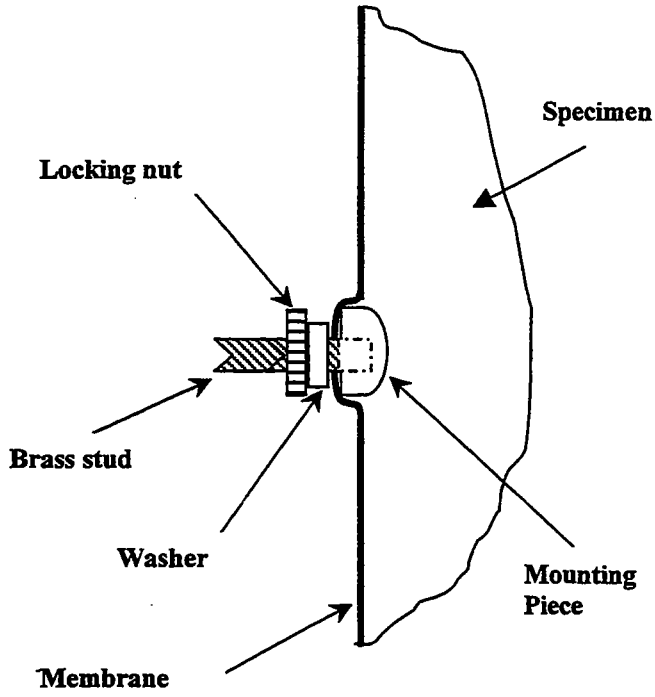

Figure 5.4 Schematic showing arrangement for radial strain measurement.

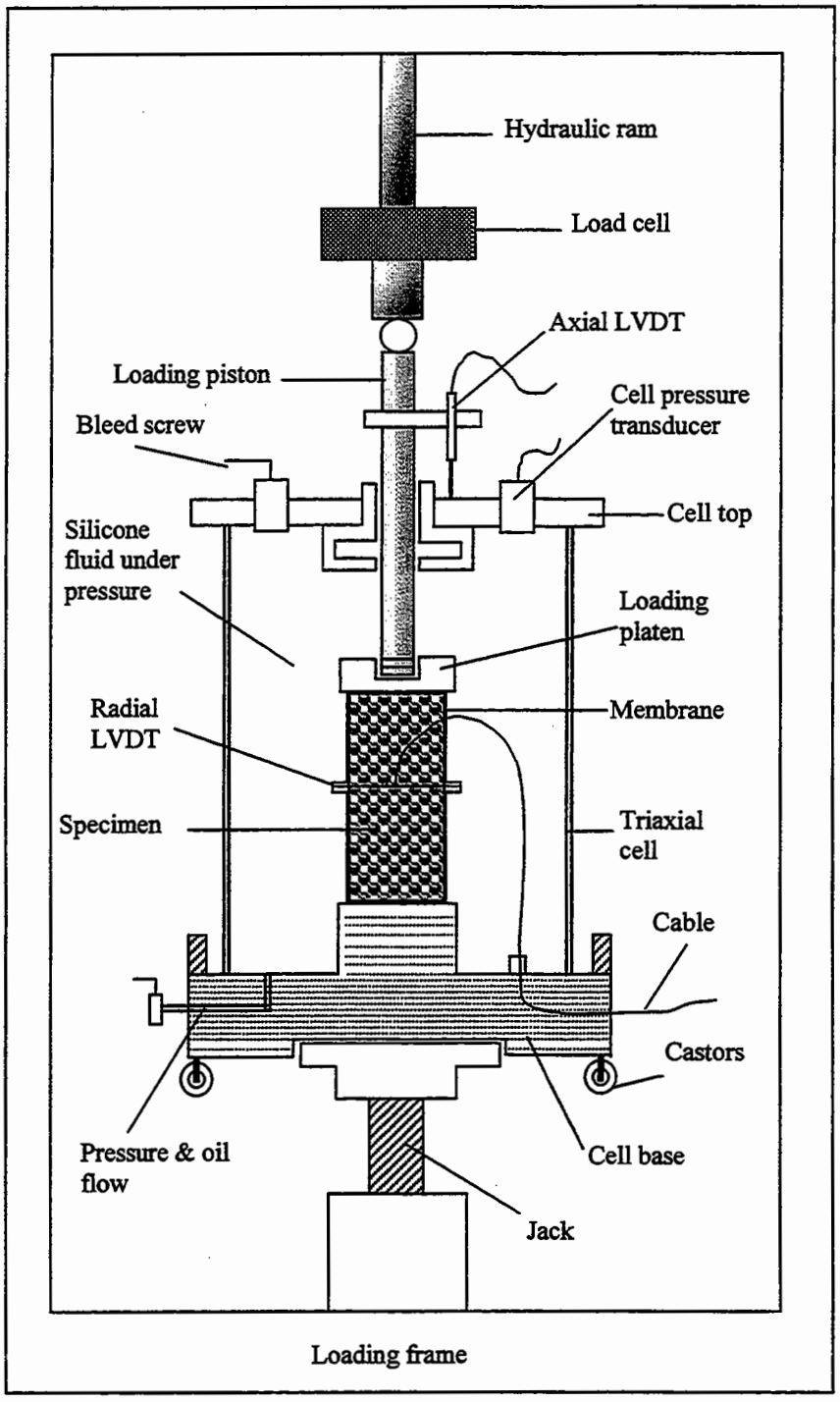

Figure 5.5 Schematic of the Triaxial Cell.

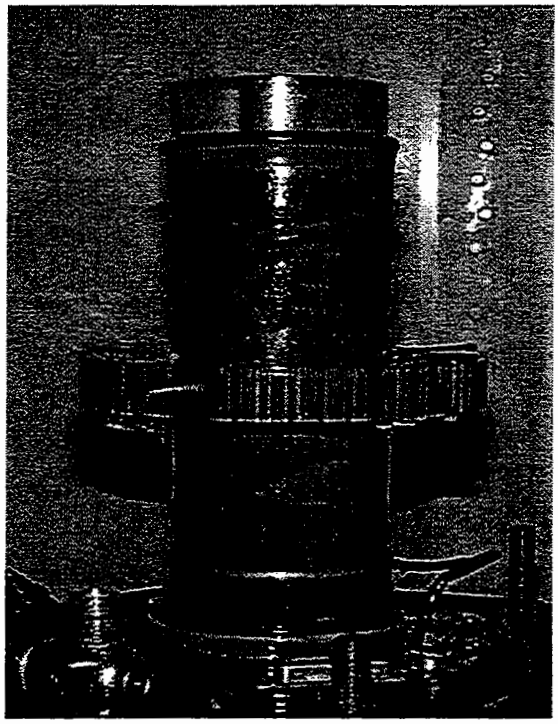

Figure 5.6 Specimen fitted with a radial strain transducer.

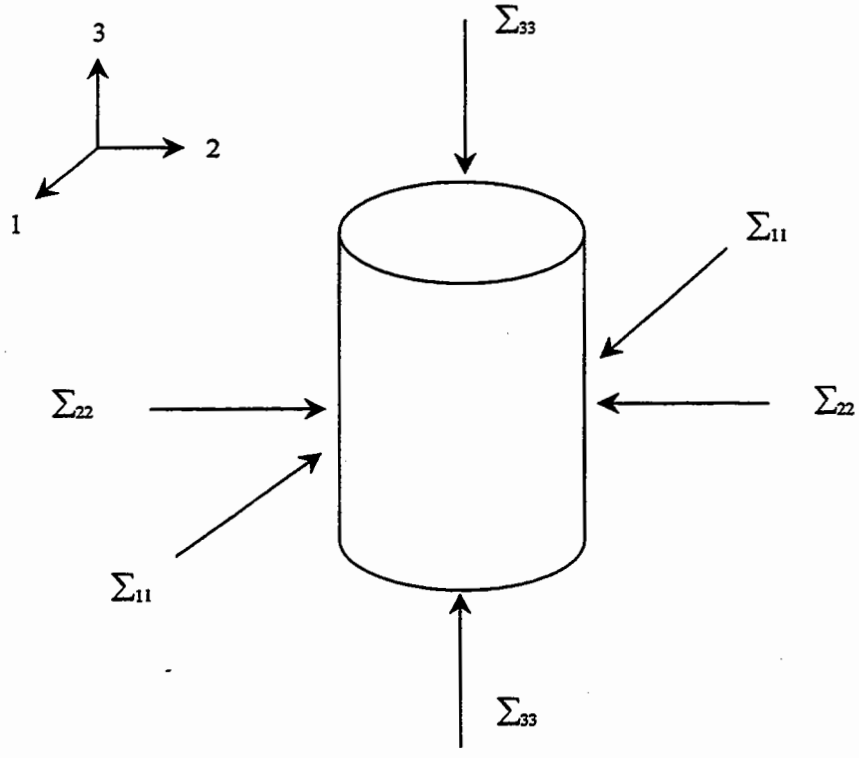

Figure 5.7 Schematic showing the triaxial co-ordinate system.

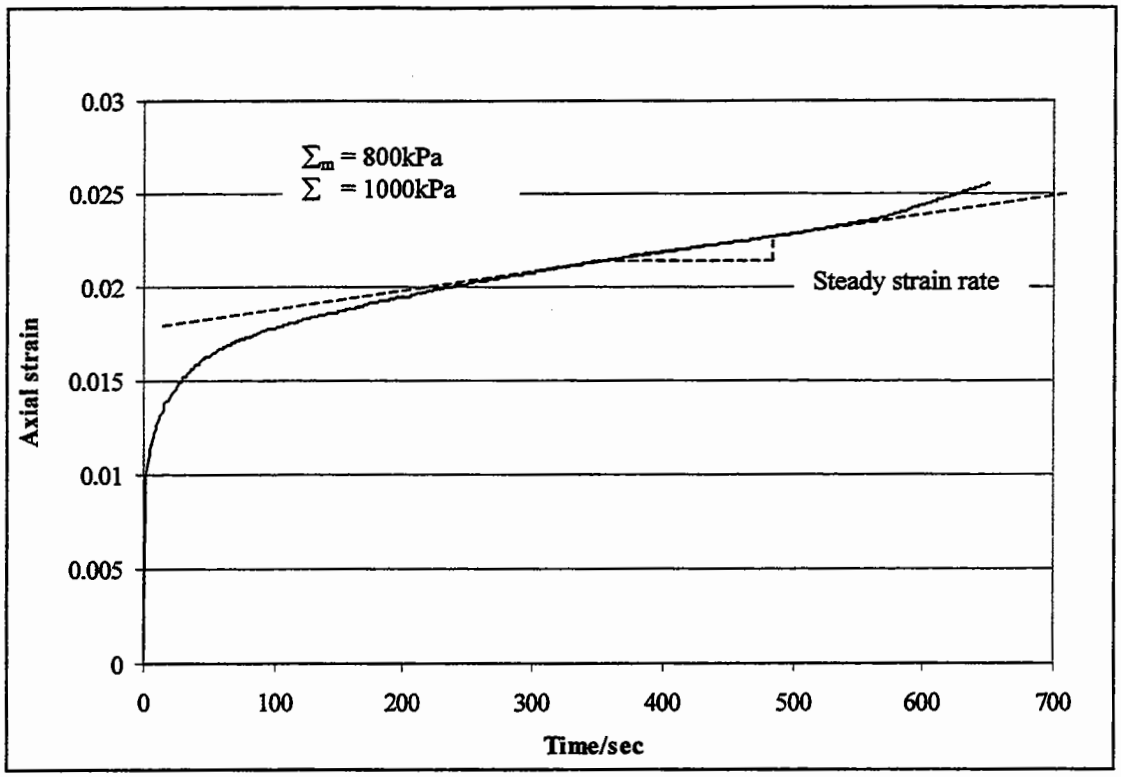

Figure 5.8 Triaxial creep test result for mixture A/D at 20°C (stress ratio 0.8).

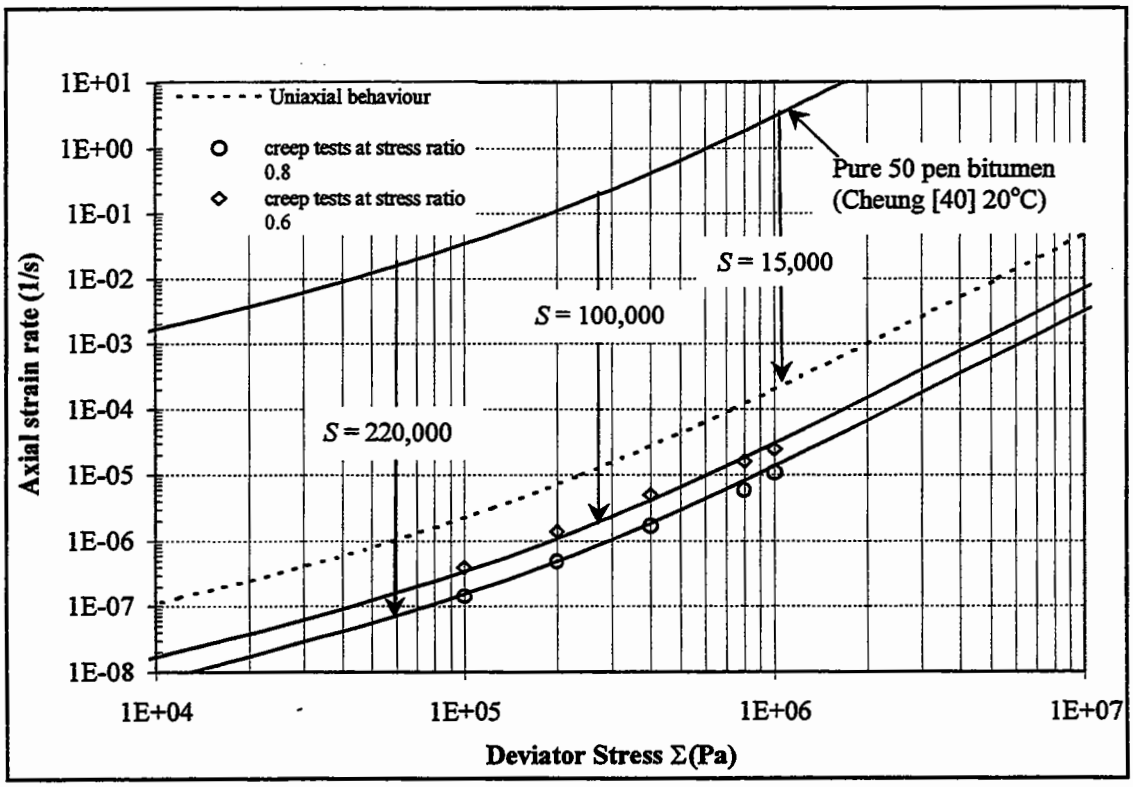

Figure 5.9 Steady-state deformation behaviour of mixture A/D at various triaxial stress states at 20°C.

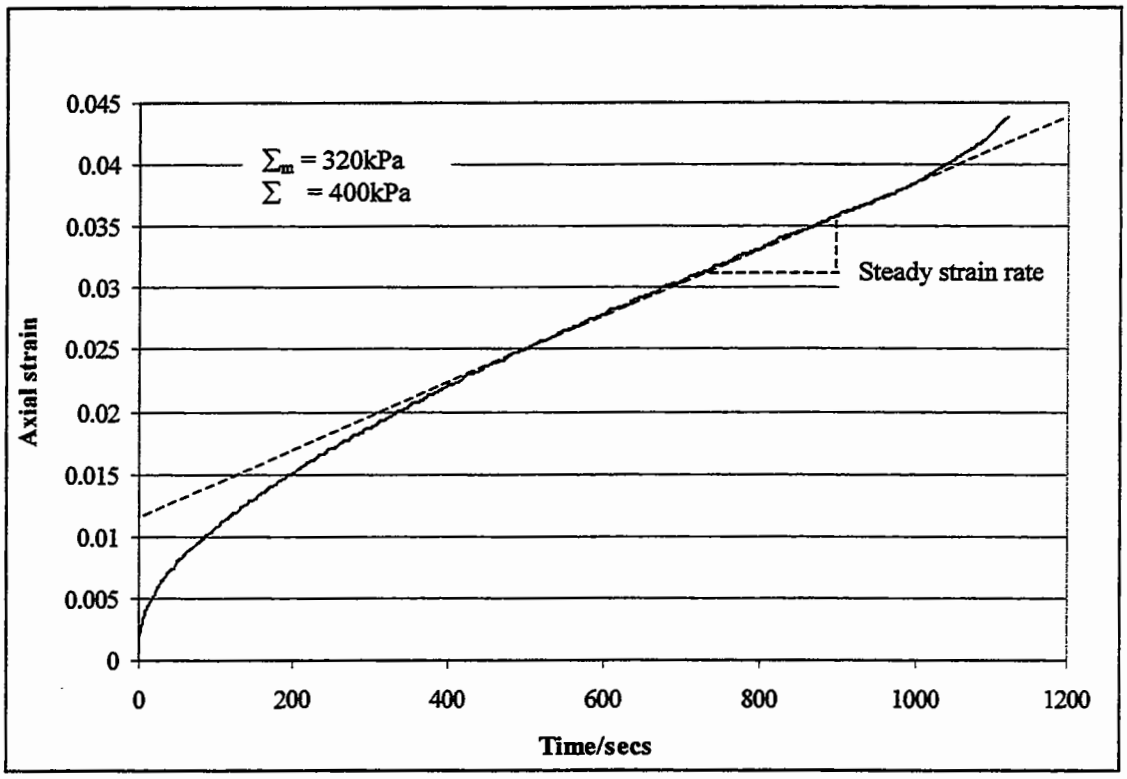

Figure 5.10 Triaxial creep test result for mixture A at 20°C (stress ratio of 0.8).

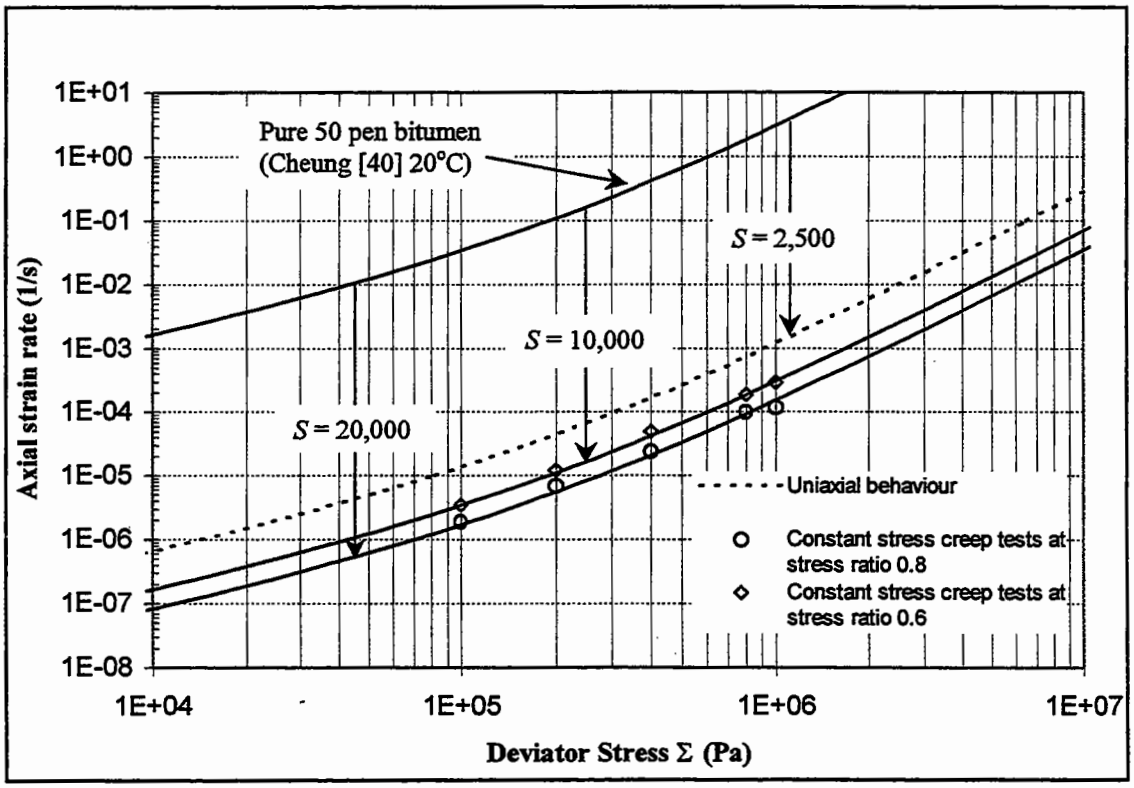

Figure 5.11 Steady-state deformation behaviour of mixture A at various triaxial stress states at 20°C.

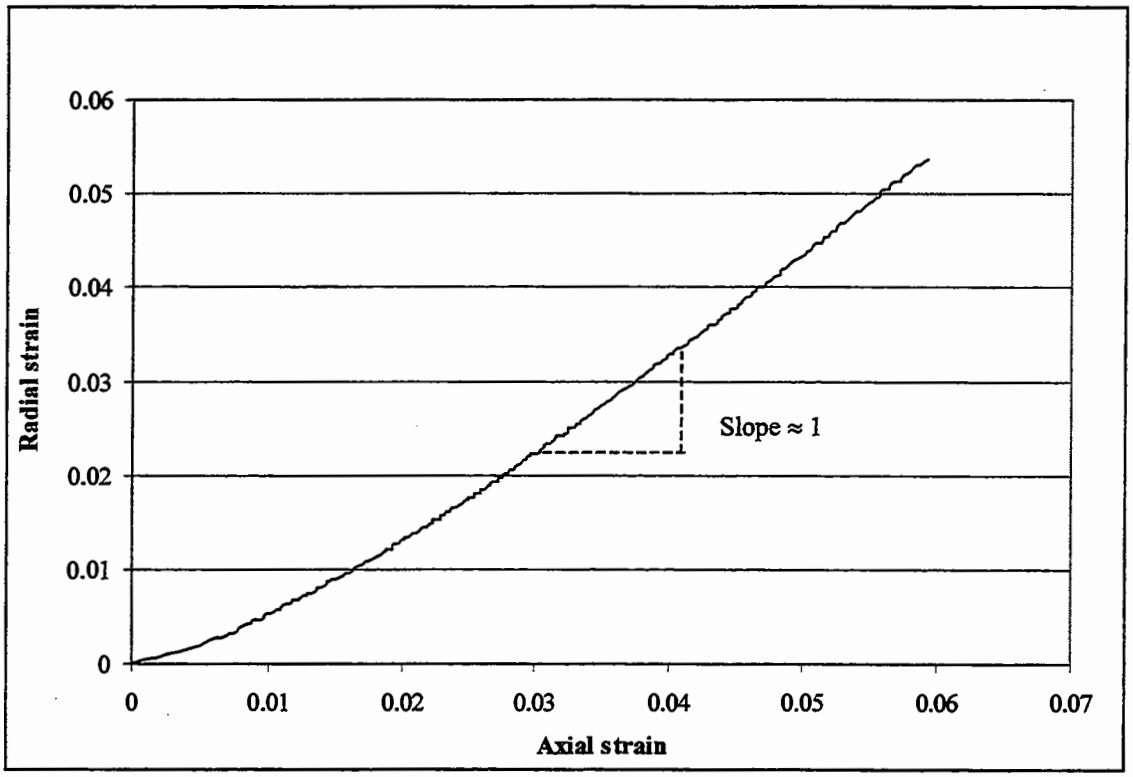

Figure 5.12 Dependence of the radial strain on the axial strain for a creep test at 20°C (mixture A).

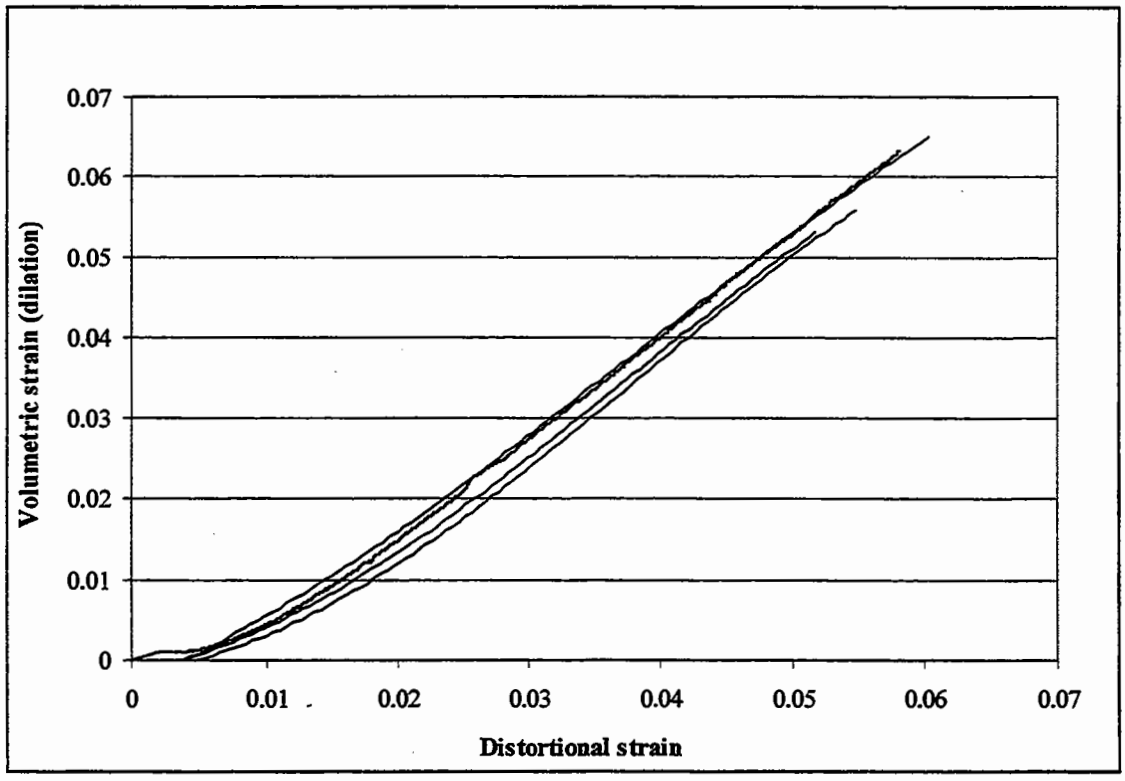

Figure 5.13 Variation of volumetric strain with distortional strain for triaxial creep tests on mixture A/D.

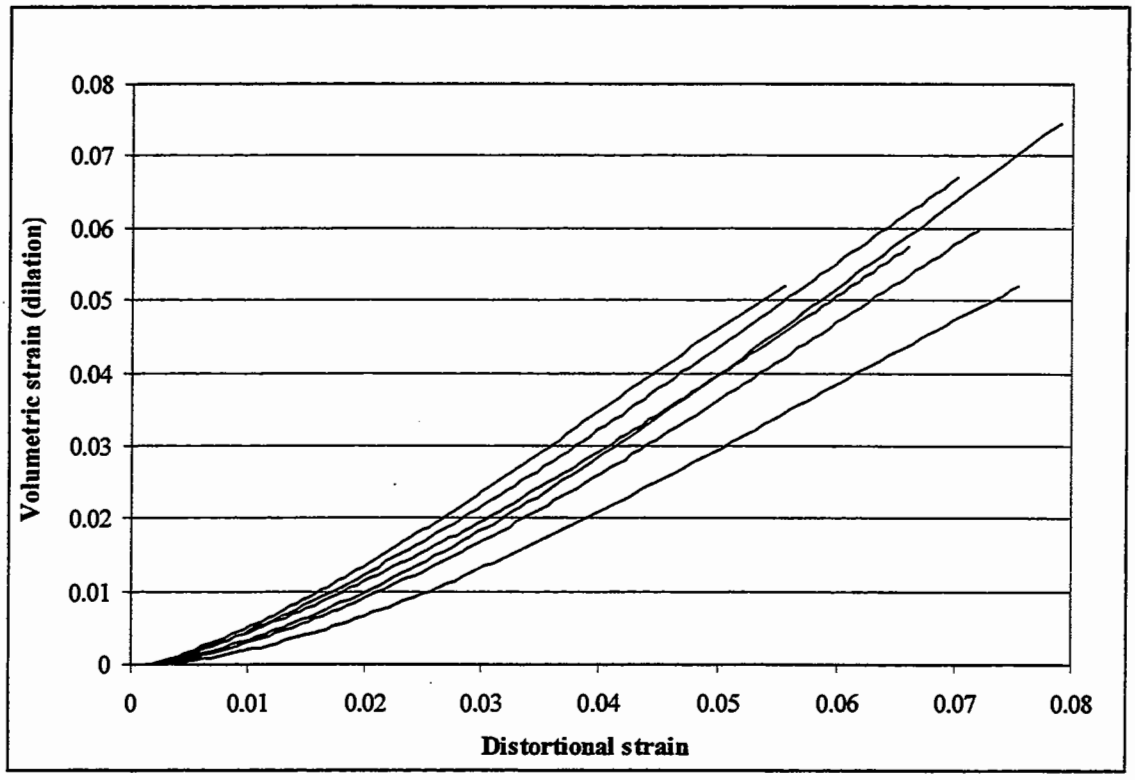

Figure 5.14 Variation of volumetric strain with distortional strain for traixial creep tests on mixture A.

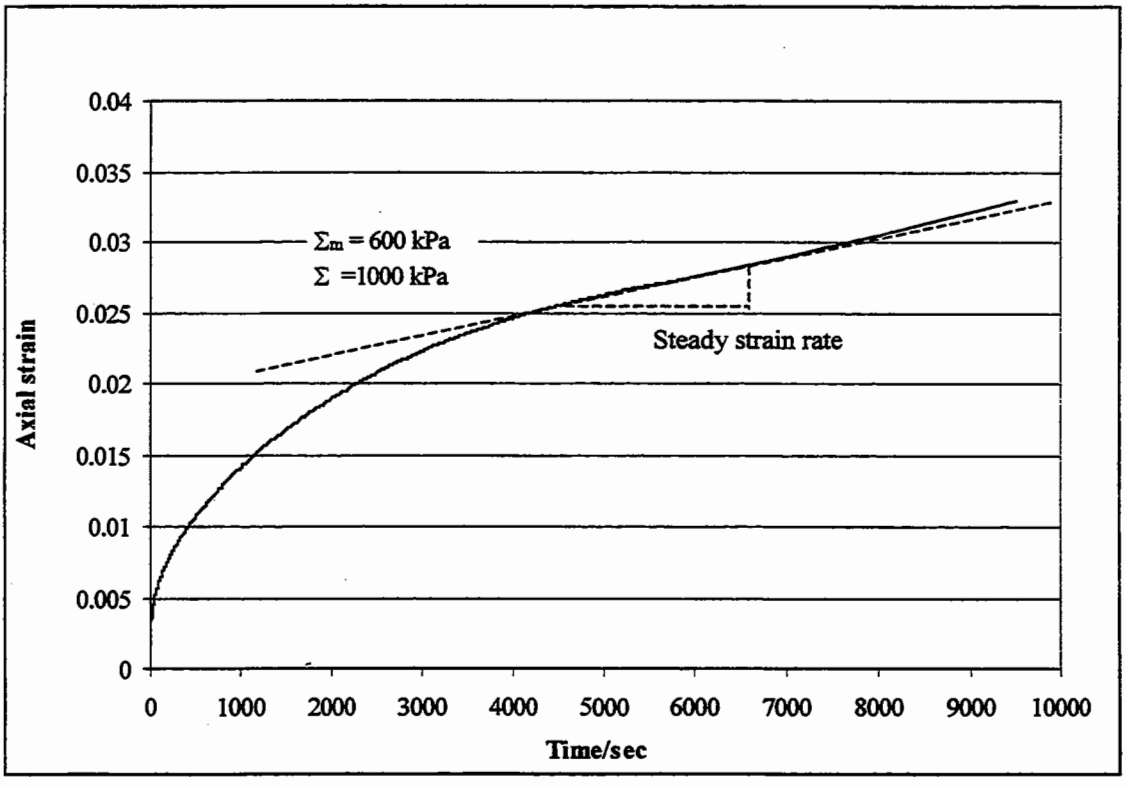

Figure 5.15 Triaxial creep test result for 30/10 HRA at 40°C (stress ratio of 0.6).

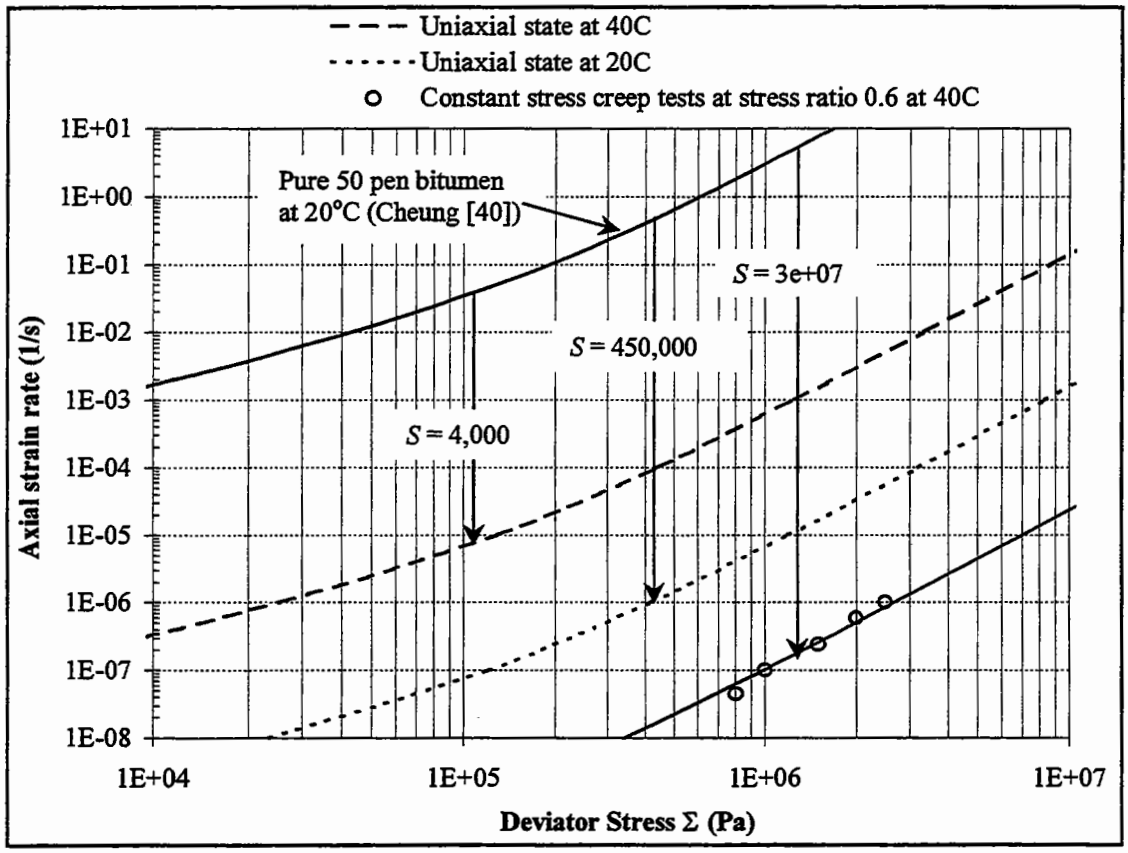

Figure 5.16 Steady-state deformation behaviour of 30/10 HRA mixture at 40°C (stress ratio of 0.6).

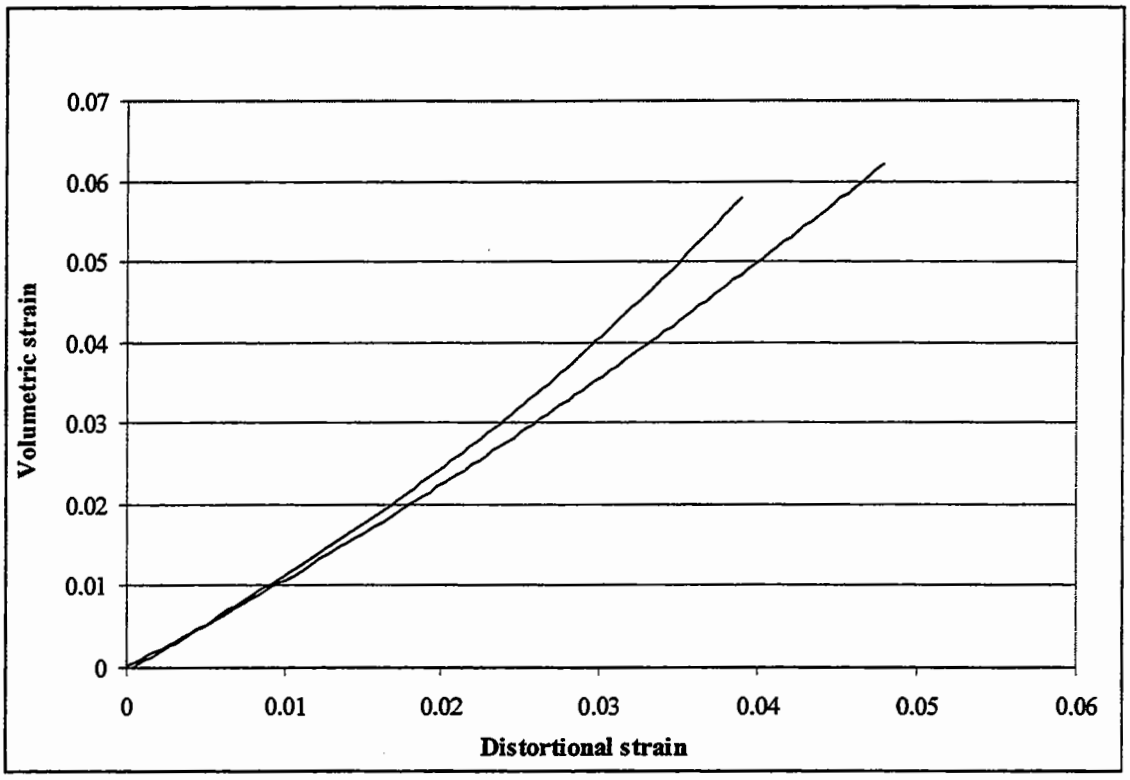

Figure 5.17 Variation of volumetric strain with distortional strain for triaxial creep test on 30/10 HRA mixture at 40°C (stress ratio of 0.6).

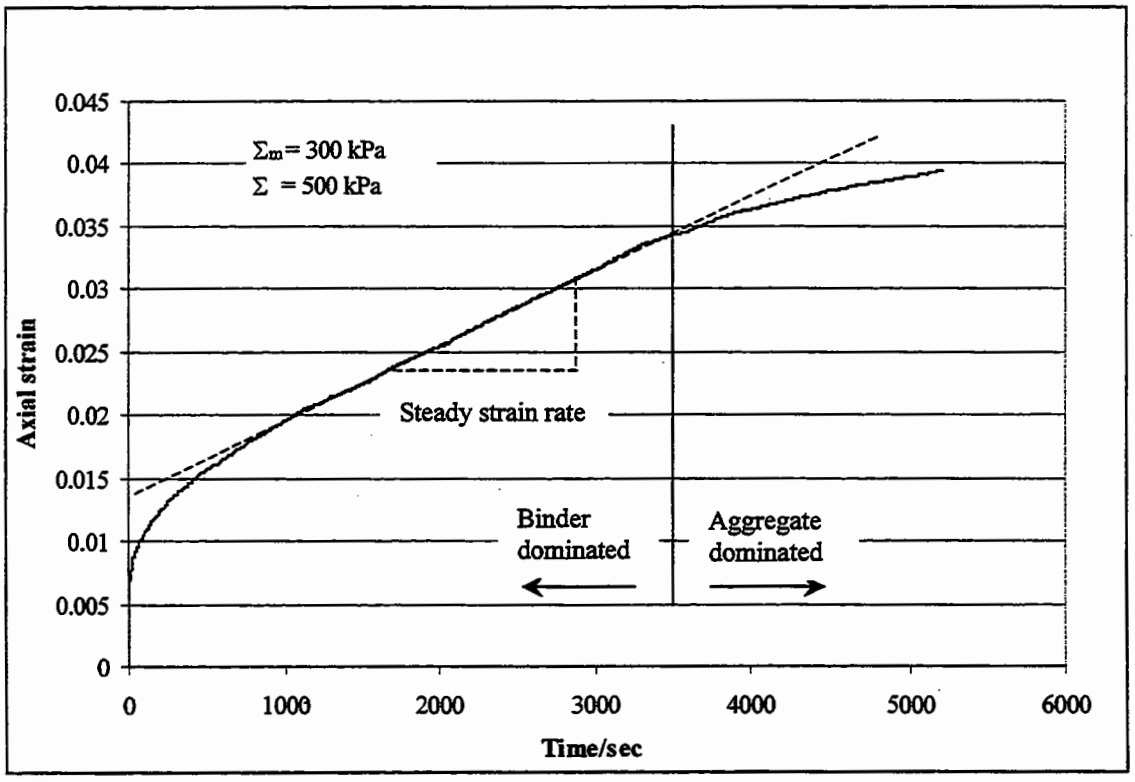

Figure 5.18 Triaxial creep test result for 10 mm DBM (100 pen) at 40°C (stress ratio of 0.6).

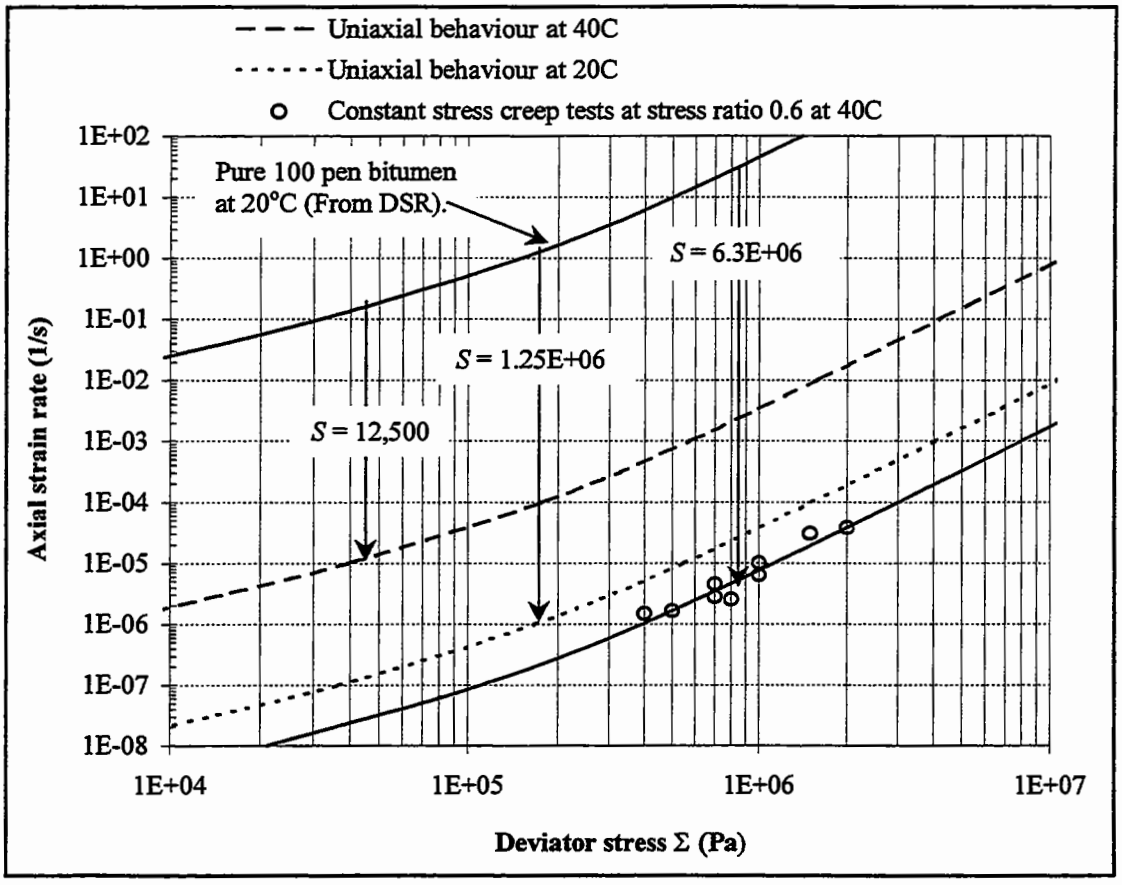

Figure 5.19 Steady-state deformation behaviour of 10 mm DBM mixture (100 pen) at 40°C (stress ratio 0.6).

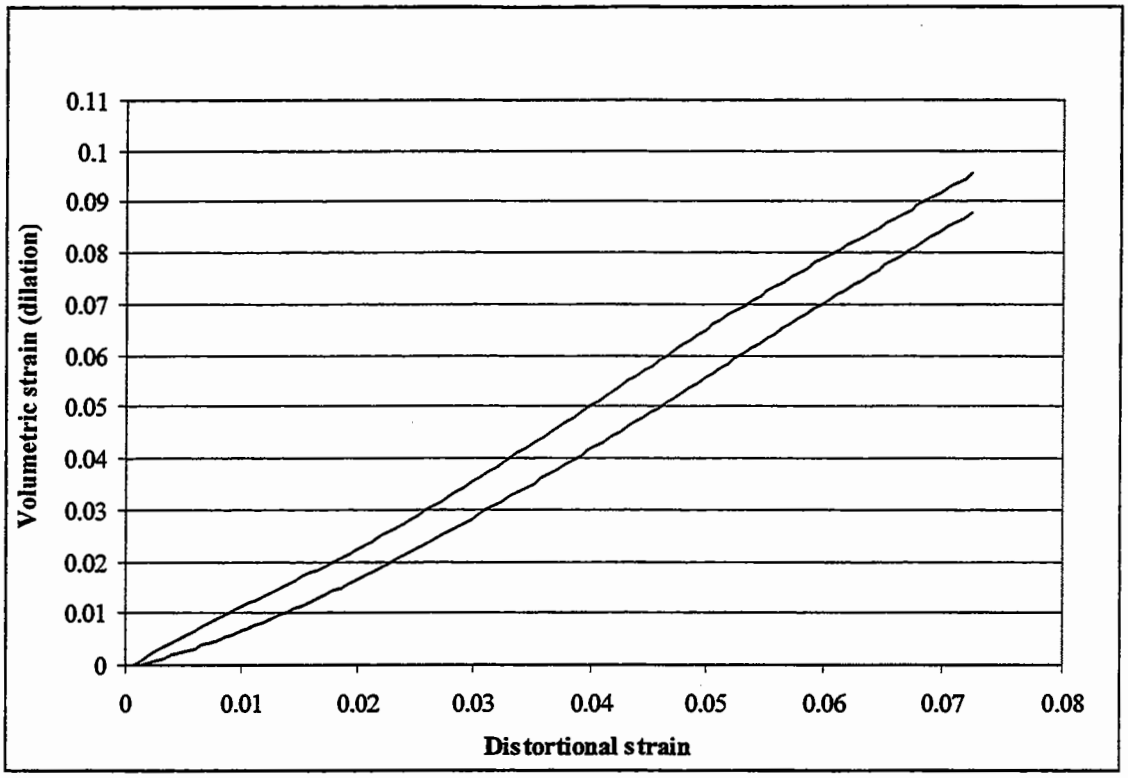

Figure 5.20 Variation of volumetric strain with distortional strain for triaxial creep test on 10 mm DBM mixture at 40°C (stress ratio of 0.6).

Figure 5.21 Specimen preparation (unbound granular material).

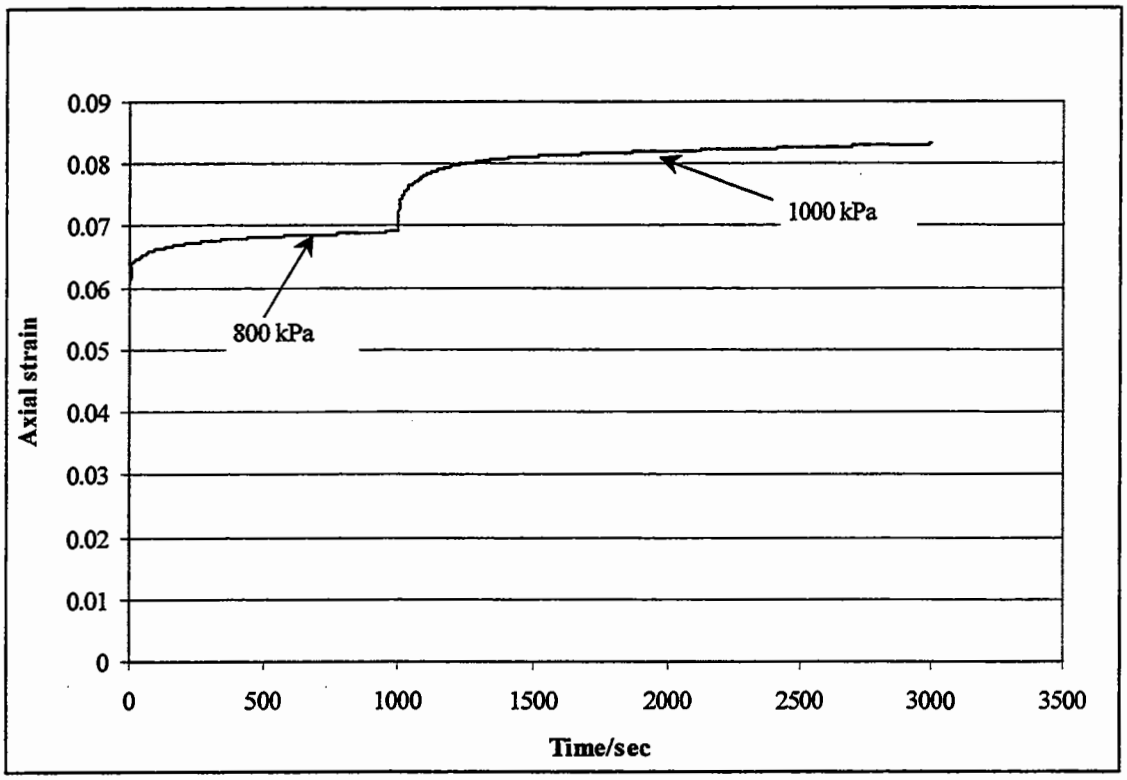

Figure 5.22 Creep test result for 10 mm DBM mixture without bitumen at stress ratio of 0.6.

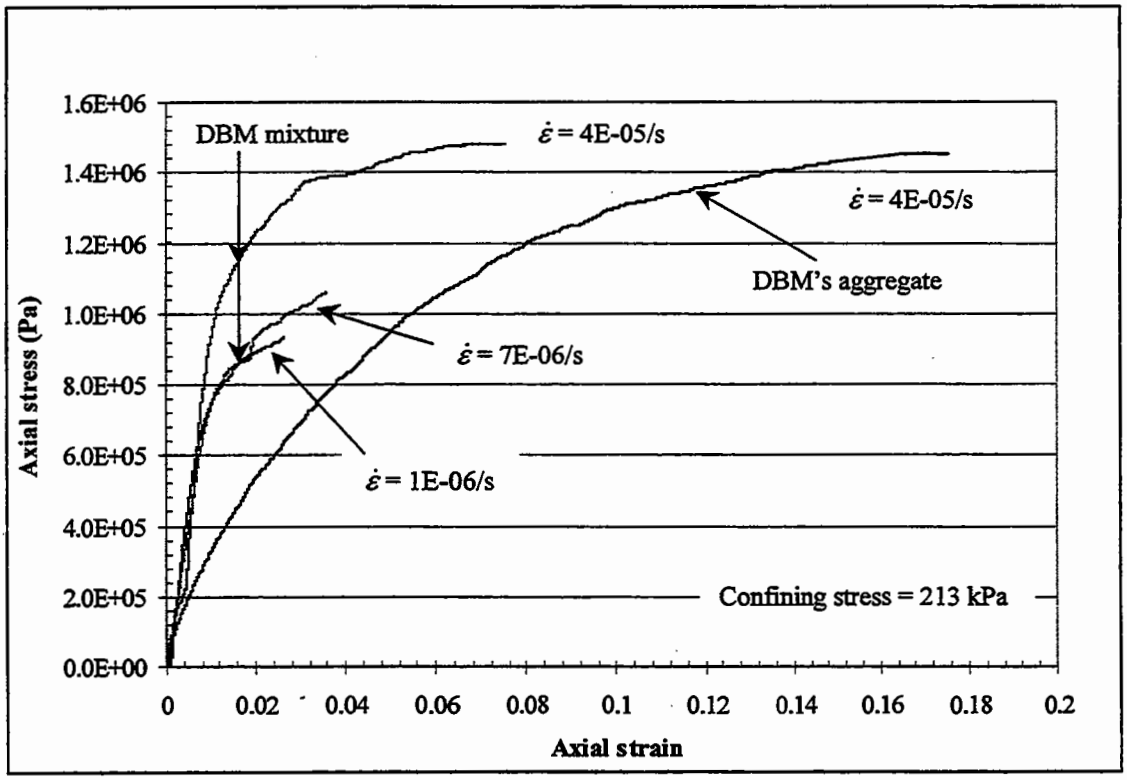

Figure 5.23 Constant strain rate test results for DBM mixture and aggregate.

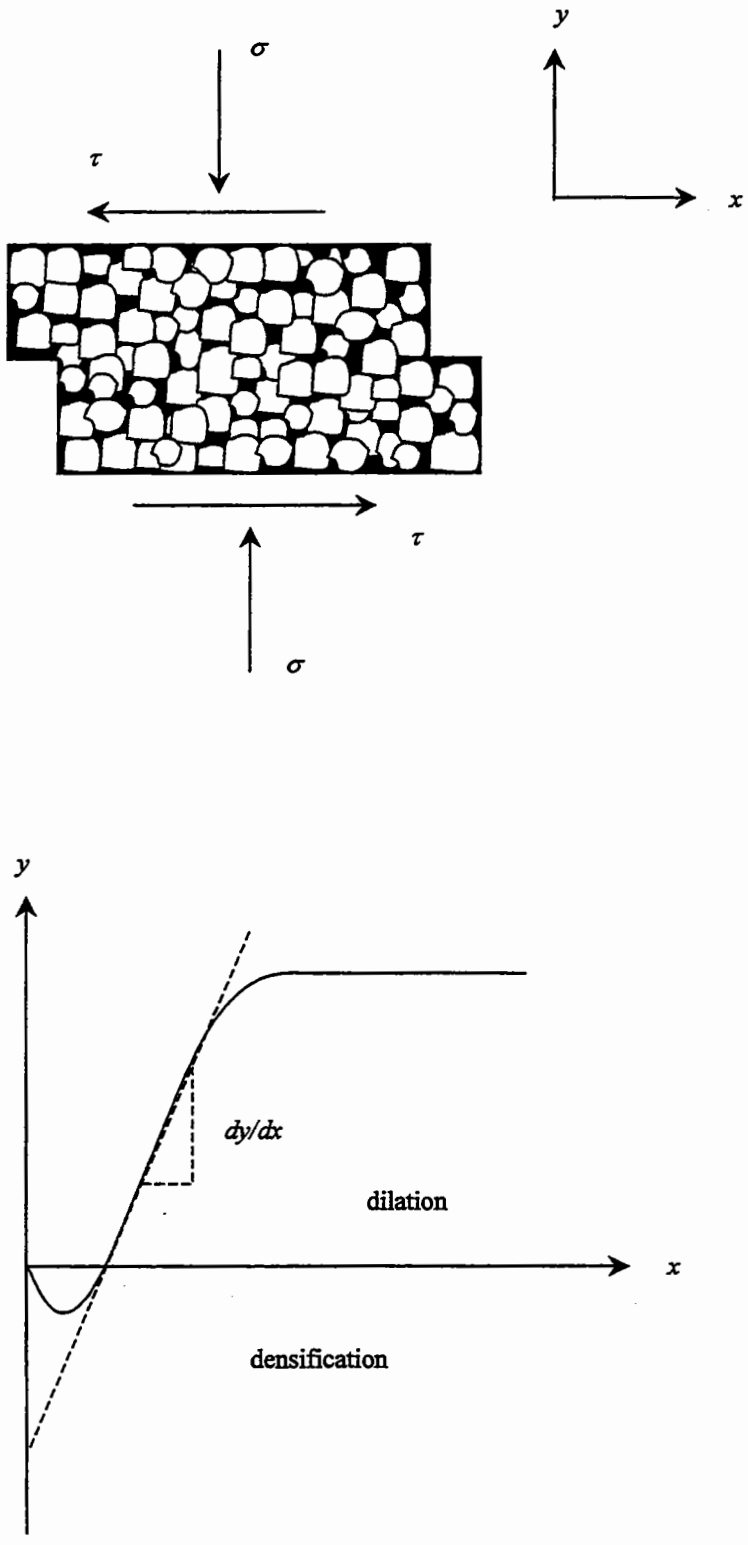

Figure 5.24 Direct shear box test.

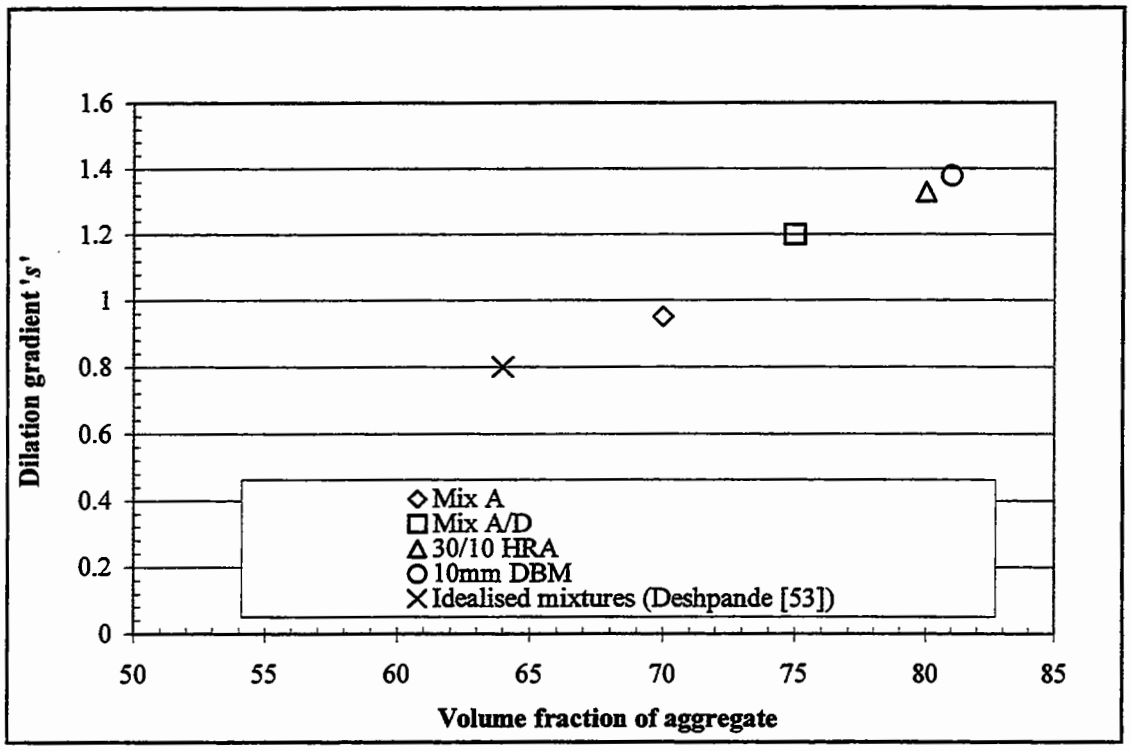

Figure 5.25 Variation of dilation gradient with volume fraction of aggregates.

Repeated Load Axial Tests on Idealised and Realistic Bituminous Mixtures

6.1 Introduction

Results from the quasi-static uniaxial and triaxial testing show that the steady-state deformation behaviour of the idealised and realistic mixtures follow the same pattern as the steady-state deformation behaviour of the bitumen. At low stress levels the response is linear whereas at higher stress levels the response is non-linear with an effective power law creep exponent of approximately 2.4. This chapter investigates the permanent deformation performance of idealised and realistic mixtures using a standard repeated load uniaxial test, performed over a range of temperatures and stress levels. The deformation behaviour of the idealised and realistic mixtures is characterised by an effective value of creep exponent for comparison with the quasi-static uniaxial and triaxial results. Finally, the results are compared to the SHRP rutting parameter for the 50 Pen grade binder, characterised using the DSR (see Chapter 3).

6.2 Repeated Load Axial (RLA) Test

The RLA test is an increasingly commonly used test in the UK for routinely assessing the permanent deformation characteristics of bituminous materials [28, 66]. The tests reported herein were carried out using the Nottingham Asphalt Tester (NAT) which is described in the following sub-section.

6.2.1 The Nottingham Asphalt Tester (NAT)

The NAT was developed at the University of Nottingham during the 1980's as a routine assessment tool for bituminous mixtures. It is capable of testing cylindrical specimens both in the indirect tensile mode and uniaxially, with either static or repeated loading [50, 51]. The indirect tensile mode is used to determine the stiffness modulus and fatigue life of the material and the uniaxial mode is used to assess the resistance of the material to permanent deformation.

In the NAT, the load is applied by a rolling diaphragm pneumatic actuator, the supply of compressed air to which is governed by a solenoid valve. The operation of this valve is controlled by a computer via a digital to analogue converter. The load applied to a specimen and the resultant deformation are monitored by a load cell and LVDT's respectively. Outputs from these devices are acquired by the computer through an analogue-digital interface. The standard pneumatic actuator is capable of applying a load of up to 4.2 kN and transient deformations as low as 1 micron can be recorded. The use of microcomputer control and data acquisition allows, through the use of suitable software, both flexibility in the application of load and also the facility to acquire data continuously and automatically throughout a test [28].

The uniaxial testing configuration used to assess the permanent deformation resistance of a bituminous material is shown in Figure 6.1 and is known as the Repeated Load Axial (RLA) test. A cylindrical specimen (with both the ends lubricated using graphite powder) is subjected to a pre-test conditioning regime consisting of the application of a static stress of 10 kPa for a duration of 10 minutes. The main purpose of conditioning is to ensure that the loading platens are properly seated on the specimen prior to the commencement of deformation measurement. A

repeated vertical stress of magnitude 100 kPa is then applied to the specimen with stress pulse duration of 1 second followed by a 1 second rest period. This is repeated for 3600 load applications at a constant temperature. The LVDT's mounted on the upper loading platen monitor the deformation which occurs over the whole length of the specimen. The permanent axial deformation is recorded after every 10^{th} load application up to 100 load applications and thereafter every 100 load applications. The permanent axial strain is calculated from the measured deformation at the end of the rest period between each successive load applications using:

$$\varepsilon_{perm},(n,T) = \Delta h / h_o \tag{6.1}$$

where, ε_{perm}, (n, T) = permanent axial strain after n load applications at temperature T

h_o = original distance between loading surfaces (specimen thickness)

Δh = measured axial permanent deformation (change in distance between specimen loading surfaces)

6.3 Test Specimens

Cylindrical specimens, approximately 100 mm in diameter and 60 mm in thickness, were tested in Repeated Load Axial (RLA) mode. For mixtures A/D, HRA and DBM, the samples were obtained by coring the slabs used for the wheel tracking test (outside the loaded area) whilst the specimens for mixture A were compacted in a gyratory compactor due to problems with coring the slabs, associated with the high bitumen content of mixture A. The gyratory samples for mixture A were compacted to similar air void contents as the wheel tracking slab samples to ensure that essentially the same material (in volumetric terms) was tested.

Table 6.1 shows the ranges of air void contents for all the mixtures characterised by a mean value, a maximum and minimum and a Coefficient of Variation.

Table 6.1 Air Void Content Analysis (RLA test specimens)

Mix	No. of Samples	Air Void Content (%)			
		Mean	Minimum	Maximum	COV (%)
A	14	9.7	8.9	10.5	4.9
A/D	17	6.9	6	7.8	8.7
30/10 HRA	7	5.9	5.2	6.7	8.9
10mm DBM	7	3.9	3.4	4.2	7.3

It can be seen from Table 6.1 and 4.2 that there is a difference between the void contents for the HRA and the DBM mixture specimens used for the RLA and the uniaxial tests. This is because the RLA specimens (with lower void contents) were cored from slabs which were compacted using a laboratory roller compactor. However, this does not affect the test results and analysis as the purpose of this testing is not to compare directly the performance of these mixtures but to investigate linearity in the RLA test compared to that in the uniaxial test.

6.3.1 Test Conditions

RLA testing was carried out using the following test conditions:

Idealised Mixtures (mixture A and mixture A/D)

- 3 temperatures (20, 30 and 40°C),
- 3 applied stress levels (50, 75 and 100 kPa).

Mixture A was only tested at 20°C and 30°C because It was found that at higher temperatures (i.e. 40°C) mixture A deformed under the weight of loading platens.

Realistic Mixtures (30/10 HRA and 10mm DBM)

- 1 temperature (40°C),
- 3 stress levels (50, 75 and 100 kPa).

6.4 Results for the Idealised Mixtures

Results from tests at different applied stress levels and temperatures are shown in Figures 6.2 to 6.4 for mixture A/D, and Figures 6.5 and 6.6 for mixture A, where the permanent strain is plotted against the number of cumulative load passes. It can be seen from these figures that, after an initial period where the strain rate decreases, the permanent strain increases approximately in proportion to the number of cumulative load passes. As before, this part of the curve can be characterised by a steady-state strain rate (gradient). It can be seen from Figure 6.2 that there is an additional tertiary region where the strain rate increases quickly before specimen failure. This is due to the large permanent strains accumulating in the RLA specimens resulting in failure. It can be also seen from these figures that, as expected, the rate of steady-state permanent deformation increases as the applied stress level increases and the temperature increases. The steady-state strain rates measured in the tests were converted into an equivalent permanent deformation rate by multiplying by the length of the specimen (for comparison with results from the wheel tracking test in Chapter 7).

6.5 Analysis of Test Results

For a linear viscous material the rutting rate would be expected to increase in proportion to the applied stress level. Assuming that a power law creep model describes viscous flow in the material [40, 53] it can be shown that the rutting rate increases as a function of the applied stress raised to a power n (creep exponent). Consequently, if the rutting rate is plotted against applied stress on double logarithmic scale the resulting curve is a straight line with gradient n (see Figures 6.7 and 6.8 for mixture A and mixture A/D respectively, for extended curve stress is shown on a linear scale). The variability in test results for mixture A and mixture A/D was

quantified by conducting three replicate tests at two different temperatures (20°C and 30°C) and two stress levels (50kPa and 100kPa). The steady-state rutting rates from all the tests (including repeats) conducted on these mixtures are also plotted in Figures 6.7 and 6.8.

To determine the value of n, the gradients for each mixture and temperature were calculated and then averaged to give an average value of n. A summary of the test results (including repeats) for mixtures A and A/D is given in Table 6.2. To evaluate the fit the COV between the measured rutting rate and the predicted rutting rate was calculated for each temperature and averaged to give a mean COV for each mixture (also shown in Table 6.2). It can be seen from the resulting values of n that they are lower than those calculated from the creep and constant strain rate tests, particularly for mixture A, indicating more linear behaviour. The implications of these results are discussed later in this chapter.

Table 6.2 Summary of Repeated Load Axial Test Results (Idealised Mixtures)

Mix	Temp (°C)	Stress (kPa)	Void (%)	Rutting rate (mm/cycle)	*n* (COV)
A	20	50	10.5	1.20E-03	1.1 (7.8%)
			10.3	6.42E-04	
			10	8.52E-04	
		75	9.9	1.80E-03	
		100	10.4	1.80E-03	
			9.8	8.52E-04	
			9.6	1.58E-03	
	30	50	8.9	5.67E-03	
			9	6.80E-03	
			9.6	5.58E-03	
		75	9.4	1.20E-02	
		100	9.1	1.83E-02	
			9.5	2.38E-02	
			9.7	1.19E-02	
A/D	20	50	7.0	3.12E-05	1.5 (5.2%)
			7.3	4.30E-05	
			7.1	4.30E-05	
		75	6.3	5.81E-05	
		100	6.3	7.92E-05	
			6.5	7.91E-05	
			6.4	6.00E-05	
	30	50	6.0	1.11E-04	
			6.2	1.50E-04	
			6.6	1.11E-04	
		75	6.7	3.08E-04	
		100	7.4	4.14E-04	
			7.8	4.00E-04	
			7.2	3.20E-04	
	40	50	7.4	6.12E-03	
		75	7.7	2.94E-02	
		100	7.8	5.08E-02	

6.6 Results for Realistic Mixtures

Data from tests at different load levels and a temperature of 40°C are shown in Figures 6.9 and 6.10 for the 30/10 HRA and the 10mm DBM mixtures respectively, where the permanent strain is plotted against the number of load passes. It can be seen from these figures that, as described above, the second part of the curve, where the permanent strain increases approximately in proportion to the number of cumulative load passes, can be characterised by a steady-state strain rate (gradient). As before, the constant steady-state strain rates measured from the tests have been converted into equivalent rutting rates by multiplying by the length of the specimen.

6.7 Analysis of Test Results

Figures 6.11 and 6.12 show the rutting gradients from the HRA and DBM mixtures plotted as a function of applied stress on a semi-logarithmic scale. To quantify variability in test results three replicate tests at two stress levels (50kPa and 100kPa) on the HRA and DBM mixtures were conducted which are also plotted in these figures. The same technique described above was used to determine the value of creep exponent n that best fits the data. A summary of the test results for the HRA and DBM mixtures are given in Table 6.3. To evaluate the fit, the Coefficient of Variation (COV) between the measured and predicted rutting rates has been calculated for each mixture and is shown in Table 6.3. It can be seen that for both the HRA and DBM mixtures, the deformation behaviour can be characterised with a value of creep exponent n = 0.8 to 0.9. The steady-state rutting rates from all the tests (including repeats) are also given in Table 6.3.

Table 6.3 Summary of Repeated Load Axial Test Results (Realistic Mixtures)

Mix	Temp (°C)	Stress (kPa)	Void (%)	Rutting rate (mm/cycle)	*n* (COV)
30/10 HRA	40	50	5.2	6.69E-05	0.8 (3.7%)
			5.8	6.74E-05	
			5.5	6.10E-05	
		75	6.2	9.06E-05	
		100	6.7	9.24E-05	
			6.3	8.65E-05	
			5.6	6.74E-05	
10 mm DBM	40	50	3.4	1.65E-04	0.9 (3.9%)
			3.5	1.09E-04	
			4	1.14E-04	
		75	4.2	2.16E-04	
		100	3.8	2.53E-04	
			4.1	2.60E-04	
			4.2	1.25E-04	

6.8 Comparison of $G^*/\sin\delta$ with RLA Test Data

Because RLA tests on the HRA and DBM mixtures were performed at only one temperature the following comparison is for the idealised mixtures only. Figure 6.13 shows a plot of $G^*/\sin\delta$ against the steady-state rutting rate normalised to the mean stress level. A loading frequency of 0.1Hz was selected for calculating $G^*/\sin\delta$ because this gave the best correlation with the RLA results. This is expected since the mixtures were designed to promote viscous permanent deformation and the lower frequency results from the DSR test are more dominated by viscous deformation for this type of bitumen.

It can be seen from Figure 6.13, that the data fall onto 3 horizontal lines corresponding to the 3 different test temperatures. Although, the stress levels were lower in the RLA test, there is still a considerable amount of scatter between the RLA test data and $G^*/\sin\delta$ values (R^2 = 0.45) [47]. This is thought to be mainly due to variability in the RLA test (see discussion).

6.9 Discussion

Results from RLA tests on idealised and realistic mixtures indicate a lower value of creep exponent than those calculated from creep and constant strain rate tests for both the idealised and realistic mixtures. This is likely to be due to the differences in applied stress levels between the tests. For example, the minimum stress applied in the RLA test is 50 kPa to 100 kPa which, according to Figures 4.10 and 4.11 (Chapter 4), means that the mixture is likely to be operating at the lower end of the transition region from linear to power law behaviour. Consequently, it may be expected that the values of n fitted to RLA test results would be nearer to 1.

This may imply that simplified tests that operate at lower stress levels (such as the RLA test) may not be sufficient to fully characterise the permanent deformation behaviour of these types of mixtures. However, this type of test may be sufficient to correctly rank the rutting potential of mixtures if all the binders have similar non-linear creep properties (this may not be the case for highly modified binders).

Results from the RLA test performed on the idealised mixtures indicate that there is a poor correlation between $G^*/\sin\delta$ and the measured steady-state rutting rates. $G^*/\sin\delta$ gives a measure of the dissipated energy which, in part, will relate to permanent viscous deformation. However, dissipated energy also relates to heating of the specimens and energy required for damage initiation so cannot be considered to be a unique measure of permanent deformation (indeed dissipated energy is also related to fatigue by SHRP). It should also be noted that different compaction methods were used for mixtures A and A/D which may have effected the orientation of the aggregates and the air void content which will result in additional scatter.

Each mixture type included 3 replicate tests at various stress levels and temperatures. The standard deviation and hence the Coefficient of Variation (COV) associated with the determination of the steady-state deformation rate in the RLA test for each mixture type at various stress levels and temperatures are shown in Table 6.4. It is quite evident from this table that the degree of variability in the results is quite high. No consistent effect was observed in the results due to small variations in void content as demonstrated in Figures 6.14 and 6.15, which show data from replicate tests of

idealised and realistic (DBM) mixtures respectively. However, for the limited number of tests on the HRA mixture there was found to be a more consistent trend due to variation in void content i.e. the deformation rate increased with an increase in void content (see Figure 6.15). The variability in the test results may be due to the fact that these results were obtained from unconfined RLA testing. The application of a confinement has previously been found to have significant effect on the performance of bituminous mixtures [30].

Table 6.4 Percentage Variation of Steady-State Rutting Rate Measured from Replicate Repeated Load Axial Tests

Mix	Temp (°C)	Stress (kPa)	No of Tests	COV (%)
A	20	50	3	18.3
		100	3	17.6
	30	50	3	13.6
		100	3	18.4
A/D	20	50	3	22.4
		100	3	1.4
	30	50	3	21.1
		100	3	23.1
30/10 HRA	40	50	3	5.5
		100	3	15.9
10 mm DBM	40	50	3	24.1
		100	3	35.7

It has been demonstrated that the RLA test operates at relatively low stress levels resulting in a mainly linear response in terms of permanent deformation. In order for the RLA to be able to characterise the permanent deformation behaviour of the materials in the non-linear range of behaviour the level of stress applied to the specimen would need to be increased, which may be possible with a larger pneumatic actuator or alternatively a hydraulic actuator. It should be noted that changing the temperature will not be directly beneficial since the non-linearity has been found to be stress related.

6.10 Conclusions

The following conclusions can be drawn from this chapter:

- RLA tests have been performed on two idealised and two realistic bituminous mixtures over a range of temperatures and applied stress levels.

- A steady-state rutting rate has been used to characterise the steady-state permanent deformation behaviour of these mixtures.

- Results show a lower effective creep exponent n = 1.1 to 1.5 for the idealised mixtures from the RLA tests.

- For the realistic mixtures the effective creep exponent was found to be in the range n = 0.8 to 0.9.

- Results for both the idealised and realistic mixtures indicate that the binder is operating in (or near to) the linear region.

- Simplified tests that operate at low stress levels (such as the RLA test) may not be sufficient to fully characterise the permanent deformation behaviour of these types of mixtures. However, this type of test may be sufficient to correctly rank the rutting potential of mixtures if all the binders have similar non-linear creep properties (this may not be the case for highly modified binders).

- The amount of scatter observed in the determination of the steady-state rutting rates is thought to be due to the unconfinement of the test specimen. A confined version of the RLA test might give better results (reduced scatter).

- $G^*/\sin\delta$ (obtained from DSR testing) has been calculated at a frequency of 0.1Hz and plotted against the measured steady-state rutting rate from the RLA tests.

- Comparison of RLA test results with $G^*/\sin\delta$ (SHRP rutting parameter) show that there is considerable scatter which is thought to be mainly due to the variability in the RLA test.

6.11 Figures

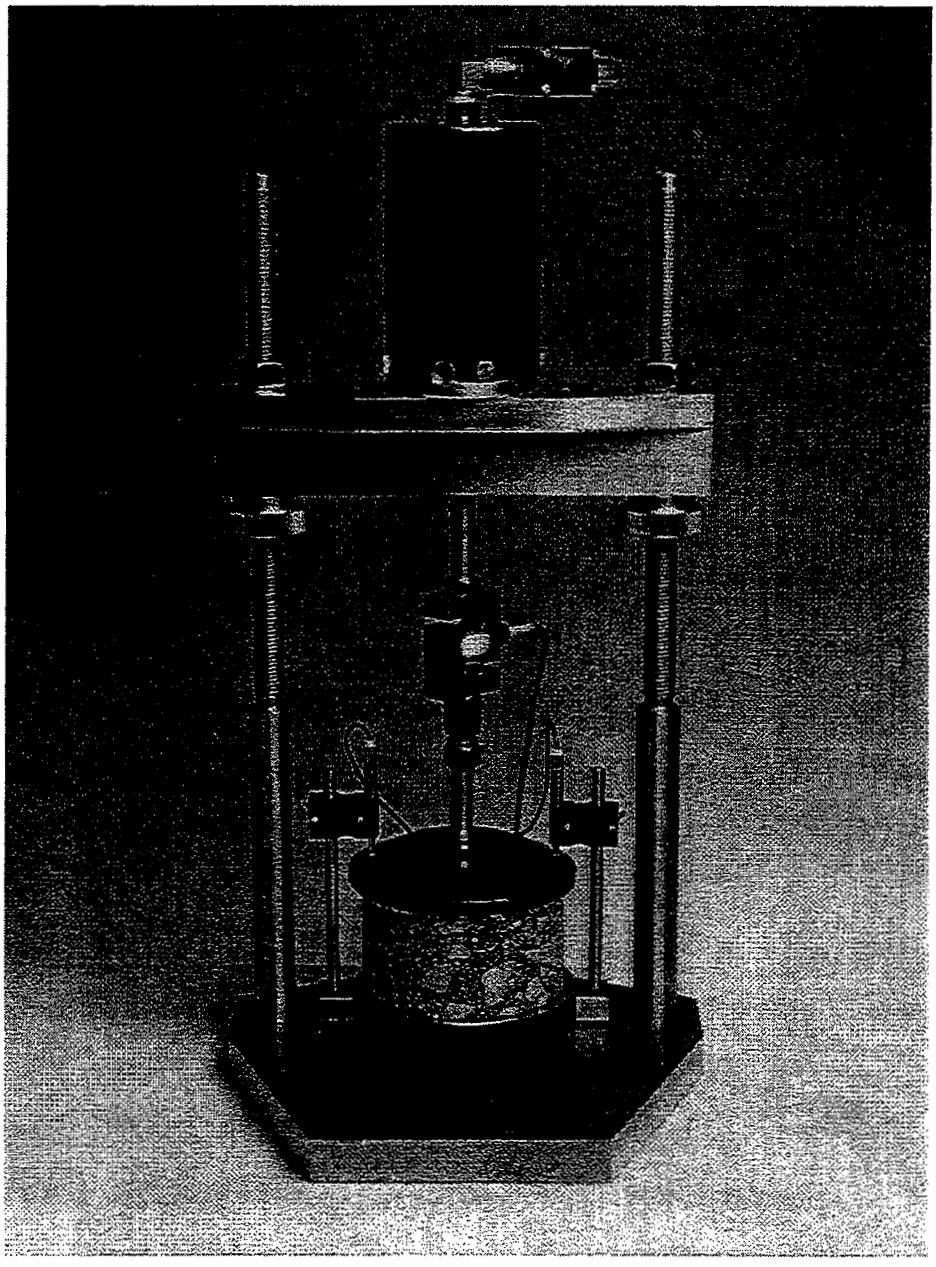

Figure 6.1 The Nottingham Asphalt Tester (NAT) configured in Repeated Load Axial (RLA) test mode.

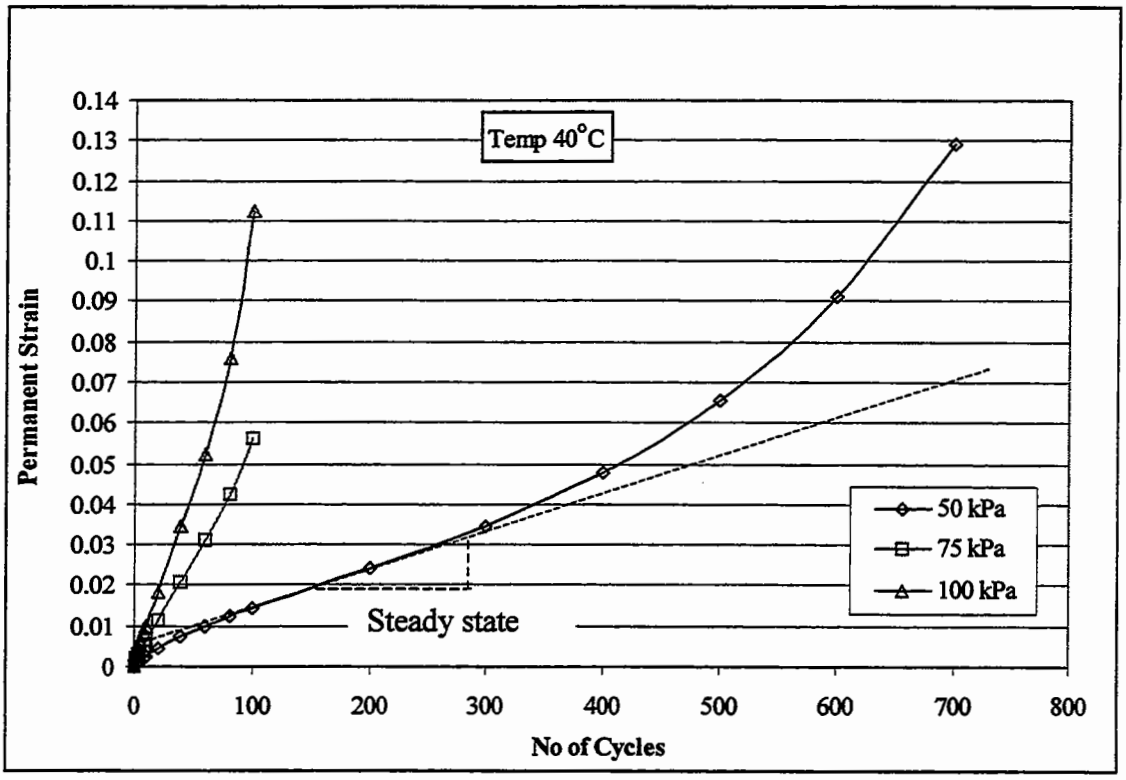

Figure 6.2 Repeated load axial tests at 40°C (Mixture A/D).

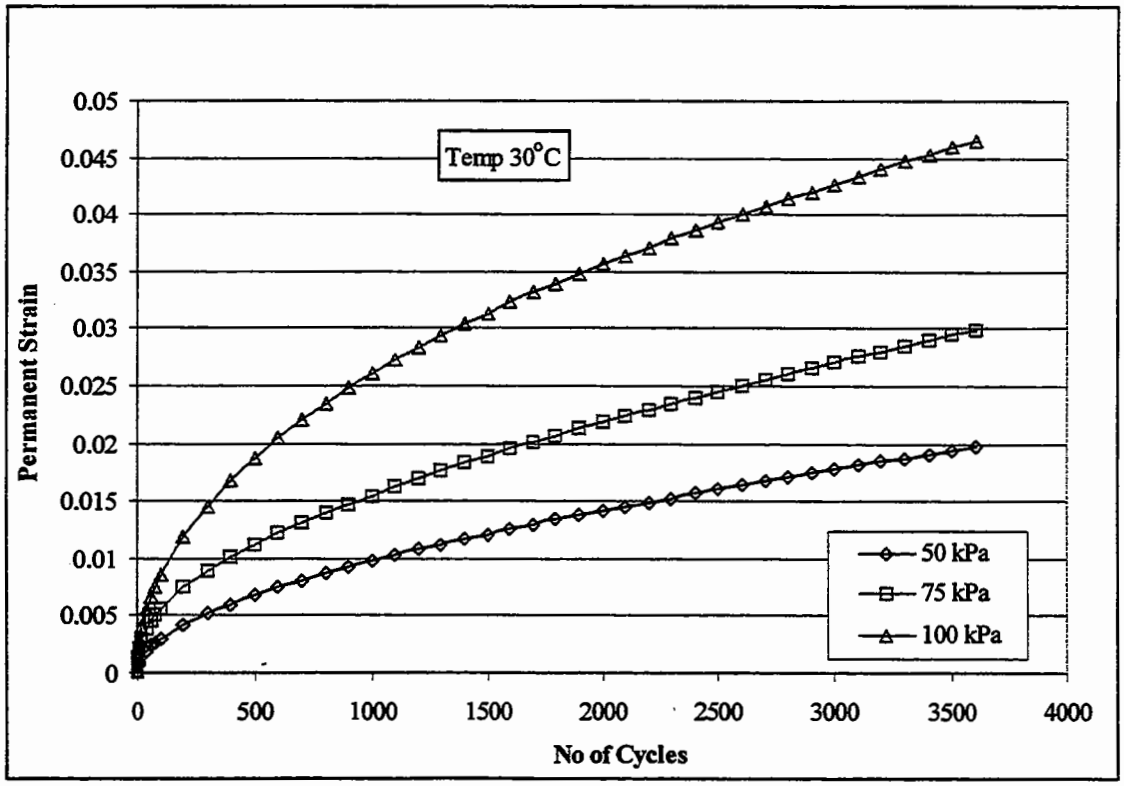

Figure 6.3 Repeated load axial tests at 30°C (Mixture A/D).

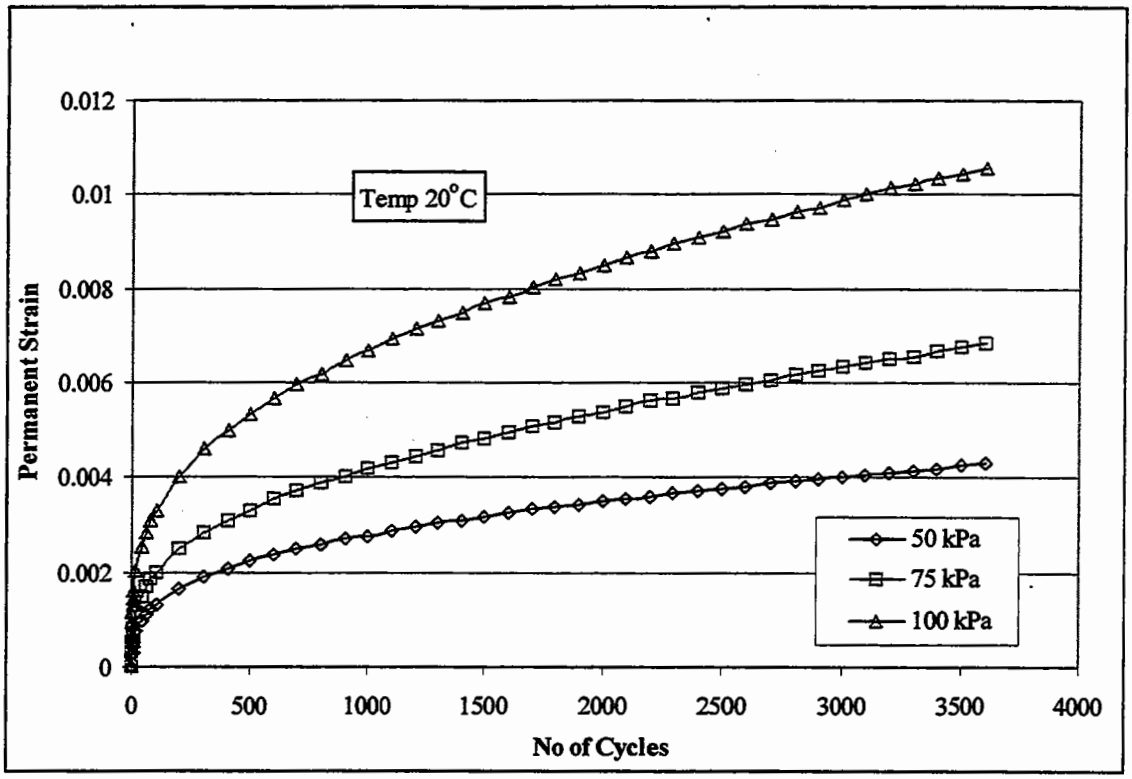

Figure 6.4 Repeated load axial tests at 20°C (Mixture A/D).

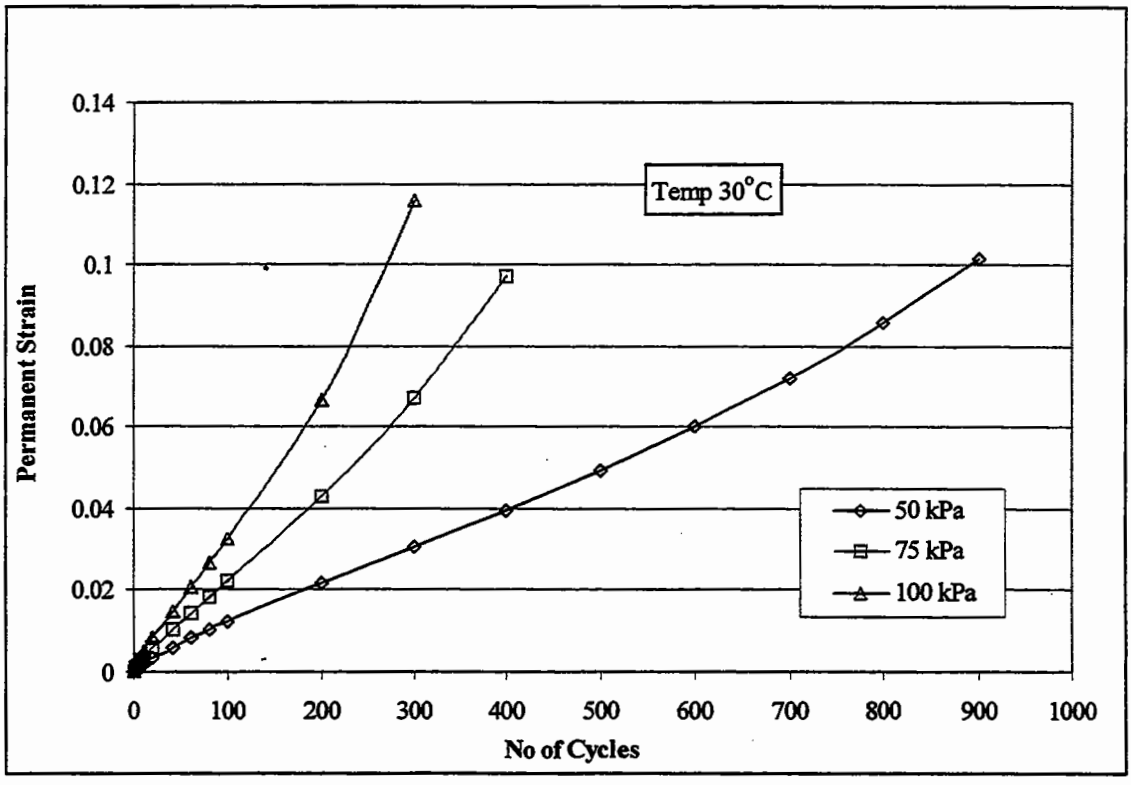

Figure 6.5 Repeated load axial tests at 30°C (Mixture A).

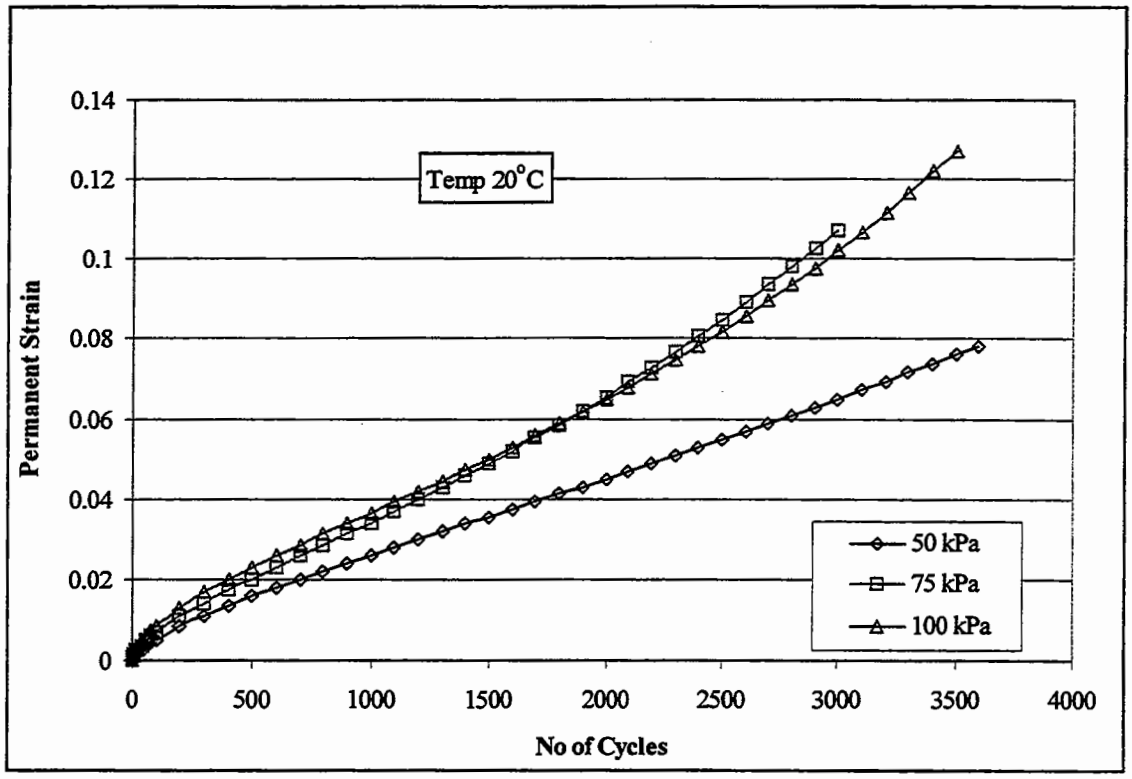

Figure 6.6 Repeated load axial tests at 20°C (Mixture A).

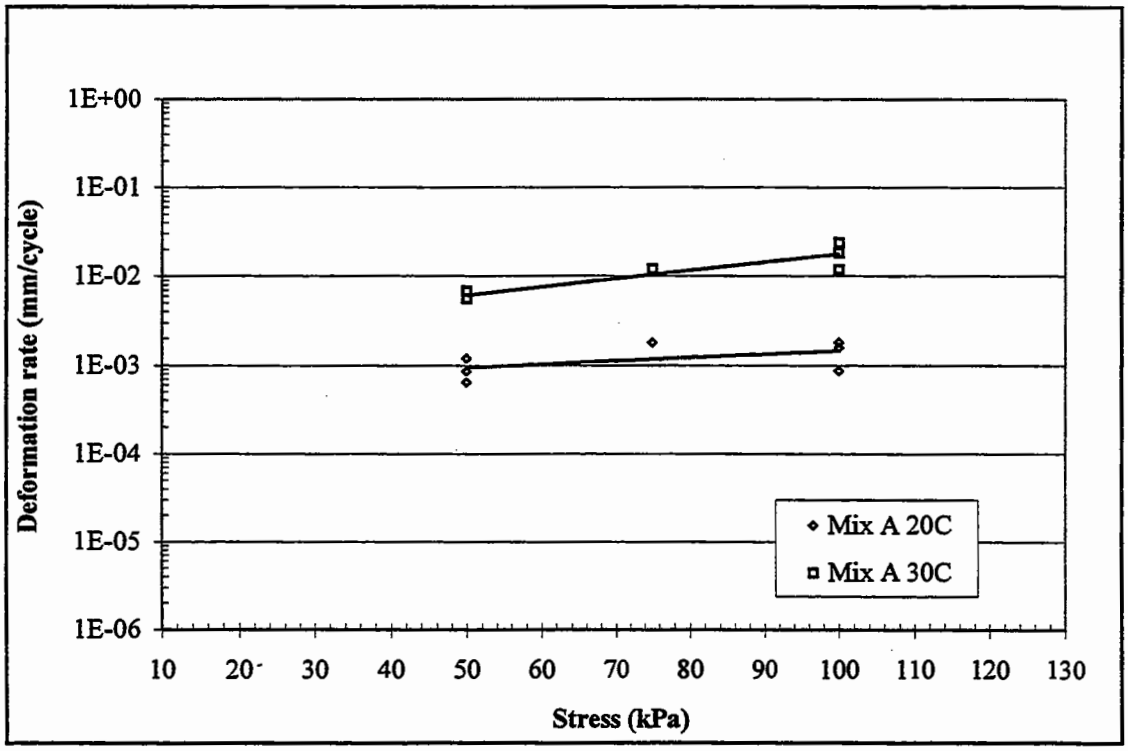

Figure 6.7 Steady-state deformation rates for mixture A.

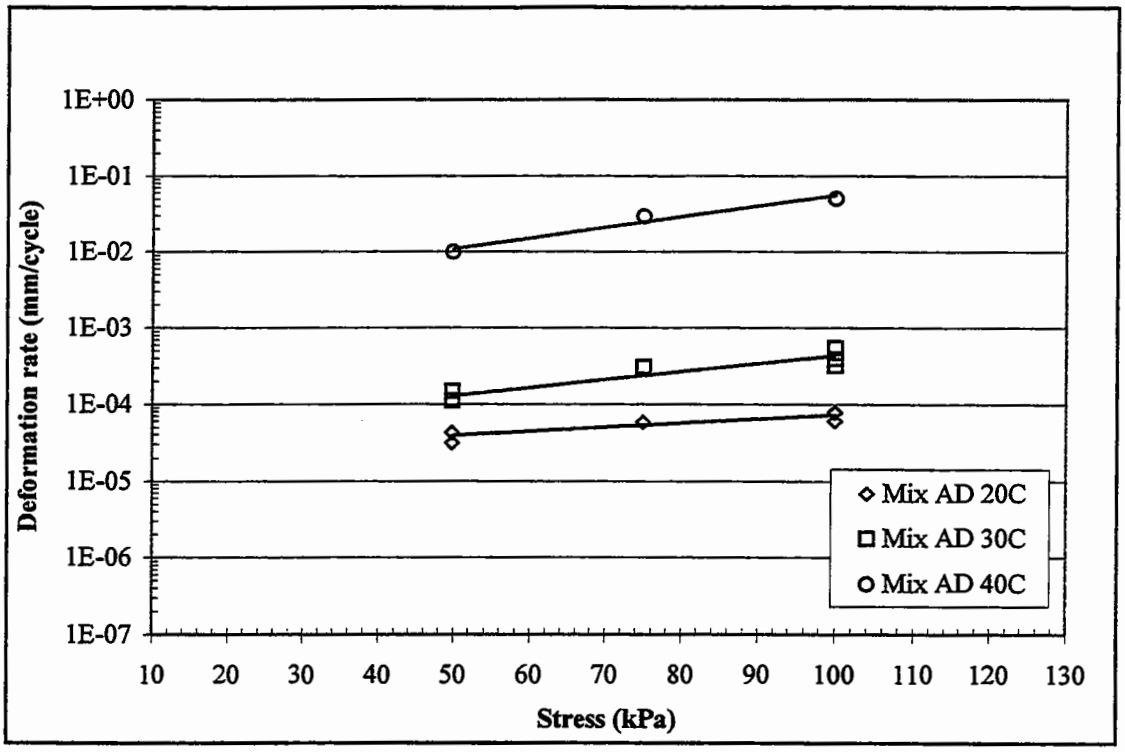

Figure 6.8 Steady-state deformation rates for mixture A/D.

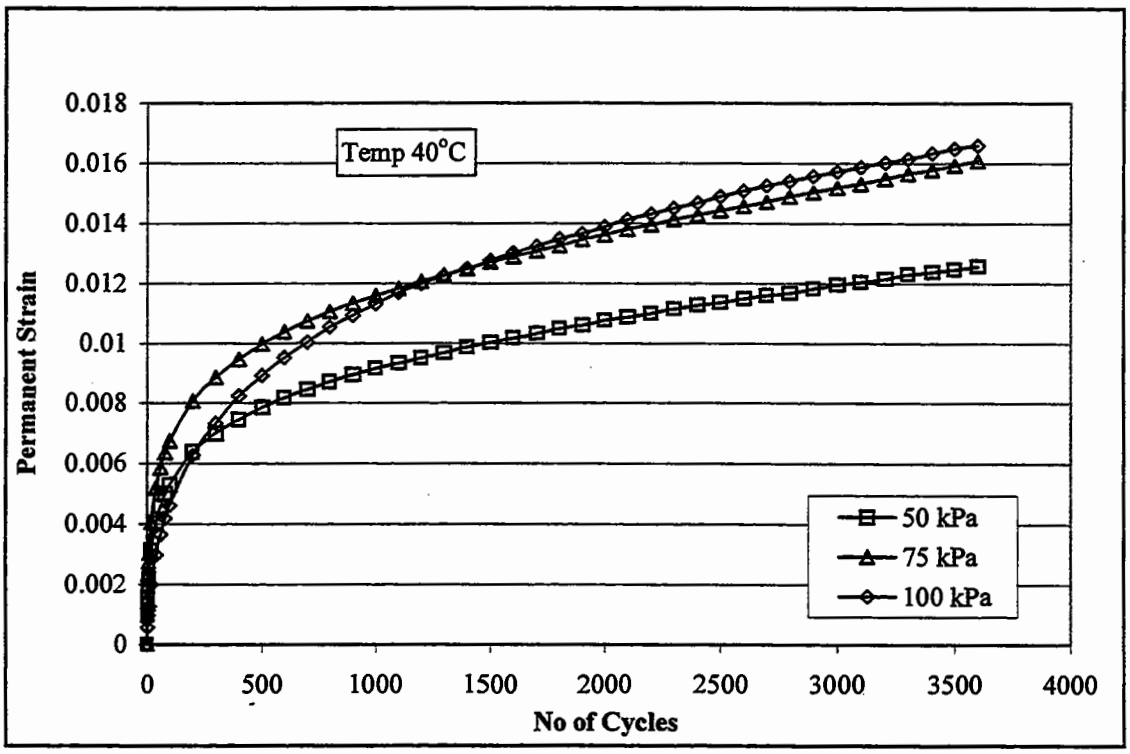

Figure 6.9 Repeated load axial test at 40°C (30/10 HRA mixture).

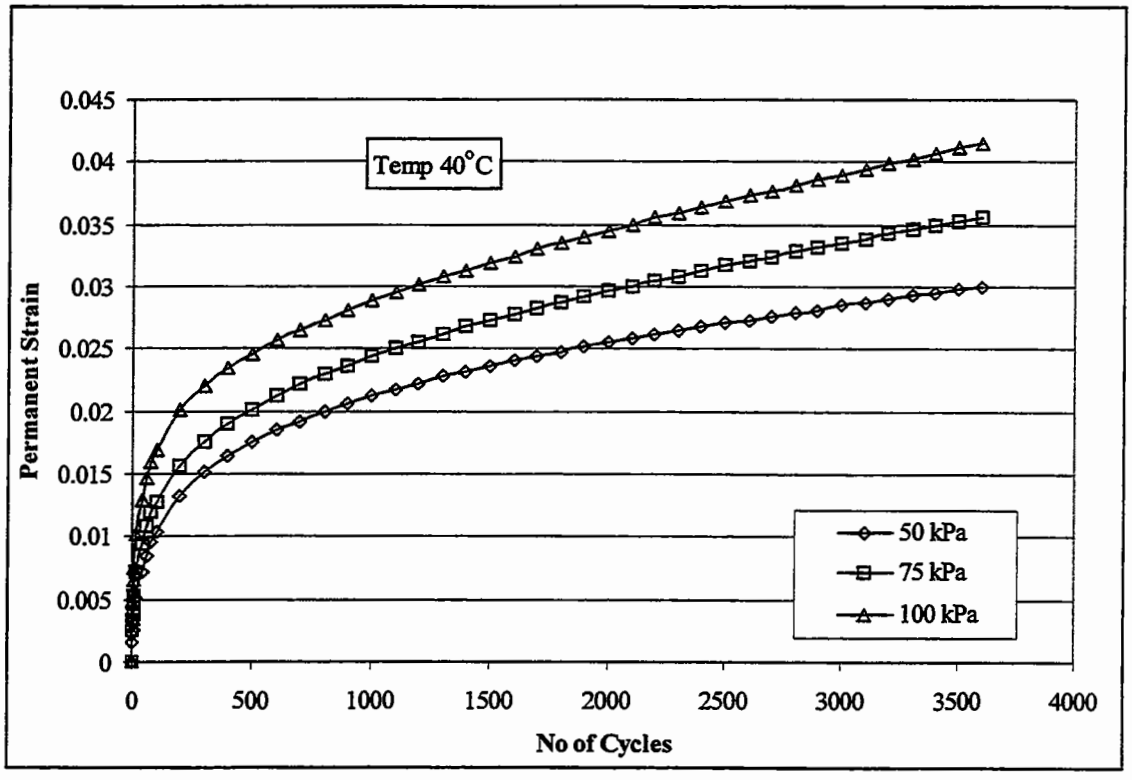

Figure 6.10 Repeated load axial test at 40°C (10 mm DBM mixture).

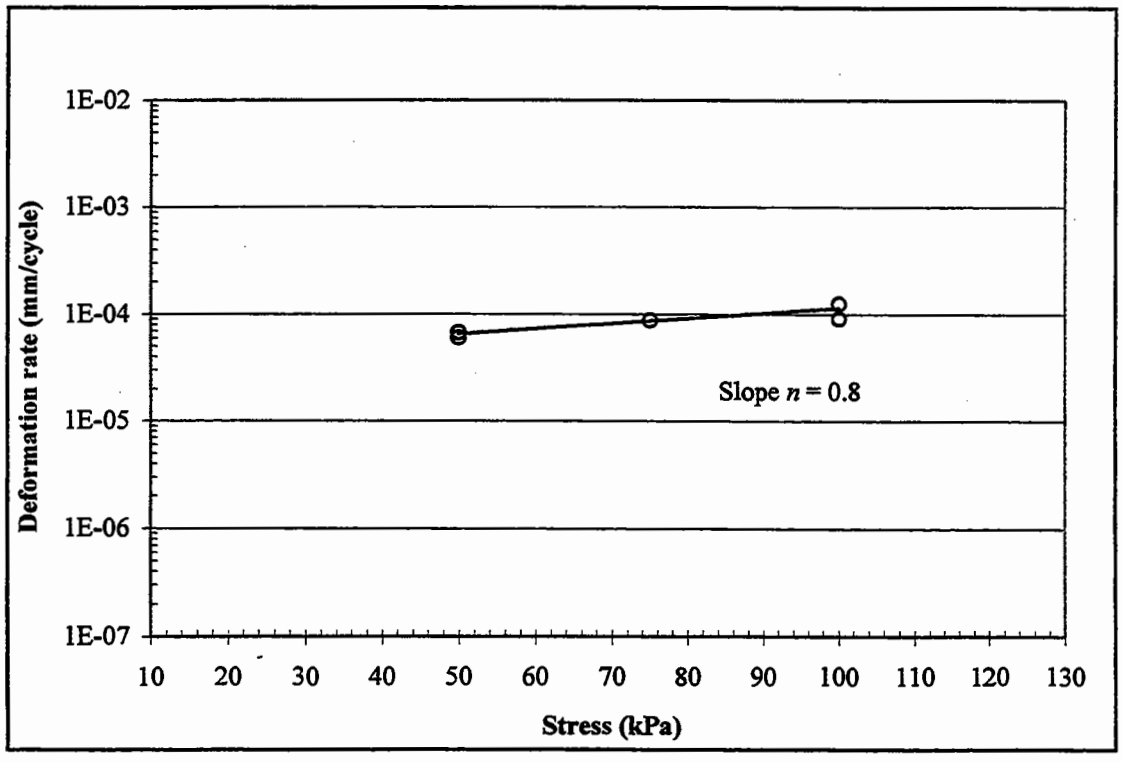

Figure 6.11 Steady-state deformation rates for 30/10 HRA mixture at 40°C.

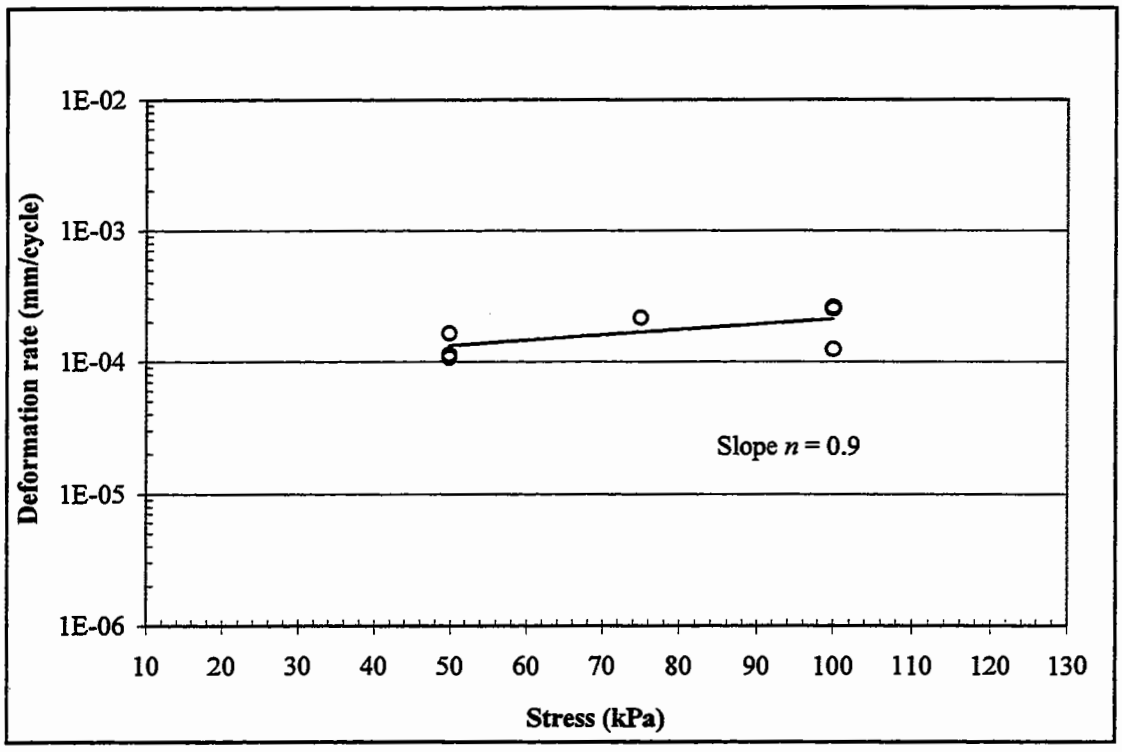

Figure 6.12 Steady-state deformation rates for 10 mm DBM mixture at 40°C.

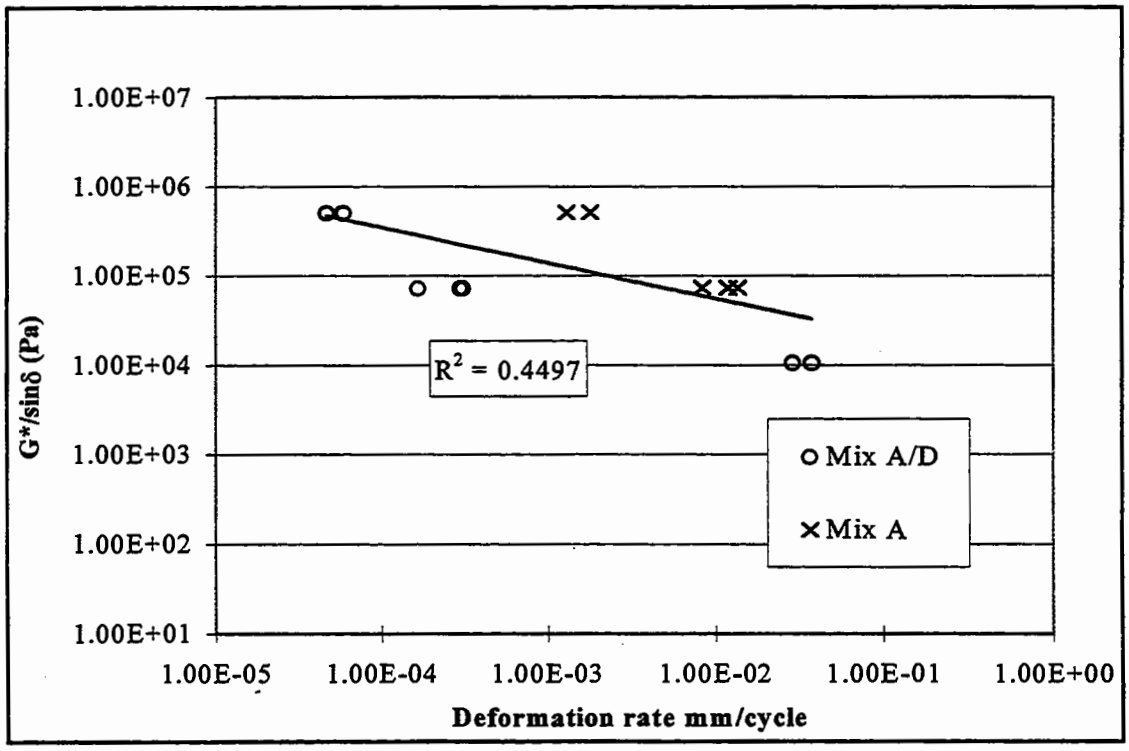

Figure 6.13 Comparison of steady-state deformation rate with G*/sin δ.

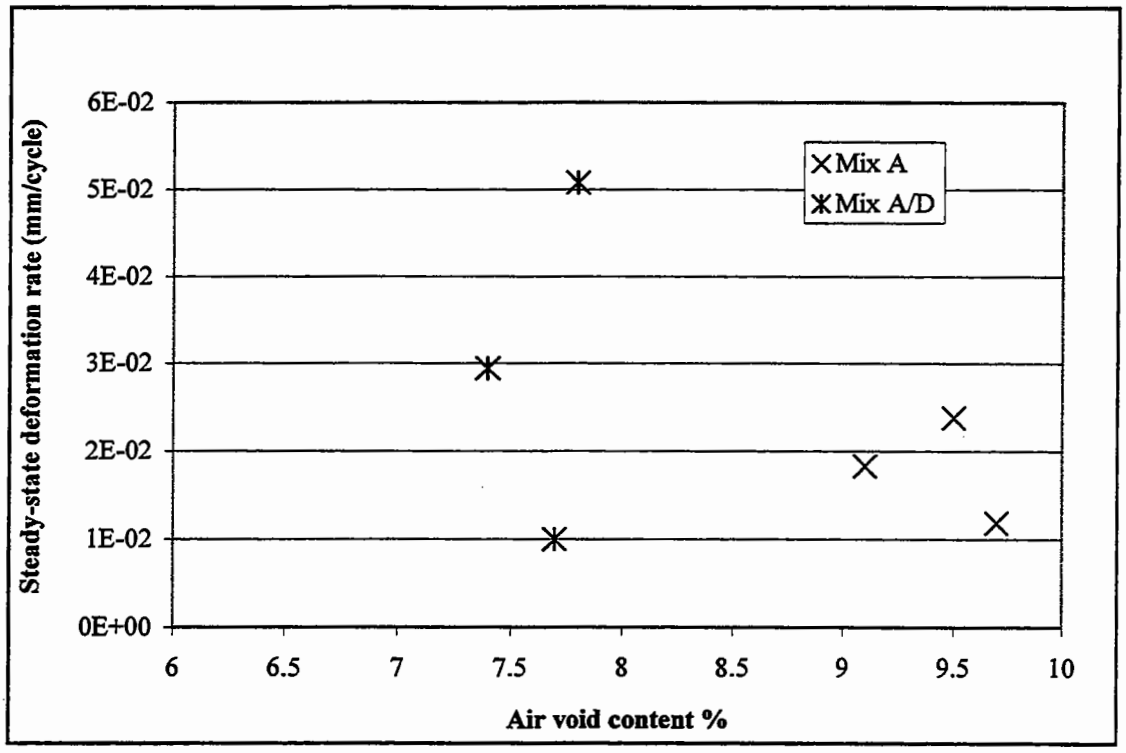

Figure 6.14 Effect of void content on steady-state deformation rate (mix A and mix A/D).

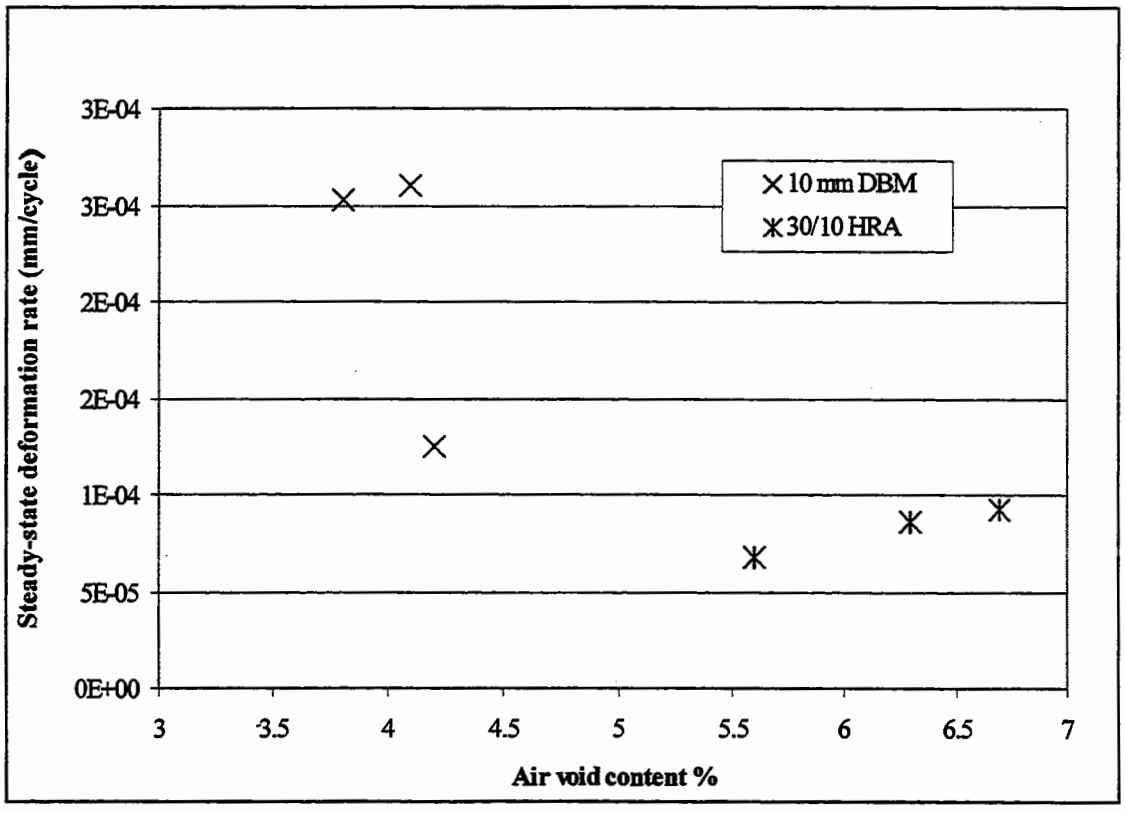

Figure 6.15 Effect of void content on steady-state deformation rate (10 mm DBM and 30/10 HRA).

Wheel Tracking Tests on Idealised and Realistic Bituminous Mixtures

7.1 Introduction

Analysis of results from a standard repeated load uniaxial test show that, due to the lower applied stress levels, the non-linear behaviour of the mixture is reduced resulting in lower values of the effective creep exponent. This chapter describes results from more realistic laboratory scale simulative wheel tracking tests performed on the two idealised and the two realistic bituminous mixtures (described in Chapter 4) over a range of temperatures and applied stress levels. The measured normalised rutting rates from the wheel tracking and RLA test on the idealised mixtures are compared. Results are also compared to the SHRP rutting parameter (see Chapter 3).

This chapter also contains details of experimental developments required for the testing programme.

7.2 Wheel Tracking Test at Nottingham

The wheel tracking test equipment at Nottingham is shown schematically in Figure 7.1. It was derived from a test developed by the Transport Research Laboratory (TRL), for assessing the rutting resistance of HRA wearing course mixtures [137].

The test specimen, which may be either a 200 mm diameter core or a slab of plan dimensions 404×280 mm, is confined in a rigid mould which is driven backwards and forwards beneath a loaded wheel mounted on a pivoted lever arm through which the load is applied. The wheel is 200 mm in diameter, 50 mm wide and is fitted with a solid rubber tyre which measures 80 on the Dunlop hardness scale [66]. The rate of oscillation is set at 40 passes per minute. To record the development of permanent deformation beneath the wheel as the test progresses the vertical position of the wheel (relative to the surface of the slab) is monitored by means of an LVDT mounted beneath the lever arm (see Figure 7.1). The longitudinal distance which the wheel travels during each pass is approximately 240 mm. At the two extremes of each pass where the wheel decelerates and accelerates causes non-uniform deformation both ends of the specimen. A slotted slide attached to the specimen passes through an optical trigger causing the LVDT signal to be captured at eleven positions at 10 mm centres along the central 100 mm of the wheel travel in each pass where the speed is constant. The data is acquired via an analogue to digital converter and is stored on a micro computer.

To fully characterise the rutting process the transverse rut profile is required as well as the peak rut depth. The following sections present the development of a transverse profilometer used to measure the transverse rut profile at various stages during the test.

7.3 Equipment development

Two basic procedures were investigated for measuring the transverse rut profile at various longitudinal positions and loading stages during the wheel tracking test.

7.3.1 Image Analysis

The principal of this technique is that an image of an object is captured from a video or still camera and is downloaded to a computer for detailed analysis. The arrangement that was investigated is shown schematically in Figure 7.2.

A camera was placed in front of (and at an angle to) the slab specimen. A ruler was placed transversely over the rut to be measured for calibration purposes on the computer screen (see Figure 7.2). Rut depth measurements were taken from the bottom of the ruler to the slab surface. To capture a smooth rut profile, measurements were taken at transverse intervals of 5 mm across the slab. However, because of the number of pixels in the picture, a digitisation error in the range of ± 2 mm was observed in the readings. Results were compared with spot LVDT measurements for validation of the measurement system. The results are shown in Figure 7.3 from which it can be seen the accuracy of the system was poor. The method was also found to be extremely time consuming and was not adopted.

7.3.2 Mechanical Profilometer

Because of the inaccuracies associated with the image analysis an alternative mechanical profilometer was developed for capturing the transverse rut profiles. The profilometer comprises an LVDT fitted to an aluminium base plate (see Figure 7.4). The base plate slides on two rigid steel bars 5 mm in diameter to a distance of 280 mm (the width of the slab). To ensure low friction, the base plate was fitted with two self lubricating bushes. The end mountings of the steel bars were fitted to the sides of the slab mould. A small wheel bearing 6.25 mm in diameter was fitted to the transducer so that it could be easily traversed across the slab surface. The LVDT measures the rut depth as a smooth profile transversely over the slab. The transverse distance travelled across the slab by the LVDT is measured by a wire coil fitted to the glide plate, which moves to and fro on the transformer windings attached to the end mountings. Data acquisition is performed using a data-logger which is connected to a personal computer.

In order to validate the measurements, a digital vernier calliper was used to take spot rut depth measurements. A rectangular alluminium base plate (100 mm×280 mm×10 mm) with its end mountings resting on the slab mould was made. Holes were drilled in the base plate at 10 mm centres across the slab width. The base of the vernier calliper was placed vertically on the base plate, over the hole while the needle was extended to touch the slab surface and a reading was taken. The results are shown in Figure 7.5. It can be seen from this figure that a good agreement has been achieved across the slab. The largest error was found to be approximately 2 microns. Consequently, this system was used in the further tests to measure the transverse rut profile.

7.4 Test Procedure

Wheel tracking tests were carried out on slab specimens of dimensions 404 × 280 × 100 mm. To ensure that the specimens were at a uniform temperature, they were placed in a temperature controlled room for at least 24 hours prior to testing. It should be noted that as stated in Chapter 4, the dummy core sample indicated that a temperature of 2 hours was sufficient for conditioning. However, due to the large volume of material in the slab sample it was considered appropriate to condition the specimens for 24 hours since there was no damaging effect on the sample as in case of cylindrical specimens (see Chapter 4). Consequently, these samples were stored in the temperature controlled room for a period of 24 hours. Prior to the commencement of the test, three profiles were captured from the central 100 mm of the slab specimen to define the initial slab transverse profile. The same procedure was repeated after approximately every 1 mm of rut depth observed during the test. The test was terminated when the maximum rut depth reached approximately 10 mm. Figure 7.6 shows a typical set of transverse rut profiles captured after every 1 mm increment in rut depth for mixture A/D tested at 30°C and a contact pressure of 750 kPa. The contact area of the tyre was measured by an imprint on a steel plate as 850mm^2 giving contact stresses in the range 500 kPa to 1500 kPa.

7.4.1 Compaction of Test Specimens

Compaction is a critical factor in specimen preparation. The purpose of any laboratory compaction process is to simulate, as closely as possible, compaction produced in the field. Factors such as the orientation and interlocking of aggregate particles, the extent of interparticle contact, air void content and void structure depend on the method of compaction. A comparison of the results of various tests conducted on the idealised and realistic mixtures indicate that within an optimum range (approximately ± 2%) of void content for a particular mixture, the actual value of air voids has no significant effect on the results. Consequently, for each particular mixture an optimum range of air voids was targetted during the compaction process. The influence of the void content on the steady-state rutting rates is discussed later in this chapter (see discussion).

The loose material was compacted in the rigid mould using a roller compactor (as shown schematically in Figure 7.7) designed to simulate the action of site compaction plant. It comprises a pivoted heated steel roller segment, which is forced into contact with the hot mixture by a vertically mounted pneumatic actuator. A horizontal ram drives the mould back and forth to simulate a rolling action. Compaction was terminated when the desired void content was reached.

7.4.2 Density Measurements

To check uniformity of compaction in the specimens a simple destructive method was used after the wheel tracking test was carried out. For mixture A/D, and the HRA and DBM specimens cores were taken from outside the tracked section to obtain three 100 mm diameter samples. Figure 7.8 shows the position of the cores in relation to the slab. A fourth core was also taken through the rutted section to investigate whether densification had occurred. Due to problems in coring mixture A specimens, the slabs were sliced along the sides of the tracked section and trapezoidal samples of dimensions 134 × 110 × 100 mm were recovered from similar positions to those shown in Figure 7.8. The cores and the cubes were cut to 60 mm height in order to obtain homogeneous samples. The void content of the samples taken from the rutted sections of mixture A and DBM specimens was found to be approximately 2% lower

then the average void content of the samples taken from other sections which indicates that some limited densification had occurred under tracking. However, based on the void content data no evidence of this was found for mixture A/D and HRA specimens. In order to further investigate this, the measured transverse rut profiles (see Figure 7.6) were used to calculate the area of material displaced from below the tyre (depression) and the area of the additional material in shoulders adjacent to the tyre. An area ratio defined between the i'th cycle and the (i+1)'th cycle was defined as:

$$R = \frac{\Delta A_1}{\Delta A_2} \tag{7.1}$$

where R = Area ratio

ΔA_1 = Area of material in the shoulders between the (i+1)'th cycle and i'th cycle

ΔA_2 = Area of material removed from the depression between the (i+1)'th cycle and i'th cycle

It can be seen from Equation 7.1 that if the material is compacting and there is no shear flow $\Delta A_1 = 0$ and $R = 0$. Conversely, if the material is deforming at constant volume $\Delta A_1 = \Delta A_2$ and $R = 1$. If the material is dilating in the rutting process $\Delta A_1 > \Delta A_2$ and R > 1. Figures 7.9, 7.10, 7.11 and 7.12 show Equation 7.1 plotted as a function of number of load passes in a wheel tracking test for mixture A, A/D, HRA and DBM respectively. Equation 7.1 has been calculated at approximately every 1 mm increment in rut depth (depression below the wheel) at the centre of the slab and has been plotted at the mean number of load passes during this period (i.e. $(N_{i+1}+N_I)/2$) for three different applied stress levels (it should be noted that for mixture A/D at 30°C, tests were carried out at two stress levels only). The rut depth readings taken were the average of the three separate readings taken along the central 100 mm of the slab to account for any uneven shear flow due to the particulate nature of the material. It can be seen from these figures that there is quite a lot of scatter in the data but generally the trend is for R to increase as the number of load passes increases. It can be seen from all these figures that at the beginning of the test $R < 1$

indicating that the material is compacting whereas later in the test the R value rises to above 1 indicating that the material is dilating as it deforms. It should be noted that this dilational behaviour could be the result of material continuing to compact under the wheel and also deforming in shear at constant volume although this is not strongly supported by the density measurements taken from under the loaded area. The amount of dilation was observed to be independent of the stress levels with an average value of around 1.5 for mixture A, A/D and HRA and 1.2 for DBM (it should be noted that the DBM mixture contained 100 Pen grade of bitumen).

It can be seen from Figure 7.17 that for mixture A, steady-state rutting conditions are reached very quickly (after approximately 100 load passes). This can also be observed from Figure 7.9 where R rises quickly to a value of approximately 1.5 indicating that the material is dilating as it deforms. A similar observation can be made by comparing Figure 7.14 with Figure 7.10 noting that, for mixture A/D, steady-state rutting conditions take longer to achieve (approx. 800 load passes), and again the material is dilating as it deforms. Similar observations can also be made for the realistic mixtures by comparing Figure 7.21 with Figure 7.11 (HRA) and Figure 7.22 with Figure 7.12 (DBM). Again it should be noted that steady-state rutting conditions take longer to achieve compared to the idealised mixtures (approx. 5,000 load applications) and again the material is dilating as it deforms. It should also be noted that under triaxial test conditions all the mixtures were observed to dilate (see Table 5.1 and Figure 5.25) which is consistent with the results shown in Figures 7.9-7.12.

Table 7.1 shows the range of air void contents for all the mixtures characterised by a mean value, a maximum and minimum and a Coefficient of Variation (COV). It can be seen by comparing Table 6.1 and Table 7.1 that the variability (COV) in air void content for all the mixtures is lower for the wheel tracking specimens (compared to the RLA test) because the void content for each tracked specimen was taken to be the average of the separate measurements made on three samples taken from the slab. It can also be seen by comparing Table 6.1 and Table 7.1 that, for mixture A, the average air void content for the gyratory specimens (9.7%) is very close to the average air void content for the wheel tracking specimens (9.5%).

Table 7.1 Air Void Content Analysis (outside loaded area)

Mix	No. of Samples	Air Void Content (%)			
		Mean	Minimum	Maximum	COV (%)
A	14	9.5	9	10.2	3.4
A/D	16	6.9	6.3	7.7	5.2
30/10 HRA	7	6.1	5.5	6.8	5.7
10mm DBM	7	4.3	3.9	4.8	6.9

7.4.3 Test Conditions

The following wheel tracking testing was carried out on the idealised and realistic mixtures:

Idealised Mixtures (mixture A and mixture A/D)

- 3 temperatures (20, 30 and 40°C),
- 3 stress levels (500, 750 and 1000 kPa).

For Mixture A/D, at 20°C, higher stress levels of 1000, 1250 and 1500 kPa were applied, to accelerate the rutting process.

Realistic Mixtures (HRA and DBM)

- 1 temperature (45°C),
- 3 stress levels (1000, 1250 and 1500 kPa).

7.5 Results for the Idealised Mixtures

Results from tests at 3 different stress levels and 3 temperatures are shown in Figures 7.13 to 7.15 for mixture A/D, and in Figures 7.16 to 7.18 for mixture A where the average rut depth is plotted against the number of load passes. The rut depth at a

particular location was taken to be the difference between the maximum depression and the top of the shoulder adjacent to the depression (similar to the straight edge method used in full-scale pavements [133]). The average rut depth was calculated by averaging together the rut depth measured at 3 longitudinal positions over the central 100 mm of the slab.

It can be seen from these figures that, after an initial period where the rutting rate decreases, the rut depth increases approximately in proportion to the number of cumulative load passes. This initial behaviour is thought to be associated with densification where the density of the material increases under early loading. This is supported by the increase in density measured under the tracked area (see section 7.4.2). The second part of the curve can be characterised by a steady-state rutting rate (gradient). It can be seen from these figures that, as expected, the rutting rate increases with increasing contact stress and increasing temperature.

7.6 Analysis of Test Results

Figures 7.19 and 7.20 show the rutting rate (gradient) measured for mixture A and mixture A/D plotted against applied contact stress on a semi logarithmic scale. The variability in wheel tracking test results for mix A and mix A/D was determined by conducting three replicate tests each at two temperatures (20°C and 40°C) and the two extremes of stress level. The steady state rutting rates from all the tests (including repeats) conducted on these mixtures are also plotted in these figures.

The same technique described in Chapter 6 for the RLA test results has been used to determine the average value of n that best fits the data from all three temperatures for each mixture. A summary of the test results (including repeats) for mixtures A and A/D are given in Table 7.2. In addition to the value of n, rutting rates and air void contents of the specimens are also given. As before, the average Coefficient of Variation (COV) has been calculated for each mixture to evaluate the fit (also shown in Table 7.2). Also given in Table 7.2 are the steady state rutting rates for just the depression (without the rut shoulder). The calculated values of n with the COV values are also given in the table. It can be seen that, although the shoulder height is not taken into account, the resulting values of n are within the range n = 1.9 to 2.4 for

both mixtures A and A/D. It can be seen from the values of n (with and without the shoulder) that the rutting process is not linear ($n = 1$) and the values of n compare well with the range of n = 1.9 to 2.4 measured from creep and constant strain rate tests performed on these mixtures and the binder.

Table 7.2 Summary of Wheel Tracking Test Results (Idealised Mixtures)

Mix	Temp (°C)	Stress (kPa)	Void (%)	Rutting Rate (Depression + Shoulder) (mm/cycle)	n (COV)	Rutting Rate (Depression) (mm/cycle)	n (COV)
A	20	500	9.0	1.11E-04	2.1 (12%)	6.88E-05	1.9 (9.4%)
			9.2	3.42E-04		2.12E-04	
			9.1	4.67E-04		2.73E-04	
		750	9.5	1.14E-03		6.46E-04	
		1000	9.3	1.90E-03		1.20E-03	
			9.6	1.60E-03		1.16E-03	
			9.2	1.52E-03		1.11E-03	
	30	500	10.1	9.00E-03		5.00E-03	
		750	10.2	1.20E-02		7.00E-03	
		1000	9.8	2.30E-02		9.03E-03	
	40	500	9.4	2.10E-02		1.44E-02	
		750	9.1	6.29E-02		4.12E-02	
			9.9	4.91E-02		3.25E-02	
			9.5	2.46E-02		1.60E-02	
A/D	20	1000	7.0	6.34E-05	2.4 (10.2%)	5.10E-05	2.4 (10%)
			6.8	6.37E-05		6.00E-05	
			6.7	6.37E-05		4.20E-05	
		1250	6.3	8.40E-05		7.70E-05	
		1500	7.4	6.34E-05		6.00E-05	
			7.6	2.57E-04		1.50E-04	
			7.5	2.59E-04		1.70E-04	
	30	750	7.7	1.96E-03		6.20E-04	
		1000	7.4	4.50E-03		2.60E-03	
	40	500	6.6	3.13E-03		1.50E-03	
			6.3	2.25E-03		1.90E-03	
			6.5	2.75E-03		2.12E-03	
		750	6.8	5.60E-03		4.14E-03	
		1000	6.8	1.74E-02		1.12E-02	
			6.7	1.90E-02		8.00E-03	
			7	1.87E-02		1.00E-02	

7.7 Results for Realistic Mixtures

Results from tests at 3 different stress levels and at a temperature of 45°C are shown in Figures 7.21 and 7.22, for the 30/10 HRA mixture and the 10mm DBM mixture respectively, where the average rut depth is plotted against the number of load passes.

It can be seen from these figures that, after an initial densification period, the rut depth increases approximately in proportion to the number of cumulative load passes. As before, this was characterised by a steady-state rutting rate (gradient).

7.8 Analysis of Test Results

Figures 7.23 and 7.24 show the rutting rate (gradient) of the HRA and DBM mixtures plotted as a function of applied stress plotted on a semi logarithmic scale. To account for variability in results, three replicate tests at two stress levels (1000 kPa and 1500 kPa) were conducted for each of the mixtures. The steady state rutting rates from all the tests (including repeats) are also plotted in the figures. The same technique described above for tests on idealised mixtures has been used to determine the value of n (creep exponent) that best fits the data for each mixture. A summary of the test results (including repeats) for 30/10 HRA and 10mm DBM mixtures is given in Table 7.3. In addition to the values of n, rutting rate and the air void contents of the specimens are also given. To evaluate the fit the COV between the measured and predicted rutting rates has been calculated for each mixture (also shown in Table 7.3).

It can be seen from Table 7.3 that the resulting values of creep exponent n are similar to those measured for the idealised mixtures (Table 7.2). It can also be seen from Tables 7.3 and 7.2 that there is less variability in the results from the realistic mixtures compared to the idealised mixtures. This is probably because wheel tracking tests on realistic mixtures were only conducted at one temperature whereas the wheel tracking tests on the idealised mixtures were conducted at 3 temperatures. Also given in Table 7.3 are the steady state rutting rates for the depression (without the rut shoulder). The calculated values of n with the COV values are also given in the table. As before, it can be seen that although the shoulder height is not taken into account the resulting values of n indicate that the rutting process in realistic mixtures is not linear ($n = 1$).

Table 7.3 Summary of Wheel Tracking Test Results

(Realistic Mixtures)

Mix	Temp (°C)	Stress (kPa)	Void (%)	Rutting Rate (Depression + Shoulder) (mm/cycle)	*n* (COV)	Rutting Rate (Depression) (mm/cycle)	*n* (COV)
30/10 HRA	45	1000	6.8	8.16E-05	2.2 (4.8%)	5.26E-05	2 (3.5%)
			6.5	9.00E-05		8.00E-05	
			5.8	5.80E-05		3.55E-05	
		1250	6.2	1.82E-04		8.33E-05	
		1500	5.5	1.94E-04		1.20E-04	
			5.9	1.75E-04		9.00E-05	
			6.1	1.70E-04		8.69E-05	
10mm DBM	45	1000	4.4	5.10E-05	1.9 (4.1%)	4.80E-05	1.6 (3.3%)
			4.2	5.90E-05		5.10E-05	
			3.9	7.90E-05		7.00E-05	
		1250	4.8	1.20E-04		9.00E-05	
		1500	4	1.33E-04		1.00E-04	
			4.3	1.39E-04		1.20E-04	
			4.4	1.21E-04		9.00E-05	

7.9 Comparison of Wheel Tracking and RLA Test Data

Because wheel tracking tests and RLA tests on the HRA and DBM mixtures were performed at two different temperatures (45°C and 40°C) the following comparisons are for the idealised mixtures only. A comparison of the average normalised steady-state rutting rates at each temperature calculated from the wheel tracking test and the RLA test (Chapter 6) is shown in Figure 7.25. For a particular temperature the average normalised rutting rates have been calculated by normalising the rutting rates to the mean stress level and then averaging these normalised rutting rates together. It can be seen from this figure that there is a reasonable correlation between the 2 tests although the scatter is quite high (R^2=0.67) and the ranking of the mixtures changes depending on the test that is used to characterise the material [47]. This is likely to be due to non-linearities that are not accounted for in the normalisation of the steady-state rutting rates and variations in air void content. The scatter in the results between the two tests may be reduced by applying a confining pressure in the RLA test although the results are limited to relatively few tests. Recently, the vacuum RLAT

was found to rank the materials in a similar order to that of the wheel tracking tests and appears to have the potential over standard RLAT to provide a realistic ranking of deformation resistance [106]. The vacuum RLAT correlated best with the wheel tracking and this test was recommended for further investigation and development. However, further research is in progress to establish the standard test conditions for the vacuum RLAT and investigate its precision [107].

7.10 Comparison of G*/sinδ with Wheel Tracking Test Data

Because wheel tracking tests and RLA tests on the HRA and DBM mixtures were performed at only one temperature the following comparisons are for the idealised mixtures only. Figure 7.26 show a plot of $G^*/\sin\delta$ against normalised steady-state rutting rate calculated by normalising the rutting rates to the mean stress level. Again a loading frequency of 0.1Hz was selected for calculating $G^*/\sin\delta$ because this gave the best correlation with the wheel tracking results. It should also be noted that the effective loading speed for the wheel tracking test is also low (0.55 km/hr) which, corresponds to a lower test frequency in the DSR.

It can be seen from Figure 7.26 that as with RLA test results (Chapter 6), the data falls onto 3 horizontal lines corresponding to the 3 different test temperatures. It can also be seen from Figure 7.26, that there is quite a large amount of scatter in the results (R^2 = 0.65) between wheel tracking and G*/sinδ values [47].

7.11 Discussion

The results from the wheel tracking tests suggest that the permanent deformation behaviour of the idealised and the realistic mixtures subjected to more realistic loading is heavily influenced by the non-linear permanent deformation properties of the binder. The measured creep exponents from the wheel tracking test for the idealised as well as the realistic mixtures are well within the range n = 1.9 to 2.4 which is very similar to the non-linear creep exponent measured from the quasi-static uniaxial and triaxial testing (see Chapters 4 and 5).

It can also be seen from Tables 7.2 and 7.3 that the values of n measured from the wheel tracking test are higher than those measured for the RLA test (Chapter 6). This is likely to be due to differences in the applied stress level between the two tests. For example, the minimum stress applied in the RLA test was 50 kPa compared to a minimum stress of 500 kPa applied in the wheel tracking test. The lower stress level in the RLA test would be expected to influence the behaviour of the bitumen which has been found to change from power law creep to linear viscous flow between 70 kPa and 500 kPa (see Figure 4.10, Chapter 4). Consequently, it seems likely that the rutting process (as measured in the wheel tracking test) for these idealised mixtures and realistic mixtures is a non-linear process, the form of which is largely determined by the non-linear viscous properties of the binder.

In the wheel tracking test program, 3 replicate tests at different stress levels and temperatures were performed on each mixture. The standard deviation and hence the COV associated with the determination of the steady-state rutting rate for each mixture type are shown in Table 7.4. It is quite evident that the degree of scatter in the wheel tracking test results is high. Comparing Table 6.4 and 7.4, it can be seen that the mean COV for the RLA test is 18.1 ± 8.8% and for the wheel tracking test is 17.4 ± 18.1%.

There is no indication from the wheel tracking test results of any consistent effect of small variations in void content on the steady-state rutting rate as demonstrated in Figures 7.27 and 7.28, which shows data from replicate tests of idealised and realistic mixtures respectively. These results are not untypical and are consistent with data reported by Gibb [66] which shows little or no effect of air voids on performance of his mixtures in the wheel tracking test. He found no consistency in the test results from mixtures with void content in the range between 4% to 8.5%. However, at very high void content (16% - 20%) the effect would be more pronounced which would indicate poorly compacted mixture. Consequently, the scatter in the results of wheel tracking tests could not be attributed confidently to the small variation in the void content and is thought to be the variability inherent in the test. Similar observations were also made for repeated load axial test.

Table 7.4 Percentage Variation of Steady-State Rutting Rate Measured from Replicate Wheel Tracking Tests

Mix	Temp (°C)	Stress (kPa)	No of Tests	COV (%)
A	20	500	3	58
		1000	3	11.9
	40	750	3	42
A/D	20	1000	3	0.27
		1500	3	0.77
	40	500	3	16.2
		1000	3	4.6
30/10 HRA	45	1000	3	21
		1500	3	7
10 mm DBM	45	1000	3	22.8
		1500	3	6.9

7.12 Conclusions

The following conclusions can be drawn from this chapter:

- Wheel tracking tests have been performed on two idealised and two realistic bituminous mixtures over a range of temperatures and applied stress levels.

- The idealised and the realistic mixtures were found to dilate in the wheel tracking test. The amount of dilation was independent of stress levels.

- The steady-state rutting rate has been used to characterise the permanent deformation behaviour of these mixtures.

- Results show a higher value of creep exponent (n = 1.9 to 2.4) from the wheel tracking tests compared to the RLA test (n = 0.8 to 1.5) for both the idealised and realistic mixtures.

- These results show that the rutting process (as measured in the wheel tracking test) for the mixtures tested can be non-linear with respect to the applied load at realistic stress levels.

- The amount of scatter observed in replicate tests for determination of steady-state rutting rate could not be attributed to small variation in void content and is thought to be due to the variability inherent in the test.

- Results shows a reasonable correlation between average normalised rutting rates from the wheel tracking and RLA tests on idealised mixtures.

- $G^*/\sin\delta$ (obtained from DSR testing) has been calculated at a frequency of 0.1Hz and plotted against the measured steady-state rutting rate from the wheel tracking test on idealised mixtures

- Results show that there is considerable scatter caused mainly by non-linearities not accounted for in the SHRP rutting parameter.

7.13 Figures

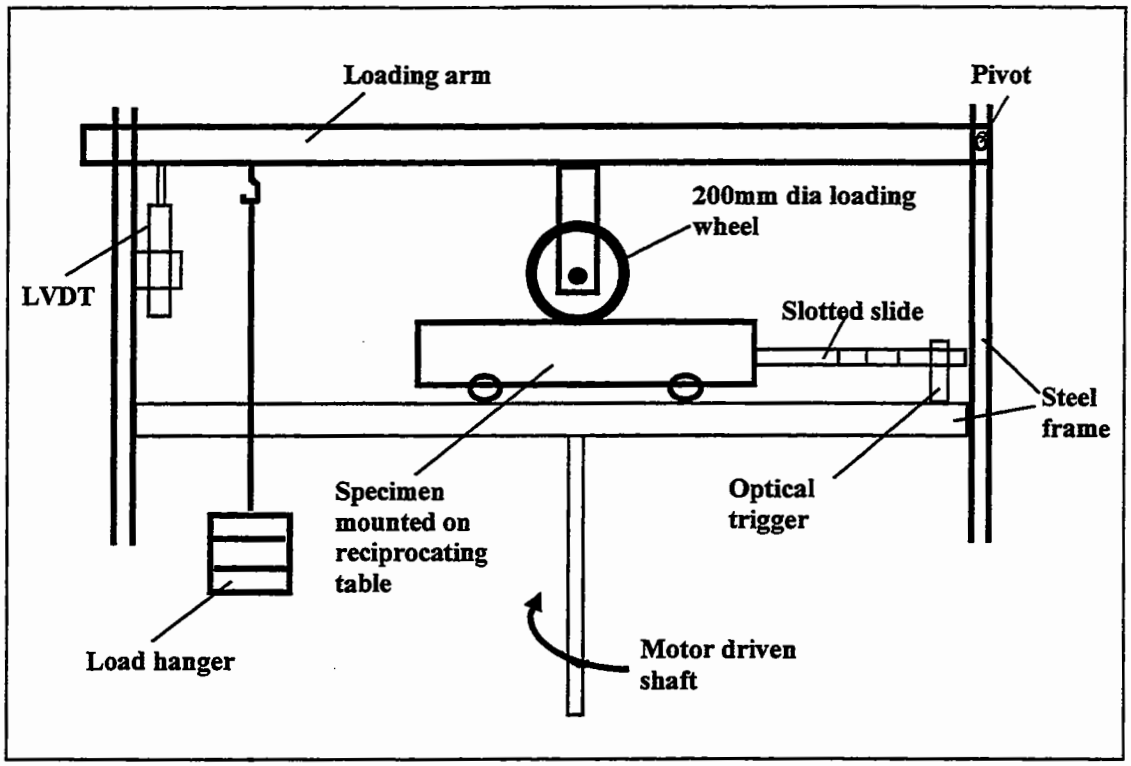

Figure 7.1 Schematic of wheel tracking apparatus at Nottingham.

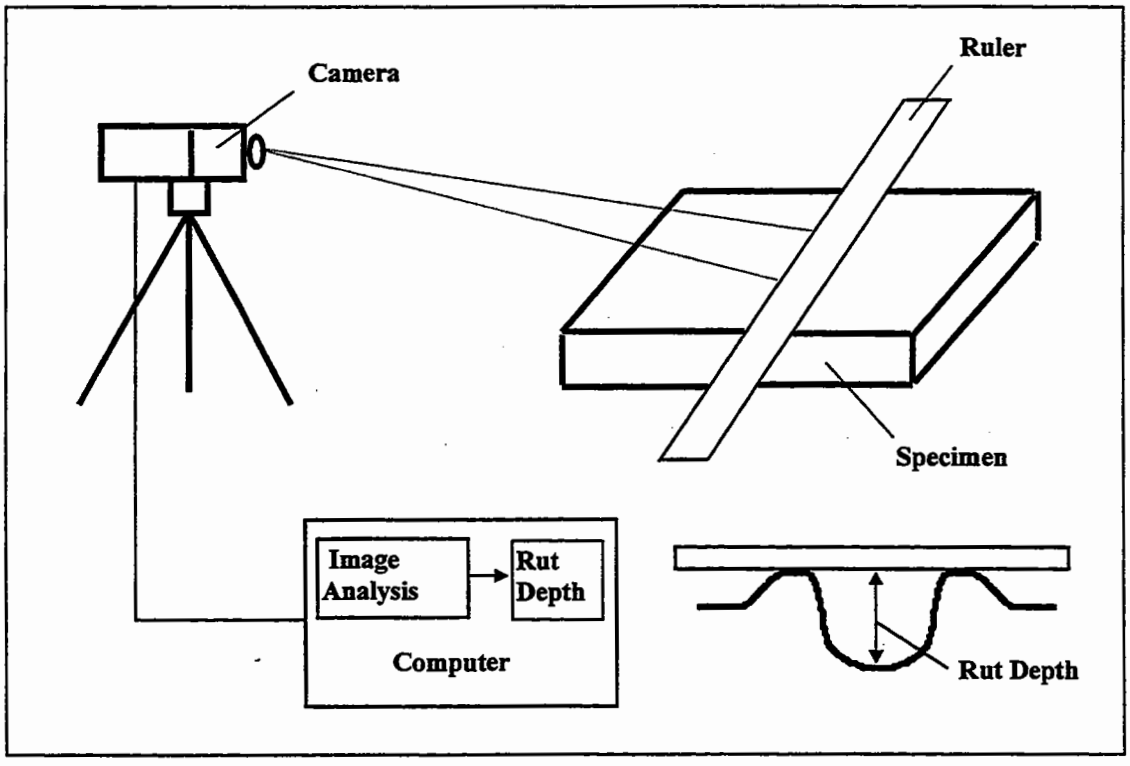

Figure 7.2 Schematic of image analysis arrangement for capturing rut profile.

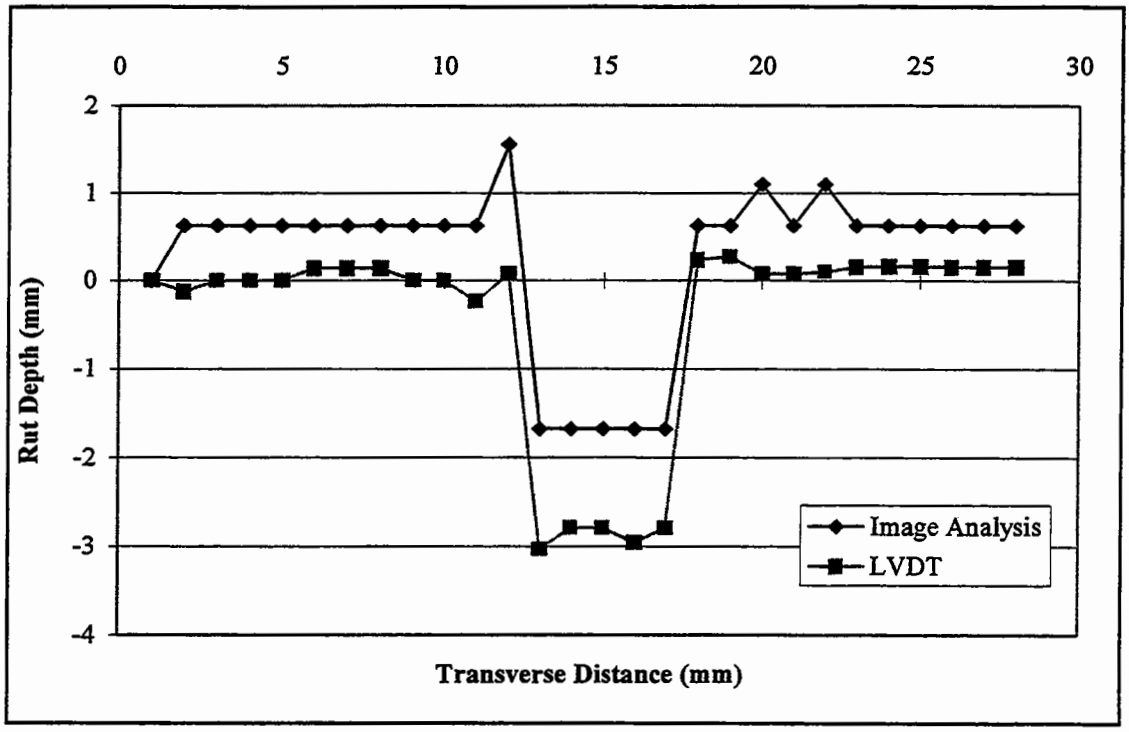

Figure 7.3 Comparison of rut profile captured by image analysis and LVDT.

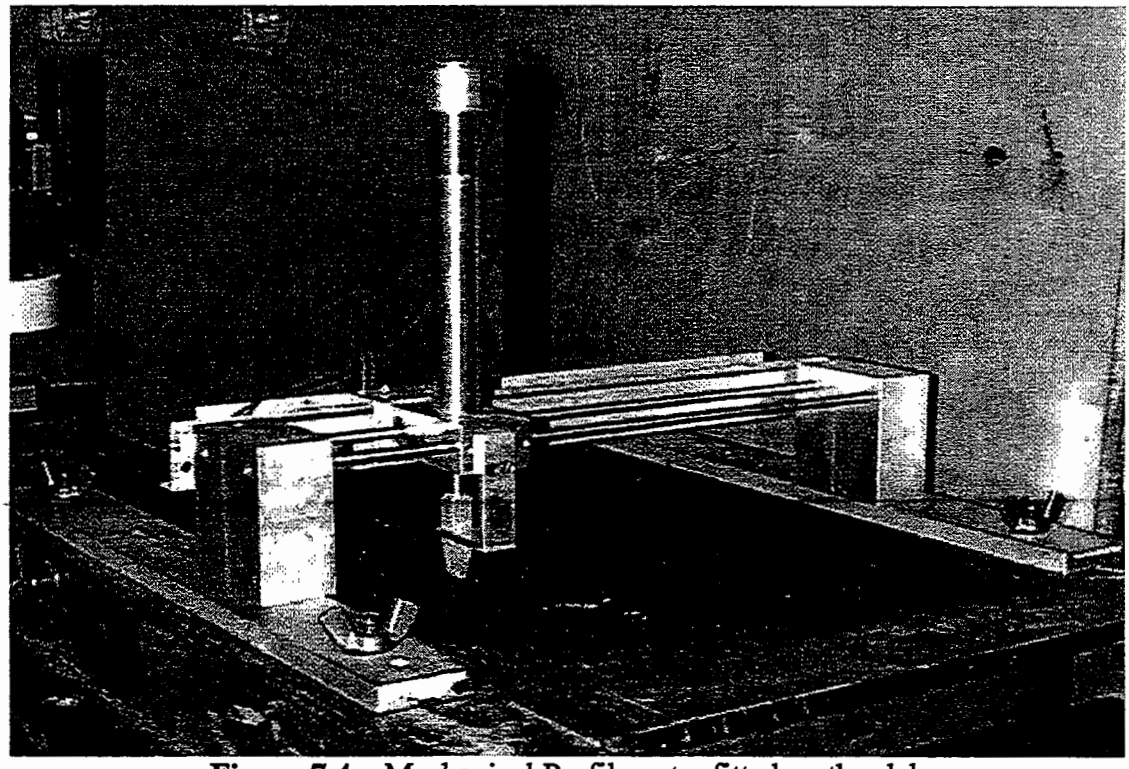

Figure 7.4 Mechanical Profilometer fitted on the slab.

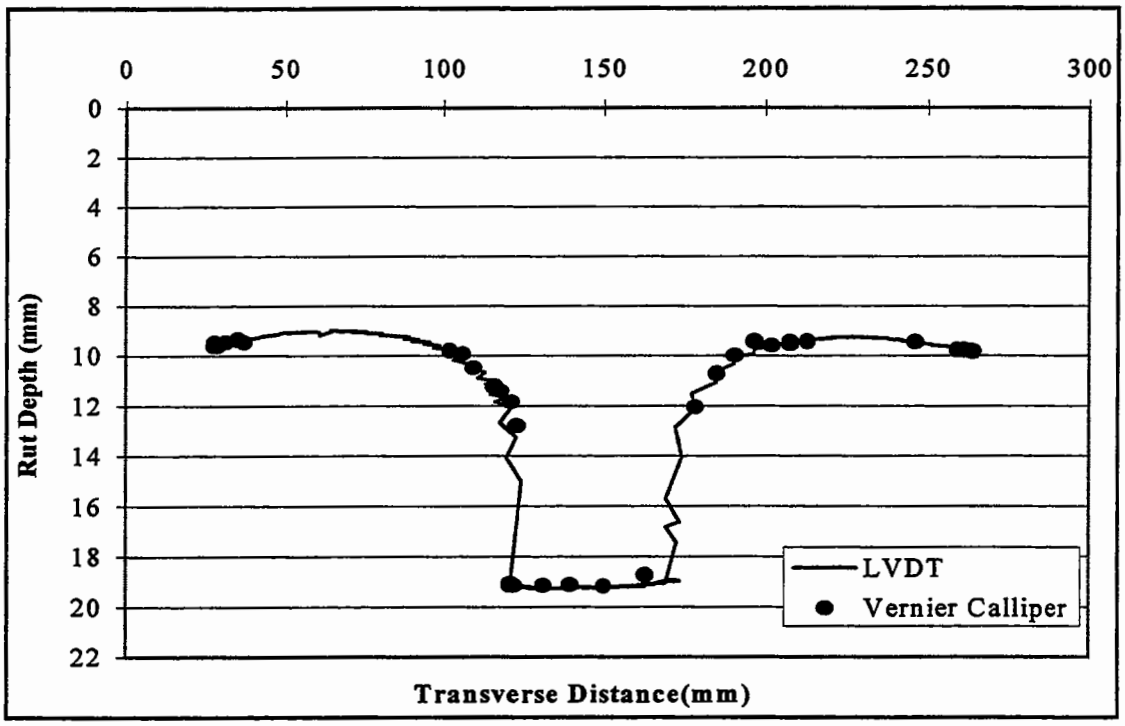

Figure 7.5 Validation of rut profile captured by mechanical profilometer with vernier calliper.

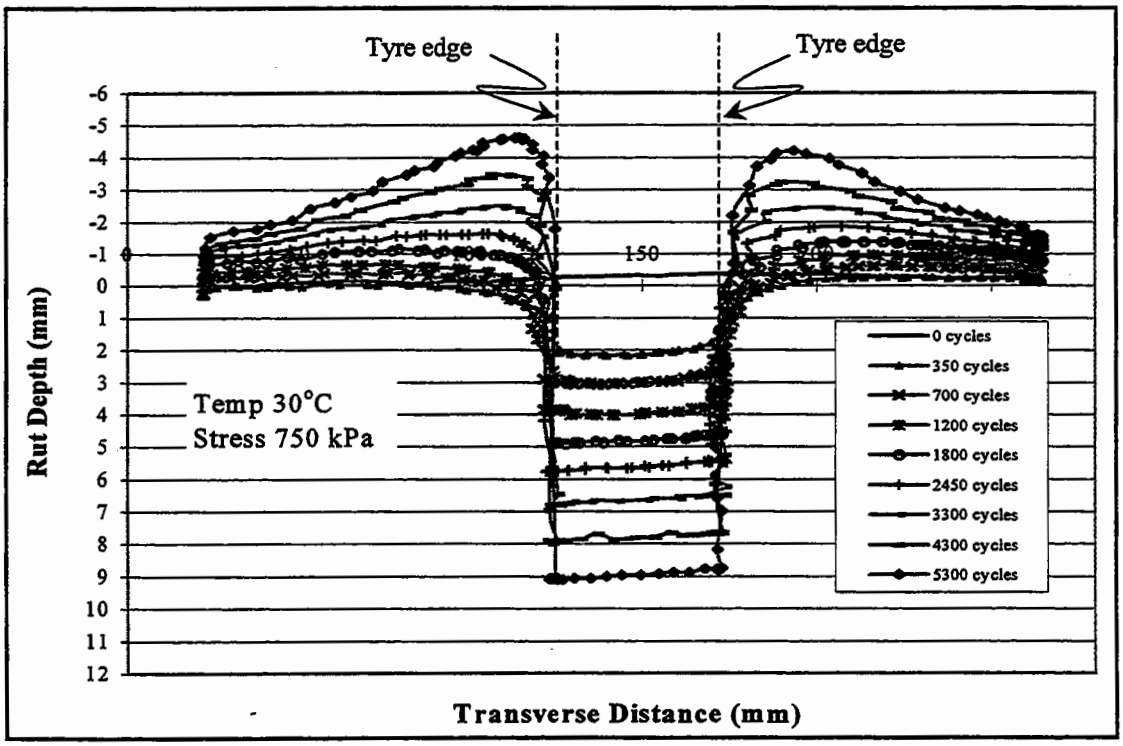

Figure 7.6 Transverse rut profile captured with Mechanical Profilometer (Mixture A/D).

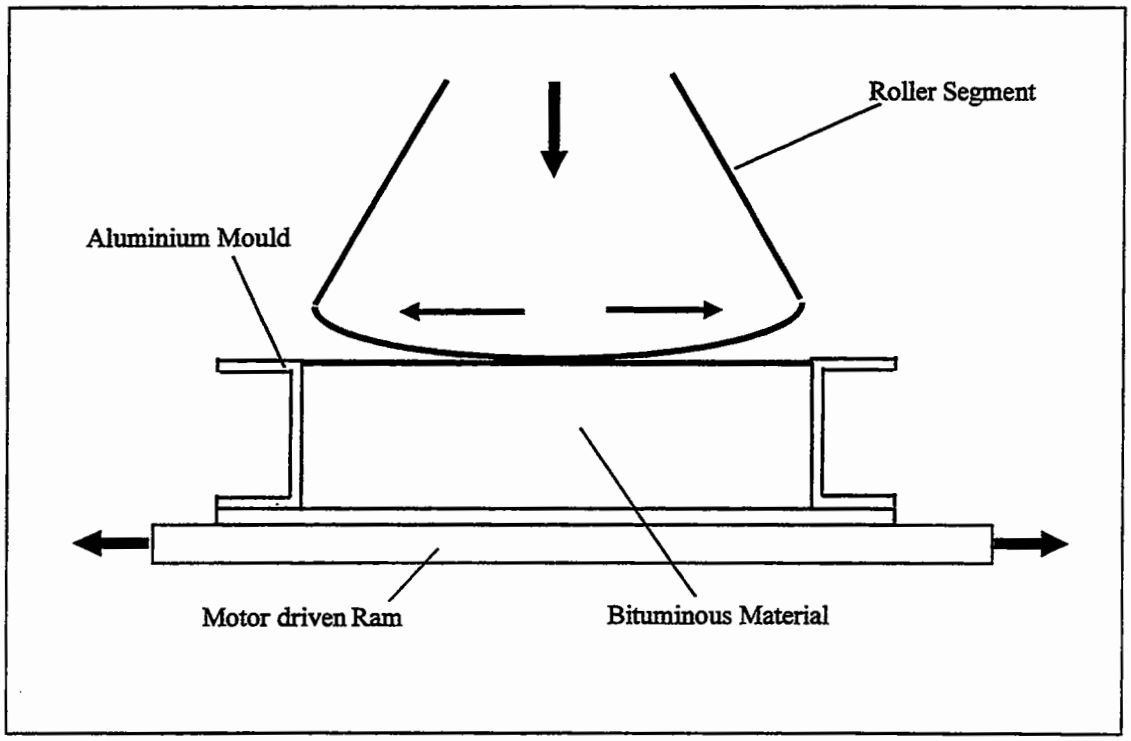

Figure 7.7 Schematic section showing Laboratory Roller Compactor.

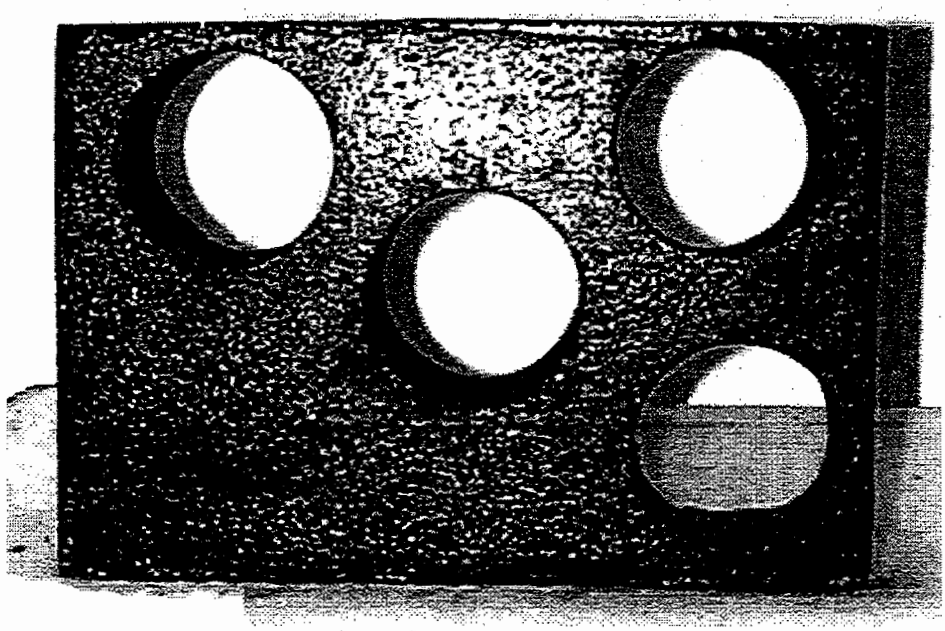

Figure 7.8 Position of core samples from Mixture A/D.

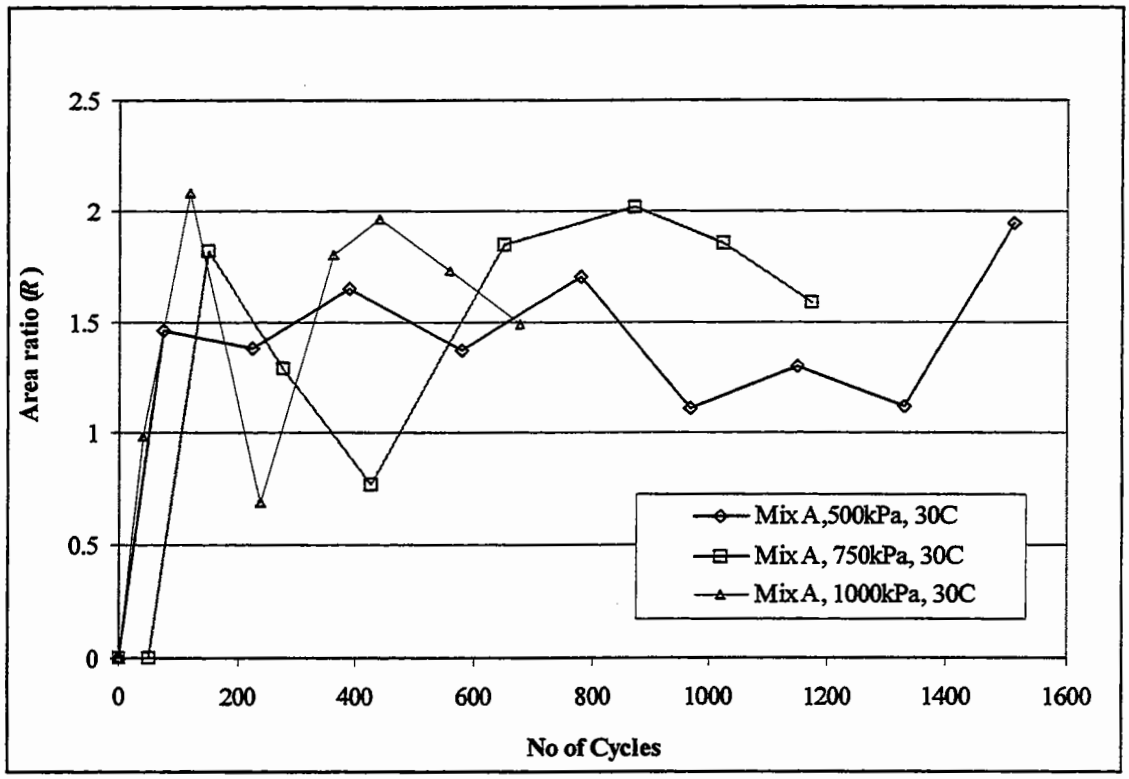

Figure 7.9 Area ratio for mixture A at 30°C.

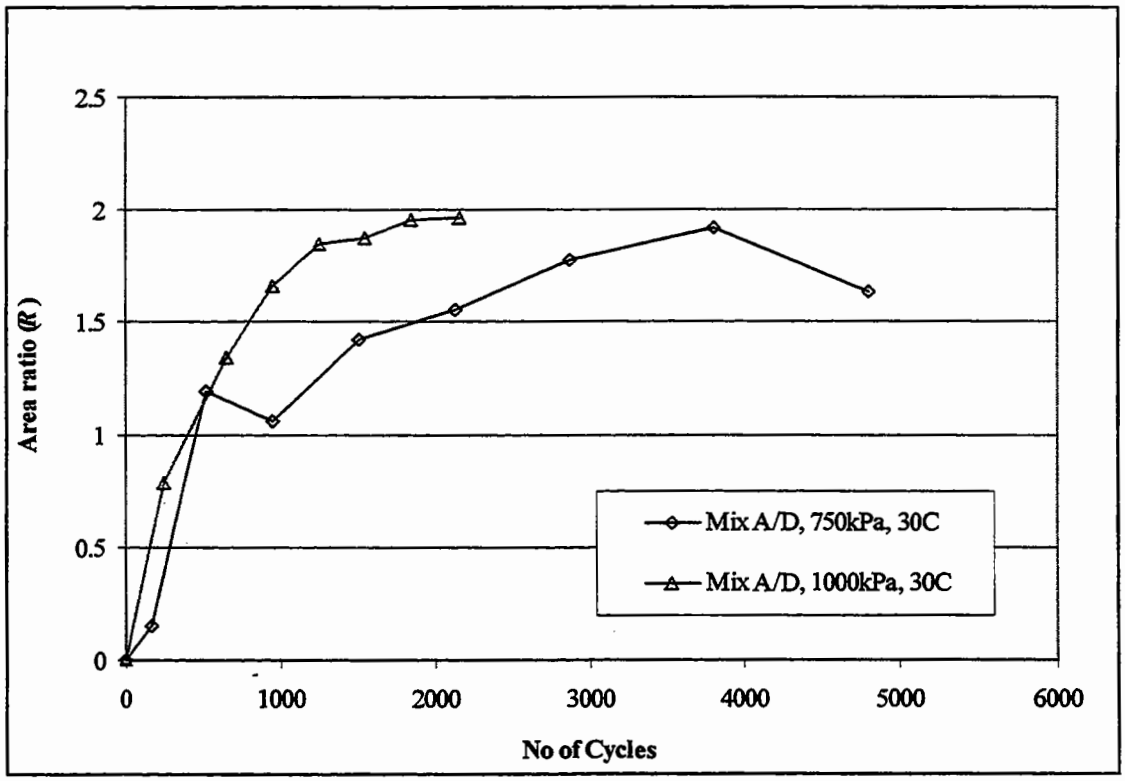

Figure 7.10 Area ratio for mixture A/D at 30°C.

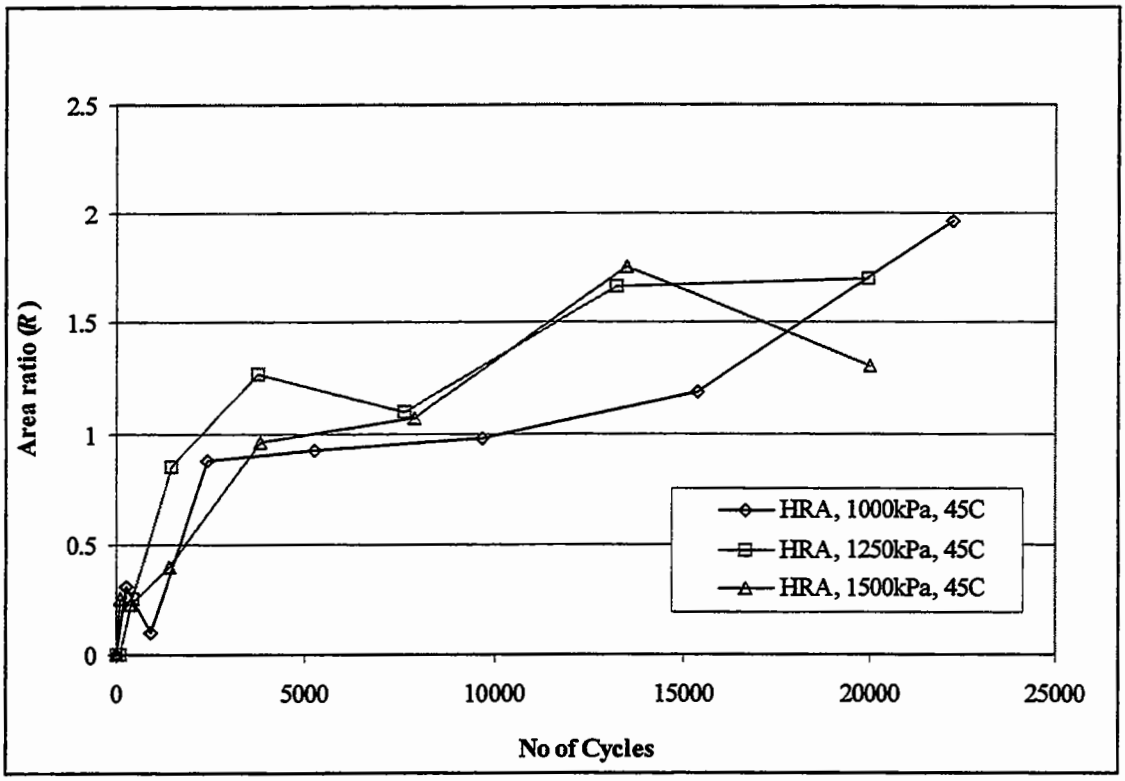

Figure 7.11 Area ratio for 30/10 HRA at 45°C.

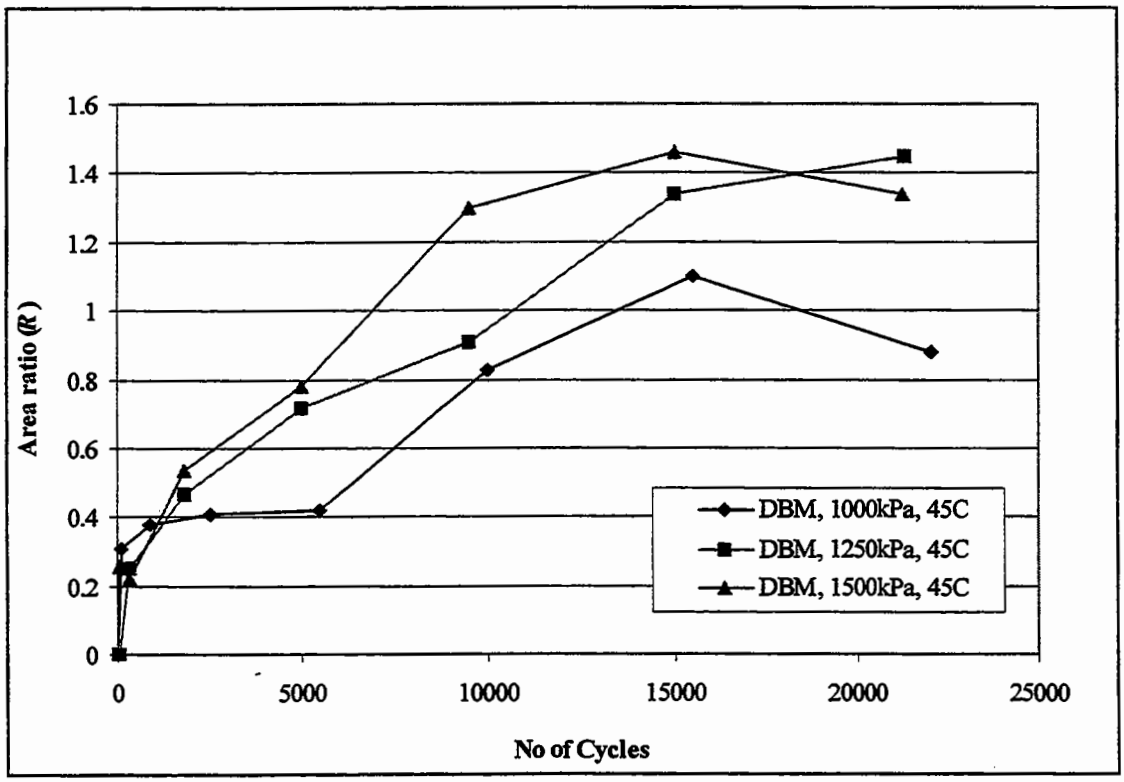

Figure 7.12 Area ratio for 10 mm DBM at 45°C.

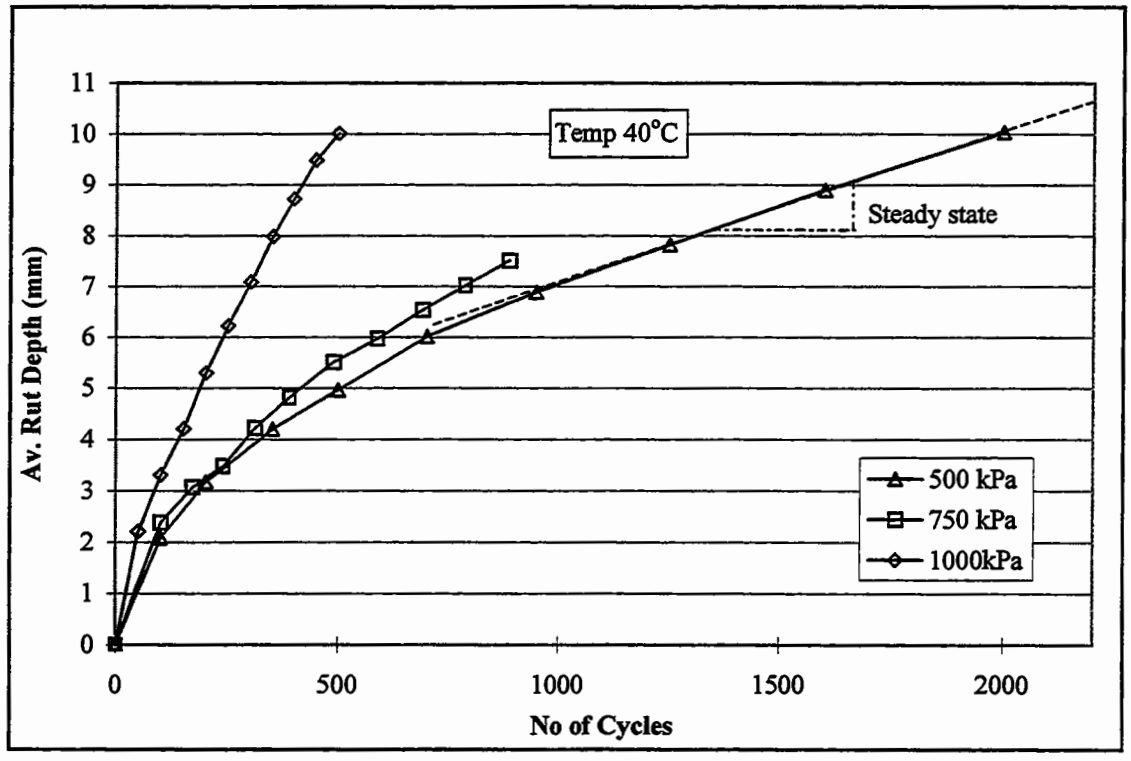

Figure 7.13 Wheel tracking tests at 40°C (Mixture A/D).

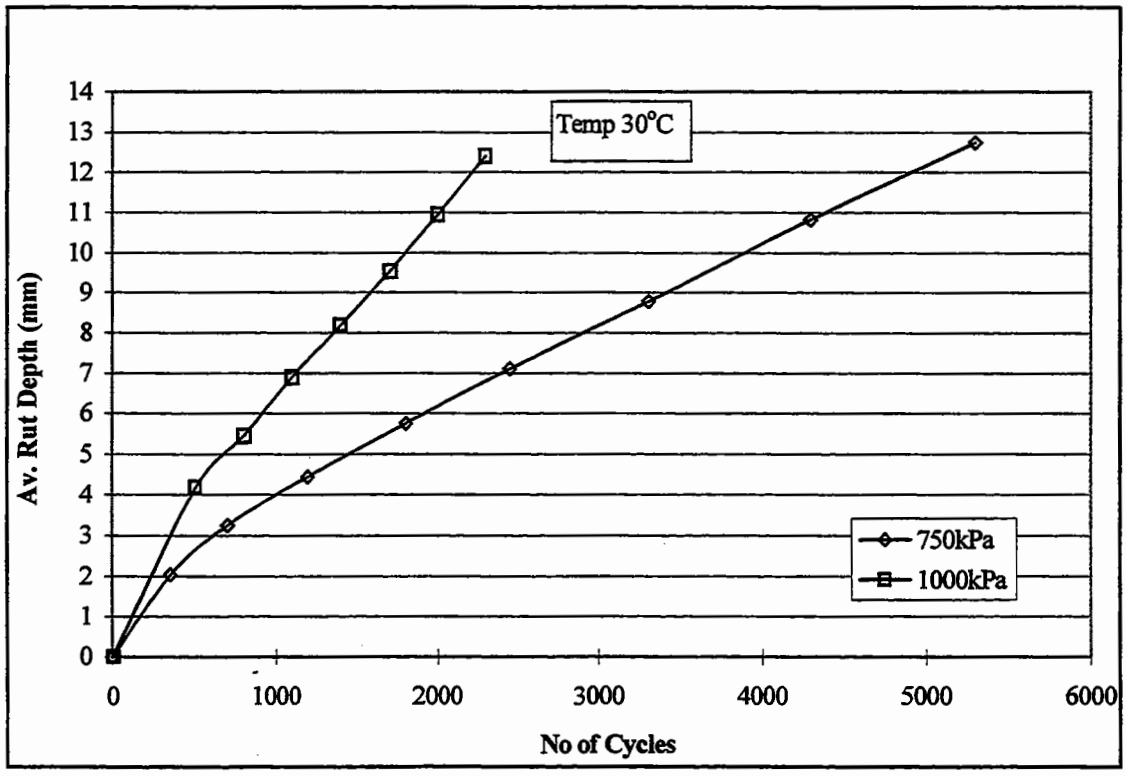

Figure 7.14 Wheel tracking tests at 30°C (Mixture A/D).

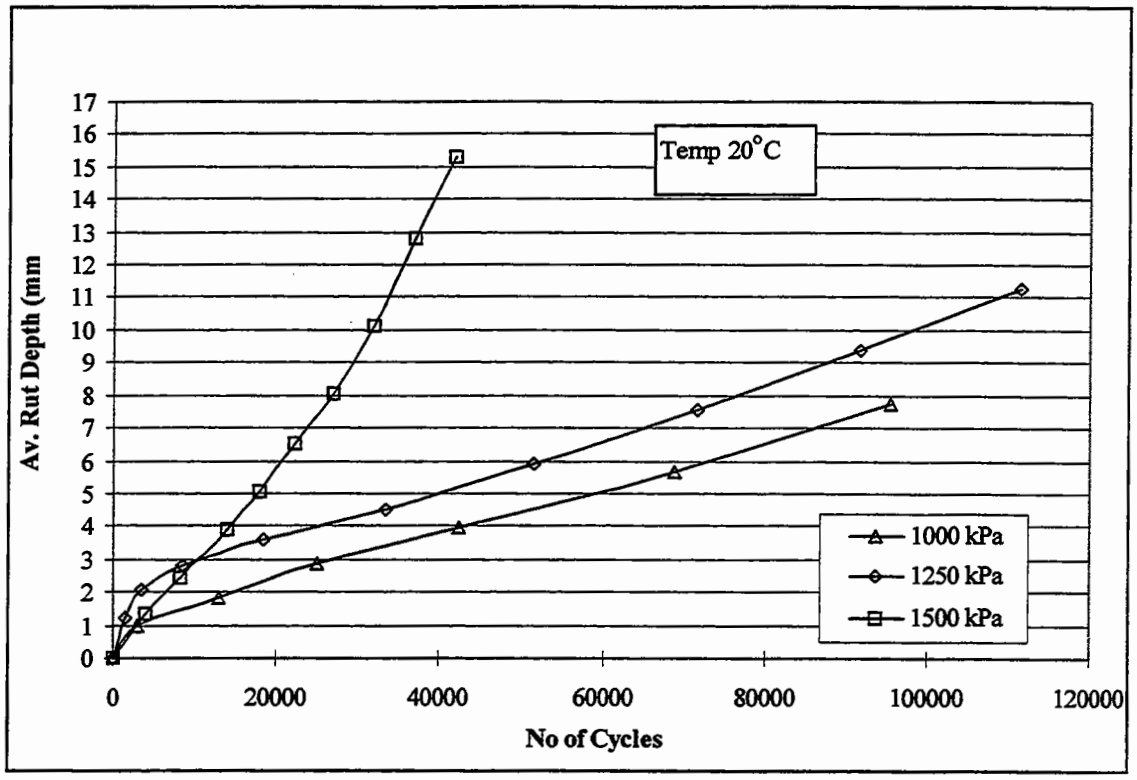

Figure 7.15 Wheel tracking tests at 20°C (Mixture A/D).

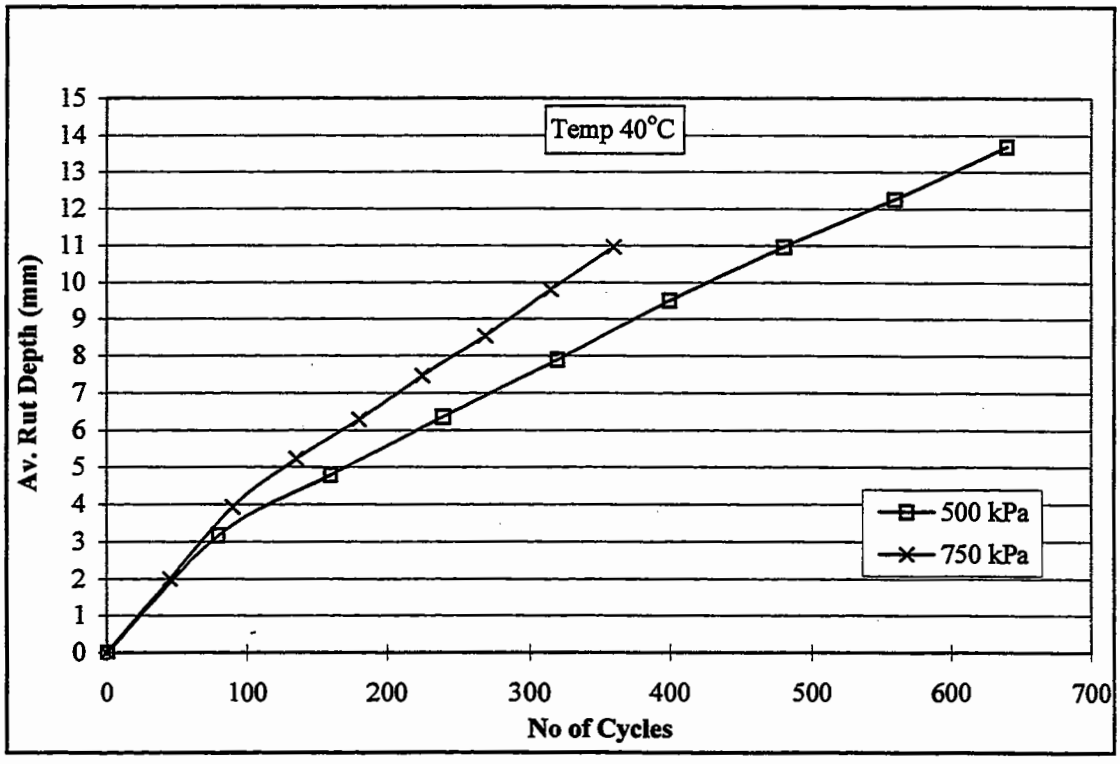

Figure 7.16 Wheel tracking tests at 40°C (Mixture A).

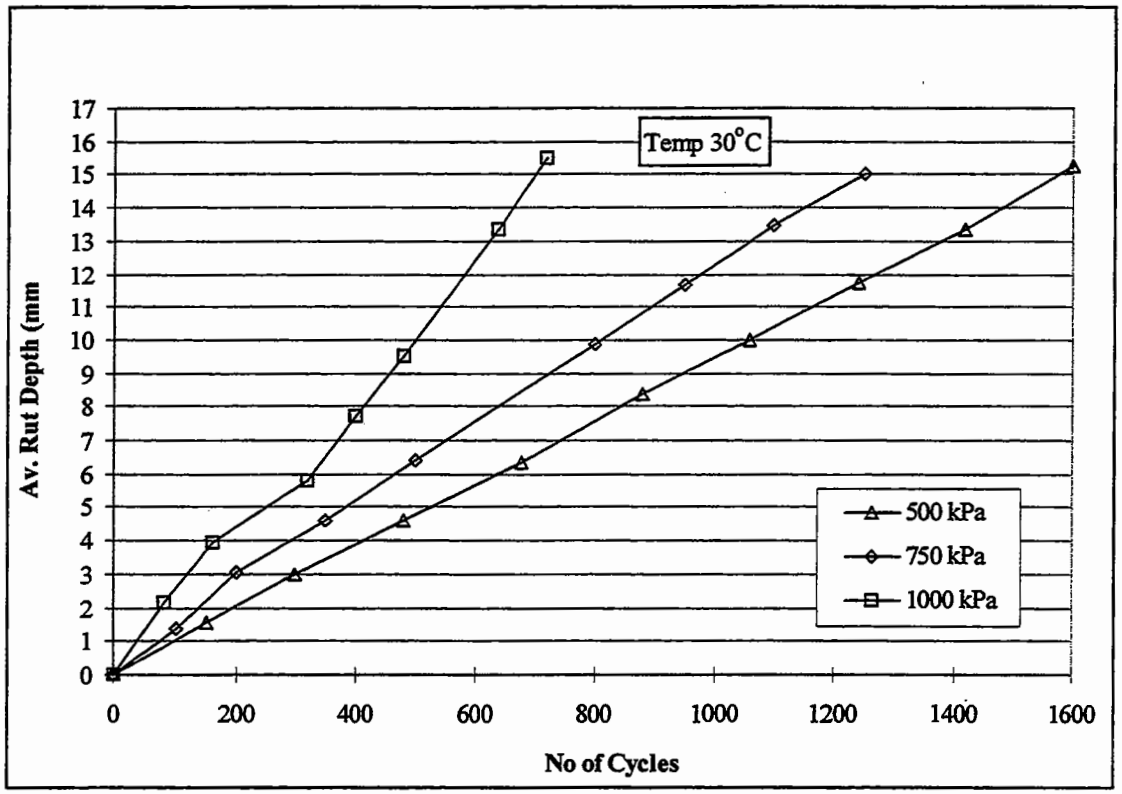

Figure 7.17 Wheel tracking tests at 30°C (Mixture A).

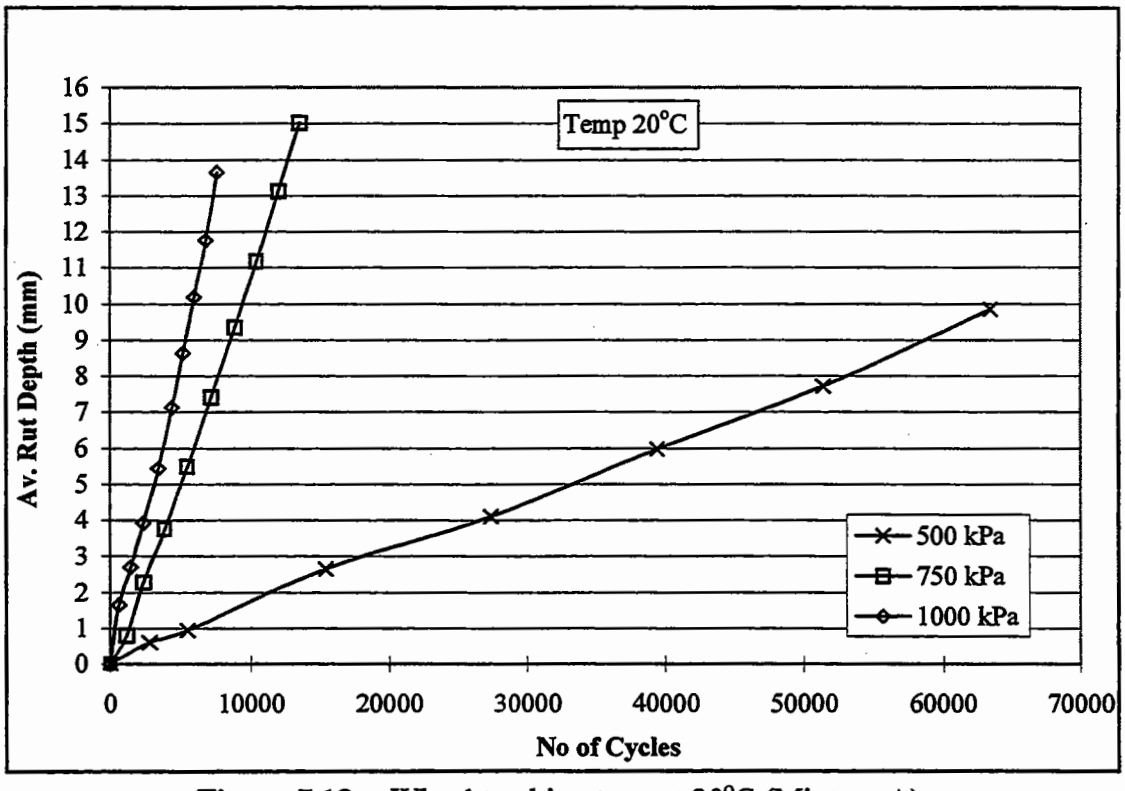

Figure 7.18 Wheel tracking tests at 20°C (Mixture A).

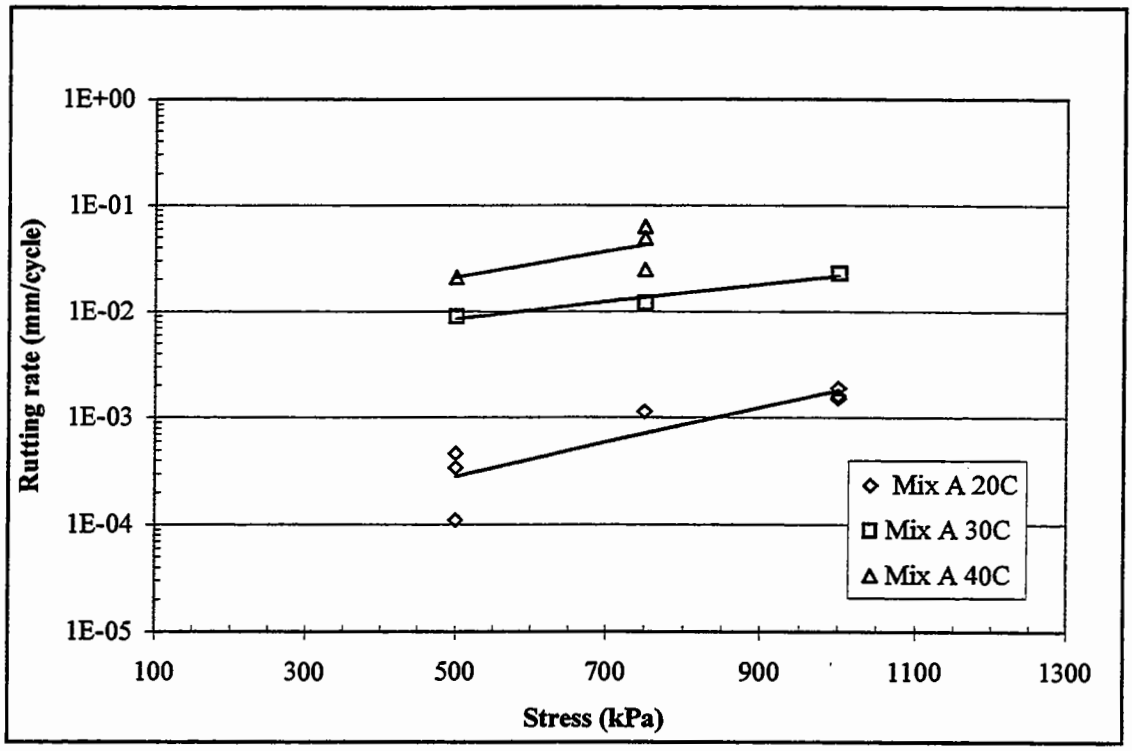

Figure 7.19 Steady-state rutting rates for mixture A.

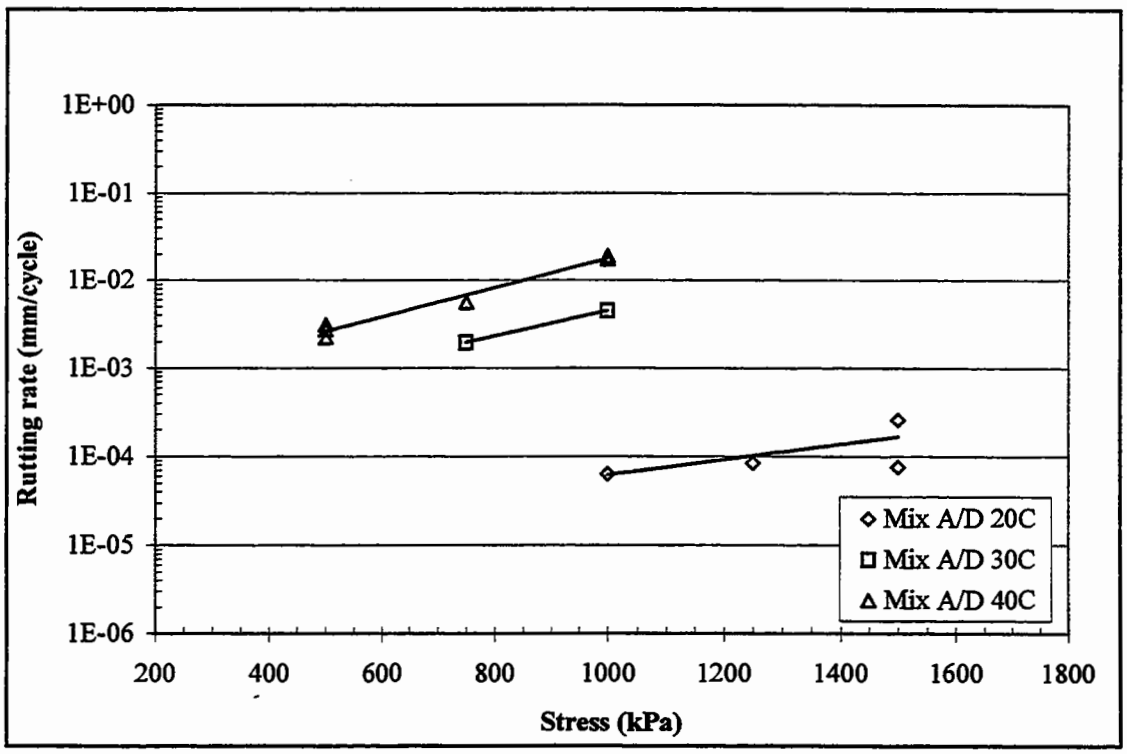

Figure 7.20 Steady-state rutting rates for mixture A/D.

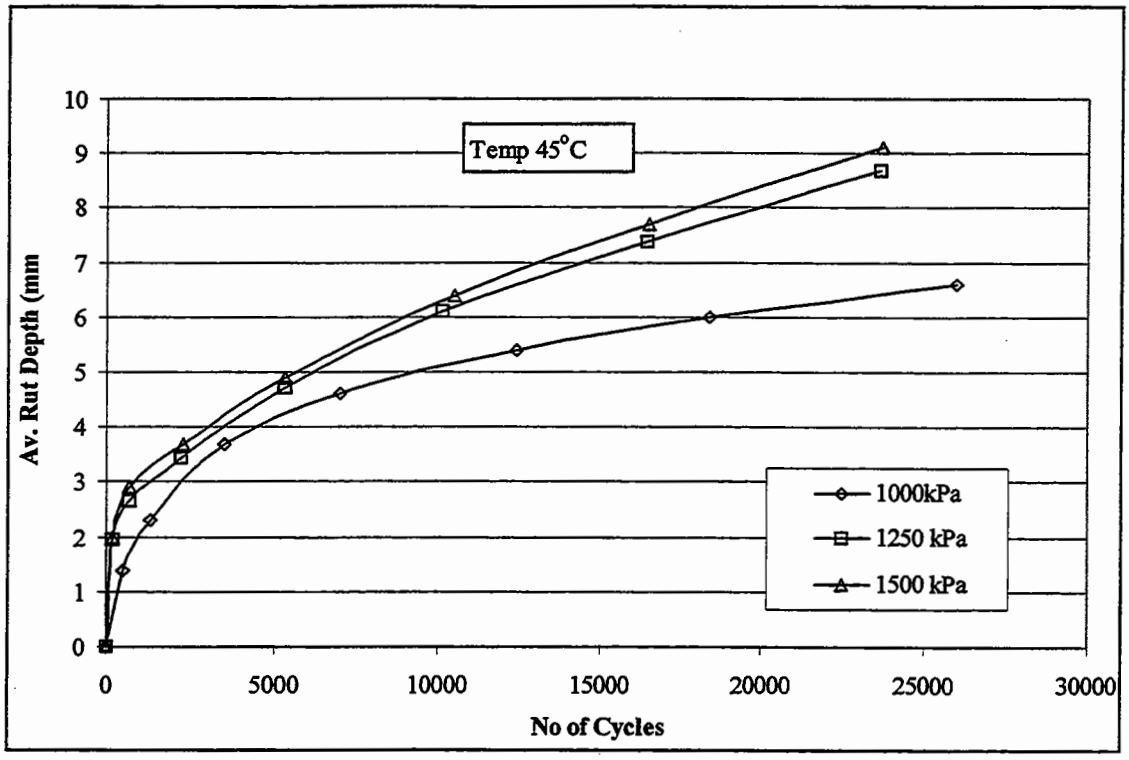

Figure 7.21 Wheel tracking test at 45°C (30/10 HRA mixture).

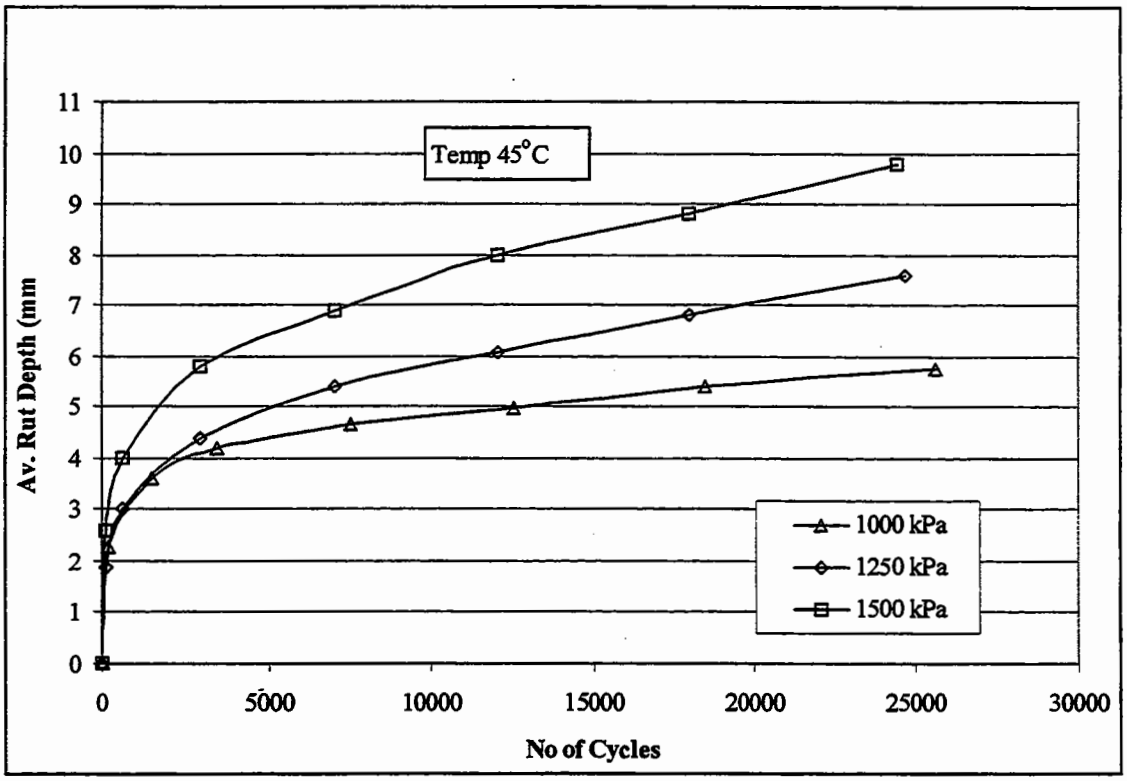

Figure 7.22 Wheel tracking test at 45°C (10 mm DBM mixture).

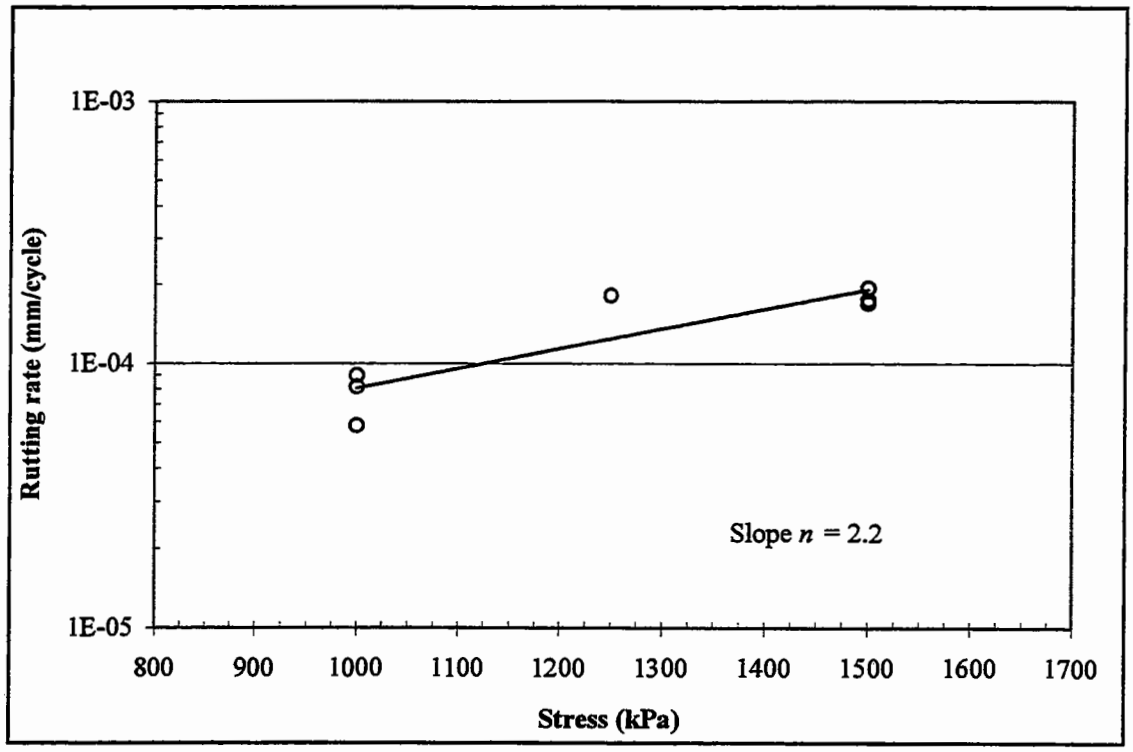

Figure 7.23 Steady-state rutting rates for 30/10 HRA mixture.

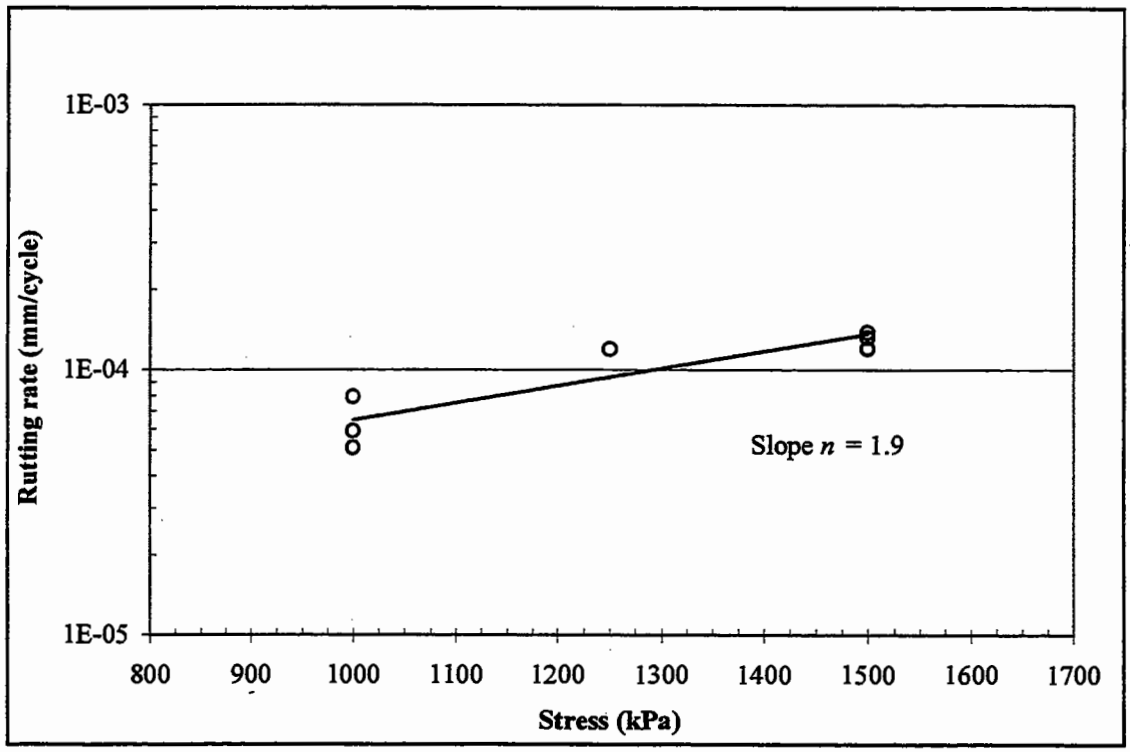

Figure 7.24 Steady-state rutting rates for 10 mm DBM mixture.

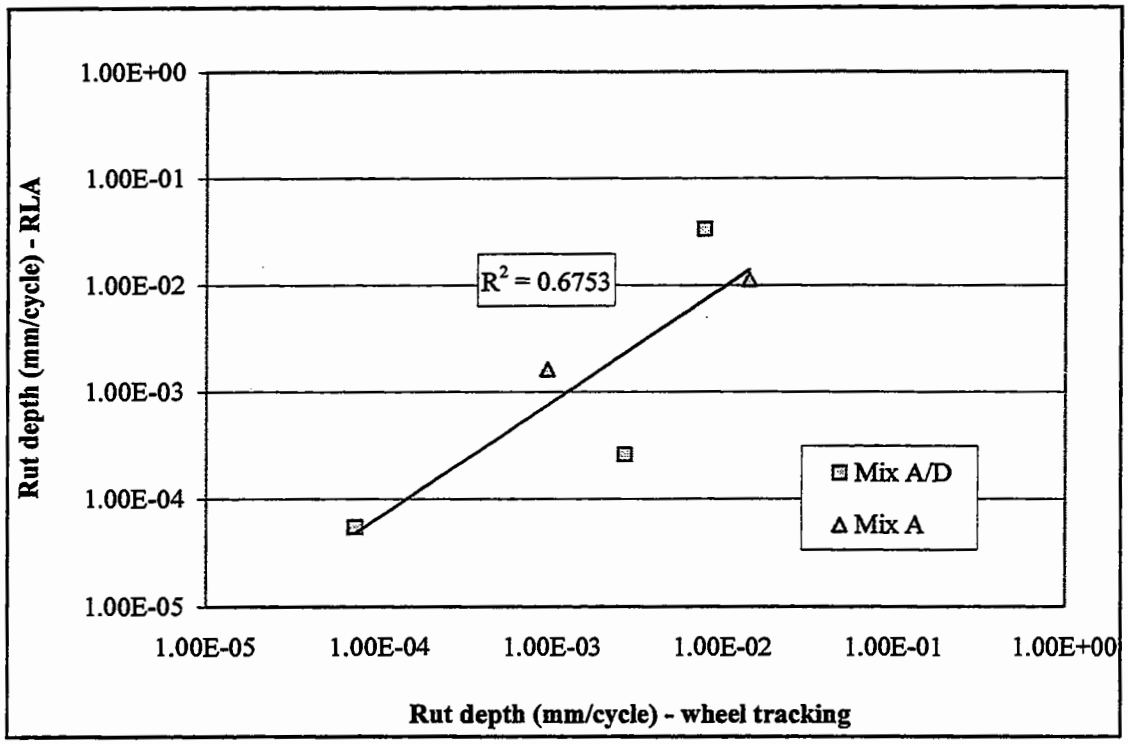

Figure 7.25 Comparison of steady-state rutting rates from the Wheel tracking and RLA tests.

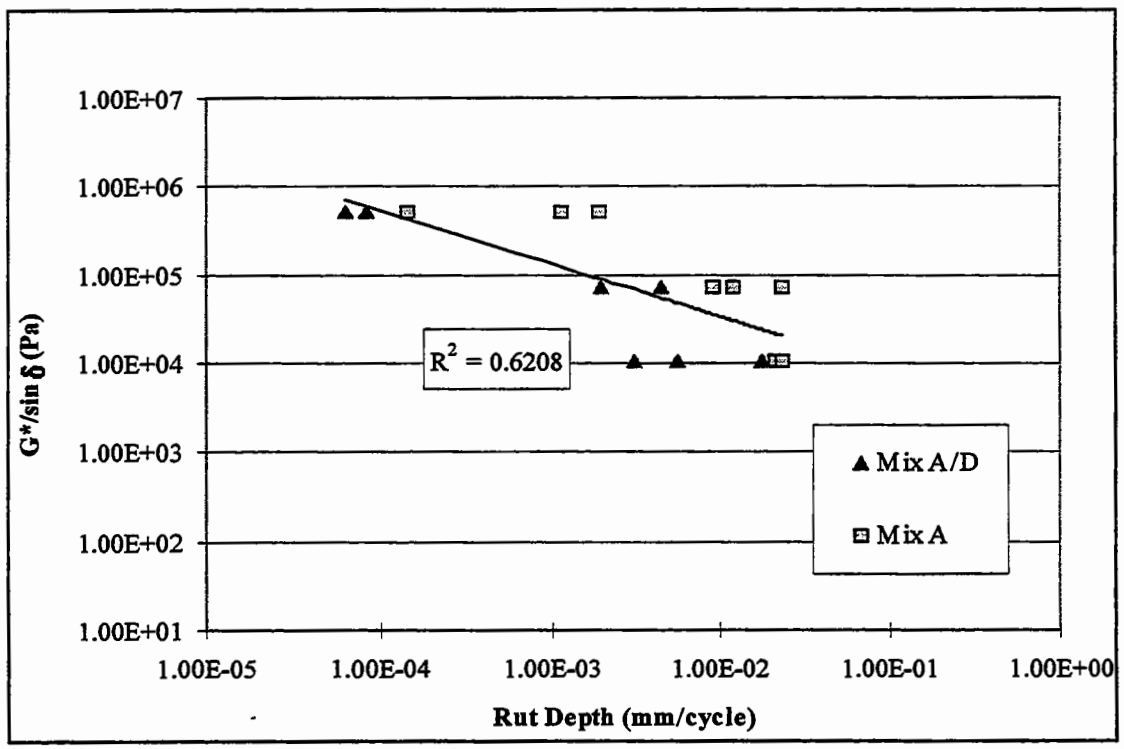

Figure 7.26 Comparison of steady-state rutting rate with G*/sin δ (wheel tracking tests).

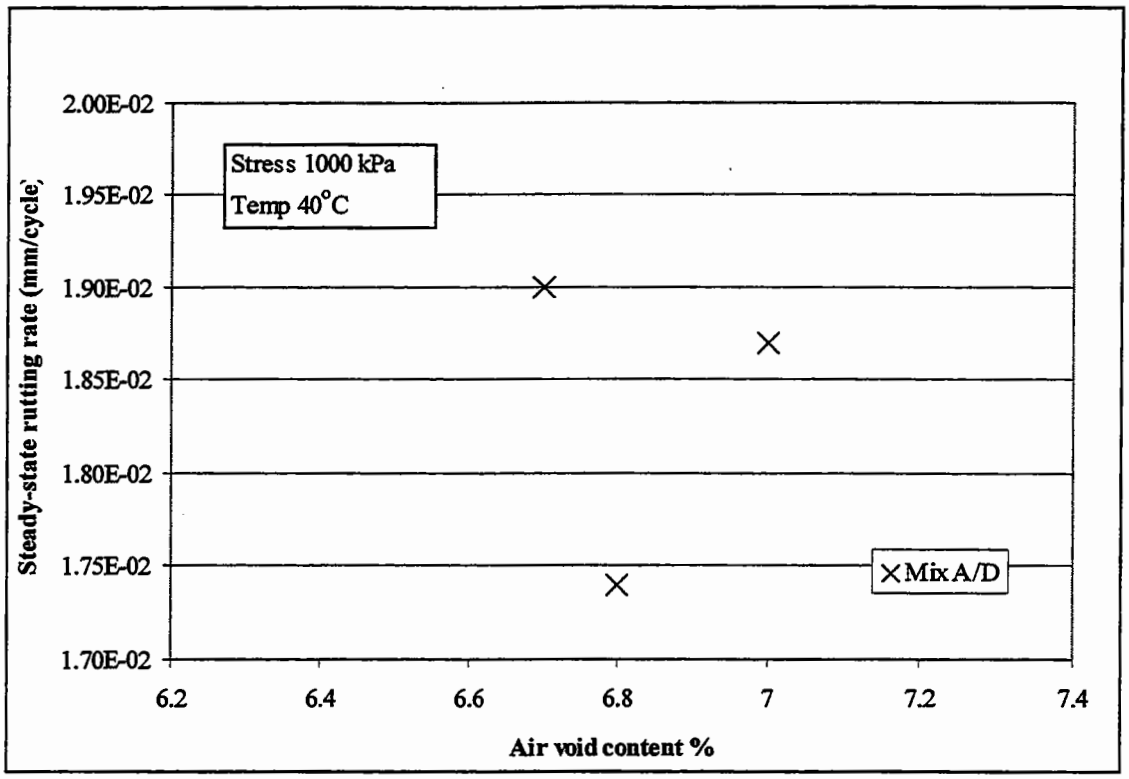

Figure 7.27 Effect of void content on steady-state rutting rate (mixture A/D).

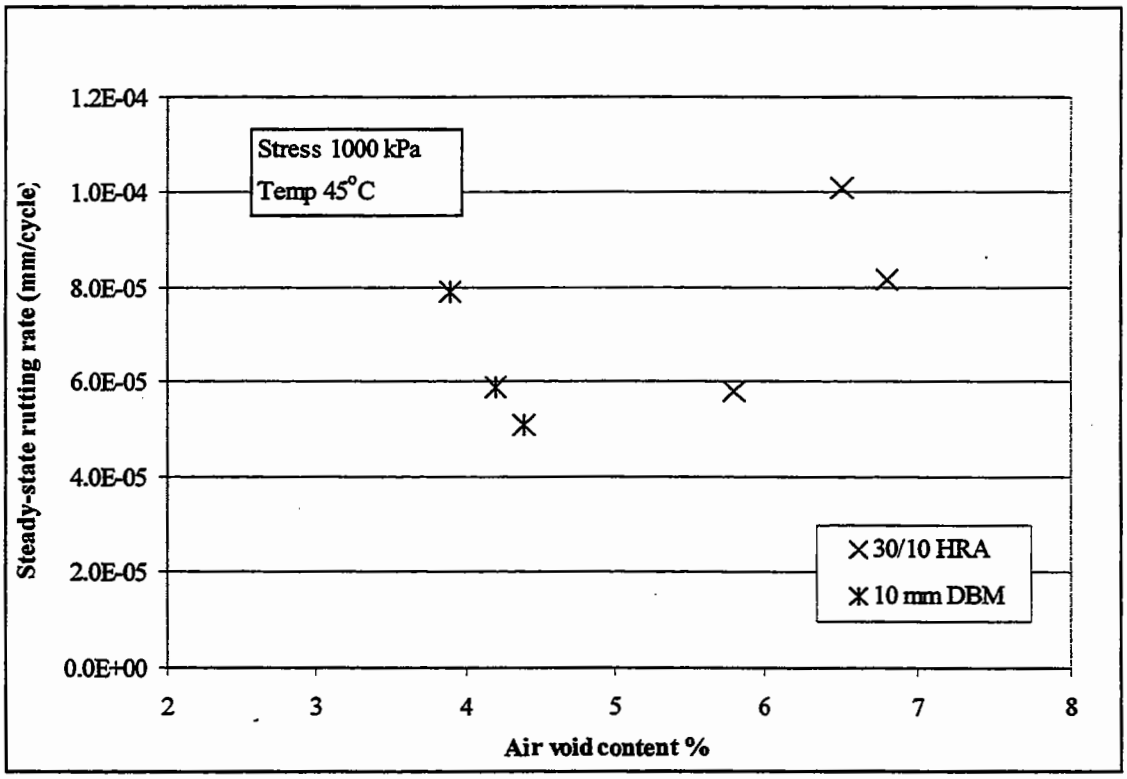

Figure 7.28 Effect of void content on steady-state rutting rate (HRA and DBM mixtures).

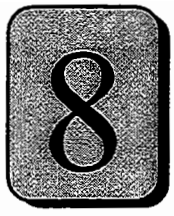

A Visco-Elastic Model for Rutting in Asphaltic Mixtures

8.1 Introduction

Research described in the preceeding chapters has indicated that the behaviour of the mixtures tested is largely controlled by the viscous deformation behaviour of the bitumen over a large range of temperatures, stress levels and strain rates. Results from the wheel tracking tests (Chapter 7) have shown that permanent deformation in the idealised and realistic mixtures is, in general, non-linear. This chapter introduces a method based on the theory of linear viscoelasticity which is used to simulate the measured non-linear deformation in the wheel tracking test using data from the uniaxial and triaxial testing. The model is verified by comparison with measured results from the wheel tracking tests.

8.2 Theoretical Rutting Model Formulation

It can be seen from the literature review presented in Chapter 2 that the two most common methodologies used to predict rutting in flexible pavements are the 'layer-strain' approach and approaches based on viscoelastic theory. Methods using the layer-strain approach account for rutting in all the pavements layers by assuming either a linear or non-linear relationship between the elastic stress field and the vertical permanent deformation in each layer. The permanent deformation characteristics of the various pavement materials are determined usually through

triaxial testing [27, 69, 98]. This method assumes that permanent deformation is only dependent on the elastic material properties and is independent of the material viscosity. Although, the 'layer-strain' approach can account for permanent deformation in each pavement layer, it cannot model the characteristic longitudinal ridge formed adjacent to the wheel path (see Chapter 2).

Viscoelastic based rutting models directly incorporate time-dependent response and moving wheel loads. This type of model assumes that ruts form primarily by shear flow of the pavement materials and can account for the characteristic ridge formed adjacent to the wheel path (see Chapter 2). In this type of approach permanent deformation is assumed to be dependent on the viscous properties of the asphalt and independent of the elastic properties. Typically, the viscoelastic properties of the asphalt are determined from confined or unconfined creep testing.

Over the years several researchers have investigated various applications of the use of 'linear viscoelastic' theories in material characterisation and rutting prediction of asphalt concrete pavements [16, 46, 60, 96, 97, 100, 102, 105, 110, 135]. The main disadvantage of this type of model is the assumption that asphalt behaves as a linear viscoelastic material. It can be seen from the results presented in Chapter 7 that the viscous behaviour of both the idealised and realistic bituminous mixtures is, in general, non-linear at higher stress levels. However, to implement the non-linear constitutive law (Equation 2.5) to calculate permanent deformation would require the use of a Finite Element (FE) program with special elements. This is beyond the scope of this research both in terms of the time required to develop special elements and since the aim was to develop a simplified approach towards modelling rut depth using a simple existing model, i.e. linear elastic layered model, and to try to incorporate the observed non-linearity in the permanent deformation process. Consequently, a simpler approximate method will be used based on a 'linearised' viscous analysis undertaken using the Elastic-Viscoelastic Correspondence Principle.

The Elastic-Viscoelastic Correspondence principle states that, for a linear viscoelastic material, the rates of permanent stress, strain and displacement can be calculated using elastic stress analysis, but with the elastic material parameters (Young's modulus and

Poisson's ratio) replaced by their viscous equivalents (further details can be found in [135]).

Previous research [46] has used this approach and shown that for a single moving static load, the permanent deformation at longitudinal position x is given by:

$$z(x) = \frac{F}{V} \int_{-x_o}^{x_o} I(y)\ dy \tag{8.1}$$

where
- $z(x)$ = permanent deformation at longitudinal position x
- V = speed of the applied static load
- $I(y)$ = rate of permanent deformation due to a unit static load applied at position x
- F = static applied force, and
- x_o = position where the permanent deformation influence function is negligible (i.e. $I(y) = 0$ for $|y| > x_o$)

It can be seen that the integral in Equation 8.1 is simply the area under the permanent deformation influence function $I(y)$. It can also be seen that permanent deformation calculated using Equation 8.1 will be proportional to the static load F (this is expected in a linear model), and inversely proportional to vehicle speed V.

According to Collop et al [46], this approach to pavement rutting has several beneficial features:

1. The distribution of permanent deformation through the layers is accounted for exactly, assuming that all the layers behave as linear visco-elastic materials.

2. The effects of vehicle speed (loading time) and dynamic loads, are accounted for exactly in the integration stage, and requires only one $I(y)$ influence function for each tyre type.

3. The effect of the pavement temperature on rut generation can be included in the analysis by using temperature sensitive viscosities, particularly for layers near the surface, where temperature can be higher.

The success of this type of model relies on the ability to determine the viscous material properties (the viscous equivalents to a Young's Modulus E, and Poisson's ratio, *v*) that need to be supplied to the elastic model. The following sections describe the procedure used to determine the viscous parameters based on results from the uniaxial and triaxial tests on the idealised and realistic mixtures presented in Chapters 4 and 5.

8.3 Determination of Asphalt Mixture Extensional Viscosity

8.3.1 Viscosity Model from Uniaxial and Triaxial Tests

It can be seen from Chapter 5 that the general triaxial steady-state strain rate versus stress curves can be used to calculate an equivalent extensional viscosity (λ_{eq}) which will be a function of stress (or strain rate) using the relationship:

$$\lambda_{eq} = \frac{\Sigma}{\dot{\varepsilon}} \tag{8.2}$$

where λ_{eq} = equivalent extensional viscosity

Σ = deviator stress

$\dot{\varepsilon}$ = uniaxial strain rate

A typical set of equivalent extensional viscosity curves plotted against deviator stress for mixture A is shown in Figure 8.1 plotted at different stress ratios. It should be noted that to show the temperature effect on viscosity (for example), data for a stress ratio of 0.3 at a temperature of 30°C is also plotted in addition to the data obtained at 20°C. Asymptotic curves in the linear and non-linear regions have also been plotted (solid lines). It can be seen from this figure that, at higher stress levels (>100kPa), the

equivalent viscosity is a function of temperature, deviator stress and stress ratio, whereas at lower stress levels (<100kPa) the equivalent viscosity is only a function of temperature and stress ratio. For simplicity the asymptotic values of viscosities have been used in the analysis with a transition stress of 100 kPa.

Previous research by Cheung [40] has shown that the steady-state deformation behaviour of bitumen above the glass transition temperature in shear is well correlated to the steady-state tensile deformation behaviour in terms of the Von Mises equivalent stress and strain rate. Consequently, since the steady-state deformation behaviour of both the idealised and realistic mixtures depend strongly on the steady-state deformation behaviour of the bitumen, and to apply the triaxial results to a three-dimensional analysis the deviator stress ($\sum$) in Equation 8.2 has been replaced by the Von Mises equivalent stress[1] (σ_e), defined as:

$$\sigma_e = \left((3/2)\times((\sigma_x-\sigma_m)^2+(\sigma_z-\sigma_m)^2+(\sigma_y-\sigma_m)^2+(2\tau_{xz})^2+(2\tau_{xy})^2+(2\tau_{yz})^2\right)^{\frac{1}{2}} \quad (8.3)$$

where $\sigma_x\ \sigma_y\ \sigma_z$ = components of stress in x, y and z direction

σ_m = mean stress $(\sigma_m = \frac{\sigma_x + \sigma_y + \sigma_z}{3})$

$\tau_{xz}\ \tau_{xy}\ \tau_{yz}$ = shear stress components in xz, xy and yz direction

To predict viscosities at different stress ratios, stress levels and temperatures, viscosity asymptotes have been fitted in the linear and non-linear regions (see Figure 8.1) of the form:

$$\log_{10}(\lambda_{eq}) = A + B(\eta) \quad \text{(linear region < 100kPa)} \quad (8.4)$$

$$\log_{10}(\lambda_{eq}) = A + B\log_{10}(\sigma_e) + C(\eta) \quad (8.5)$$

(non-linear region >100kPa)

[1] The Von Mises equivalent stress is equivalent to the deviator stress for triaxial conditions.

where λ_{eq} = equivalent viscosity

σ_e = Von Mises equivalent stress

η = stress ratio

A, B, and C = constants that depend on temperature for each mixture

Values for the constants A, B, and C are given in Table 8.1. It can be seen from Equations 8.4 and 8.5 that, provided the stress ratio and the Von Mises equivalent stress can be determined and the temperature is known, an equivalent extensional viscosity λ_{eq} can be calculated. The method used to calculate these quantities for the wheel tracking test slabs is explained in the following sub-sections.

Table 8.1 Viscosity Constants for Equations 8.4 & 8.5.

Mix	Temp (°C)	Linear region		Non-linear region		
		A	B	A	B	C
A	20	9.424	1.832	16.574	-1.366	1.835
	30	8.705	1.859	15.670	-1.391	1.830
	40	7.826	1.734	14.639	-1.368	1.830
A/D	20	10.405	2.410	17.421	-1.396	2.362
	30	9.321	2.353	16.246	-1.382	2.359
	40	8.465	2.356	15.413	-1.389	2.369
30/10 HRA	45	7.089	10.393	13.982	-1.376	10.369
10 mm DBM	45	7.421	7.682	14.376	-1.384	7.662

8.3.2 Calculation of Stress Ratio and Von Mises Equivalent Stress in Wheel Tracking Test

To calculate the Von Mises equivalent stress and the stress ratios in the wheel tracking slabs an axi-symmetric semi-infinite layered linear elastic model has been used. By using linear elastic analysis rather than using the non-linear constitutive law (Equation 2.5), the compatibility of displacement fields is ignored although the resulting stress field satisfies equilibrium (this is effectively an upper bound type of approach). The upper layer was modelled as a bituminous material of thickness 100 mm (thickness of

the slab) with a Poisson's ratio of 0.35 which is typical for bituminous material [114]. Because the layered elastic model used was infinite in vertical extent, the lower layer (of infinite thickness) was assigned an infinite stiffness modulus[2] to represent the rigid boundary conditions at the base of the slabs. Because the ratio of the stiffness modulus of the lower layer to the stiffness modulus of the upper layer is effectively infinite, the resulting stresses (and strains and displacements) do not depend on the value of stiffness modulus assigned to the upper layer. Consequently, a nominal value of 1000 MPa was used in the analysis. The computer program BISAR 3 was used to perform the calculations [126, 141].

Figures 8.2 and 8.3 show the resulting contours of Von Mises equivalent stress and mean stress for an applied stress of 1000 kPa as a function of depth 'z' beneath the surface of the slab and horizontal distance 'x' from the wheel load. The contact width of the tyre was taken to be 0.025 m (25 mm). It can be seen from Figure 8.2 that the Von Mises equivalent stress tends to reach a maximum value at a depth of approximately one contact radius below the surface under the loaded area. Since the Von Mises equivalent stress is a measure of the shear stress, the maximum deformation would be expected to occur in this region. It can be seen from Figure 8.3 that, the highest value of mean stress occurs directly under the contact area (it should be noted that the mean stress is compressive). This is the expected result since in this location the vertical stress (contact pressure) is highest. The stress ratio, which is the ratio of mean stress divided by the Von Mises equivalent stress, can also be evaluated at different depths in the bituminous layer. Figure 8.4 shows contours of constant stress ratio plotted as a function of depth 'z' and horizontal distance 'x' from the wheel load. Note that as the mean stress is compressive and the stress ratio is negative, hence absolute values of stress ratio have been plotted. These figures, together with Figure 8.1, can now be used to determine contours of equivalent extensional viscosity in the wheel tracking slabs.

[2] In the model an infinite value is not possible so a high value of elastic stiffness (1E+19MPa) was taken for the rigid layer.

8.3.3 Predicted Viscosities

Figure 8.5 shows the contours of equivalent viscosity for mixture A at an applied stress level of 1000 kPa and a temperature of 20°C plotted as a function of depth 'z' and horizontal distance 'x' from the wheel load. It can be seen from this figure that, as expected, the viscosity is not constant due to the variations in stress ratios and Von Mises equivalent stresses. It can also be seen from this figure that the viscosities are lowest in a semi circular zone from the edge of the contact area (x = 0.025 m) to a depth of about 40 mm.

8.4 Linearisation Approach

For a viscous analysis using the Elastic-Viscoelastic Correspondence Principle constant values are required for the viscosity of each layer. Consequently, the bituminous slab was divided into a number of sub-layers where the viscosity was taken to be constant. It can be seen from Figure 8.5 that the effective viscosity varies as a function of horizontal distance from the load (x) as well as depth beneath the surface of the slab (z). This is illustrated in Figure 8.6 where the effective extensional viscosity is plotted as a function of horizontal distance from the load at different depths below the surface of the slab. It can be seen from this figure that, due to the high stress ratios directly beneath the wheel (see Figures 8.4 and 8.7), the resulting viscosities become very high towards the surface of the slab (it should be noted that the curves shown in Figure 8.6 start at a depth of z = 0.02m). It can be seen from Figure 8.5 that the viscosity nearer to the surface is significantly higher. However, it can also be seen from this figure that from the edge of the contact area (x = 0.025 m) there is a reduction in viscosity as the stress ratio decreases (see Figure 8.5). It is not possible to include this horizontal variation in viscosity in the modelling approach because the model assumes that the layers, which are infinite in horizontal extent, have constant properties. Consequently, a methodology is required to choose a representative viscosity for each sub-layer. To correctly calculate the permanent deformation directly under the contact area (where the majority will occur) the value of the viscosity that should be used is the one under the tyre. However, since the model used is of infinite extent horizontally, this will mean that near to the surface the

lower viscosities outside the loaded region will be significantly higher than they should be. This, in turn, will broaden the calculated rut profile due to the presence of an artificially high viscosity in the zone where upheaval of material is expected at the surface near to the edge of the tyre. This is illustrated in Figure 8.8 where a high value for the viscosity has been used directly under the tyre. It can be seen from this figure that the shoulder of predicted rut is well away from the edge of the tyre compared to the measured rut (see Figure 7.6). Consequently, only the steady-state rutting rates of the depression directly under the wheel were modelled. It should be noted that a simplified linear elastic Finite Element (FE) approach could be used instead of the layered elastic model to allow the properties to vary laterally as well as vertically in the rutting model. However, this adds an extra layer of complexity to the calculation procedure and would mean that readily available standard layered elastic pavement models could not be utilised.

Viscosity versus depth profiles were plotted for particular values of x (0 to 0.025m which corresponds to the contact width of the tyre) are shown in Figure 8.9. Because of the variation of viscosity with depth (discussed above) it was necessary to sub-divide the bituminous layer into sub-layers at different depths where the viscosity was assumed to be constant. A number of different options were investigated and it was found that a satisfactory trade-off between the number of layers required and convergence of the results was achieved when the bituminous layer was divided into four sub-layers as shown in Figure 8.10. Each sub-layer was assigned an average value of equivalent viscosity derived from the viscosity depth profiles. It should be noted that based on this particular simplified approach using a layered elastic model the sub-division of layers will depend on the stress ratios, particularly those at the surface directly beneath the wheel. For the wheel tracking test geometry the method used to calculate the stress ratios does not depend on the stiffness modulus of the asphaltic material so the sub-division technique should work for other types of bituminous materials. However, it should be noted that the stress ratio calculation does depend on the value of Poisson's ratio assumed for the bituminous material. Consequently, different sub-layer divisions may be required for bituminous materials with a different Poisson's ratio from that assumed in the analysis (0.35).

8.5 Calculation of Rutting Influence Function

A standard layered elastic pavement model was used to generate the deformation-rate influence function $I(y)$ required by the Equation 8.1. The contact width of the tyre was taken to be 25 mm (0.025 m) and the velocity V of the tyre was calculated to be 0.153m/s (0.55km/hr) in the central region (100mm) of travel. In order to calculate the deformation rate influence function, the model was supplied with the viscous equivalents of Young's modulus E, and Poisson's ratio v. For both the idealised and realistic mixtures the bituminous layer was divided into four sub-layers (described earlier). The viscosities for sub-layers for each mixture at the corresponding test temperature were determined from the procedure described above and Poisson's ratio was taken to be 0.5 indicating that permanent deformation is due to the shear flow only, without any volume change. The value of the viscous equivalent to Poisson's ratio of 0.5 was used because this is the simplest situation where the viscous deformation occurs at constant volume. In reality the experiments have shown this not to be the case (there is dilation of the material) but it should be noted that the effect of confinement on the deformation process is accounted for correctly. The viscosity assigned to the rigid layer was effectively infinite (1E+19 MPa.s) thus restricting all the viscous permanent deformation to the bituminous sub-layers.

8.6 Rut Depth Predictions

8.6.1 Idealised Mixtures (mixtures A and A/D)

Because of the very high stress ratios directly under the load near to the surface (Figure 8.7), the resulting viscosities are also very high (Figure 8.6). It was found that if this thin layer of high viscosity material was included in the model, the predicted rutting rates were unrealistically low probably due to the presence of this artificially high viscosity material at the edge of the contact area where upheaval is expected. Consequently, the top 5 mm of the material was not included in the analysis and hence a 95 mm thick bituminous layer was modelled. Physically, this can be interpreted as having a small volume of material due to the surface of the slab (under the wheel) that does not deform viscously due to the high stress ratios and consequent viscosities.

Unfortunately, because of the nature of the model used to represent the slab in the wheel tracking test it is not possible to include this effectively rigid material directly under the tyre (not away from the tyre) with any degree of accuracy.

Figures 8.11 to 8.13 show the predicted and measured steady state rutting rates for mixture A at temperatures of 20°C, 30°C and 40°C respectively, plotted as a function of the applied stress. The thickness of the sub-layers for both mixtures A and A/D was kept the same. The error bars shown in Figures 8.11 and 8.13 represent the variation in the steady state rutting rates from the three replicate tests performed at two extremes of the stress level and temperature. It can be seen from these figures, that the predicted steady state rutting rates agree reasonably well with the measured steady state rutting rates at the corresponding stress levels and at all the three test temperatures. The corresponding predicted and measured steady state rutting rates for mixture A/D are shown in Figures 8.14 to 8.16 at temperatures of 20°C, 30°C and 40°C respectively, plotted as a function of the applied stress on linear axes. It can also be seen from these figures that the agreement between the predicted and measured steady state rutting rates is often within a reasonable range bearing in mind the simplified nature of the approach. However, it should be noted that the error in rutting rate could in some cases produce a reasonably large difference in final rut depth (see also discussion) and that the prediction approach therefore needs to be used with caution.

As discussed in Chapter 7, the permanent deformation behaviour of the idealised mixtures in the wheel tracking test has been characterised by an effective creep exponent of n = 1.9 to 2.4. In order to quantify the predicted rutting rates in terms of an effective creep exponent, the same technique as described in Chapter 7 was used to determine the value of n that best fits the predicted data from all temperatures for each mixture. A summary of the measured and predicted rutting rates is given in Table 8.2. It can be seen from this table that the values of n for the predicted rutting rates are in the range of 2.2 and 2.4 for both the mixture A and A/D respectively and are similar to those for the measured rutting rates although a linear model is used in the calculation procedure. It can therefore be seen from this that the current approach to predicting rutting is capable of reproducing the non-linear effects observed from the wheel

tracking tests. (To evaluate the fit for the predicted rutting rates the Coefficient of Variation (COV) is also given in Table 8.2).

Table 8.2 Measured and Predicted Steady-State Rutting Rate Data Analysis (Idealised Mixtures)

Mix	Temp (°C)	Stress (kPa)	Rutting Rate (Measured) (mm/cycle)	*n* (COV)	Rutting Rate (Predicted) (mm/cycle)	*n* (COV)
A	20	500	6.88E-05	1.9 (9.4%)	2.40E-04	2.2 (12.1%)
			2.12E-04			
			2.73E-04			
		750	6.46E-04		5.70E-04	
		1000	1.20E-03		1.10E-03	
			1.16E-03			
			1.11E-03			
	30	500	5.00E-03		2.60E-03	
		750	7.00E-03		6.30E-03	
		1000	9.03E-03		1.20E-02	
	40	500	1.44E-02		2.00E-02	
		750	4.12E-02		4.70E-02	
			3.25E-02			
			1.60E-02			
A/D	20	1000	5.10E-05	2.4 (10%)	7.80E-05	2.4 (8%)
			6.00E-05			
			4.20E-05			
		1250	7.70E-05		1.70E-04	
		1500	6.00E-05		2.60E-04	
			1.50E-04			
			1.70E-04			
	30	750	6.20E-04		6.60E-04	
		1000	2.60E-03		1.30E-03	
	40	500	1.50E-03		2.10E-03	
			1.90E-03			
			2.12E-03			
		750	4.14E-03		4.90E-03	
		1000	1.12E-02		9.30E-03	
			8.00E-03			
			1.00E-02			

8.6.2 Realistic mixtures (HRA and DBM)

It can be seen from the steady-state strain rate versus stress curves in Chapter 5 that, as expected, both the HRA and the DBM mixtures are significantly stiffer than mixture A and A/D at corresponding stress ratios. These curves re-plotted as a function of equivalent viscosity versus stress, result in higher values of equivalent viscosity. It was found in the analysis that the predicted rutting rates were too low if only the top 5 mm of the layer was ignored. Consequently, to better match the predictions to the measurements, the top 10 mm of the material was not included in the model. It should be noted that, although this will change the absolute value of the predicted rut, it is not expected to significantly alter the sensitivity of the predicted rut to the level of applied load (i.e. the degree of non-linearity). As before, for both the HRA and the DBM, the bituminous layer was divided into four sub-layers at different depths. The thickness of each sub-layer was kept the same for the two mixtures. The measured and the predicted steady state rutting rates for the HRA and DBM mixtures are shown in Figures 8.17 and 8.18 respectively, plotted as a function of applied stress. It can be seen from Figures 8.17 and 8.18 that the agreement between the predicted and measured steady state rutting rates is generally good for the DBM mixture (Figure 8.18). However, for the HRA mixture (Figure 8.17) it can be seen that predicted rutting rates are significantly lower than the measured rutting rates which would result in significant differences in the final rut depths. The exact reason for this is not known but it should be noted that the prediction is sensitive to the above assumption of the 5 or 10mm surface layer not included in the calculation. This requires further investigation (see also discussion).

To quantify the predicted steady state rutting rates in terms of an effective creep exponent the same technique described above for the idealised mixtures was used. The measured and the predicted steady state rutting rates are given in Table 8.3. Also given in the table are the values of an effective creep exponent n for both the HRA and the DBM mixture for the predicted steady state rutting rates. It can be seen from the values of n for both the mixtures that they fall in the range of 2 to 2.4 which is very similar to the measured wheel tracking results. To evaluate the fit to the predicted rutting rates the COV values are also given in Table 8.3. It should be noted that the

calculated value of n for the predicted rutting rate for the DBM mixture was found to be 2.4 which is higher than the measured value of 1.6. The reason for the lower value of n may be principally increased scatter due to the fact that the behaviour of this type of continuously graded mixture is influenced by inter-particle contact as well as shear deformation in the thin films of bitumen between particles. It should be noted that, as stated in Chapter 7, the scatter associated with the wheel tracking results for DBM is high.

Table 8.3 Measured and Predicted Steady-State Rutting Rate Data Analysis (Realistic Mixtures)

Mix	Temp (°C)	Stress (kPa)	Rutting Rate (Measured) (mm/cycle)	n (COV)	Rutting Rate (Predicted) (mm/cycle)	n (COV)
30/10 HRA	45	1000	5.26E-05	2 (3.5%)	1.20E-05	2.3 (3.7%)
			8.00E-05			
			3.55E-05			
		1250	8.33E-05		2.00E-05	
		1500	1.20E-04		3.00E-05	
			9.00E-05			
			8.69E-05			
10mm DBM	45	1000	4.80E-05	1.6 (3.3%)	5.30E-05	2.4 (4.6%)
			5.10E-05			
			7.00E-05			
		1250	9.00E-05		9.10E-05	
		1500	1.00E-04		1.40E-04	
			1.20E-04			
			9.00E-05			

8.7 Discussion

The measured uniaxial and triaxial properties have been used in a viscous model to predict the rutting measured from wheel tracking tests. A method has been presented for incorporating the observed non-linear behaviour of these materials in a linearised viscous approach for estimating rutting in bituminous mixtures based on the use of existing linear elastic layered models of a pavement structure supplied with viscous rather than elastic properties. The occurrence of high stress ratios near the surface

(directly under the wheel) leads to very high viscosities effectively limiting the viscous flow that can occur in that region. However, if an effectively rigid horizontally infinite layer is included in the analysis it artificially restricts the upward flow of material outside the loaded area where the stress ratios at the surface are much lower. Consequently, a thin layer at the surface of the pavement has not been included in the analysis. To implement the full non-linear constitutive model would have required purpose written Finite Elements which was far beyond the scope of this project. However, the degree of non-linearity has been correctly accounted for showing that this simple linearised approach is reproducing this important feature. As with every other rutting model a calibration factor may be required but the initial results seem to be promising and are based on a simplified physical model of the deformation process (i.e. viscous flow).

8.8 Conclusions

The following conclusions can be drawn from this chapter:

- A method for estimating the rutting behaviour of bituminous mixtures has been presented. The calculation uses existing linear elastic layered models of a pavement supplied with viscous rather than elastic properties.

- The method uses non-linear material properties determined from the uniaxial and triaxial testing.

- The predicted rutting rates are based on a previously developed model which predicts that permanent deformation per wheel pass in bituminous mixtures is proportional to the static axle load and inversely proportional to vehicle speed.

- A method has been presented for predicting asphalt mixture viscosity from the uniaxial and triaxial test results.

- Most of the predicted and the measured rutting rates for both the idealised and realistic mixtures showed reasonable agreement over a range of stress levels and temperatures bearing in mind the simplified nature of the approach.

- The predicted rutting rates have been characterised by an effective creep exponent of n = 2.2 to 2.4 for both the idealised and realistic mixtures. This range agrees well with the creep exponents from the measured rutting data.

- The predicted creep exponent n = 2.2 to 2.4, shows that the model has the ability to predict the non-linear permanent deformation behaviour of bituminous mixtures.

8.9 Figures

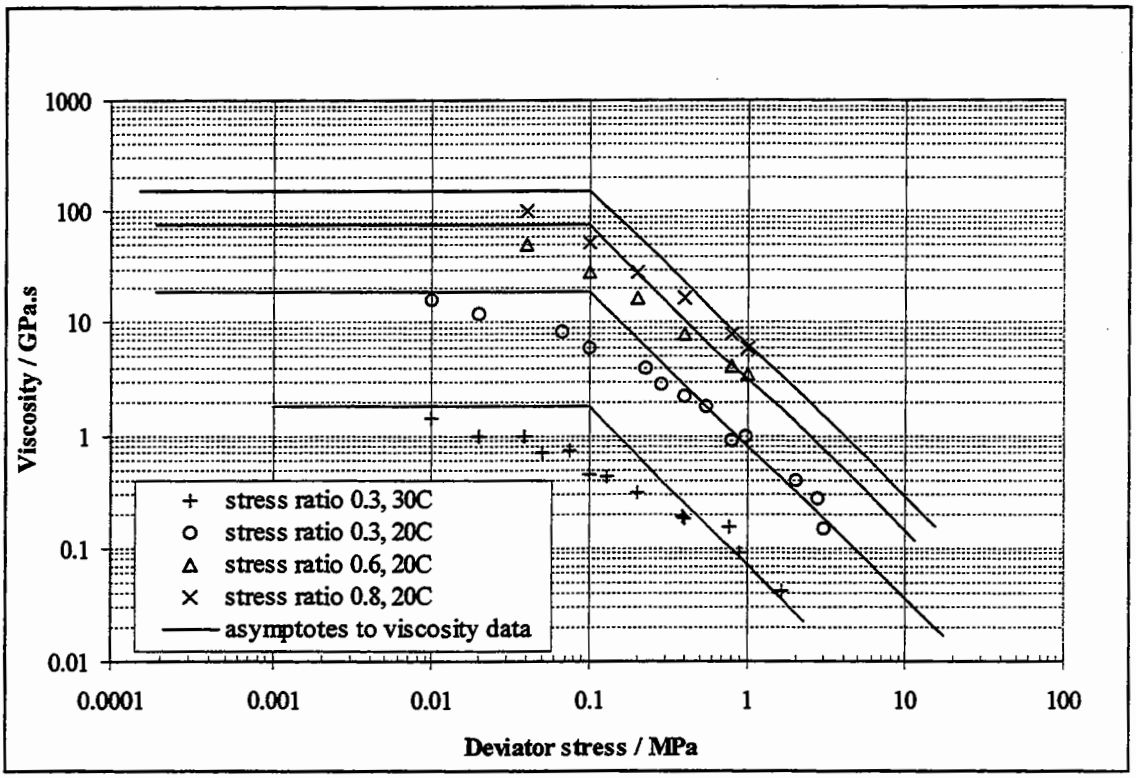

Figure 8.1 Viscosity asymptote at various stress ratios (mixture A at 20°C).

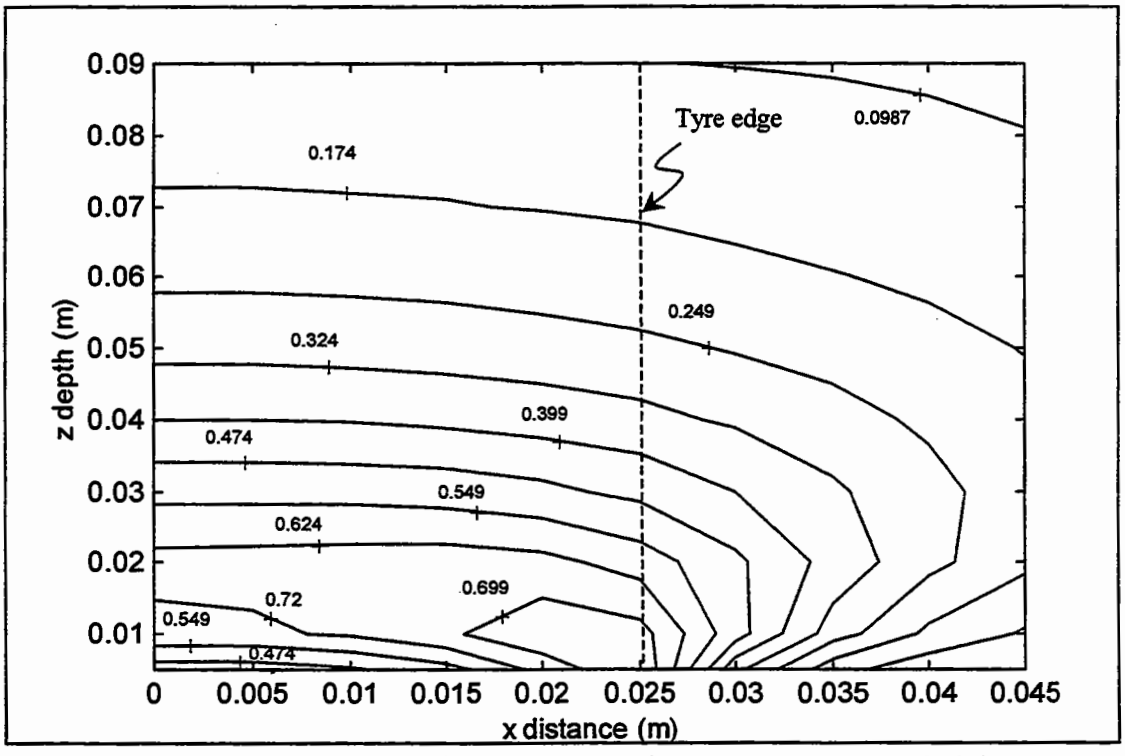

Figure 8.2 Contours of Von Mises equivalent stress (values in MPa).

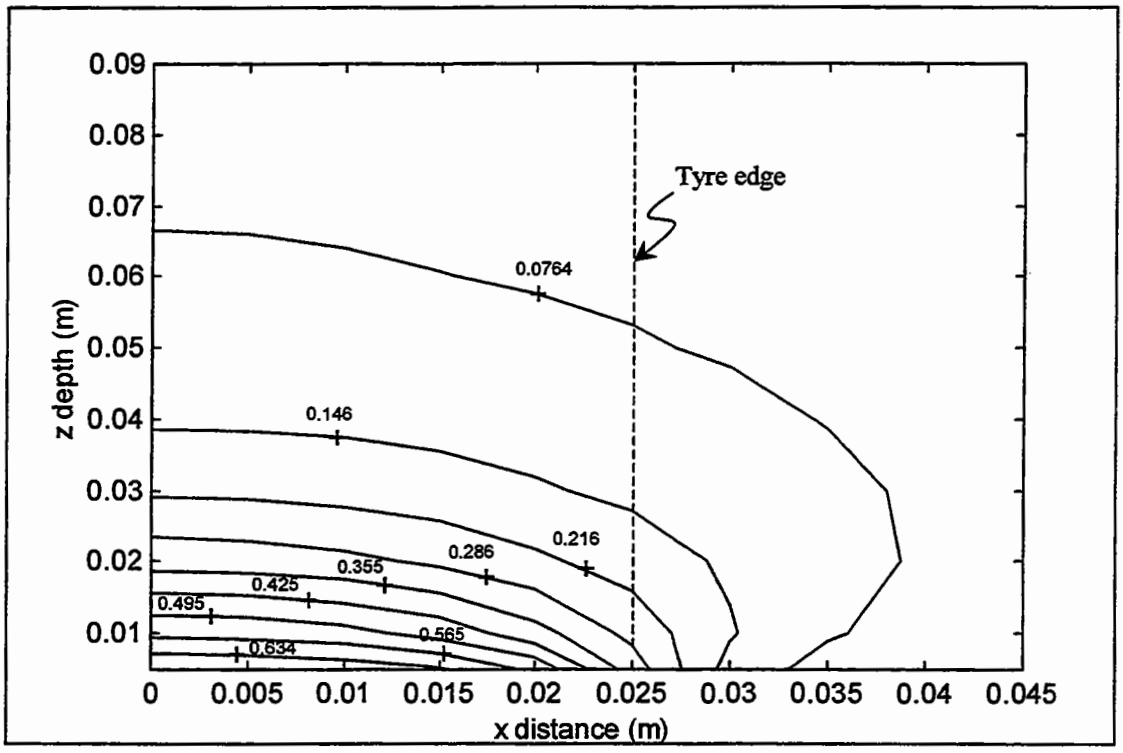

Figure 8.3 Contours of constant mean stress (values in MPa).

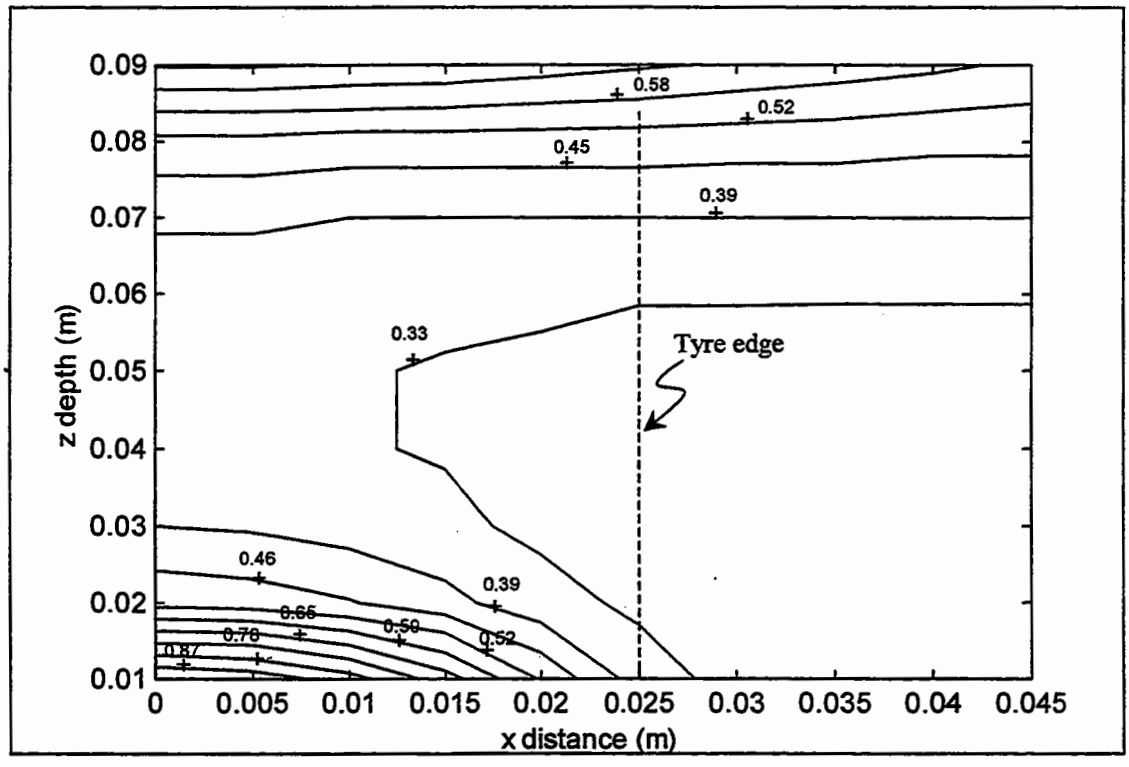

Figure 8.4 Contours of constant stress ratio.

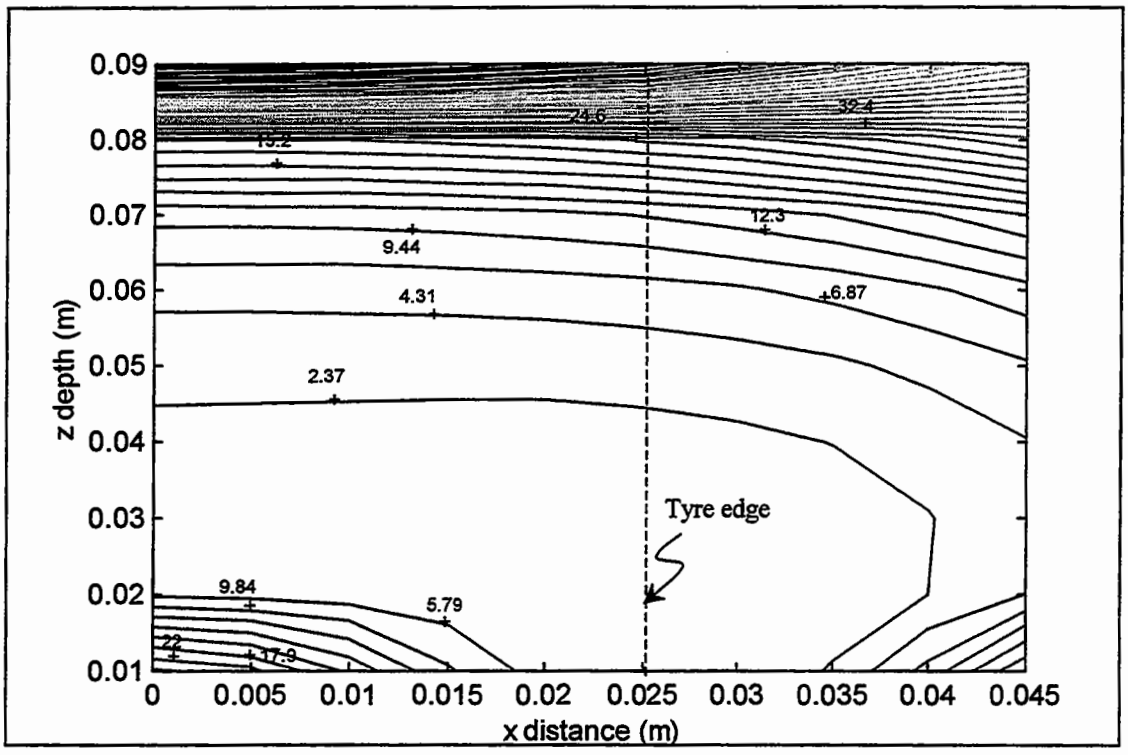

Figure 8.5 Contours of constant viscosity mixture A at 20°C (values in GPa.s).

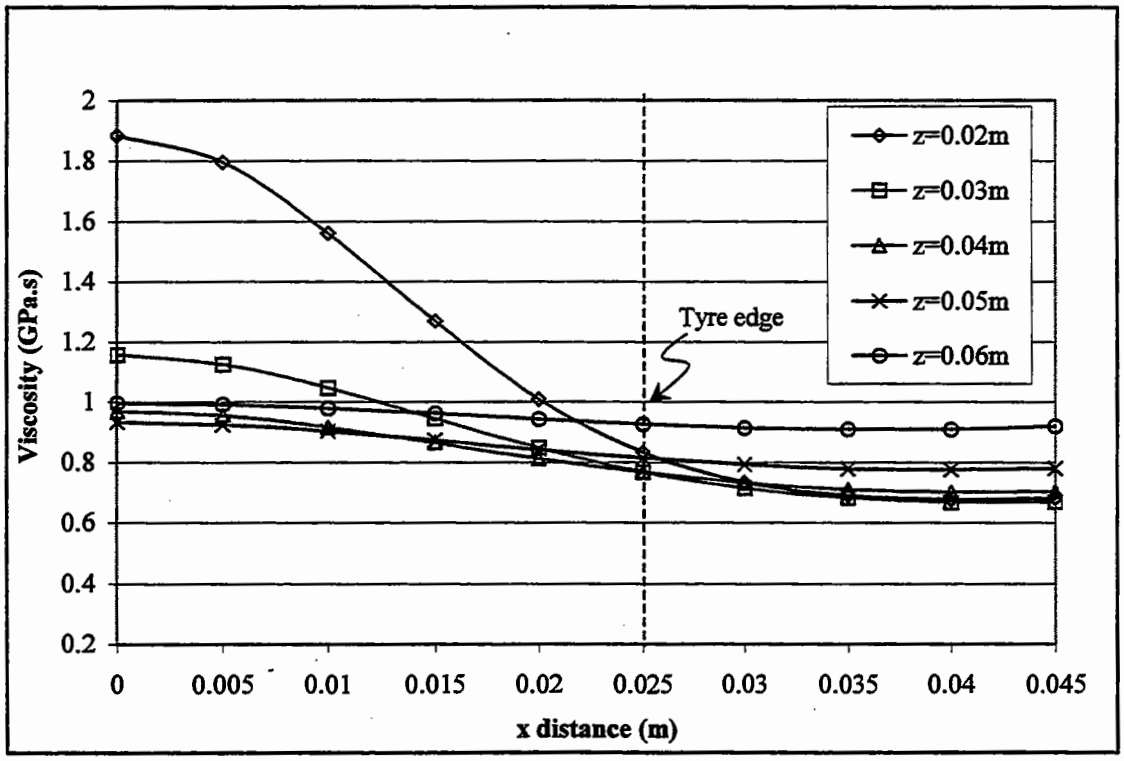

Figure 8.6 Variation of viscosity with depth 'z' and 'x' distance (HRA at 45°C).

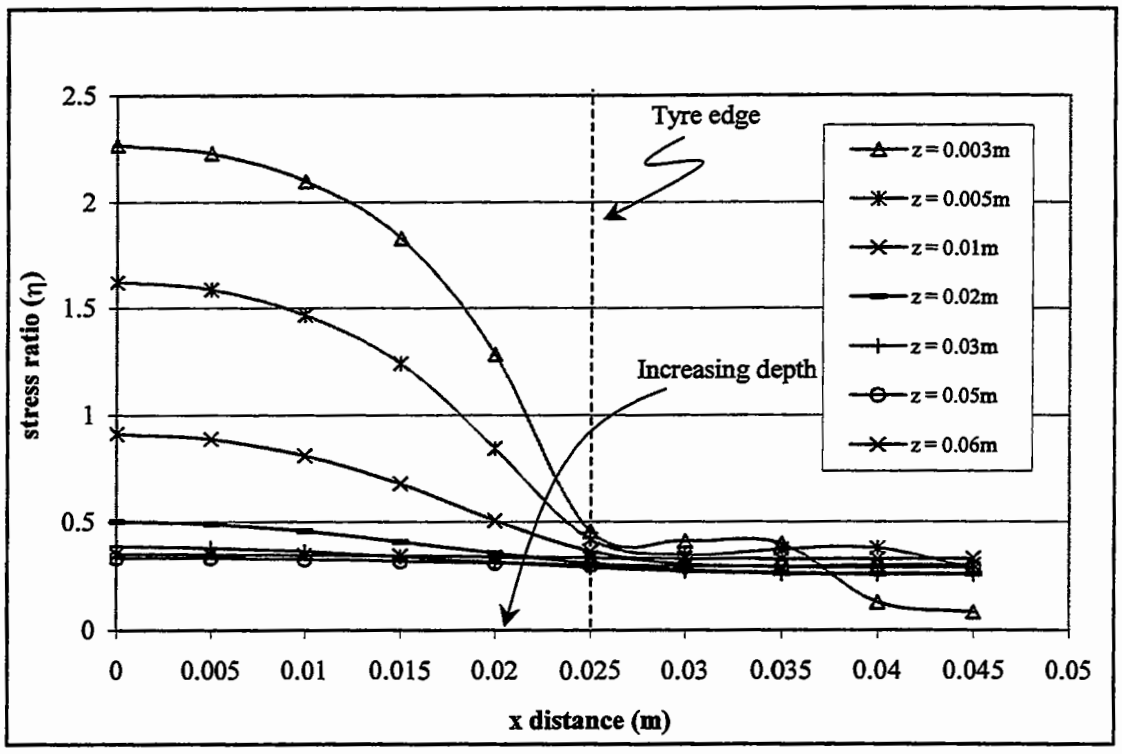

Figure 8.7 Variation of stress ratios with depth 'z' and radial distance 'x'.

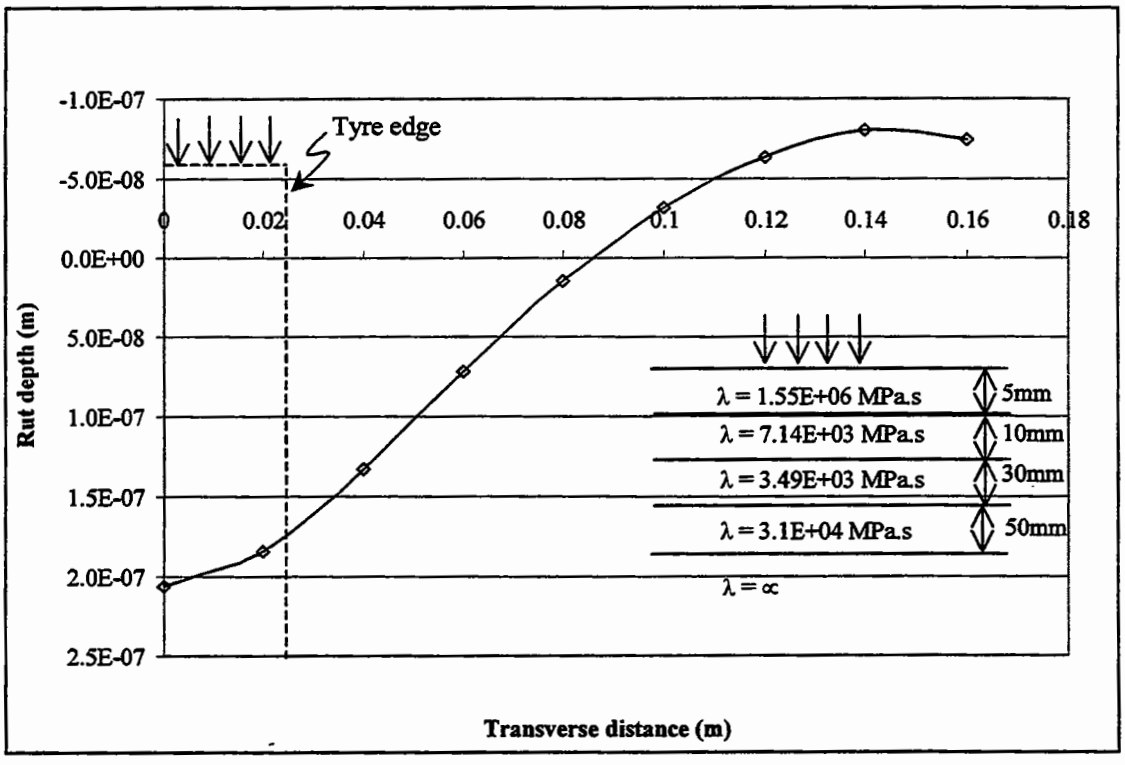

Figure 8.8 Transverse rut profile for higher viscosity value (mixture A at 20°C & 1000kPa).

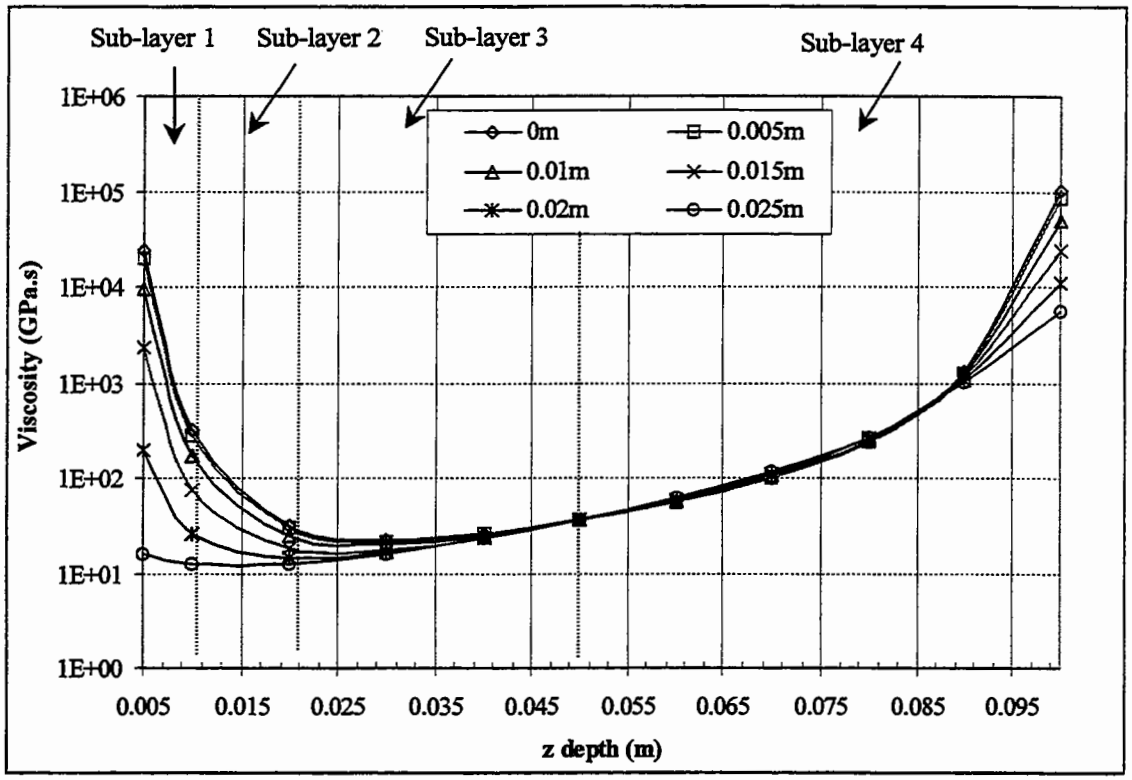

Figure 8.9 Viscosity-depth profiles (mixture A/D at 20°C).

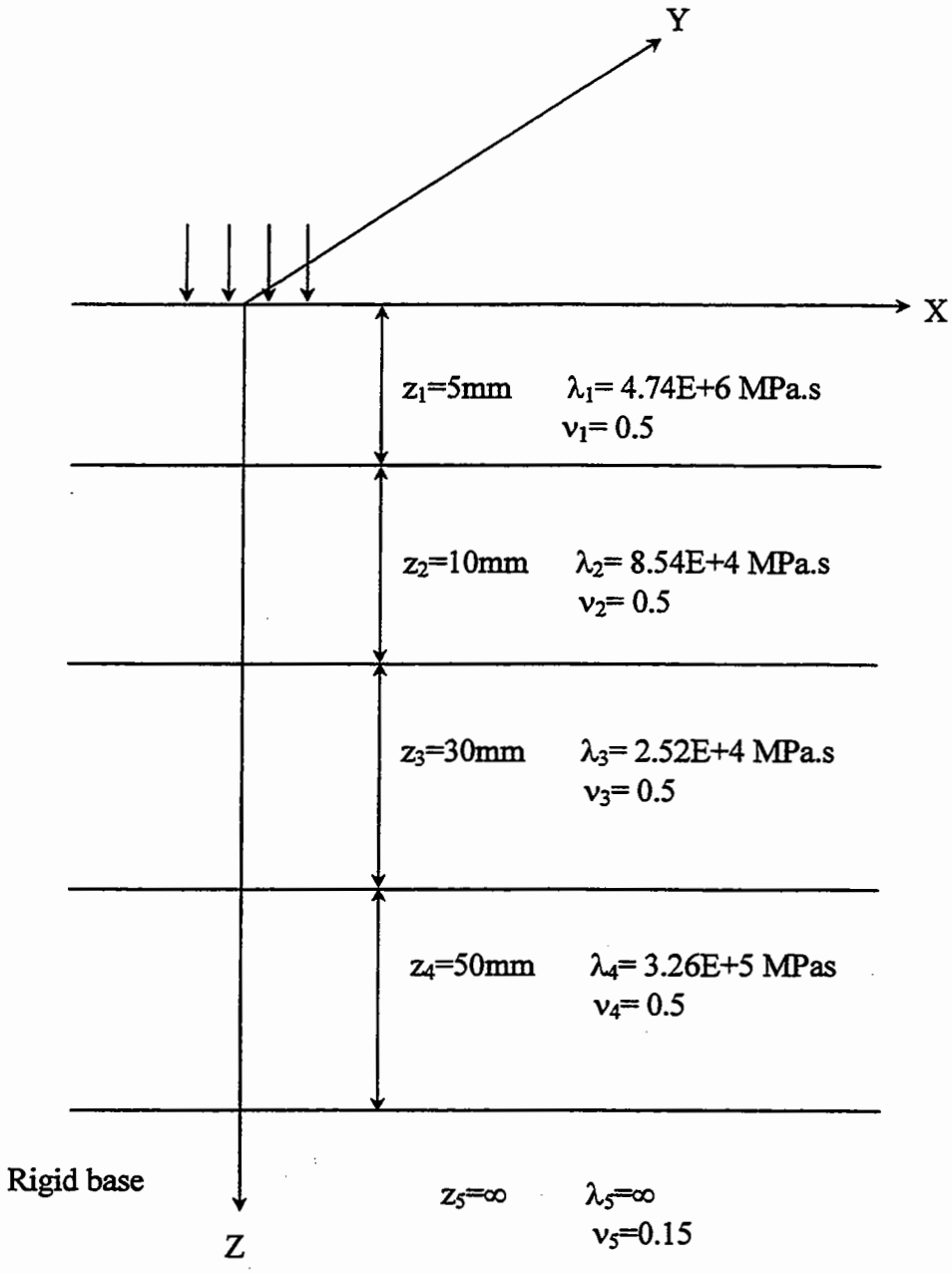

Figure 8.10 Slab section divided into sub-layers (mixture A/D at 20°C).

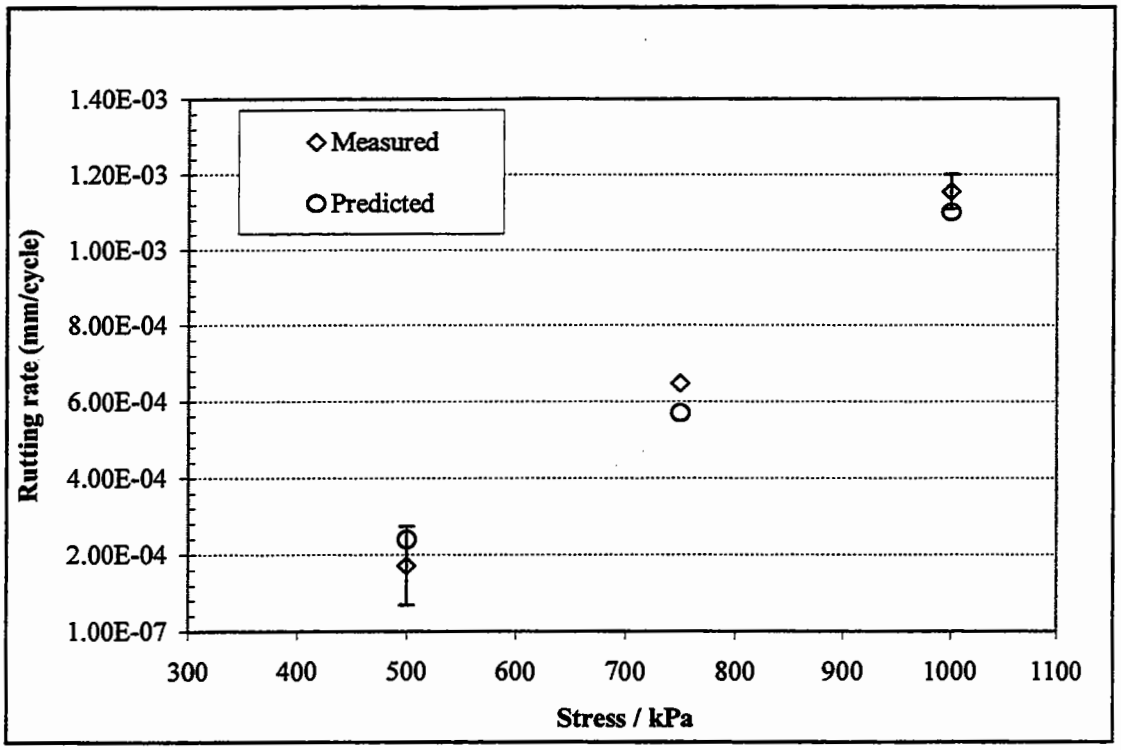

Figure 8.11 Predicted and measured rutting rates for mixture A at 20°C.

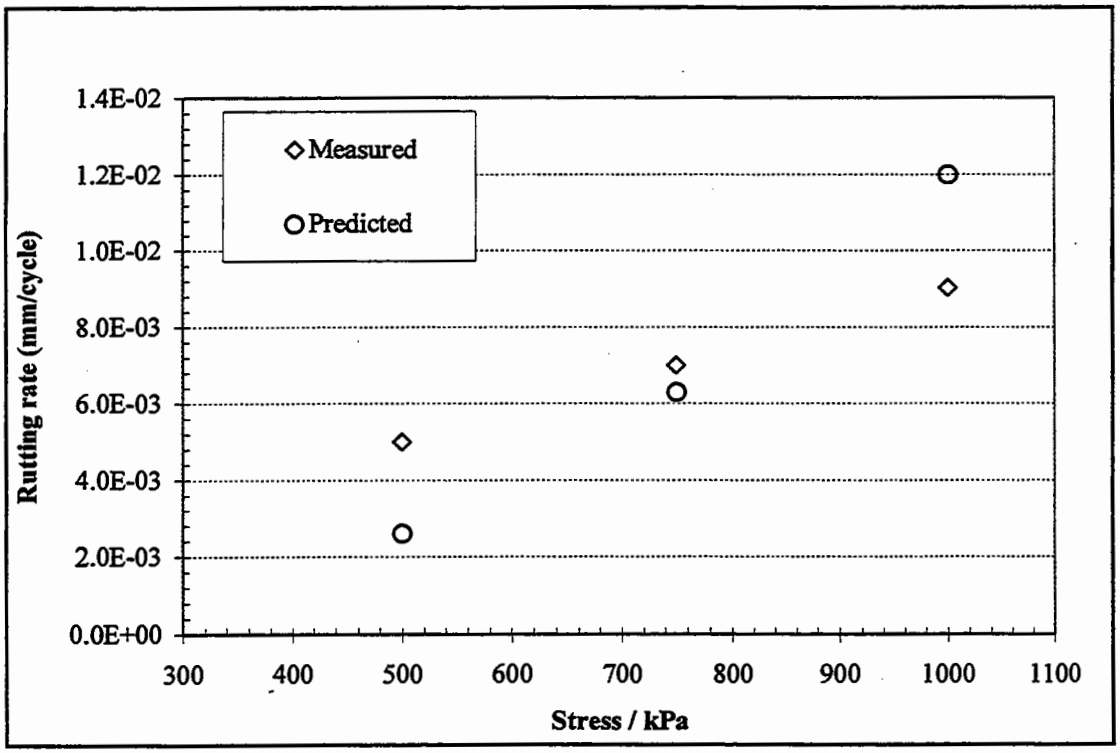

Figure 8.12 Predicted and measured rutting rates for mixture A at 30°C.

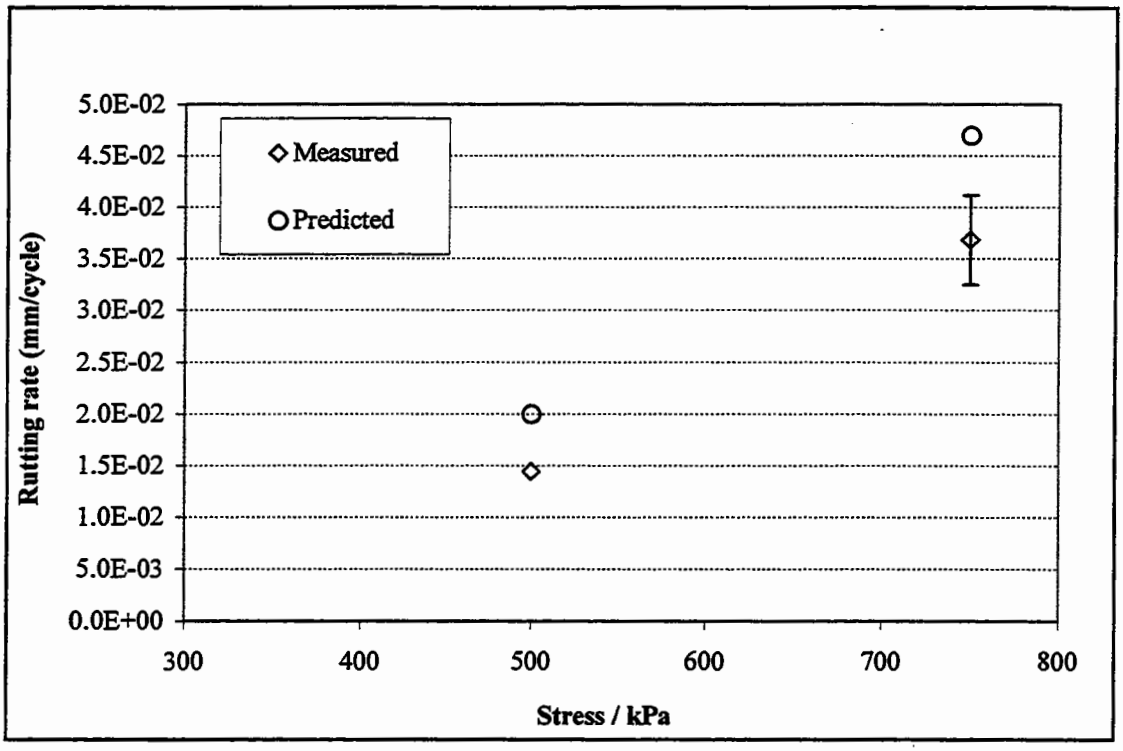

Figure 8.13 Predicted and measured rutting rates for mixture A at 40°C.

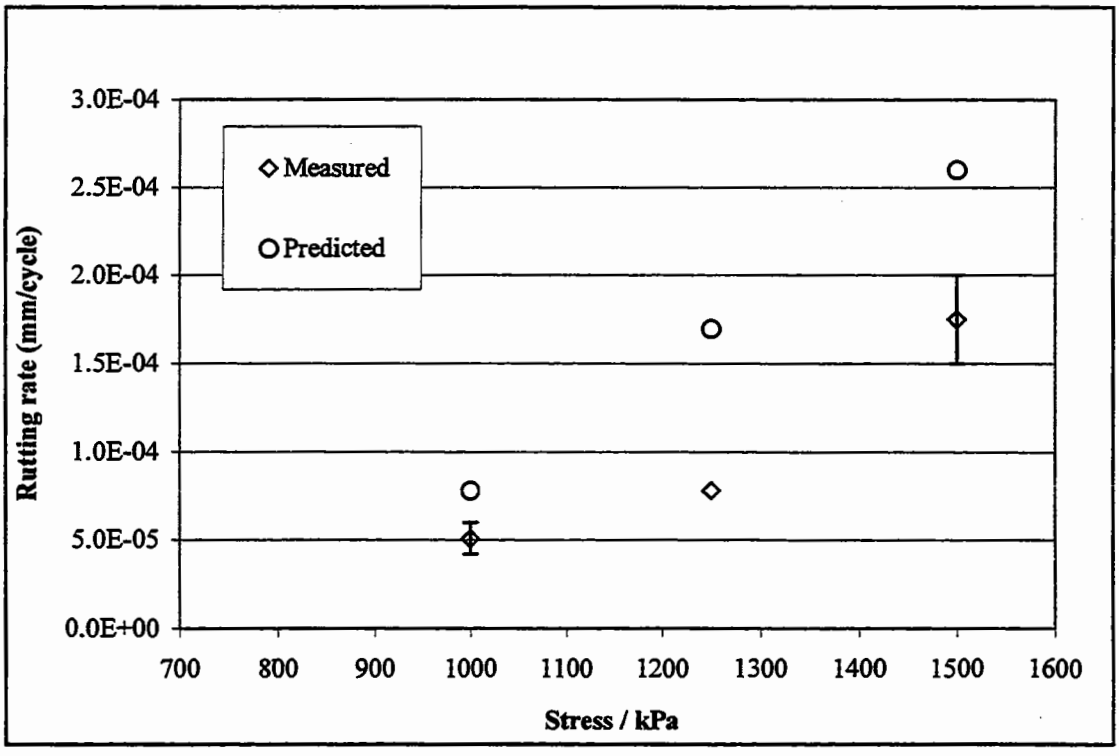

Figure 8.14 Predicted and measured rutting rates for mixture A/D at 20°C.

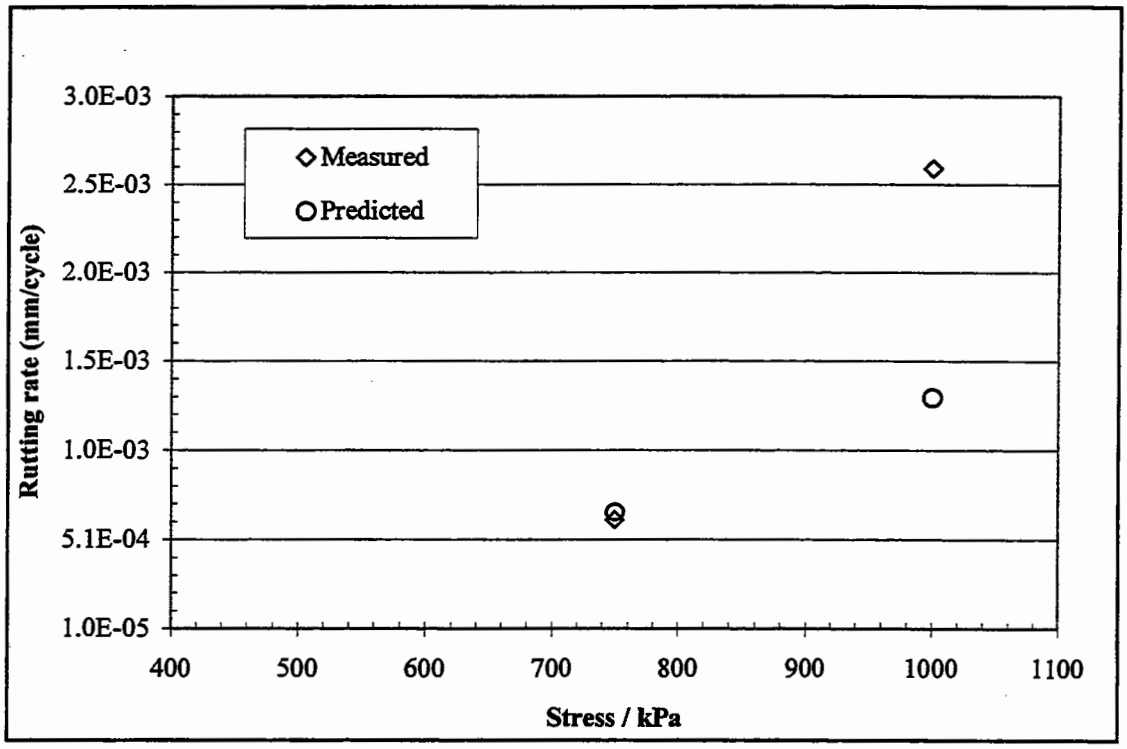

Figure 8.15 Predicted and measured rutting rates for mixture A/D at 30°C.

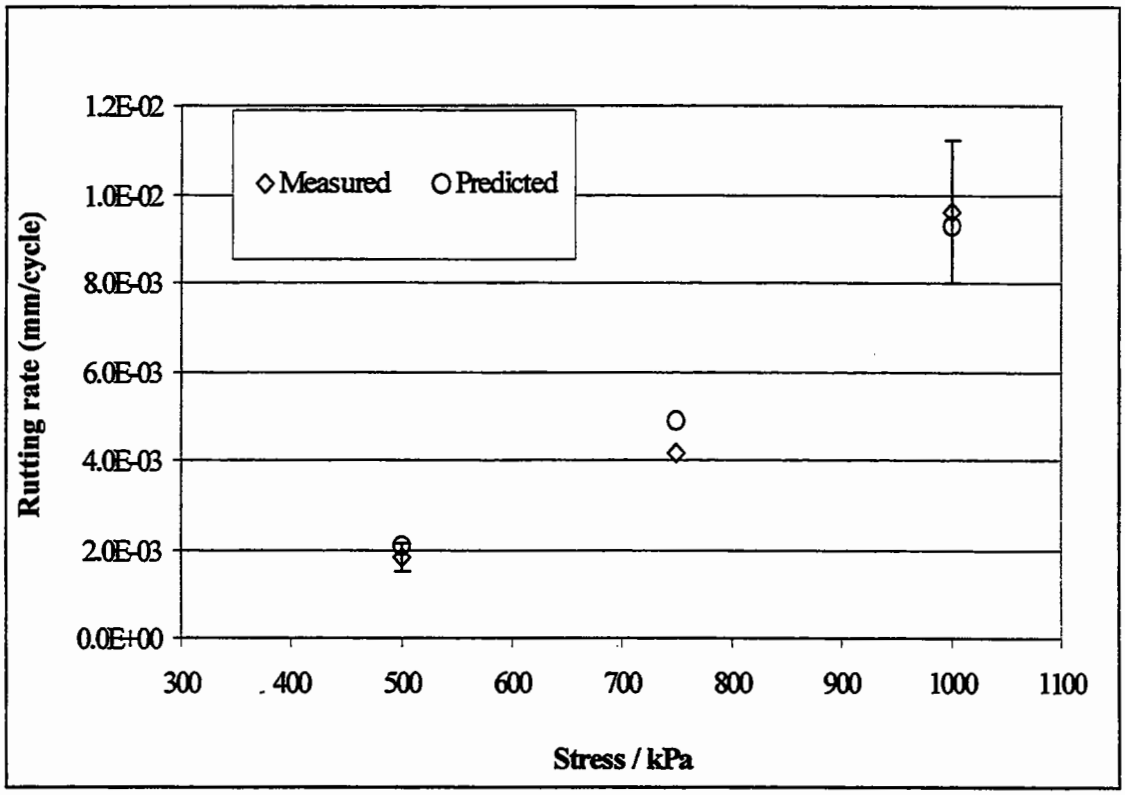

Figure 8.16 Predicted and measured rutting rates for mixture A/D at 40°C.

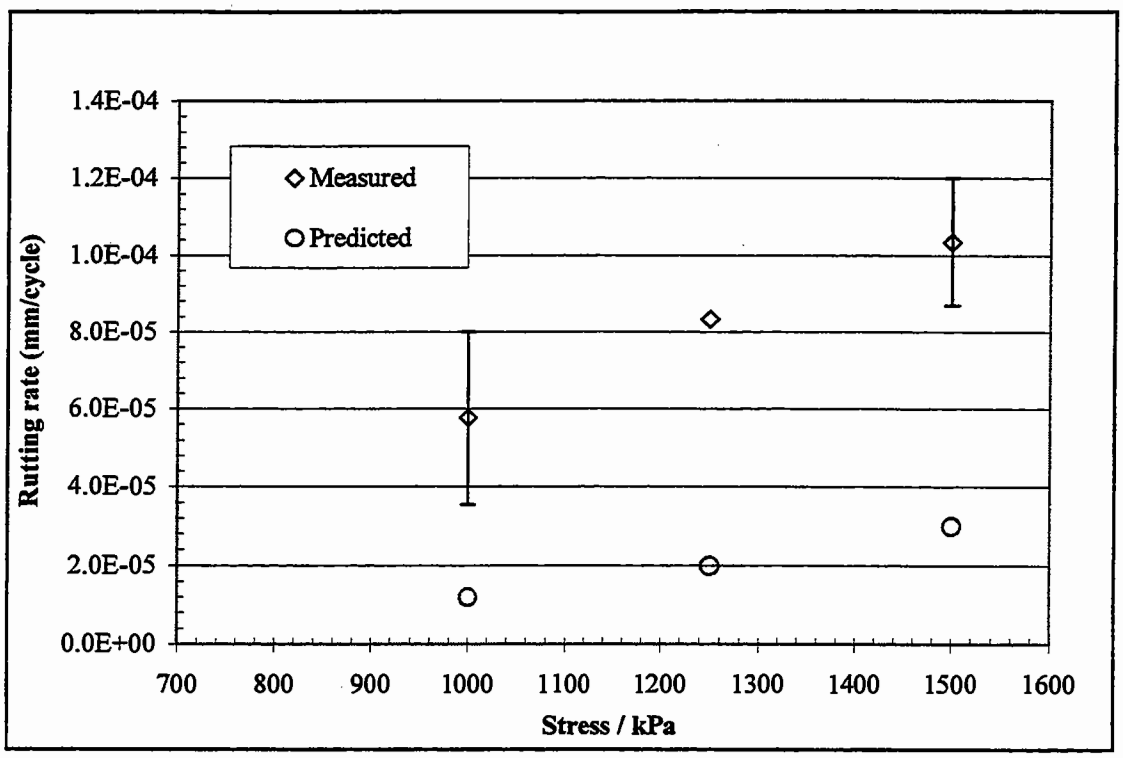

Figure 8.17 Predicted and measured rutting rates for 30/10 HRA at 45°C.

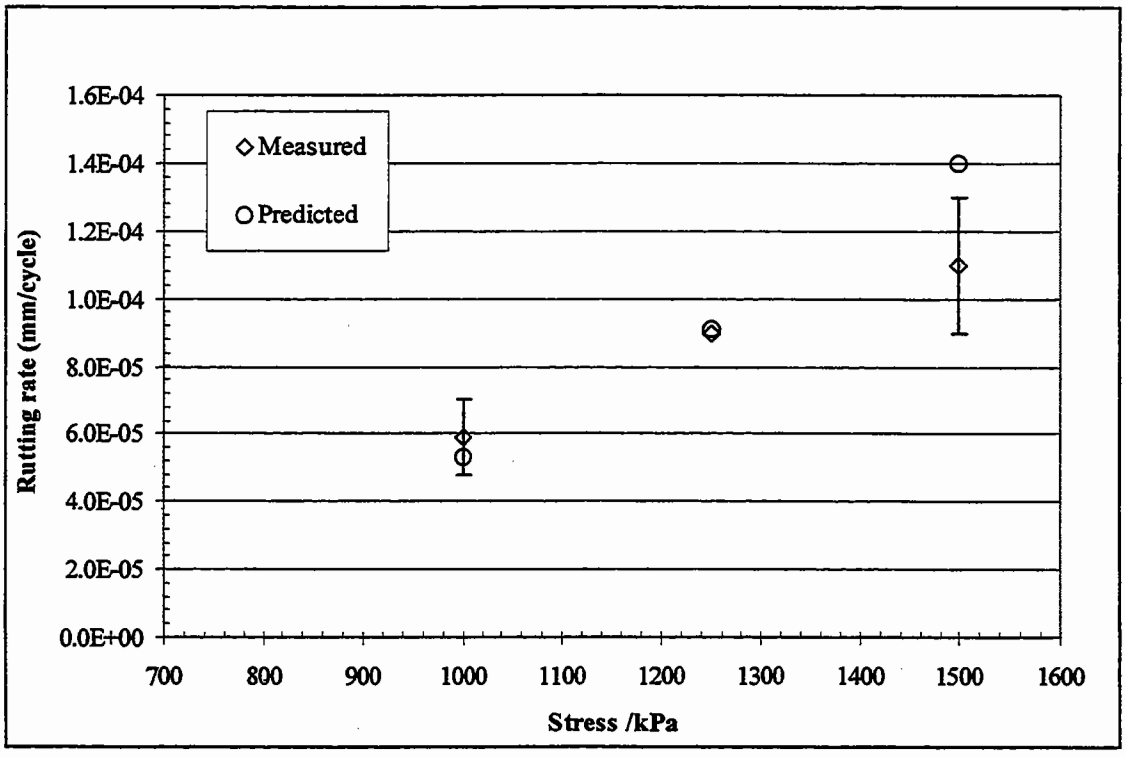

Figure 8.18 Predicted and measured rutting rates for 10mm DBM at 45°C.

Summary, Conclusions and Recommendations

9.1 Summary

This research investigated the permanent deformation (rutting) behaviour of the two idealised and two realistic bituminous mixtures. The research was built up in various stages starting with the selection and characterisation (using the DSR) of the two bitumens (50 Pen and 100 Pen) to be used as binders in the idealised and realistic bituminous mixtures.

The DSR has become accepted as a simple test tool for determining the performance related properties of the bitumen equally for its straightforward procedures and simplicity. However, the interpretation of shear tests results is more complicated and the reasons are not fully understood. In a DSR testing geometry the strain rate varies from the centre to the outer perimeter of the disc, thus it was found that the DSR could be used to characterise the permanent deformation behaviour of the pure bitumen. The results from creep shear tests performed on these two types of bitumens were presented and the results were compared to previous results from uniaxial creep testing. A model has been developed which describes the deformation behaviour of the bitumen subjected to shear loading in the DSR. The model relates steady-state shear stress to steady-state shear strain rate. The results indicate that at low stress

levels (≤ 70kPa) the deformation behaviour of the pure bitumen is linear $n = 1$, whereas at higher stress levels the deformation behaviour is non-linear and can be characterised by an effective creep exponent of $n = 2.4$.

The permanent deformation behaviour of the idealised mixtures (mixture A and A/D) and realistic mixtures (30/10 HRA and 10mm DBM) has been assessed using simplified quasi-static uniaxial and triaxial laboratory tests performed over a range of temperatures, stress levels, strain rates and stress ratios. Results from the quasi-static uniaxial testing showed that the deformation behaviour of the idealised and the realistic mixtures tested follows the same pattern as the deformation behaviour of the bitumen used in these mixtures. At low stress levels the response is linear with a creep exponent of 1 whereas at higher stress levels the response is non-linear with a power law creep exponent of approximately 2.4. The effect of the aggregate was found to reduce the strain rate corresponding to a particular applied stress level (i.e. stiffening effect). Results from the triaxial testing also show similar binder dominated behaviour and indicate that the stiffening effect depends on the ratio of mean stress to deviator stress as well as mixture volumetrics and temperature.

Analysis of results from a standard repeated load uniaxial (RLA) test often used as a practical tool to assess the permanent deformation resistance of bituminous mixtures shows that, due to the lower applied stress levels (50kPa to 100kPa), the non-linear behaviour of the mixture is reduced resulting in lower values of the effective creep exponent (nearer to 1) when compared with results from uniaxial tests. It has been demonstrated that the RLA test operates at relatively low stress levels resulting in a mainly linear response from the two idealised and two realistic mixtures in terms of permanent deformation. In order for the RLA to be able to characterise the permanent deformation behaviour of the materials in the non-linear range of behaviour the level of stress applied to the specimen would need to be increased, which may be possible with a larger pneumatic actuator or alternatively a hydraulic actuator. However, changing the temperature will not be directly beneficial since the non-linearity has been found to be stress related.

Results from more realistic laboratory scale simulative wheel tracking tests on the idealised and realistic mixtures, show a similar value of creep exponent (nearer to 2.4) to that measured in the quasi-static uniaxial and triaxial tests due to the higher applied stress levels (500kPa to 1500kPa) under the tyre in this test. While a repeated load axial test showed reasonable correspondence with a wheel tracking test it is assumed that it is influenced greatly by testing configuration of the RLA test. Consequently, it appears that the application of confining stress in the RLA test is beneficial for reducing the scatter in the test results. Moreover, the application of a confining stress is also considered desirable since it is more representative of in situ loading than the unconfined condition. These findings are of concern since both the test methods are used to make a quantitative assessment of mixture performance. Comparison of RLA and wheel tracking tests performed on the idealised mixtures with $G^*/\sin\delta$ (SHRP rutting parameter) indicates that there is a poor correlation between $G^*/\sin\delta$ and the measured steady-state deformation rates obtained from these tests.

The measured uniaxial and triaxial properties have been used in a viscous model to predict the rutting measured from wheel tracking tests. A method has been presented for incorporating the observed non-linear behaviour of these materials in a linearised viscous approach for estimating rutting in bituminous mixtures based on the use of existing linear elastic layered models of a pavement structure supplied with viscous rather than elastic properties. The model predicts that permanent deformation per wheel pass in bituminous mixtures is proportional to the static wheel load and inversely proportional to loading speed. The predicted and the measured rutting rates from the wheel tracking test for both the idealised and realistic mixtures show reasonable agreement over a range of stress levels and temperatures bearing in mind the simplified nature of the approach. The predicted rutting rates were characterised by an effective creep exponent of $n = 2.2$ to 2.4 for both the idealised and realistic mixtures, and were found to be in range with the effective creep exponent calculated from the measured rutting rates. The predicted creep exponent indicate that the model has the ability to predict the degree of non-linearity observed in the deformation behaviour of bituminous mixtures and this simple approach was capturing this important feature.

9.2 Conclusions

The following conclusions have been drawn from the various chapters of this thesis.

9.2.1 Literature Review (Chapter 2)

Various theories describing the mechanism of permanent deformation of bituminous material were reviewed in Chapter 2. The aim of the review was to examine the applicability of these theories to model the deformation behaviour of bituminous mixtures. Recent research on pure bitumen and idealised bituminous mixtures was reviewed which concluded that the steady-state behaviour of the idealised mixtures followed a similar pattern to the steady-state behaviour of pure bitumen.

Two basic methodologies for predicting rutting in asphaltic pavements were reviewed. These were the 'layer-strain' approach and models based on viscoelastic theory. Methods using the first approach assume that permanent deformation is only dependent on the elastic stresses in the pavement and is independent of the material viscosity. Methods using the second approach typically use linear viscoelastic material models where properties are derived from cyclic or creep tests. Both these proposed methods have limitations in accurately predicting rutting in non-linear bituminous materials. However, rutting models based on viscoelastic theory can effectively model the shear deformation that results in the formation of a ridge adjacent to the wheel path. Consequently, this type of approach was adopted.

9.2.2 Binder Testing (Chapter 3)

DSR testing has been used to investigate the rheological behaviour of two grades of bitumen (50 Pen and 100 Pen) over a range of frequencies (0.1Hz-10Hz) and 3 temperatures (20°C, 30°C and 40°C). The main objective of dynamic shear testing was to compare the SHRP rutting parameter with the RLA and wheel tracking results.

Shear creep tests were also performed on the 50 Pen and 100 Pen grades of bitumen to investigate the quasi-static deformation behaviour. A simple model was developed

which describes the deformation behaviour of the bitumen subjected to shear loading in the DSR. The model relates steady-state shear stress to steady-state shear strain rate. The results indicate that at low stress levels (≤ 70kPa) the deformation behaviour of the pure bitumen is linear $n = 1$, whereas at higher stress levels the deformation behaviour is non-linear and can be characterised by an effective creep exponent of $n = 2.4$. A correction factor of 3 was found to give good results when DSR model was corrected for uniaxial tensile conditions. This factor of 3 also agrees with previous results obtained by Cheung [40] for his range of shear tests conducted on same grade of bitumen and according to him, in the non-linear region, reflects the collapse behaviour of the elastic asphaltene network prior to the steady-state creep behaviour where the expected correlation factor should be $\sqrt{3}^{n+1} \cong 6$. However, interpretation of shear tests results is more complicated and the reasons are not fully understood. In the non-linear region the strain rates are predominantly high and there may be damage accumulating in the specimen. This requires further investigation.

9.2.3 Uniaxial Tests on Idealised and Realistic Bituminous Mixtures (Chapter 4)

Two idealised mixtures with different fractions of sand aggregates were tested in uniaxial compression. The uniaxial steady-state deformation behaviour of the idealised mixtures (denoted mixture A/D & mixture A) was found to follow the same form as the steady-state deformation of the bitumen, with the aggregate acting to stiffen the mixture. Mixture A/D, which had two fractions of sand aggregates, was found to be stiffer than mixture A which had only one fraction of sand aggregate. The temperature dependence of both the mixtures was found to be the same as that of the pure bitumen. For both the mixtures (mixture A/D and mixture A), steady-state conditions were observed at strain levels greater than approximately 3%.

This research was further extended to understand the steady-state behaviour of realistic mixtures in uniaxial compression. The uniaxial steady-state deformation behaviour of an HRA mortar and a 30/10 HRA mixture were found to have the same form as the steady-state deformation of the pure bitumen and idealised mixtures. The aggregates were found to stiffen the mortar without changing the form of deformation

behaviour. The steady-state conditions for HRA mixture and HRA mortar were observed at strain levels of greater than approximately 3%.

The uniaxial steady-state deformation behaviour of a 10mm DBM mixture was also found to be of a similar form to that of the pure bitumen and the idealised mixtures. The steady-state conditions for the DBM mixture were also observed at strain level of greater than approximately 3%. The DBM mixture was found to be stiffer than the HRA mixture. A reduction in the stiffening effect was observed when the 100 Pen grade bitumen was used as the binder in the DBM mixture.

The stiffening effect was found to be susceptible to variations in specimen air void content, especially for the HRA and DBM mixtures. The stiffening factor was also found to be dependent on the volume fraction of aggregates. The experimental results indicate that the behaviour of the bituminous mixtures tested was not strongly dependent on the shape or angularity of the aggregate particles (for the limited number of mixtures tested). The deformation behaviour of all the mixtures was found to be dominated by the binder over the regimes tested.

9.2.4 Triaxial Tests on Idealised and Realistic Bituminous Mixtures (Chapter 5)

In this chapter triaxial creep tests performed on the idealised mixtures (mixture A/D and mixture A) and the realistic mixtures (30/10 HRA and 10 mm DBM) under various compressive stress states were described. At a constant stress ratio, the steady-state deformation behaviour of the idealised mixtures (mixture A and A/D) and the realistic mixtures (HRA and DBM) was found to be of the same form as that of the pure bitumen and the results from the uniaxial testing. The steady-state deformation behaviour of the idealised and the realistic mixtures was found to be dependent on the mean stress and the deviator stress. The stiffening factor S (between the bitumen and the mixture) was found to be a function of the volume fraction of the aggregate and the stress ratio ($\eta = \Sigma_m/\Sigma$). In the later stages of the creep test, the deformation behaviour of the DBM mixture was found to be dependent on the properties of the aggregate skeleton. A limited number of triaxial tests were performed on the dry DBM aggregate to investigate this further. The results from the triaxial strain rate tests

indicate that the steady-state stress for the dry mixture occurs at an axial strain of approximately 14%. For the DBM mixture (with bitumen) the steady-state stress as observed from uniaxial tests was found to reach its limiting value of 1.5 MPa at an axial strain of approximately 6%. It was found that the dry mixture tested at the same strain rate tends towards a similar value of stress but at a much larger value of strain (>18%). Consequently, on the basis of these limited tests it is assumed that the mixture has a certain limiting value of stress at which it fails, the form of which is determined by the aggregate grading.

Both the idealised and realistic mixtures were observed to dilate under compressive triaxial stresses. For the idealised and realistic mixtures the volumetric strain was found to vary linearly with the distortional strain and was found to be independent of the stress ratio and deviator stress. The value of the dilation gradient s was observed to be dependent on the volume fraction of aggregates. The mean value of s for mixture A was found to increase from 0.95 to 1.2 for mixture A/D. For the HRA and DBM mixtures the mean values of dilation gradient s were observed to be higher than for the idealised mixtures. The dilation gradient s was found to have a significant effect on the deformation behaviour of the mixtures. It was hypothesised that above a critical stress ratio mixtures with high value of s are expected to lockup (i.e. no further deformation is possible).

9.2.5 Repeated Load Axial Tests on Idealised and Realistic Bituminous Mixtures (Chapter 6)

RLA tests were performed on the idealised and the realistic bituminous mixtures over a range of temperatures and applied stress levels. A steady state rutting rate was used to characterise the steady state permanent deformation behaviour of these mixtures. Results showed a lower effective creep exponent n = 1.1 to 1.5 for the idealised mixtures from the RLA tests. For the realistic mixtures the effective creep exponent was found to be in the range n = 0.8 to 0.9. Results from both the idealised and realistic mixtures indicated that the binder was operating in (or near to) the linear region. It was suggested that simplified tests that operate at low stress levels (such as the RLA test) may not be sufficient to fully characterise the permanent deformation

behaviour of these types of mixtures. However, this type of test may be sufficient to correctly rank the rutting potential of mixtures if all the binders have similar non-linear creep properties (this may not be the case for highly modified binders).

$G^*/\sin\delta$ (obtained from DSR testing) was calculated at a frequency of 0.1Hz and was plotted against the measured steady-state rutting rate from the RLA tests. Comparison of RLA tests performed on the idealised mixtures with $G^*/\sin\delta$ (SHRP rutting parameter) indicate that there is a poor correlation between $G^*/\sin\delta$ and the measured steady-state deformation rates. $G^*/\sin\delta$ gives a measure of the dissipated energy which, in part, will relate to permanent viscous deformation. However, dissipated energy also relates to heating of the specimens and energy required for damage initiation so cannot be considered to be a unique measure of permanent deformation (indeed dissipated energy is also related to fatigue by SHRP). It should also be noted that different compaction methods were used for mixtures A and A/D which may have effected the orientation of the aggregates and the air void content which will result in additional scatter.

9.2.6 Wheel Tracking Tests on Idealised and Realistic Bituminous Mixtures (Chapter 7)

Wheel tracking tests were performed on the idealised and the realistic bituminous mixtures over a range of temperatures and applied stress levels. A steady-state rutting rate was used to characterise the permanent deformation behaviour of these mixtures. Results showed a higher value of effective creep exponent (n = 1.9 to 2.4) from the wheel tracking tests compared to results from the RLA test (n = 0.8 to 1.5) for both the idealised and realistic mixtures. The results indicate that the rutting process (as measured in the wheel tracking test) for the mixtures tested can be non-linear with respect to the applied load at realistic applied stress levels.

Results showed a reasonable correlation between the average normalised rutting rates from the wheel tracking test and RLA tests on the idealised mixtures. $G^*/\sin\delta$ (obtained from DSR testing) was calculated at a frequency of 0.1Hz and plotted against the measured steady-state rutting rate from the wheel tracking test on idealised

mixtures. Results showed that there was considerable scatter that is thought to be mainly caused by non-linearities not accounted for in the SHRP rutting parameter.

9.2.7 A Visco-Elastic Model for Rutting in Asphaltic Mixtures (Chapter 8)

A method for estimating rutting in bituminous mixtures was presented based on the use of existing linear elastic layered models of a pavement structure supplied with viscous rather than elastic properties. The model predicts that permanent deformation per wheel pass in bituminous mixtures is proportional to the static wheel load and inversely proportional to loading speed. The method uses non-linear material properties determined from the uniaxial and triaxial testing. A linearised approach has been developed to predict the non-linear deformation behaviour of bituminous mixtures.

The predicted and the measured rutting rates from the wheel tracking test for both the idealised and realistic mixtures showed good agreement over a range of stress levels and temperatures. The predicted rutting rates were characterised by an effective creep exponent of n = 2.2 to 2.4 for both the idealised and realistic mixtures, and were found to be similar to the effective creep exponent calculated from the measured rutting rates. The predicted creep exponent n = 2.2 to 2.4, showed that the model has the ability to predict non-linear deformation behaviour of bituminous mixtures.

9.3 Recommendations for Further Work

9.3.1 Quasi-Static Behaviour of Modified Binders and Mixtures

This research has highlighted the influence of the steady-state binder properties on the steady-state deformation behaviour of idealised and a limited number of realistic bituminous mixtures. In order to obtain more quantitative data for other types of mixtures (i.e. Stone Mastic Asphalt, Porous Asphalt etc) it is suggested that a programme of mixture testing over a range of temperatures and stress levels should be carried out using the research framework describe in this thesis. The testing should be extended to include polymer modified binders and mixtures which might alter the

form of steady-state deformation behaviour of bituminous mixtures. It is recommended that further binder testing should be undertaken to characterise the deformation behaviour of modified binders in the linear and non-linear regions.

9.3.2 Further Investigation into the Dilation Gradient '*s*'

A very important area of research, which this thesis has only touched on, is the dilation gradient '*s*'. It has been found that increasing the dilation gradient results in a higher stiffening factor for a mixture with the same volume fraction of aggregates subjected to the same stress ratio. The dilation gradient was found to be an important factor and needs to be taken into consideration while designing bituminous mixtures. However, the relationship between *s* and the aggregate properties like particle shape, size gradation and volume properties is not fully understood. Further research is needed to understand the factors affecting *s* to improve mixture design.

9.3.3 Field Verification

The approach for predicting rutting in bituminous materials requires validation with data collected from in-service pavement structures. Currently, the approach has only been validated using a limited number of tightly controlled small-scale wheel tracking tests. Data from in-service pavements will include other factors such as temperature variations, variation in contact pressure and area, lateral wander of traffic etc.

9.3.4 Finite Element Implementation of Rutting Model

A simplified approach to modelling permanent deformation in bituminous mixtures was presented in this thesis. The simplified modelling approach is subject to a number of limitations and there is a difficulty in adequately dealing with the large variations in viscosity that occur near to the surface of the slab. There are also the limitations associated with using a linear elastic model to calculate the Von Mises equivalent stress and the stress ratios rather than using the true non-linear constitutive law for the calculation. Further research needs to be undertaken aimed at incorporating the true

non-linear constitutive law into a Finite Element program to improve the prediction procedure.

9.3.5 Extension to Transient Behaviour

When a pavement is loaded by a moving tyre the response will be a combination of transient and steady-state responses. This research has assumed that the most important factor in rutting of bituminous materials is the steady-state response. This assumption needs investigating in more detail (experimentally and theoretically) to characterise the role that the transient response has on permanent deformation in bituminous mixtures.

REFERENCES

1. **Ahlborn, G.,** 'ELSYM, computer program for determining stresses and deformations in five layered system.' University of California, Berkeley, 1972.

2. **Airey, G. D.,** 'Rheological characteristics of polymer modified and aged bitumens.' PhD Thesis, Department of Civil Engineering, University of Nottingham, 1997.

3. **Alavi, S. H.,** 'Viscoelastic and permanent deformation characteristics of asphalt aggregate mixes tested as hollow cylinders and subjected to dynamic axial and shear loads.' Ph.D. Thesis, Civil Engineering Department, University of California at Berkeley, 1992.

4. **Alavi, S. H., Monismith C. L.,** 'Time and temperature dependent properties of asphalt concrete mixes tested as hollow cylinders and subjected to dynamic axial and shear loads.' Journal of Association of Asphalt Paving Technologists, Vol. 63, pp 152-181, 1994.

5. **American Association of State Highway and Transportation Officials.** AASHTO TP5., 'Standard test method for determining the rheological properties of asphalt binder using Dynamic Shear Rheometer (DSR).' AASHTO, Washington, D. C., 1995.

6. **Anon,** 'Shell pavement design manual – Asphalt pavements and overlays for road traffic'. Shell 1978.

7. **Anon,** 'Pavement design; A guide to the structural design of road pavements'. National Association of Australian State Road Authorities (NAASRA), 1987.

8. **Anon,** 'AASHTO guide for design of pavement structures'. Vol. 1, American Association of State Highway and Transportation Officials (AASHTO), 1986.

9. **Anon,** 'Thickness design – Asphalt pavements for highways and streets'. The Asphalt Institute, Manual Series No: 1 (MS – 1), September 1981.

10. **Anderson, D.A. and Kennedy, T.W.,** 'Development of SHRP binder specification.' Journal of the Association of Asphalt Paving Technologists Vol. 62, pp 481-507, 1993.

11. **Anderson, D. A., Christensen, D. W., Bahia, H.,** 'Physical properties of asphalt cement and the development of performance related specifications.' Journal of Association of Asphalt Paving Technologists, Vol. 60, pp 437-475 1991.

12. **Austin, G.,** 'The behaviour of keuper marl under undrained creep and repeated loading.' Ph.D. thesis, University of Nottingham, 1979.

13. **Autret, P., Gramsammer, J. G.,** 'The LCPC's circular test track and innovation.' Special report, Laboratoire central des ponts et chaussees. 1990.

14. **Barksdale, R. D.,** 'Laboratory evaluation of rutting in base course materials.' Proc. 3rd Int. Conf. on the Structural Design of Asphalt Pavements, London, pp 161-174, 1972.

15. **Barksdale, R. D.,** 'Compressive stress pulse times in flexible pavements for use in dynamic testing.' Highway Research Record, No. 345, Highway research Board, pp 32-34, 1971.

16. **Battiato, G., Ronco, F., Verga, C.,** 'Moving loads on a viscoelastic double layer : Prediction of recoverable and permanent deformation.' Proc. 4th Int. Conf. on the Structural design of Asphalt Pavements, Ann Arbor, pp 459-466. 1977.

17. **Bonnot, J.,** 'Asphalt aggregate mixtures.' Transportation Research Record, 1096, Transportation Research Record, pp 42-51, 1986.

18. **Bolton, M. D.,** 'A Guide to Soil Mechanics.' Macmillan, 1979.

19. **Bromhead, E. N.,** 'A Simple Shear Apparatus.' J. of Ground Engineering 12, No. 5, pp. 40-44. 1979

20. **Brown, S. F., Brunton, J. M.,** 'An introduction to the analytical design of bituminous pavements.' 3rd Edition, University of Nottingham, 1986.

21. **Brown, S. F., Brunton, J. M.,** 'Improvements to subgrade strain criterion.' J. of Transportation Engineering, Vol. 110, No. 6. American Society of Civil Engineers. November 1984.

22. **Brown, S. F.,** 'Laboratory testing for use in the prediction of rutting in asphalt pavements.' Transportation Research Record, No. 616, Transportation Research Board. Washington D.C., pp 22-27, 1976.

23. **Brown, S. F., Cooper, K. E.,** 'Permanent deformation of dense bitumen macadam under creep and repeated loading.' Proc. Colloquium 77, Plastic deformability of Bituminous Mixes, pp 173-215. Zurich 1977.

24. **Brown, S. F., Cooper, K E.,** 'The mechanical properties of bituminous materials for road bases and basecourses.' J. of Association of Asphalt Paving Technologists, Vol. 53, 1984.

25. **Brown, S. F., Cooper, K E.,** 'A fundamental study of stress-strain characteristics of a bituminous material.' J. of Association of Asphalt Paving Technologists, Vol. 49, 1980.

26. **Brown, S. F., Snaith, M. S.,** 'The permanent deformation characteristics of a dense bitumen macadam subjected to repeated loading.' J. of Association of Asphalt Paving Technologists, Vol. 43, pp 224-252, 1974.

27. **Brown, S. F., Bell, C. A.,** 'The validity of design procedures for the permanent deformation of asphalt pavements.' Proc. 4th Int. Conf. on the Structural Design of Asphalt Pavements, Ann Arbor, pp 467-482, 1977.

28. **Brown, S. F., Gibb, J. M., Read, J. M., Scholz, T. V.,** 'Laboratory protocols for the design and evaluation of bituminous mixtures.' Proc. Eurasphalt & Eurobitume Congress, Strasbourg France, May 1996.

29. **Brown, S. F., Gibb, J. M.,** 'Validation of experiments for permanent deformation testing of bituminous materials.' Journal of Association of Asphalt Paving Technologists, Vol. 65, pp 255-289, 1996.

30. **Brown, S. F., Scholz, T. V.,** 'Permanent deformation characteristics of porous asphalt determined in the confined repeated load axial test.' J. of the Institution of Highways and Transportation. Vol. 45, No 12, pp 7-10. December 1998.

31. **Brodrick, B. V.,** ' The development and performance of a wheel tracking facility and in-situ instruments for pavement experiments.' MPhil thesis, University of Nottingham, 1977.

32. **Brown, E. R., Foo, K. Y.,** 'Comparison of unconfined and confined creep tests for hot mix asphalt.' Journal of Materials in Civil Engineering, Vol. 6, No. 2. pp 307-326. May 1994.

33. **British Standards Institution,** London, 'Softening point of bitumen (ring and ball). BS 2000 : Part 58, 1983.

34. **British Standard Institution,** London, 'Bitumens for building and civil engineering. Part 1. Specifications for bitumens for road purposes. BS 3690 : Part 1, 1989.

35. **BS 4987,** 'Coated macadam for roads and other paved areas.' Part1. Specification for constituent materials and for mixtures. British Standards Institution. London, 1993.

36. **BS 594,** 'Hot rolled asphalt for roads and other paved areas.' Part1. Specification for constituent materials and for mixtures. British Standards Institution. London, 1993.

37. **BS 598, Part 104,** 'Sampling and examination of bituminous mixtures for roads and other paved areas.' Methods of test for the determination of density and compaction, 1989.

38. **Buseck, H.,** ' Condition rating and failure criteria in full-scale tests and on real pavements.' International colloquium on full scale pavement tests, Zurich, Switzerland, 1982.

39. **Chan F. W. K.,** 'Permanent deformation resistance of granular layers in pavements.' Ph.D. Thesis, Civil Engineering Department, University of Nottingham, 1990.

40. **Cheung, C. Y.,** 'Mechanical behaviour of bitumens and bituminous mixes.' Ph.D. Thesis, University of Cambridge, 1995.

41. **Cheung, C.Y. and Cebon, D.** 'Experimental study of pure bitumen in tension, compression and shear.' Journal of Rheology, Vol. 41(1), pp 45-73, (1997).

42. **Cheung, C.Y. and Cebon, D.** 'Deformation mechanisms of pure bitumen.' Journal of Materials in Civil Engineering, Vol. 9(3), pp 117-129, (1997).

43. **Cheung, C.Y. and Cebon, D.** 'Thin film deformation behaviour of power-law creeping materials.' ASCE Journal of Engineering Mechanics, Vol. 123(11), pp 1138-1152, (1997).

44. **Claessen, A. I. M., Edwards, J. M., Sommer, P., Uge P.,** 'Asphalt pavement design - The Shell method.' Proc. 4th Int. Conf. on the Structural Design of Asphalt Pavement. Ann Arbor, pp 39-74, 1977.

45. **Collop, A.C., Potter T. E. C., Cebon, D., Cole, D. J.,** 'Investigation of spatial repeatability using a tire force measuring mat.' Presented at the 72nd Annual meeting of the Transportation Research Board, Washington DC, 1993.

46. **Collop, A. C., Cebon, D., Hardy, M. S.,** 'Viscoelastic approach to rutting in flexible pavements.' Journal of Transportation Engineering, Vol. 121, pp 82-92, 1995.

47. **Collop, A. C., Khanzada, S.,** 'Permanent deformation in idealised mixtures and bitumen properties.' Eurobitume workshop'99 on performance related properties for bituminous binders. Paper No. 124, Luxembourg, 1999.

48. **Collop, A. C., Khanzada, S.,** 'Permanent deformation behaviour of idealised bituminous mixtures.' Proc. 3rd European symposium on performance and durability of bituminous materials and hydraulic stabilised composites. Leeds (UK), 1999.

49. **Corte, J. F., Brosseaud, Y., Kerzreho, J. P.,** 'Study of rutting of wearing courses on the L.C.P.C. test track.' Proc. 8th Int. Conf. on the Asphalt Pavements, Seattle, pp. 1555-1568, 1997.

50. **Cooper, K. E., Brown, S. F.,** 'Development of simple apparatus for the measurement of the mechanical properties of asphalt mixes.' Proceedings, 4th Eurobitume Symposium, Vol. 1, pp 494-498, Madrid 1989.

51. **Cooper, K. E., Brown, S. F.,** 'Assessment of the mechanical properties of asphaltic mixes on a routine basis using simple equipments.' Proceedings, Eurobitume Congress, Vol. 1B, pp 872-876, Stockholm 1993.

52. **Cooper, K. E., Brown, S. F., Pooley, G. R.,** 'The design of aggregate gradings for asphalt basecourses.' Proc. AAPT, Vol. 54, pp 324-346, 1985.

53. **Deshpande, V.,** 'Steady-State Deformation Behaviour of Bituminous Mixes.' PhD Thesis, University of Cambridge, 1997.

54. **Deshpande, V., Cebon, D.,** 'Steady-state constitutive relationship for idealised asphalt mixes.' *Mechanics of Materials*, Vol. 31(4), pp 271-297, (1999).

55. **Department of the Environment and Road Research Laboratory,** 'Road Note 29 – A guide to the structural design of pavements for new roads – Third edition'. HMSO, 1970.

56. **DD 228** 'Methods for determination of maximum density of bituminous mixtures'. 1996.

57. **Dormon, G. M.,** 'The extension to practice of a fundamental procedure for the design of flexible pavement.' Proc. 1st Int. Conf. on the Structural Design of Asphalt Pavements, Ann Arbor, pp 785-793, 1962.

58. **Dormon, G. M., Metcalf, C .T.,** 'Design curves for flexible pavements based on the layered elastic theory.' Highway Research Board Record No. 71, pp 69-84, 1965.

59. **Eisenmann, J., Hilmer, A.,** 'Influence of wheel load and inflation pressure at asphalt pavements - experiments and theoretical investigations.' Proc. 6th Int. Conf. on the Structural Design of Asphalt Pavements, Ann Arbor, pp. 392-403, 1987.

60. **Elliot, J. F., Moavenzadeh. F.,** 'Analysis of stresses and displacements in three-layered viscoelastic systems.' Highway research record, No. 345, pp 45-57. 1971.

61. **Finn, F., Monismith, C. L., Markevich, N. J.,** 'Pavement performance and asphalt concrete mix design.' Journal of Association of Asphalt Paving Technologists, Vol. 52, 1983.

62. **Flotz, R. B., Elliot, W. J.,** 'Effect of lowered tyre pressures on road erosion.' Transportation Research Record, No. 1589, Transportation Research Board. Washington D.C., pp 19-25, 1997.

63. **Fordyce, D.,** 'The compaction mechanism of rolled asphalt and its influence on material design.' Euroasphalt and Eurobitume Congress, Strasbourg, 1996.

64. **Francken, L.,** 'RILEM interlaboratory test on the rheology of bituminous binders.' Bituminous Binders and Mixes, Report of RILEM Technical Committee 152-PBM, No. 17.

65. **Freeme, C. R., Maree, J. H., Viljoen, A. W.,** 'Mechanistic design of asphalt pavements and verification using heavy vehicle simulator.' Proc. 5th Int. Conf. on the Structural Design of the Asphalt Pavements, Netherlands, Vol. 1, August 1982.

66. **Gibb, J. M.,** 'Evaluation of resistance to permanent deformation in the design of bituminous paving mixtures.' Ph.D. Thesis, University of Nottingham, 1996.

67. **Groenendijk, C. H., Molenaar, A. A., Mante, B. R., Dohmen, L. J.,** 'Linear tracking response measurements determining effects of wheel-load configurations.' Transportation Research Record, No. 1570, Transportation Research Board. Washington D.C., pp 1-9, 1997.

68. **Groenendijk, J., Vogelzang, C. H., Molenaar, A. A. A., Dohmen, L. J. M.,** 'Analysis of stresses, strains and FWD deflections in a full depth asphalt pavements under accelerated loading using LINTACK.' VTI 1A, Part 4, Swedish Road and Transport Research Institute, Stolkholm, 1994.

69. **Haas, R. C. G., Papagianakas, A. T.,** 'Understanding pavement rutting.' Special workshop on rutting in asphalt pavements. Roads and Transportation Association of Canada, 1986.

70. **Hadipour, K., Anderson, K. O.,** 'An evaluation of permanent deformation and low temperature characteristics of some recycled asphalt concrete mixtures.' J. of Association of Asphalt Paving Technologists, Vol. 57, pp 615-645, 1988.

71. **Harrigan, E. T., Leahy, R. B., Youtcheff, J. S.,** 'The Superpave mix design system manual of specification, test methods and practices.' Report No. SHRP-A-379. Strategic Highway Research Program, National Research Council. Washington D.C., 1994.

72. **Highway Research Board,** 'The AASHO Road Test: Special Report 73-Pavement Research.' Publication No. 1012, Washington D.C., 1962.

73. **Hills, J. F., Brien, D., Van de Loo, P. J.,** 'The correlation of rutting and creep tests on asphalt mixes.' Journal of institute of petroleum, London, England, IP 74-001. 1974.

74. **Hills, J. F.,** 'The creep of asphalt mixes.' J. of the Institute of Petroleum, Vol. 59, No. 570, November 1973.

75. **Hilster, de E., van de loo.,** 'The creep test: Influence of test parameters.' Proc. Colloquium 77, Plastic deformability of Bituminous Mixes, pp 173-215. Zurich 1977.

76. **Hight D. W., Gens A., Symes M. J.,** 'The development of a new hollow cylinder apparatus for investigating the effects of principal stress rotation in soils.' Geotechnique 33, 1983.

77. **Hofstra, A., Klomp, A. J. G.,** 'Permanent deformation of flexible pavements under simulated road traffic conditions.' Proc. 3rd Int. Conf. on the Structural Design of Asphalt Pavements, pp. 613-621, London, 1972.

78. **Hopman, P. C., Pronk, A. C., Kunst, P. A. J. C., Molenaar, A. A. A., Molenaar, J. M. M.,** 'Application of the viscoelastic properties of asphalt concrete.' Proc. 7th Int. Conf. on the Structural Design of Asphalt Pavements, Nottingham, UK, pp 73-88. 1992.

79. **Hopman, P. C., Maagdenberg, A. C., Coppens, M. H. M., Dijkink, J. H.,** 'Comparison of mechanical properties of drum mix and batch mix asphaltic concrete through dynamic testing.' J. of Association of Asphalt Paving Technologists, Vol. 57, 1988.

80. **Horak, E., Kleyn, E. G., du Plessis, J. A., de Villiers E. M., Thompson, A. J.,** 'The impact and management of Heavy Vehicle Simulator Fleet in South Africa.' Proc. 7th international conference on structural design of asphalt pavements, University of Nottingham, U.K., 1992.

81. **Huschek, S.,** 'Evaluation of rutting due to viscous flow in asphalt pavements.' Proc. 4th Int. Conf. on the Structural Design of Asphalt Pavements, Ann Arbor, pp 497-508, 1977.

82. **Hussain, E. H., Mohammad., Yue Z.,** 'Criteria for evaluation of rutting potential based in repetitive uniaxial compression test.' Transportation Research Record, No. 1454, Transportation Research Board. Washington D.C., pp 74-81, December 1994.

83. **Huhtala, M., Pihlajamaki, J., Pienimaki, M.,** 'Effects of tyres and tyre pressures on road pavements.' Transportation Research Record, No. 1227, Transportation Research Board. Washington D.C., pp 107-114, 1989.

84. **Kadar, P.,** 'Accelerated full scale testing of heavy duty pavements – experience with the Australian Accelerated Loading Facility (ALF).' Proc. 6th international conference on structural design of asphalt pavements, University of Michigan, Ann Arbor, 1987.

85. **Kenis, W. J.,** 'Predictive design procedures - A design method for flexible pavements using the VESYS structural subsystem.' Proc. 4th Int. Conf. on the Structural Design of Asphalt Pavements, Ann Arbor, pp 100-110, 1977.

86. **Kennedy, T. W., Huber, G. A., Harrigan, E.T., et al.,** 'Superior performing asphalt pavements (superpave): The product of the SHRP asphalt research program.' Report No. SHRP-A-410. Strategic Highway Research Program, National Research Council. Washington D.C., 1994.

87. **Kestler, M. A., Berg, R. L., Moore, T. L.,** 'Reducing damage to low-volume roads by using trucks with reduced tyre pressures.' Transportation Research Record, No. 1589, Transportation Research Board. Washington D.C., pp 9-17, 1997.

88. **Kirwan, R. W., Snaith, M. S., Glynn, T. E.,** 'A computer based subsystem for the prediction of pavement deformation.' Proc. 4th Int. Conf. on the Structural Design of the Asphalt Pavements, Ann Arbor, pp 509-518, 1977.

89. **LA Roche, C., Odeon, H., Simoncelli, J. P., Spernol, A.,** 'Study of fatigue in asphalt pavements using the LCPC's test track in Nantes-France.' 73rd annual meeting, Transportation research board. Washington, D. C., 1994.

90. **Lister, N. W., Powell, W. D., Goddard, R. T. N.,** 'A design for pavements to carry very heavy traffic.' Proc. 5th Int. Conf. on the Structural Design of the Asphalt Pavements, Netherlands, Vol. 1, August 1982.

91. **Low, B. H., Tan, S. A., Fwa, T. F.,** 'Analysis of marshall test behaviour with triaxial test determined material properties'. J. of Testing and Evaluation 21(3), 192. 1993.

92. **May, R. W., Witczak, M. W.,** 'Integrating flexible pavement mix and structural design.' Proc. 7th Int. Conf. on the Structural Design of Asphalt Pavements, Nottingham, UK, pp 141-151, 1992.

93. **Metcalf, J. B.,** 'Application of full-scale accelerated pavement testing.' National Cooperative Research Programme, Synthesis of Highway Practice 235, Transportation Research Board, Washington DC, 1996.

94. **Meyer, F. R. P., Haas, R. C. G.,** 'A working design subsystem for permanent deformation in asphalt pavements.' Proc. 4th Int. Conf. on the Structural Design of Asphalt Pavements, Ann Arbor, pp 519-528, 1977.

95. **Molenaar, A. A. A.,** 'Permanent deformation characterization of asphalt mixtures.' Proc. 10th International Flexible Pavements Conference, Australian Asphalt Pavement Association. Perth, Australia. Vol. 2, 1997.

96. **Monismith, C. L., Alexander, R. L., Secor, K. E.,** 'Rheological behaviour of asphalt concrete.' Proc. of the Association of Asphalt Paving Technologists, Vol. 35, pp 400-420, 1966.

97. **Monismith, C. L., Secor, K. E.,** 'Viscoelastic behaviour of asphalt concrete pavements.' Proc. of the 1st international conference on the structural design of asphalt pavements, pp 476. 1962.

98. **Monismith, C. L., Inkabi, k., Freeme, C. R., Mclean, D. B.,** 'A subsystem to predict rutting in asphalt concrete pavements.' Proc. 4th Int. Conf. on the Structural Design of Asphalt Pavements, Ann Arbor, pp 529-539, 1977.

99. **Monismith, C. L., Tayebali, A. A.,** 'Permanent deformation (rutting) considerations in asphalt concrete pavement sections.' J. of Association of Asphalt Paving Technologists, Vol. 57, 1988.

100. **Moavenzadeh, F., Carnaghi, R. A.,** 'Viscoelastic response of sand asphalt beams on elastic foundations under repeated loading.' Proc. of the Association of Asphalt Paving Technologists, Vol. 35, pp 514-, 1966.

101. **Morris, J., Haas, R. C. G., Reily, P., Hignell, E.,** 'Permanent deformation in asphalt pavements can be predicted.' Proc. AAPT, Virginia, 1974.

102. **Nair, K., Smith, W. S., Chang, C.Y.,** 'Applicability of a linear viscoelastic characterisation for asphalt concrete.' Proc. 3rd international conference on the structural design of asphalt pavements, Vol. 1, pp 277-289, Michigan. 1962.

103. **Nievelt, G., Thamfald, J.,** 'Evaluation of the resistance to deformation of different road structures and asphalt mixtures determined in the pavement rutting tester.' J. of AAPT, Vol. 57, pp. 320-345, 1988.

104. **Nunn, M, E., Leech, D.,** 'Deterioration mechanisms in flexible roads.' 2nd European conference on the durability and performance of bituminous materials, University of Leeds, 1997.

105. **Nunn, M. E.,** 'Prediction of permanent deformation in bituminous layers.' Research report no. 26, Transport and Road Research Laboratory, Department of Transport, 1986.

106. **Nunn, M. E., Brown. A., Lawrence, D.,** 'Assessment of practical tests to measure deformation resistance of asphalt'. Proc. 3rd European Symposium on Performance and Durability of Bituminous Materials and Hydraulic Stabilised Composites. Leeds, 1999.

107. **Nunn, M. E., Brown. A., Lawrence, D.,** 'Standardisation trial of RLAT:Draft Report'. Unpublished Project Report, Transport Research Laboratory, 1999.

108. **O'Reilly M. P.,** 'Mechanical properties of granular materials for use in thermal energy loading.' Ph.D. Thesis, Civil Engineering Department, University of Nottingham, 1985.

109. **Organisation for Economic Cooperation and Development (OECD).,** 'OECD full-scale pavement test.' Rep. No. IRRD No. 837329, Paris, France. 1991.

110. **Pagen, C .,** 'Dynamic structural properties of asphalt pavement mixtures.' Proc. 3rd international conference on the structural design of asphalt pavements, Vol. 1, pp 290-315, Michigan. 1962.

111. **Petersen, J. C., Robertson, J. F., Branthaver, J. F., Harnsberger, P. M., Duvall, J. J and Kim S. S.,** 'Binder characterization and evaluation, Volume 1.' SHRP-A-367, Strategic Highway Research Program, National Research Council, Washington, D. C., 1994.

112. **Phillips, M. C., Robertus, C.,** 'Binder rheology and asphaltic pavement deformation: The zero shear viscosity.' Euroasphalt and Eurobitume Congress, Strasbourg, 1996.

113. **Pidwerbesky, B. D., Steven, B. D., Arnold, G.,** 'Subgrade strain criterion for limiting rutting in asphalt pavements.' Proc. 8th Int. Conf. on the Asphalt Pavements, Seattle, pp 1529-1544, 1997.

114. **Powell, W. D., Polter, J. F., Mayhew, H. C., Nunn, M. E.,** 'The structural design of bituminous roads.' Report No. 1132, Transport and Road Research Laboratory, Crowthorne, Berkshire. 1984.

115. **Proceedings International Conference on Accelerated Pavement Testing,** Reno, Nevada, October 1999.

116. **Read, J. M.,** 'Fatigue cracking of bituminous paving mixtures.' Ph.D. Thesis, University of Nottingham, 1996.

117. **Read, J. M., Collop, A. C.,** 'Practical fatigue characterisation of bituminous paving mixtures.' Journal of the Association of Asphalt Paving Technologists, Vol. 66, pp 74-108. 1997.

118. **Richardson, I. R.,** 'The stress-strain behaviour of dry granular material subjected to repeated loading in a hollow cylinder apparatus.' Civil Engineering Department, University of Nottingham, 1999.

119. **Roberts, F. L., Quintus, V. H., Hudson, W. R.,** 'Design procedure for premium flexible pavements.' Proc. 5th Int. Conf. on the Structural Design of Asphalt Pavements, Netherlands, Vol. 1, August 1982.

120. **Romain, J. E.,** 'Rut depth prediction in asphalt pavements.' Proc. 3rd Int. Conf. on the Structural Design of Asphalt Pavements, London, pp 705-710, 1972.

121. **Rowe, G. M., Cooper, K. E.,** 'A practical approach to the evaluation of bituminous mix properties for the structural design of asphalt pavements.' J. of Association of Asphalt Paving Technologists, Vol. 57, 1988.

122. **Roque, R., Myers, L. A., Ruth, B.E.,** 'Loading characteristics of modern truck tyres and their effects on surface cracking of asphalt pavements.' Proc. 5th international conference on the bearing capacity of Roads and Airfields. Trondheim, Norway, July 1998.

123. **Scholz, T. V.,** 'Durability of bituminous paving mixtures.' PhD Thesis, Department of Civil Engineering, University of Nottingham, 1995.

124. **Scarpas, A., Al-Khoury, R., van Gurp, C and Erkens, S.,** 'Finite element simulation of damage development in asphalt concrete pavements.' Proc. 8th International Conference on Asphalt Pavements, Vol. 1, pp672-692, Seattle, (1997).

125. **Sebaaly, P., Tabatabaee, N.,** 'Effect of tyre pressure and type on response of flexible pavement.' Transportation Research Record, No. 1227, Transportation Research Board. Washington D.C., pp 115-127, 1989.

126. **'Shell Pavement Design Manual'** Shell International Petroleum Company Ltd. London 1978.

127. **Smith, H. A.,** 'Truck tyre characteristics and asphalt concrete pavement rutting.' Transportation Research Record, No. 1307, Transportation Research Board. Washington D.C., pp 1-7, 1991.

128. **Snaith, M. S., Brown, S. F.,** 'Electro-hydraulic servo-controlled equipment for the dynamic testing of bituminous materials.' RILEM International Symposium on the Deformation and the Rupture of Solids subjected to Multiaxial Stresses, 3, Cannes, pp 139-154, 1972.

129. **Sousa, J. B., Craus J., Monismith, C. L.,** 'Summary report on permanent deformation in asphalt concrete.' SHRP-A/IR-91-104. Institute of Transportation Studies, University of California Berkeley, 1991.

130. **Sousa, J.B. and Weissman, S.L.,** 'Modelling permanent deformation of asphalt-aggregate mixes.' Asphalt Paving Technology, Vol. 63, pp 224-257, (1994).

131. **Sousa, J.B., Weissman, S.L., Sackman, J.L. and Monismith, C.L.,** 'A non-linear elastic viscous with damage model to predict permanent deformation of asphalt concrete mixes.' Presented at 72nd Annual Transportation Research Board Annual Meeting, Washington DC, 1993.

132. **Sosnovske, D., Leahy, R. B., Hicks, R. G.,** 'Evaluation of rutting potential of Oregon surface mixtures.' Journal of the Association of Asphalt Paving Technologists, Vol. 63, 1994.

133. **Specification for Highway works,** Vol. 1, July 1998.

134. **'SUPERPAVE binder specification and testing'**. Superpave series No. 1 (SP-1), Asphalt Institute Kentucky, USA, 1995.

135. **Thrower, E. N.,** 'Methods of predicting deformation in road pavements.' Proc. 4th Int. Conf. on the Structural Design of Asphalt Pavements. Ann Arbor, pp 540-554, 1977.

136. **Thom N. H.,** 'Design of road foundations.' Ph.D. Thesis, Civil Engineering Department, University of Nottingham, 1988.

137. **'The Wheel Tracking Test.'** Leaflet 50, Road Research Laboratory. Crowthorne, 1971.

138. **Transport research Laboratory and Overseas Development Administration,** 'A guide to the structural design of bitumen surfaced roads in tropical and sub-tropical countries – Overseas road note 31'. Crown Copyright, 1993.

139. **Uge, P., Van de Loo, P. J.,** 'Permanent deformation of asphalt mixes.' Shell Laboratorium, Amsterdam, 1974.

140. **Uzan, J.,** 'Asphalt concrete characterisation for pavement performance prediction.' J. Asphalt Paving Technology, Vol. 65, pp 573-607, (1996).

141. **Valkering, C. P., Stapel, F. D. R.,** 'The Shell pavement design method on a personal computer.' Proc. 7th Int. Conf. on the Structural design of Asphalt Pavements, Nottingham, UK, pp. 351-374.

142. **Van der Poel C.,** 'A general system describing the visco-elastic properties of bitumen and its relation to routine test data.' J. of Applied Chemistry, Vol. 4, pp. 221-236, 1954.

143. **Van de loo P. J.,** 'The creep test: A key tool in asphalt mix design and in the prediction of pavement rutting.' J. of Association of Asphalt Paving Technologists, Vol. 47, pp 522-557, 1978.

144. **Van de loo P. J.,** 'Practical approach to the prediction of rutting in asphalt pavements: The Shell Method.' Transportation Research Record, No. 616, Transportation Research Board. Washington D.C., pp 15-21, 1976.

145. **Van de loo P. J.,** ' Creep testing, a simple tool to judge asphalt mix stability.' J. of Association of Asphalt Paving Technologists, Vol. 43, pp 253-285, 1974.

146. **Verstraeten, J., Veverka, V., Francken, L.,** 'Rational and practical designs of asphalt pavements to avoid cracking and rutting.' Proc. 5th Int. Conf. on the Structural Design of Asphalt Pavements, Holland, pp 45-58, 1982.

147. **Whiteoak, D.,** 'Shell bitumen handbook.' 1990

148. **Williams, M. L., Landel, R. F., Ferry, J. D.,** 'The temperature-dependence of relaxation mechanisms in amorphous polymers and otherglass forming liquids.' J. of the American Chemical Society, Vol.77, pp. 3701-3706, 1955

149. **Wood, D. M.,** 'Soil Behaviour and Critical State Soil Mechanics.' pp 231-234. Cambridge University Press, 1990.